Fuel Reforming for High Efficiency and Dilution Limit Extension of Spark-ignited Engines

by

Yan Chang

A dissertation submitted in partial fulfillment
of the requirements for the degree of
Doctor of Philosophy
(Mechanical Engineering)
in The University of Michigan
2018

Doctoral Committee:

Professor André L. Boehman, Co-Chair
Dr. Stanislav V. Bohac, U.S. Environmental Protection Agency, Co-Chair
Professor Galen Fisher
Professor Johannes Schwank
Senior Research Staff Dr. James P. Szybist, Oak Ridge National Laboratory
Professor Margaret Wooldridge

Yan Chang
yanchang@umich.edu
ORCID iD: 0000-0001-8432-9812

To my family

ACKNOWLEDGMENTS

TABLE OF CONTENTS

LIST OF FIGURES

x

LIST OF TABLES

LIST OF ABBREVIATIONS

BMEP	Brake Mean Effective Pressure
BSFC	Brake Specific Fuel Consumption
CAD	Crank Angle Degree
CA50	Crank Angle of 50% Mass Fraction Burned
CFD	Computational Fluid Dynamics
CI	Compression Ignition
COV	Coefficient of Variation of IMEP
DI	Direct Injection
EGR	Exhaust Gas Recirculation
ETC	Electric Turbo-compounding
EVC	Exhaust Valve Closing
GDI	Gasoline Direct Injection
GHG	Green House Gas
HCCI	Homogeneous Charge Compression Ignition
ICE	Internal Combustion Engine
IMEP	Indicated Mean Effective Pressure
LLNL	Lawrence Livermore National Laboratory
NVO	Negative Valve Overlap
ORC	Organic Rankine Cycle
ORNL	Oak Ridge National Laboratory
SACI	Spark Assisted Compression Ignition
SI	Spark Ignited
SOI	Start with Injection Timing
SwRI	Southwest Research Institute
TCR	Thermochemical Recuperation
TDC	Top Dead Center
TEG	Thermoelectric Generators
TPA	Three Pressure Analysis
TWC	Three-Way Catalytic Converter
VGT	Variable Geometry Turbocharger
VVL	Variable Valve Lift
VVT	Variable Valve Timing

ABSTRACT

Engine efficiency improvement can help combustion powertrains, which include conventional, hybrid, and plug-in hybrid systems, to meet the strict emissions standards and the increasing demand from customers for performance, drivability, and affordability of vehicles. Cooled exhaust gas recirculation (EGR) can reduce fuel consumption and NO_x emissions of gasoline engine systems while keeping the capability of using a conventional three-way catalyst for effective emissions reduction. However, too much EGR would lead to combustion instability and misfire.

This thesis identified opportunities to improve efficiency in internal combustion engines by high EGR dilution SI combustion by using thermodynamics-based approaches. This goal has been achieved by using fuel reforming in a thermodynamically-favorable way. Exhaust heat was used to drive endothermic reforming reactions to increase the chemical fuel energy to attain thermochemical recuperation (TCR), a form of waste heat recovery, with robust integrated systems and the regular gasoline.

Three strategies for fuel reforming, along with the unique designs of corresponding integrated engine systems, a committed in-cylinder reformer, a catalytic EGR-loop reforming system, and fuel reforming by fuel injection during Negative Valve Overlap (NVO), have been proposed and investigated with unique engine system setups and corresponding experimental and simulation research.

The concept and the system to use one cylinder to serve as a committed fuel reformer without spark ignition is first demonstrated. The committed in-cylinder reformer

engine system achieves 8% brake thermal efficiency improvement through EGR and cylinder deactivation effects, even though there is low fuel conversion.

The novel catalytic EGR-loop reforming integrated engine system was designed and tested. The experiments and thermodynamic equilibrium calculations reveal that the suppression of H_2 and CO caused by the enthalpy limitation could be countered by adding small amounts of O_2 by running one-cylinder lean. As much as 15 volume % H_2 at the catalyst outlet is produced when the fuel and air equivalence ratio is between 4 and 7 under quasi-steady-state conditions. It is also found that this catalytic EGR reforming strategy makes it possible to sustain stable combustion with a volumetric equivalent of 45%–55% EGR, compared to a baseline EGR dilution limit which is under 25%. This catalytic EGR-loop reforming strategy results in a decrease of more than 8% in fuel consumption with significant potentials for even higher brake thermal efficiency. This novel design also opens up a new control method to control the amount of fuel reforming and the fraction of the partial oxidation reaction and steam reforming reaction by adjusting the lambda value of the cylinder which is running lean. Through this design, the engine is serving as an active system, which can also be adapted to respond to the needs of the passive catalyst system so that even better more significant benefit can be achieved.

The results demonstrate fuel injection during NVO can extend the dilution limit, improve brake specific fuel consumption (BSFC), and reduce CO and NO_x emissions on the engine modified with the capability of variable intake and exhaust valve timing and higher compression ratio.

A comprehensive comparison of different reforming strategies for engine application and analysis of critical factors contributing to the performance of integrated fuel reforming engine systems is also provided.

The research of this dissertation has demonstrated new pathways and scientific outcomes for technology development of internal combustion engine powertrain systems that can operate significantly more efficiently and cleanly.

Chapter 1. Introduction

1.1 Motivation

Reciprocating internal combustion engines, in general, called IC engines, have been one of the most graceful inventions that have played significant roles in society, the economy, and environment [1]–[3]. The spark-ignited (SI) engine qualities of robustness, low production and operating cost, and good efficiency are the essential reasons that the automobile is so widespread [4]. However, significant technical challenges in aspects of engine operation, efficiency, and emission still exist even after more than a century of research and engineering exploration [5]–[9].

One type of emission from the internal combustion engine is carbon dioxide. According to the information from the United States Energy Information Administration, the transportation sector has been and will continue to be the most significant source of human-produced carbon dioxide out of the five industry sectors (shown in Figure 1.1). The industry sectors are residential, commercial, industrial, electric power and transportation [10]. As carbon dioxide plays a significant role as a greenhouse gas in global warming [11]–[13], the U.S. Environmental Protection Agency (EPA) has established national GHG emissions standards under the Clean Air Act. The Department of Transportation's National Highway Traffic Safety Administration (NHTSA) has established Corporate Average Fuel Economy (CAFE) standards under the Energy Policy and Conservation Act, as amended by the Energy Independence and Security Act (EISA) [14]. The average fuel efficiency of U.S. light-duty new vehicles was 36.4 mpg for passenger cars and 26.3 mpg for light trucks in 2014 [15]. EPA Light duty vehicle Green House Gas (GHG) standards require about 50% reduction in GHG emissions from 2012 to 2025 [16]. Regarding mid-term, to improve the efficiency of

internal combustion engines is one of the most promising and cost-effective approaches to increasing fuel economy of light-duty vehicles is [17].

U.S. energy-related carbon dioxide emissions (Reference case)
billion metric tons of carbon dioxide
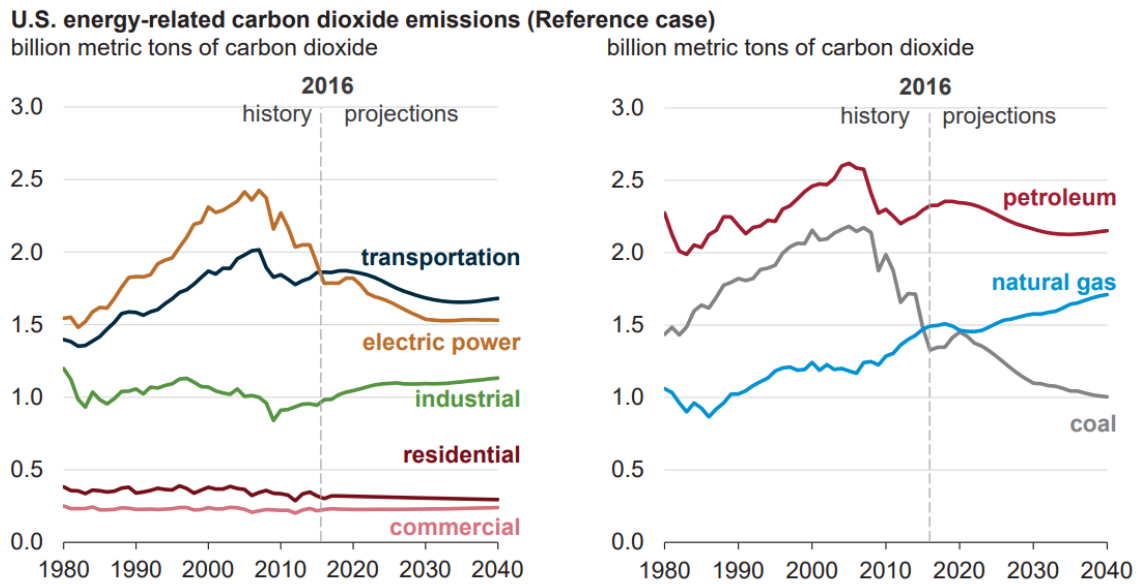
Figure 1.1. U.S. energy-related carbon dioxide emissions (Data and figure are sourced from Annual Energy Outlook 2017 with projections to 2050 – EIA) [10].

Additionally, in the current transportation infrastructure, petroleum-derived liquid fuels are the dominant source of energy. Many countries import oil at an unprecedented rate because the distribution of oil supply does not coincide with the location of the demand. These factors can lead to a significant balance of trade and national-security challenges[18]. Improvements in the energy efficiency of vehicles, development of alternative fuels, and the corresponding design of internal combustion engines can significantly reduce oil dependency [19].

Future IC engines and powertrain systems of vehicles also need to meet consumers' increasing demands for performance, drivability, and affordability. Even incremental improvements in engine efficiency, perhaps previously not considered worth pursuing, can be critical under the conditions that engine efficiency, performance, and emissions will be squeezed to the utmost in the future. In such a context, traditional internal combustion engine systems might need new system design to be continuously competitive [20].

The hybrid powertrain systems leverage positive attributes of both engines and electric motors. These characteristics include an enabling path for moving engine operating

conditions to high-efficiency areas and eliminating low-load engine operation, or conditions close to knocking limit [21]. If engine efficiency can be increased through new combustion regimes or new system design, hybrid powertrains can leverage and compound engine efficiency even further to improve fuel economy [4]. Hybrid powertrain systems are not independent of, but rather closely coupled with, engine advancement. This conclusion can also be seen in the case of the Toyota Prius, which is the best-selling hybrid vehicle in the U.S [22]. The peak efficiency of Prius' internal combustion engine has been improved from 37% for its first generation to 41% for its current generation [23]. The engine efficiency improvement can help combustion powertrains, which include conventional, hybrid, and plug-in hybrid systems, to gain future higher competitiveness.

It can be seen from a breakdown of the average losses of internal combustion engine cars (fleet make up 70% gasoline engines and 30% diesel engines in Figure 1.2) that 33% of energy from fuel is lost to the exhaust [19]. Therefore, it would be very promising to recover work from the exhaust and increase brake work directly.
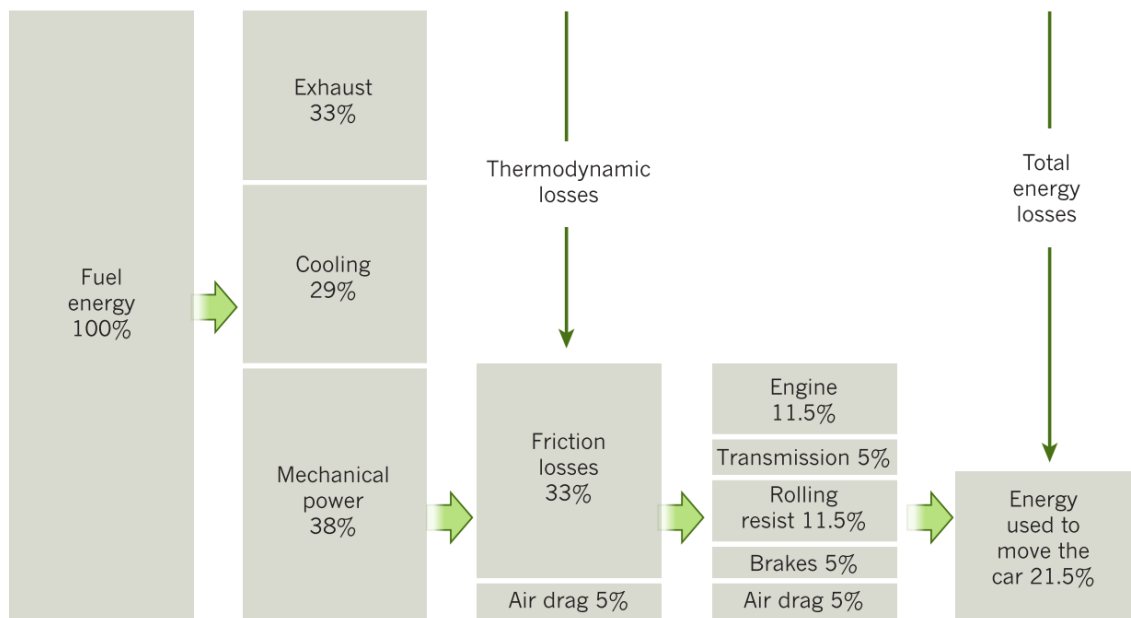
Figure 1.2. Vehicle energy losses (a breakdown of the average losses of internal combustion engine cars, fleet makes up 70% gasoline and 30% diesel) [19].

External cooled exhaust gas recirculation (EGR) provides known thermodynamic benefits while maintaining compatibility with conventional 3-way catalysts for emissions control [24].

The implementation of EGR is an attractive way to improve spark ignition engine efficiency. The thermodynamic benefits of EGR include reduced pumping work at part-load conditions, decreased heat transfer due to lower cylinder temperature, and an increased ratio of specific heats [25]. External EGR is also a proven way to lower the knocking propensity for a given fuel [26]. Also, EGR reduces NO_x emissions over a broad range of speed and load conditions [27]. However, the amount of EGR dilution is limited due to engine combustion stability issues [28].

Technical challenges need to be addressed for the implementation of EGR. Fuels with high flame speed such as hydrogen complete the early flame kernel development process faster, making them less susceptible to the stochastic cycle-to-cycle differences in turbulence and ultimately providing more stable combustion [29].

The work presented in this dissertation investigates the feasibility of thermochemical recuperation which converts exhaust heat to usable chemical energy by providing heat for endothermic reactions of fuel reforming to improve the SI engine efficiency. Reforming products support dilute combustion because H_2 allows the dilution limit to be extended. The goal is to achieve exhaust heat recovery through fuel reforming to get higher engine efficiency and the extension of dilution limit in a single and optimal engine system with new combustion regimes.

1.2 Objective

The overarching goal of the research of this thesis is to use a thermodynamics-based approach to identify and pursue opportunities for improved efficiency in internal combustion engines by high EGR dilution SI combustion enabled by the fuel reforming in the most thermodynamically-favorable way possible while keeping the capability of using current mature after-treatment systems. Ideally, this involves using exhaust heat to drive endothermic reforming reactions to increase the chemical fuel energy to achieve thermochemical recuperation (TCR) and generate H_2, a form of waste heat recovery with a robust system and the regular gasoline.

Three strategies for fuel reforming are investigated, and the corresponding integrated engine systems are designed and tested. These three strategies include committed in-cylinder reformer, catalytic EGR-loop reforming, and fuel reforming by fuel injection during Negative Valve Overlap (NVO). Unique engine systems are set up, and corresponding experimental and simulation research are done. The effect of fuel on EGR dilution limit and engine efficiency is also investigated. A comprehensive comparison of different reforming strategies for engine application and analysis of critical factors contributing to the performance of integrated fuel reforming engine systems are provided.

1.3 Summary of Dissertation

This dissertation is organized into seven chapters.

In Chapter 1, the background and motivation of fuel reforming for high efficiency and dilution limit extension of SI engines are discussed.

Chapter 2 provides a literature review of previous research and challenges focusing on EGR, state of the art of EGR dilution limit extension technologies, and waste heat recovery technologies.

Chapter 3 describes the investigation of fuel effects on combustion with EGR dilution in spark ignited engines. It sets up the baseline of dilution limit of EGR and engine efficiency of the stock configuration engine platform that was used for comparison with other strategies with fuel reforming. The EGR dilution tolerance is investigated in a multi-cylinder engine for two pure components: iso-octane, which has a relatively slow flame speed, and ethanol, which has a fast flame speed. Low sulfur gasoline is also included in the study. The comparisons are conducted at an early combustion phasing and a late combustion phasing condition to understand how the combustion process and cyclic stability changes with combustion phasing and with fuel type.

The investigation in Chapter 4 tests the feasibility of in-cylinder reforming to achieve thermochemical recuperation and extended EGR dilution limits in SI engines. In this research,

an in-cylinder reforming technique in a multi-cylinder configuration, in which one of the engine cylinders acts as the reformer, is used. The reforming cylinder breathes in from the exhaust manifold and exhausts into the intake. It requires input work from the crankshaft to the reforming cylinder rather than work being extracted from it. In this configuration, the advantageous fuel properties of reformate are utilized to determine if a sufficiently large efficiency benefit can be realized in the combustion cylinder to overcome the added friction and thermodynamic penalties associated with the reforming process.

The study shown in Chapter 5 investigates the feasibility of catalytic reforming to achieve thermochemical recuperation and extended EGR dilution limits in SI engines. In this research, one of the cylinders has an isolated intake and exhaust manifold. The entirety of the exhaust from this cylinder (cylinder 4) is fed directly to the reforming catalyst, which then feeds into the intake for cylinders 1-3. A small amount of oxygen is provided to the reformer by operating the main combustion event in cylinder 4 fuel-lean, but then using a post-injection when the exhaust valve opens to feed the catalyst the appropriate mixture.

The goal of the study in Chapter 6 is to quantify the combustion and emissions benefits of dilute SI combustion with fuel injection during NVO and to investigate the effectiveness of this strategy towards extending the low load dilution limit of SI combustion. A high-pressure EGR system, Variable Valve Timing, Variable Valve Lift, and customized cylinder head were installed in a General Motors "Ecotec LNF" platform to enable the capability of NVO control and sweep of EGR.

Chapter 7 provides a comparison of different fuel reforming strategies regarding the feasibility of engine efficiency improvement, the feasibility of dilution limit extension, system complexity, and other factors for engine integrated system application.

Finally, Chapter 8 gives a summary of work accomplished, conclusions from each research, and ideas about future work.

Chapter 2. Literature Review

2.1 Exhaust Gas Recirculation (EGR)

2.1.1 General Information

EGR was first introduced for diesel engine systems. It has been a common way to control in-cylinder NO_x production, especially on most modern high-speed direct injection diesel engines [30]–[41]. The main contents of EGR are N_2, CO_2, H_2O, and O_2. With the downsizing direction of gasoline engines driven by the stringent regulation of vehicle emission and fuel economy, EGR is also commonly used in gasoline engines [24], [27]–[29], [42]–[59].

Exhaust gas is one type of cylinder charge dilution. EGR can be classified into two categories: Internal EGR and external EGR. A controllable amount of internal EGR can be achieved through a cam system with the capability for variable valve timing to control negative valve overlap (NVO), which is one way to get internal EGR. External EGR is taken from the engine exhaust port and then put back into the engine intake.

Regarding external EGR, it can be further classified as hot EGR and cooled EGR. The hot EGR is the exhaust gas that is recycled directly to the intake [30]. The cooled EGR is the recycled exhaust after a cooling process. The hot EGR can heat the intake, enhance the flame propagation, and decrease HC emission, while cooled EGR increases the intake density, which increases the volumetric efficiency and increases the HC emission and suppresses knock (reduces the need for enrichment).

The percentage of EGR is defined as the percentage of recirculated exhaust percentage in the total intake mixture [39]. The amount of CO_2 in the intake manifold with that in the exhaust

pipe can also be used to calculate EGR percentage with the following Equation 2.1.

$$EGR \ (\%) = \frac{[CO_2]_{Intake \ gas} - [CO_2]_{Ambient}}{[CO_2]_{Exhaust \ gas} - [CO_2]_{Ambient}}$$

<div align="right">Equation 2.1</div>

2.1.2 Benefits of EGR

External EGR is a popular in-cylinder method to reduce NO_x. The NO_x emission increases exponentially with the increase of the combustion temperature [1] based on the Zeldovich mechanism. The decrease in NO_x with the increase of EGR rate is due to lower combustion temperatures coming from the thermal effect, chemical effect, and dilution effect, which are explained in detail as follows:

- The thermal effect: Recirculated CO_2 and H_2O have higher specific heat capacity compared to O_2 and N_2, resulting in lower flame temperature [60].
- The chemical effect: The water vapor and CO_2 recirculated back to the intake from the exhaust are dissociated during combustion, which modifies the combustion process and NO_x formation [39].
- The dilution effect: The decrease of inlet O_2 concentration leads to the deceleration of the mixing process between O_2 and fuel, which extends the flame region. Also, the reduction of oxygen partial pressure causes a negative effect on the kinetics of the reaction of elementary NO formation [58].

EGR is also very effective for fuel economy improvement for spark-ignited direct-injection engines, as proven by many researchers. Li et al. [46] did an in-depth first law and second law thermodynamics analysis of the effects of cooled EGR on fuel conversion efficiency on a boosted, spark-ignited, direct injection gasoline engine at high, medium, and low loads with engine experiment and simulation. It was found that EGR improves the fuel economy mainly due to the increase of the ratio of specific heat of working gases, the reduction of heat transfer through the combustion chamber walls, and the reduction of pumping loss during the gas

exchange. Also, EGR may replace the fuel enrichment at high loads, and increase the degree of constant volume heat release at medium and high loads. The effect of the reduction of loss from the heat transfer due to EGR is the dominant factor for the improvement of fuel economy at a constant air-fuel ration. And at high load, the replacement of fuel enrichment with EGR is most effective. Alger et al. [24] showed the addition of EGR resulted in higher fuel consumption benefits of 10-20% as well as the expected NO and CO reductions at high loads. The fuel economy benefits at high loads came from the reductions in exhaust temperatures that eliminated the requirement for over-fueling, a decrease in knock tendency, and a subsequent improvement in combustion phasing. Addition of EGR at low-load and part-load decreased NO and CO emissions and reduced fuel consumption by up to 4%, mainly due to the reduction in pumping losses. Duchaussoy et al. [61] proposed a comparative analysis between cooled EGR operation and lean burn as the method at full load on a turbocharged engine. They found that cooled EGR is more advantageous than lean-burn regarding performance, heat exchange, and specific fuel consumption.

EGR also substantially decreases the knocking propensity of the SI engine. Hoepke et al. [62] reported an improvement of 5% in gross thermal efficiency with 18% EGR on a boosted direct-injection spark ignition engine. The knocking tendency decrease is due partly to slower combustion, which is equivalent to a spark retard, as manifested by a retarded value of the 50% burn point (CA50). Also, it is due partly to slower ignition chemistry of the diluted charge. A 10% increment of the EGR rate corresponds approximately to a 3% increase in the effective fuel octane number. Splitter et al. [63] also showed that the maximum load limit in a single-cylinder engine was increased by more than 10% by using 15% EGR, due to the reduction of knock propensity.

The most commonly used method to limit knock at high load is to inject excess fuel into the mixture to decrease the air-fuel ratio to reduce the combustion temperature. However, under the fuel enrichment condition, HC and CO will increase, and TWC could not work appropriately when the air-fuel ratio is not stoichiometric, which causes issues for fuel economy and emissions. Using EGR allows the use of the stoichiometric air-fuel ratio, which still ensures a good conversion of HC, CO, and NO_x. Cooled EGR to inhibit knock and to

reduce emission is a more efficient method for gasoline engines. Szybist et al. [64] also illustrated that under highly boosted conditions relevant to modern downsized boosted SI engines, the in-cylinder pressure is higher and the temperature is colder than the conventional one. The charge reactivity increases compared to naturally aspirated conditions, and the attenuation of knock by EGR is reduced.

2.1.3 Challenges of EGR Implementation

However, higher EGR levels increase cycle-to-cycle variability and decrease the level of improvement in fuel consumption. High-level homogeneous EGR causes reduction of burning speed, increase of cycle to cycle variation, and even misfire so that the steady-state combustion is difficult to achieve [55]. As reported in the research of Li et al. [46], the engine can only get the smooth operation up to 25% EGR, and the coefficient of variation in IMEP was beyond the acceptable limit (5%) at high EGR rate. Similar results were also obtained from research of Cairns et al. [65] and Duchaussoy et al. [61]. The most significant factor is the substantial decrease in flame speed that occurs with EGR, as reported by Stone et al. [66] and Szybist et al. [50]. The decrease of mixture flame speed results in significantly increased combustion initiation periods and burn durations. In a literature review by Ozdor et al. [67], it was shown that flame speed effects on combustion stability are related to the early flame kernel development. Fuels with high flame speed complete the early flame kernel development process faster, making them less susceptible to the stochastic cycle-to-cycle differences in turbulence, and ultimately providing more stable combustion. Also, the technical challenges of EGR dilution limit need an investigation to get more benefits from high levels of EGR.

2.2 State of the Art of EGR Dilution Limit Extension Technologies

Technical challenges need to be addressed for the implementation of EGR. Researchers have shown several potential ways to extend the dilution limit of EGR.

2.2.1 Advanced Ignition Systems

Sevik et al. [68] used a low-energy transient plasma ignition system to extend the EGR tolerance and lean limit by as much as 20% (from 22.7 to 27.1% EGR) and nearly 10% (from $\lambda = 1.55$ to 1.7). It has been shown that the energy delivery process of the low-energy transient plasma generated by nanosecond pulses significantly improves part-load dilution tolerance by reducing the early flame development period.

Alger et al. [69] developed a new, continuous discharge ignition system, which allows for variable duration ignition events in high dilution SI engines. It resulted in a larger improvement in burn rate and stability compared to that was achieved by either one coil in multi-strike mode or both coils in a multi-strike mode with simultaneous discharge. This system provided an improvement of EGR tolerance of 5-10% EGR over the stock system and 2-5% over the multi-strike system, and it improved the initial burn rates in the engine system by 5-15 Crank Angle Degree (CAD) over the single-strike and multi-strike system.

2.2.2 Special Intake Port Design

Wheeler et al. [70] investigated increasing the EGR tolerance of the combustion system through the use of very high tumble ratios exceeding that of current production systems, enhanced ignition, and increased compression ratio. An externally boosted single-cylinder research engine and computational fluid dynamics (CFD) are used to understand the effect of high tumble intake ports on the mixture preparation and turbulence differences. This system was found to provide high EGR dilution tolerance, improved thermal efficiency, and higher load capability through the advancement of the knock limited combustion phasing. However, extremely high tumble ratios were not beneficial due to the increase of the knocking tendency of the engine and heat loss.

2.2.3 Stratified EGR

The stratified exhaust gas recirculation could minimize exhaust gas concentration at the spark plug region by separating EGR air and fresh air in the combustion chamber. This system needs to make stratification of EGR and fuel-air mixture in the intake stroke and maintain the stratification in the compression stroke before ignition [58]. The technical challenge for this concept is to keep a substantial separation between EGR gas and an air-fuel mixture or to minimize the mixing between these two zones to an acceptable level for stable and complete combustion. Radial EGR stratification seems to be the most appropriate flow structure for compression stroke compared to lateral stratification and axial stratification due to the less complexity of implementation. For the radial EGR stratification, the central air-fuel cylinder and the outer EGR tubular cylinder are concentric with the engine cylinder, and the two cylinders will be compressed in the axial direction as the piston moves upwards in the compression stroke.

Dong et al. [42] did a series of computational fluid dynamics (CFD) studies to model in-cylinder turbulent flow, temperature, pressure, and EGR concentration fields and to simulate EGR stratification process of the corndog concept (radical EGR stratification) and conjugate vortex (lateral stratification) in a typical pent-roof gasoline engine cylinder during intake and compression strokes. This research work showed that in-cylinder flow structure and characteristics highly depend on intake and exhaust system configurations, such as valve opening, port geometry, and valve curtain geometry.

Xu et al. [71] used KIVA3V to simulate mixing and combustion processes in a typical pent-roof gasoline engine cylinder during compression and expansion strokes with swirl-type stratified EGR and air-fuel flow structure. The effects of centrifugal force on the differences in velocity, temperature, and density between the air and the EGR gas were discussed. This research showed that the swirl motion could preserve the stratified EGR structure very well during the compression stroke. To minimize the adverse effect from the in-cylinder swirl motion, which deteriorates the combustion, the swirl ratio should not exceed 2. The combustion performance of this concept is susceptible to the in-cylinder flow turbulence.

Alger et al. [24] investigated the feasibility of improvement in EGR tolerance of a semi-stratified charge generated by a split injection strategy at low load conditions. The results show that the improvement in burn duration leads to an increase in combustion stability and a reduction in fuel consumption and emissions. The addition of a second injection event late in the compression stroke leads to a reduction in initial burn duration within a narrow window of the injection timing and the amount of fuel.

2.2.4 Additive of Fuel Reformate

The additive of fuel reformate primarily consists of H_2 and CO into the intake manifold. Hydrogen addition increases combustion rate, allows retarded spark timing leading to lower NOx, and improves efficiency, as indicated by Conte et al. [72].

D'Andrea et al. [73] showed that hydrogen addition effect on the engine performance highly depends on the fuel/air equivalence ratio. The added hydrogen resulted in improved work output and a reduction in burn duration and cycle-to-cycle variation while operating under lean conditions ($\Phi < 0:85$).

Ji et al. [74] found that the maximum brake thermal efficiency was increased from 26.37% in the original spark ignition gasoline engine to 31.56% in the engine with a 6% hydrogen blending level at lean conditions. However, NO_x emissions increased with the increase of hydrogen addition due to the increased cylinder temperature.

Tahtouh et al. [75] used the experiment of a single cylinder SI engine with different rates of nitrogen dilution (0 to 20 percent by volume in the total mixture) and hydrogen/iso-octane blends to show that pumping losses, combustion efficiency, and indicated efficiency are also improved with the addition of hydrogen. When hydrogen addition and lean and/or diluted conditions are combined, high values of indicated engine efficiency with low amounts of HC, NO_x, and CO emissions can be achieved.

Alger et al. [29] found that the addition of 1% (vol) hydrogen could extend the EGR limit from 25% to over 50% for gasoline and from 20% to 28% for CNG.

Ivanič et al. [44] tested the effect of adding plasmatron-produced reformer gas (H_2, CO, N_2 mixture) from isooctane and n-heptane fuel on a single cylinder SI engine. Their results show that lean dilution can improve engine efficiency by as much as 12%, while EGR dilution delivers 8% improvement under part-load conditions.

In summary, the addition of H_2 has excellent potential to improve the engine combustion stability and the engine efficiency.

2.3 Waste Heat Recovery

2.3.1 Overview of Waste Heat and Recovery Technologies

Researchers used experimental and theoretical results to state that the 30-40% of the fuel energy from the internal combustion engine is lost to the environment as waste heat [76]–[80]. For example, Teng et al. [79] demonstrated a comprehensive energy flow analysis for a typical turbocharged heavy-duty diesel engine with a high-pressure EGR system. At medium and high engine speeds, the brake power was about 40% while the net exhaust energy was about 30%. Heat rejection from the radiator was about 18%, and heat rejection from the charge air cooler was < 10%. Radiation from the exhaust system/engine block and the miscellaneous loss was about 3% of the fuel energy. Therefore, the heat contained in exhaust gas and coolant is considered to be the most promising for recovery from various waste heat [81].

Major waste heat recovery technologies can be classified into eight categories: thermodynamic organic Rankine cycle (ORC), thermoelectric generators (TEG), electric turbo-compounding (ETC), hybrid pneumatic power systems (HPPS), six-stroke internal combustion engine cycle, turbocharger, non-catalytic fuel reformates generation, and catalytic fuel reformates generation. Some waste heat recovery technologies can be incorporated with each other and with other technologies. For example, TEG technology can be combined with other technologies such as turbocharger, photovoltaic, or Rankine cycle technique to get higher energy efficiency and low emissions [78]. The recovered heat can be

reused within the same process. It can also be transferred to another thermal, electrical, or mechanical process.

2.3.2 Rankine Cycle

There are several different thermodynamic cycles that can be used to generate electricity from exhaust heat. These technologies include organic Rankine [76], [82]–[88], supercritical Rankine [89], Rankine bottoming cycle [90]–[94], Kalina, trilateral flash, and Goswami cycles. However, the low-grade heat from the engine exhaust cannot be converted to electrical power very efficiently by using conventional methods. Research has shown that thermodynamic cycle of organic Rankine cycle and Rankine bottoming cycle are promising technologies to improve the engine system efficiency [80], [90]–[99].

A Rankine cycle is a closed-loop system where a working fluid repeatedly circulates through four components (evaporator, turbine, condenser, and pump) to transform waste heat into mechanical or electrical power. If the selected working fluid is organic in nature, researchers often refer to this system as an Organic Rankine Cycle (ORC). Brief schematic setup of organic Rankine cycle system is shown in Figure 2.1 [77].
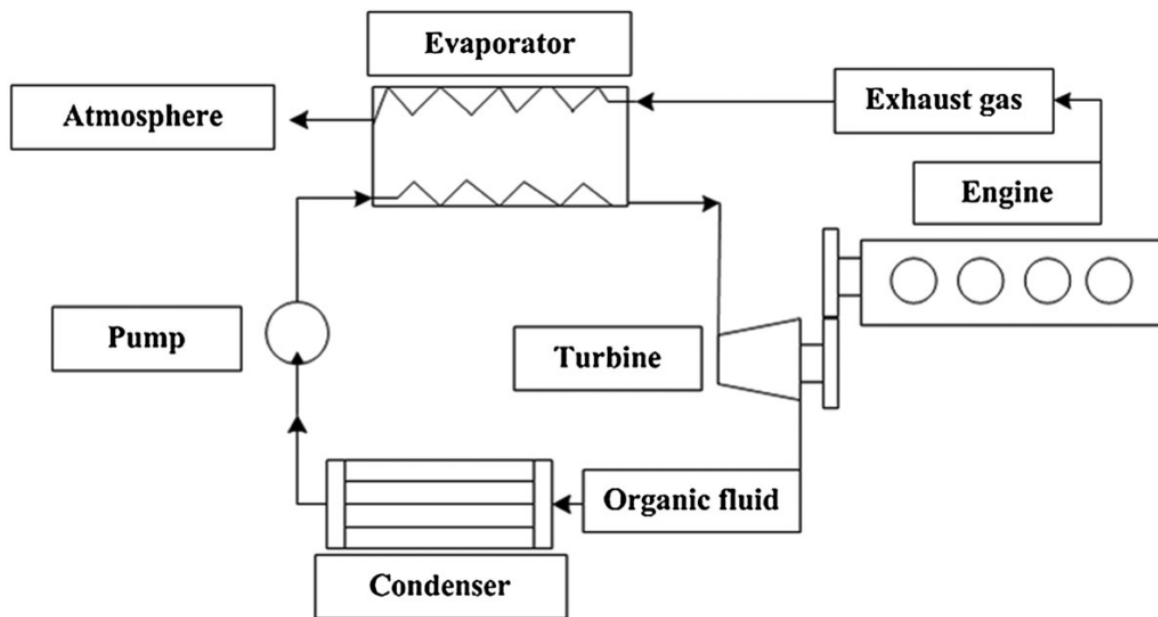
Figure 2.1. The brief schematic setup of organic Rankine cycle system. [77].

DiBella et al. [100] demonstrated an average of 12.5% improvement in fuel consumption in a diesel organic Rankine-cycle in a 288-Bhp, Class 8, long-haul vehicle diesel engine. Srinivasan et al. [101] showed that the compounding hot EGR and ORC engine could get an average 7% improvement in fuel conversion efficiency and 18% reduction of NO_x and CO_2. He [102] demonstrated more heat recovered by the combined cycle, which consists of an ORC using cyclopentane as the working fluid of the ORC for recovering the waste heat of lubricant and exhaust gas, and a Kalina cycle for recovering the waste heat of cooling water.

Vaja et al. [91] performed a second law analysis of the bottoming ORC matched to a stationary internal combustion engine and demonstrated that a 12% increase in the overall efficiency could be achieved concerning the engine with no bottoming, but the efficiency improvement is also dependent on the working fluid of ORC. Endo et al. [82] demonstrated that the thermal efficiency was increased from 28.9% to 32.7% (13.2% increase) at 100 km/h constant vehicle speed in a hybrid vehicle where the Rankine cycle system was installed, and an automatic control system to change steam temperature and pressure according to the load variation was constructed.

In summary, the Rankine cycle waste heat recovery technology could get higher thermal efficiency with no increase of pumping loss and a small effect on the engine load. However, it has disadvantages such as complex structure, increased volume and weight for the vehicle system, and toxic working fluid [77].

2.3.3 Thermoelectric Generators (TEG)

Thermoelectric materials can generate electricity from waste heat or be used as solid-state Peltier coolers [103]. The mobile charge carriers at the hot end tend to diffuse to the cold end when a temperature gradient is applied to a material. The thermoelectric effects arise because charge carriers in metals and semiconductors are free to move while carrying charge and heat. Thermoelectric devices contain many thermoelectric couples consisting of n-type (containing free electrons) and p-type (containing free holes) thermoelectric elements wired electrically in series and thermally in parallel, as shown in Figure 2.2. Due to the Seebeck effect, the

temperature difference provides the voltage. The thermoelectric generator uses the heat flow across a temperature gradient to power an electric load through the external circuit. Investigations of TEG technology have shown it could be a promising new technology to recover waste heat from internal combustion engines [104]–[114].
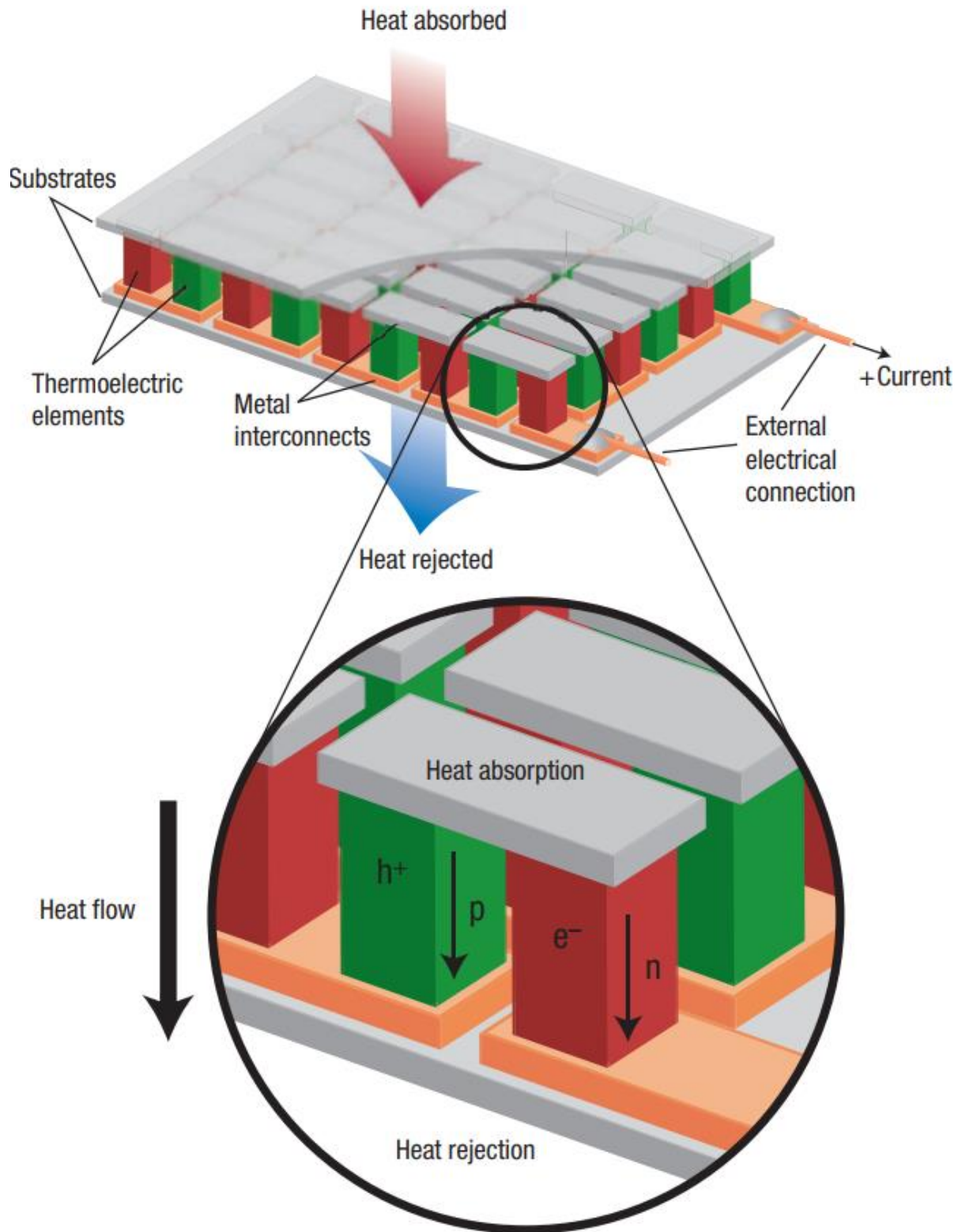
Figure 2.2. The thermoelectric module is showing the direction of charge flow on both cooling and power generation [103].

Hussain et al. [110] developed a 1-D model to simulate the thermoelectric exhaust heat recovery for hybrid vehicles. The model predicted the potential to generate 300 W to 400 W under EPA highway drive cycle conditions for a 2.5L gas-electric hybrid vehicle.

Weng et al. [106] used simulations to explore the influences of the number and the coverage rate on the heat-exchanger of the TEGs. It was found that implementing more thermal electric couples does not necessarily generate more power in total, and the average power per thermal-electric couple decreases rapidly.

Zhang et al. [115] adopted a maximum power point tracker controller into the proposed system as a tool for power conditioning and transfer to the TEG and engine system. They also proposed and implemented a new automotive thermoelectric–photovoltaic (TE–PV) hybrid energy system. Both the TEG and PVG branches can achieve maximum power transfer independently. The experimental results of a 100 W prototype successfully verified the validity of the proposed system. Power improvement as much as 4.8% to 17.9% can be achieved. They mentioned that the proposed system would be very promising for different types of automobiles by scaling up the power ratings proportionally up to 1 kW.

After reviewing the potential for fuel saving, Stobart et al. [104] concluded that the potential for fuel economy efficiency improvement from thermoelectric devices could be up to 4.7%. Thermoelectric generator technologies have advantages such as lightweight, no increase of pumping loss, environmentally friendly material, and no moving parts. However, the thermal efficiency improvement is relatively low, and it requires extensive exhaust surface areas and high investment, with a payback period of 3-6 years for the thermoelectric device with current thermoelectric materials and costs [104].

2.3.4 Electric Turbo-compounding (ETC) System

The electric Turbo-compounding (ETC) system can be used to recover the pressure energy contained in the waste energy. It is based on the Brayton cycle, which is named after George Brayton, which describes the workings of a constant-pressure heat engine. The exhaust

energy can be transferred either to shaft work through the turbine [116] or to electricity through the compound turbine power generation systems [117] [118].

A typical setup of electric turbo compound system in a diesel engine is shown in Figure 2.3 [117]. Algrain [117] used simulation to show that the overall fuel consumption could be reduced by about 5% for a Class-8 on-highway truck engine with an ETC system installed.

Hopmann [119] demonstrated ETC technology could bring an overall fuel saving of 3-5% based on an MY 2000 engine. The system cost is $2000 to $3400. Power-electronics account for half of the total cost. The payback period is 13 to 38 months.

Hountalas et al. [120] used an engine simulation code to examine the effect of two exhaust heat recovery technologies, mechanical and electrical turbo-compounding, on overall engine fuel economy, power output, and pollutant emissions. Mechanical turbo-compounding can offer a maximum fuel consumption reduction of 0.5% to 4.5%, while electrical turbo-compounding can provide a maximum fuel consumption reduction of 3.3% to 6.5% with a highly efficient turbocharger and 1 bar exhaust pressure increase. Also, the reduction of NO_x of mechanical turbo-compounding systems is around 12-17% while that of electrical turbo-compounding systems is 7%.
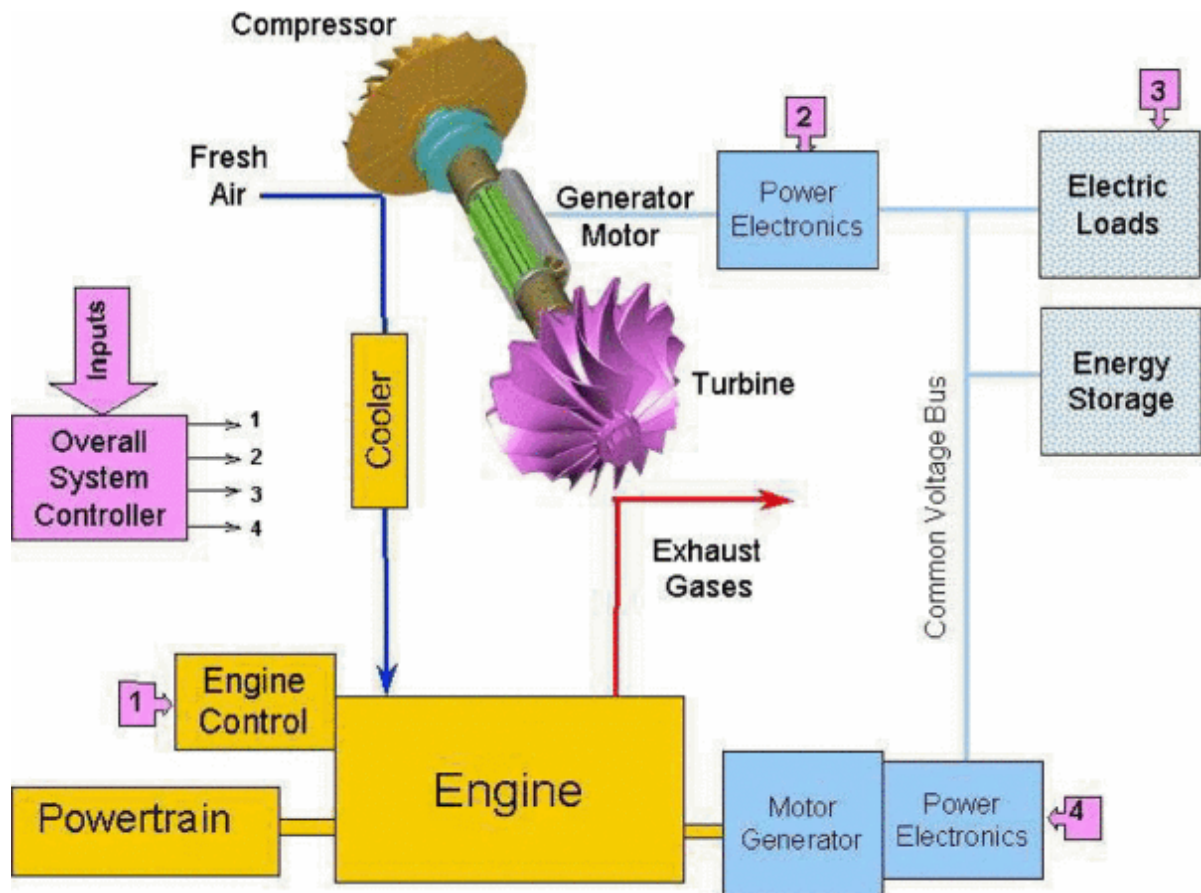
Figure 2.3. An electric turbo compound system for exhaust gas energy recovery in a diesel engine [117].

The electrical turbo-compounding system has a relatively simple structure and low volume, but it is highly dependent on the engine working cycles.

2.3.5 Turbocharger

Turbocharger technology is currently widely used to enable engine downsizing by increasing the specific work, and the pumping work is also reduced through this technology [65], [121]–[124]. This technology uses the gas turbine to reuse the heat and pressure in the expanding exhaust gas to increase engine power by compressing the air that goes to the engine's combustion chambers.

Petitjean et al. [123] used extensive data comparing production turbocharged and non-turbocharged engines/vehicles. It was shown that the turbocharging technology enables gasoline engine downsizing by about 30% and improves torque and acceleration performance

of the vehicle. Also, it improves fuel economy by 8-10% for the engine with same power, and it gives as much as 18% improvement in fuel economy for the vehicle.

Also, by varying the degrees of boost through turbocharger technology, engine families with a much wider range of rated power can be developed from the same basic engine [123].

However, turbocharger technology suffers turbo-lag from the engine system with traditional turbochargers. Variable Geometry Turbocharger (VGT) technology was developed to use small movable vanes to direct the incoming exhaust flow through the turbine blades. The flow of the exhaust gas can be optimized by varying the angle of the vanes at different engine speeds. Andersen et al. [125] concluded that 10% improvement in fuel economy during low and high engine speed and torque could be achieved by using VGT compared to fixed geometry turbochargers.

The electrically assisted turbocharging system was also developed to use electrical machines in a motoring mode to give additional power to the common shaft during low load operation to improve the transient engine performance. The typical diagram of an electrically assisted turbocharger is shown in Figure 2.4 [126]. Terdich et al. [127] showed that the combination of the electric turbocharger assist and variable geometry turbine is a very effective way to recover the transient response of a turbocharged engine whose boost is optimized for pumping losses reduction, and it can achieve fuel economy improvement as high as 4.2%.
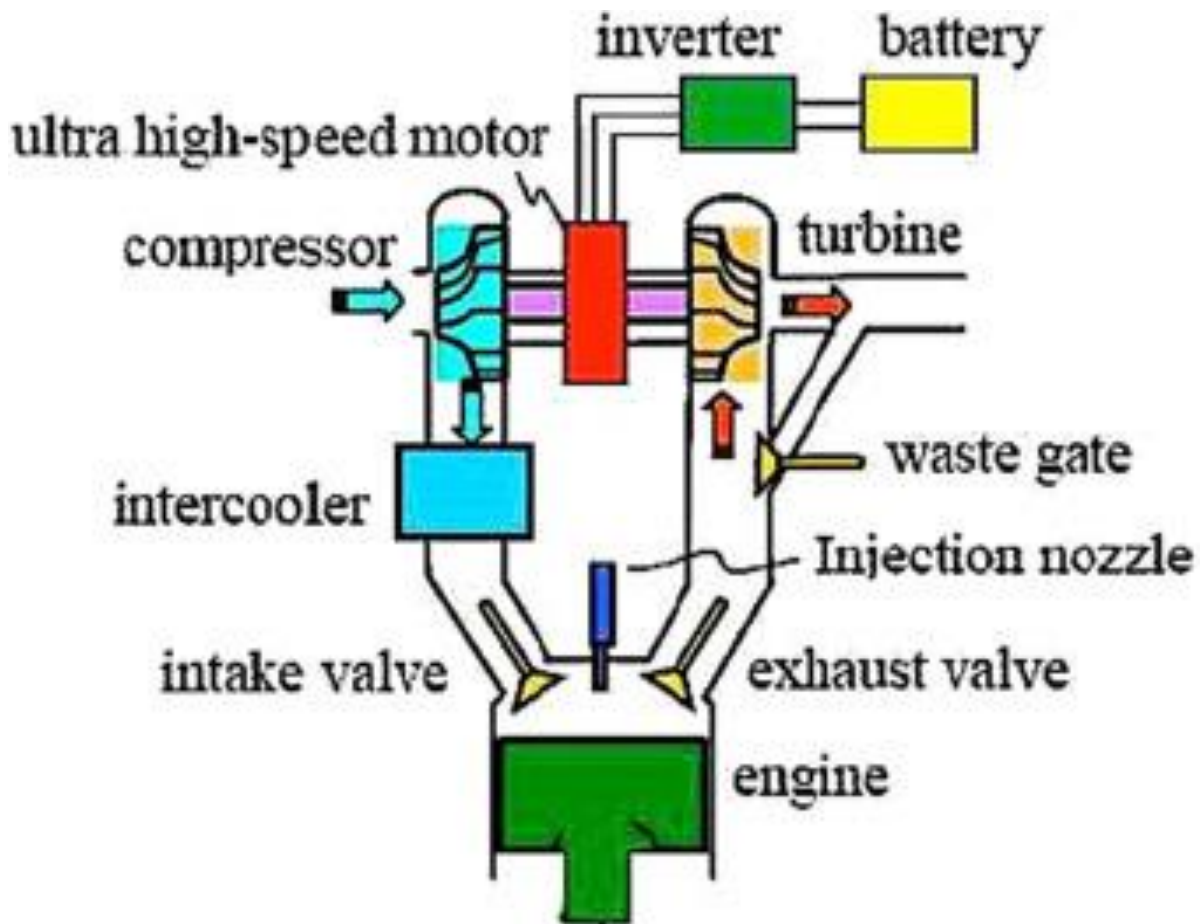
Figure 2.4. Diagram of an Electrically Assisted Turbocharger [126].

2.3.6 Long-stroke engine design

Newer engines that are highly tolerant of EGR dilution are under-square (stroke > bore). The new Toyota 1.2-Liter ESTEC 2ZR-FXE gasoline engine has a stroke to bore ratio of 1.097 [128]. The long-stroke engine design is one of the keys to the high-efficiency engines which achieved >40% engine efficiency [129]. High-speed combustion is an effective way of expanding the EGR limit and intensifying in-cylinder turbulence by increasing the tumble ratio is an effective way of increasing the combustion speed. A long stroke engine design with under-square geometry raises the mean piston speed and, by extension, the in-cylinder turbulence, which scales with mean piston speed [130]. Higher turbulence shortens the duration of the early flame kernel development by transitioning to turbulent combustion sooner, thereby increasing combustion stability, and shortening combustion duration, which extends the EGR dilution limit.

2.3.7 Hybrid Pneumatic Power Systems (HPPS)

A hybrid pneumatic power system (HPPS) was developed to store the flow work and recycle the exhaust gas energy of the ICEs, which could help the ICEs to operate in the maximum efficiency region [131]–[135]. Typically, the HPPS system consists of an ICE, an air compressor, a storage tank, an energy merger tank, and a turbine, as shown in Figure 2.5.

By using the HPPS system, energy can be recovered from a braking phase or a combustion phase by pumping the exhaust gas or the pressurized air into the air tank during the low load of the vehicle. Then the energy stored in the air tank can be used to start the engine, or to provide additional power for the vehicle during the strong transient acceleration, or to use the pressurized air to overcome the turbo-lag problem, mentioned in section 2.3.5 [77].

Huang et al. [131] conducted experimental research on the exhaust gas energy recycling efficiency of HPPS. They found that exhaust-gas energy recycling efficiency could reach approximately 75–81%, and the efficiency of the vehicle equipped with HPPS can achieve approximately 40% under optimal conditions. Exhaust gas energy recycling is highly dependent on the cross-sectional area adjustment.

Higelin et al. [134] used simple thermodynamics cycle modeling to simulate the hybrid pneumatic combustion engine and showed that the global fuel consumption could be reduced by around 15% without any specific optimization under a transient driving cycle.
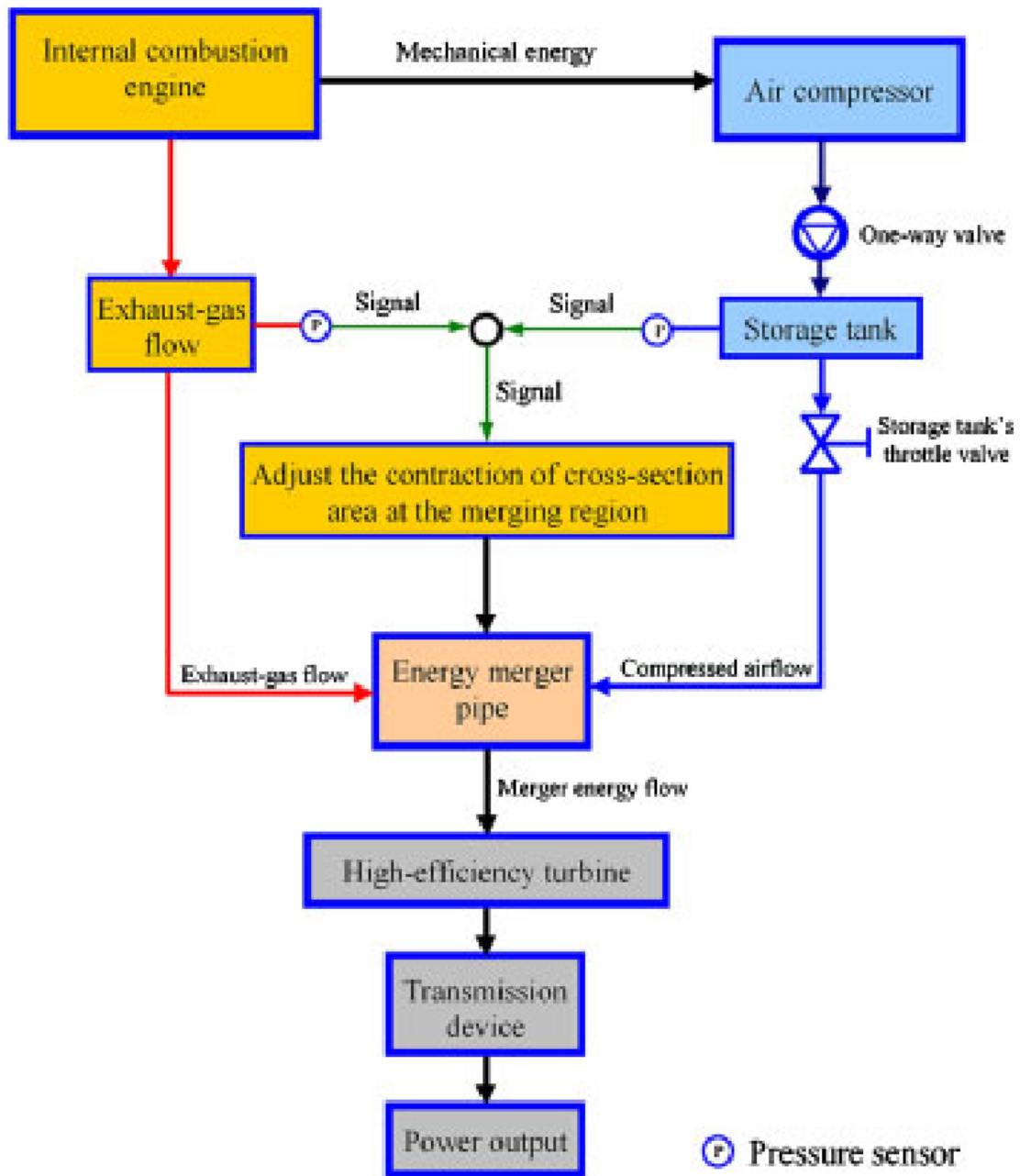
Figure 2.5. The framework of the hybrid pneumatic-power system [131].

2.3.8 Six-stroke Internal Combustion Engine Cycle

A six-stroke engine cycle adds a two-stroke steam cycle after a four-stroke Diesel cycle. The additional power stroke produces more output work without adding additional fuel into the engine so that the fuel efficiency can be improved. This concept was first proposed by Dyer [136]. Then other patents [137], [138] showed more detailed designs for this idea. These

designs utilize the complete exhaust stroke from 540 Crank Angle Degree (CAD) to 720 CAD and use the combustion chamber surfaces as the primary sources of heat to vaporize the water for the steam stroke.

Conklin and Szybist [139] proposed another highly efficient six-stroke ICE cycle with water injection for the in-cylinder exhaust heat recovery. The two additional strokes involve trapping and compression of part of the exhaust from the fourth piston stroke, followed by a water injection event and an expansion event of the steam/exhaust mixture. The schematic of this concept is shown in Figure 2.6. The water injected during the 5th stroke is heated by the engine coolant so that this concept recovers heat from both the engine coolant and exhaust gas. It has been shown from the calculation that the net mean effective pressure of the steam expansion stroke can range from 0.75 to 2.5 bar, which indicates the great potential to increase the engine efficiency.
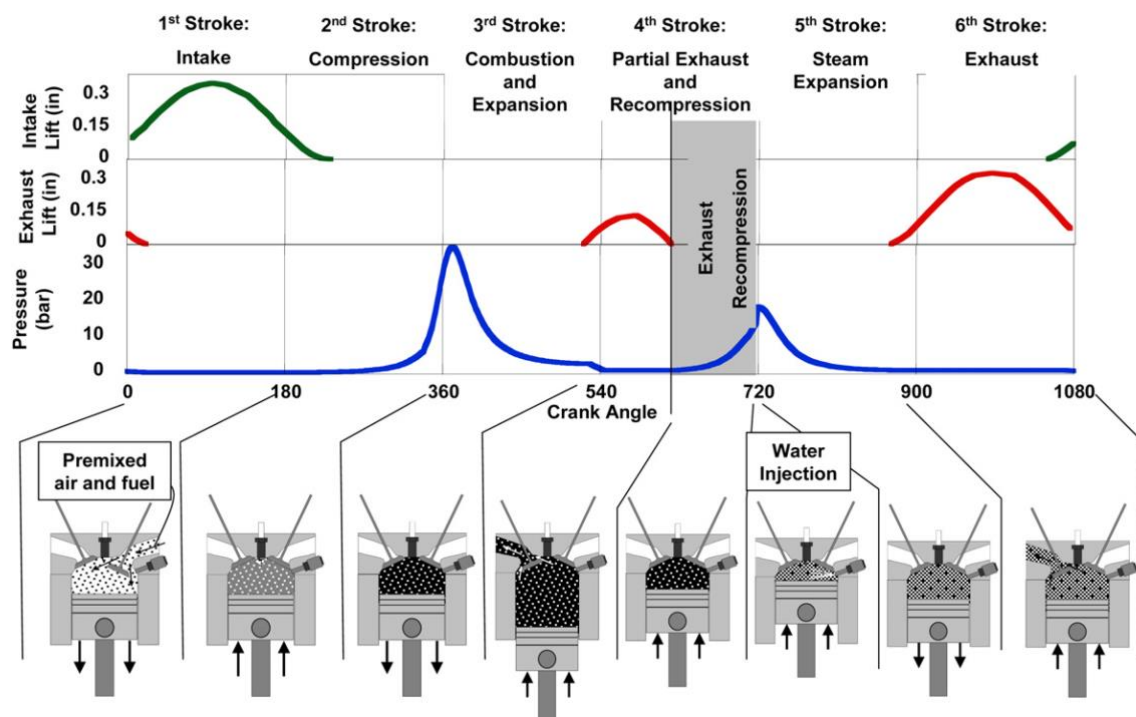
Figure 2.6. Schematic of the six-stroke engine cycle [139].

2.3.9 Non-catalytic Fuel Reformate Generation

Benefits from fuel reforming products attract significant interest from researchers to do investigations on on-board fuel reforming.

In terms of the non-catalytic in-cylinder reforming process in the engine systems, Alger and Mangold [140] from Southwest Research Institute (SwRI) proposed a Dedicated EGR (D-EGR) concept in which one cylinder is converted to operate under fuel-rich conditions to produce reformate, and reformate is exhausted to the intake manifold and consumed in spark-ignited (SI) combustion, as shown in Figure 2.7. Their SwRI D-EGR demonstrator shows an improved engine efficiency and reduced fuel consumption of at least 10% across the performance map [141]–[146].
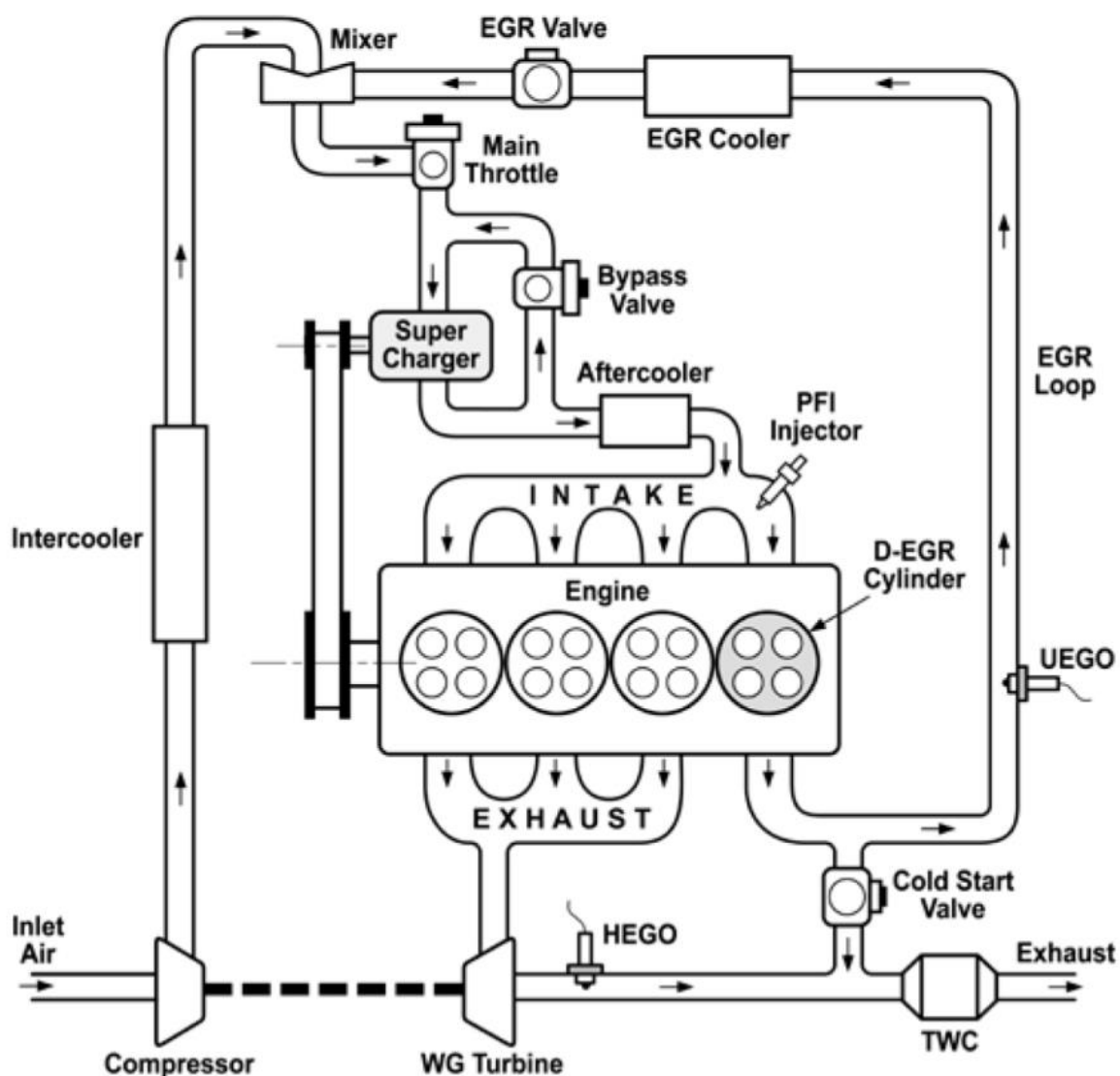
Figure 2.7. Schematic of Dedicated EGR Concept from SWRI [140].

Another way to accomplish in-cylinder fuel reforming is to inject fuel during Negative valve overlap (NVO). Negative valve overlap, which is a common way of controlling HCCI combustion phasing, incorporates early exhaust valve closing (EVC) and late intake valve opening (IVO) to retain internal residual gases [147], [148]. NVO provides thermal and dilution advantages compared to external EGR strategies. Additionally, because the residuals are recompressed (reheated), NVO can enable reaction or reformation of fuel during the NVO period [149]. The effects of reformed gases include charge heating, dilution (reduced oxygen concentrations), increased heat capacity, changed chemical reactivity, and increased stratification. Reactions and heat release accompanying NVO fuel injection can change the temperature and composition of the charge before the main combustion, which can be used to control ignition, rate of pressure rise, peak pressure, combustion noise, misfire, and emissions [150]. The amount of fuel reforming can be controlled by injection timing and the ratio of split fuel injection [150]. Szybist et al. [151] investigated the non-catalytic in-cylinder reforming process during the NVO using a unique 6-stroke engine cycle and a conventional 4-stroke cycle and found that substantial concentrations of H_2, CO, methane, and other short-chain hydrocarbon species are produced during the reforming process under low-O_2 conditions. From the energy analysis, it was found that increased NVO-period global equivalence ratio, either from lower NVO period oxygen concentrations or higher fueling rates, in general, led to a higher fraction of net recovered fuel energy and work as heat losses were minimized [152]. Kalaskar et al. [153] investigated the chemistry of a range of fuels injected during NVO under low oxygen conditions. Fuels investigated included iso-octane, isobutanol, ethanol, and methanol. It has been found that products from NVO chemistry were highly dependent on fuel type and injection timing, with isooctane producing less than 1.5% hydrogen and methanol producing more than 8%. They also found that the kinetic mechanisms investigated are unable to accurately predict the magnitude and trends of major species observed in their experiment.

These results indicate that an O_2 deficient operation approach may be a pathway toward a chemical reforming process that is not thermodynamically expensive, and may even enable thermodynamic recuperation.

2.3.10 Catalytic Fuel Reformate Generation

Catalytic fuel reforming technology is used for on-board clean hydrogen generation in fuel cells. Edwards et al. [154] demonstrated that 24 individual full-size prototype methanol fuel-processors could be combined to supply hydrogen to generate 20 kW of electrical power in a hybrid (battery + fuel cell) drivetrain. However, the concentration of CO needs to be reduced below 20 ppm to avoid poisoning the fuel cell anodes.

Tsolakis et al. [155] tested the feasibility of producing hydrogen "on-board" by using a laboratory reforming mini reactor (shown in Figure 2.8) in the exhaust system of compression ignition engine fueled by conventional diesel and biodiesel mixture. It has been shown that the partial replacement of the hydrocarbon fuel by hydrogen combined with EGR resulted in simultaneous reductions of smoke and NO_x without significant changes to engine efficiency. Also, the reformer contained up to 15% hydrogen produced by the mini-catalytic reactor.
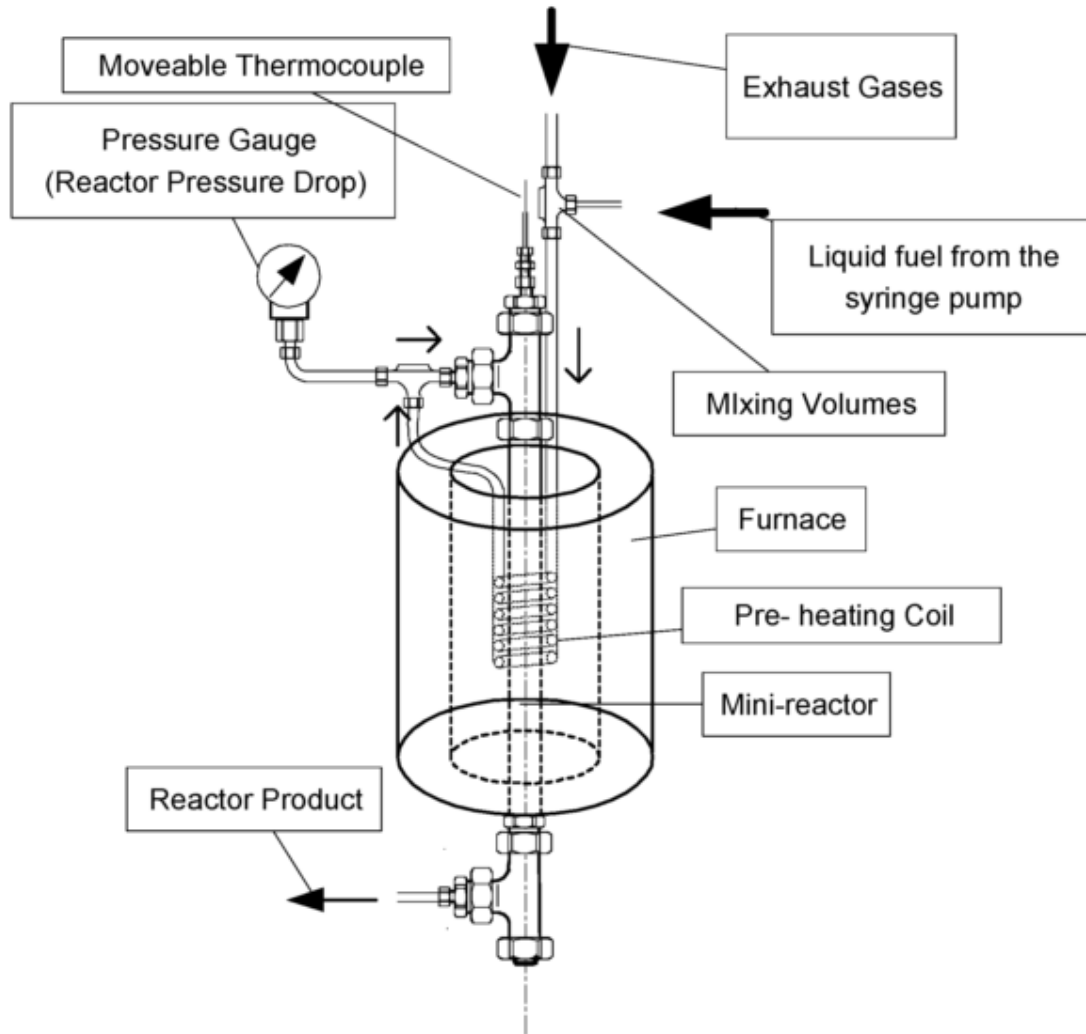
Figure 2.8. Schematic of the liquid fuel reforming system from University of Birmingham [155].

Regarding catalytic fuel reforming, Ashida et al. [156] proposed an on-board fuel reforming system by adding a steam reforming catalyst and a reformer injector to the EGR supply line, as shown in Figure 2.9. They showed that hydrogen-containing reformate produced on-board is capable of expanding the EGR limit to the same extent as the addition of hydrogen alone, which is around 36%. However, the aged catalyst generated only half of the hydrogen as compared to a fresh catalyst.
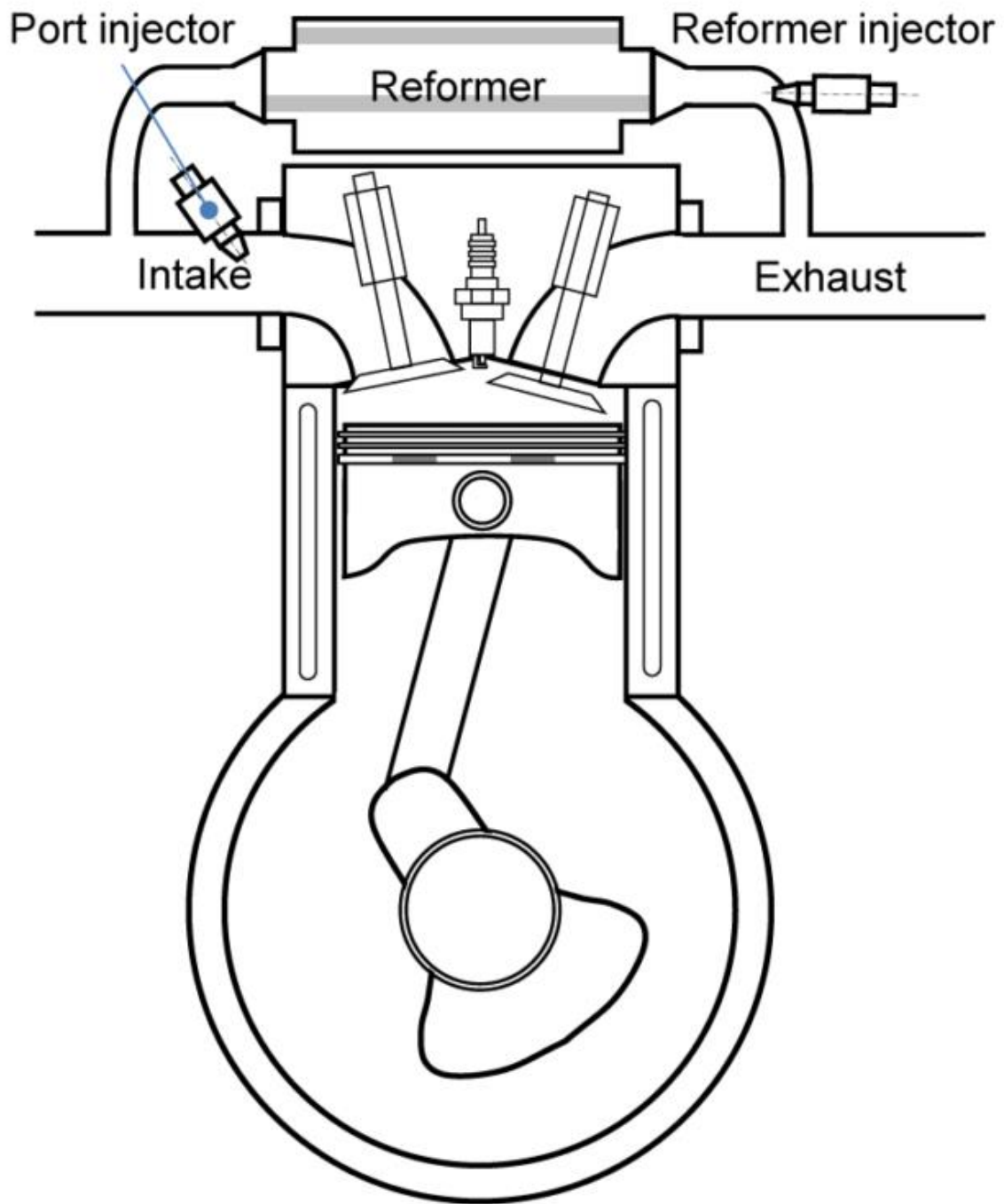
Figure 2.9. On-board steam reformer integrated engine system from Nissa Motor. [156].

Kirwan et al. [157], [158] demonstrated that gasoline combustion was able to preheat the catalytic fuel reforming system rapidly and the preheat period of 5-10 seconds with pre-vaporized gasoline enabled the production of good quality reformate for fast engine starting. And the HC mass emissions from reformate fueled cold starts in a single-cylinder engine was up to 75% lower than with gasoline fueling.

Fowler et al. [159] demonstrated an integrated engine-reformer system suitable for vehicle integration with a compression ratio of 12:1 utilizing low-temperature reforming of E85 by using 119 g of Cu/Pd/C pellet catalysts and 105 g of copper-plated nickel sponge catalyst. They also showed that use of 25% reformate in the fuel enabled stable engine operation with extreme valve overlap and delivered efficiency improvement of about 10% over E85.

Hwang et al. [160] demonstrated a thermally integrated reforming reactor (shown in Figure 2.10) with a high conversion efficiency of fuel for diesel engines. This system produced 12% peak hydrogen concentration, but the overall engine efficiency was decreased.
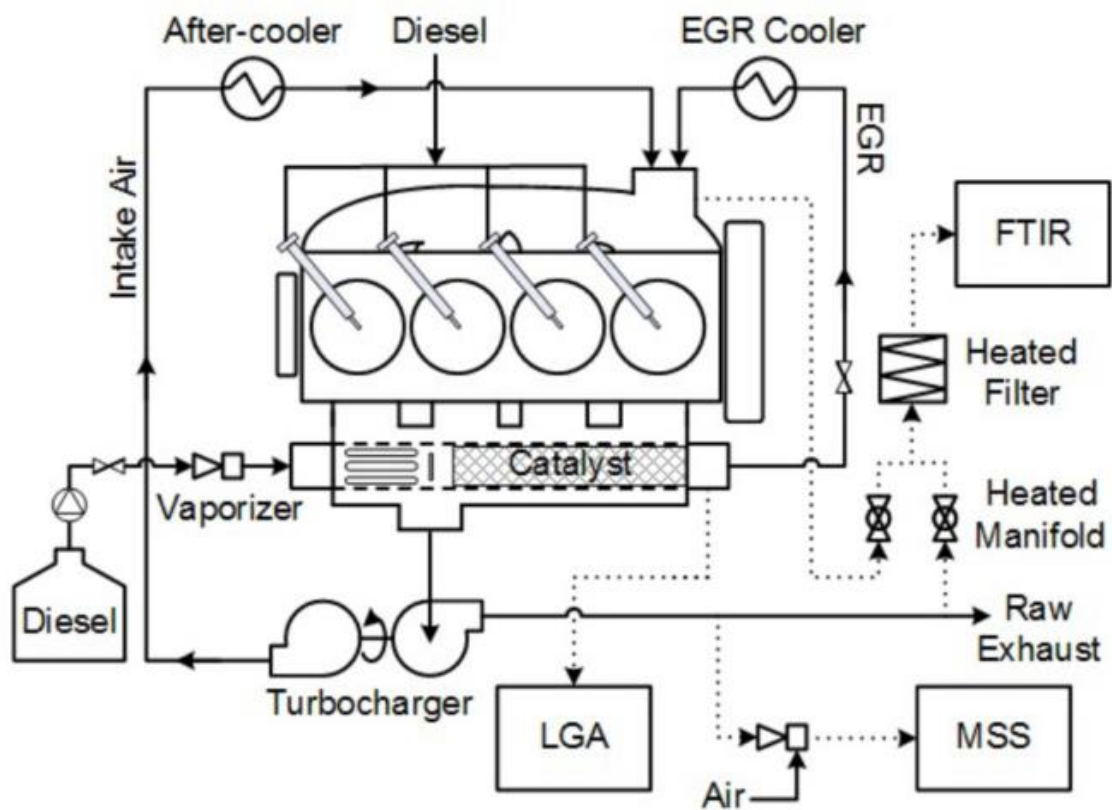
Figure 2.10. A thermally integrated reforming reactor using exhaust gas recirculation mixed with vaporized diesel fuel as reactants from University of Minnesota [160].

Fennell et al. [161], [162] demonstrated a prototype of exhaust gas fuel reformer integrated with a modern, turbocharged, 4-cylinder gasoline direct injection engine. The reformer is positioned in the exhaust stream after TWC. The schematic of this system is shown in Figure 2.11. This method reduces NO_x emissions by up to 91% and improves engine fuel

consumption by up to 8%. The presence of hydrogen and exhaust gas diluents in the combustion charge also reduces particle formation for lower total particulate matter emissions (up to 78% and 84% for number and mass, respectively).
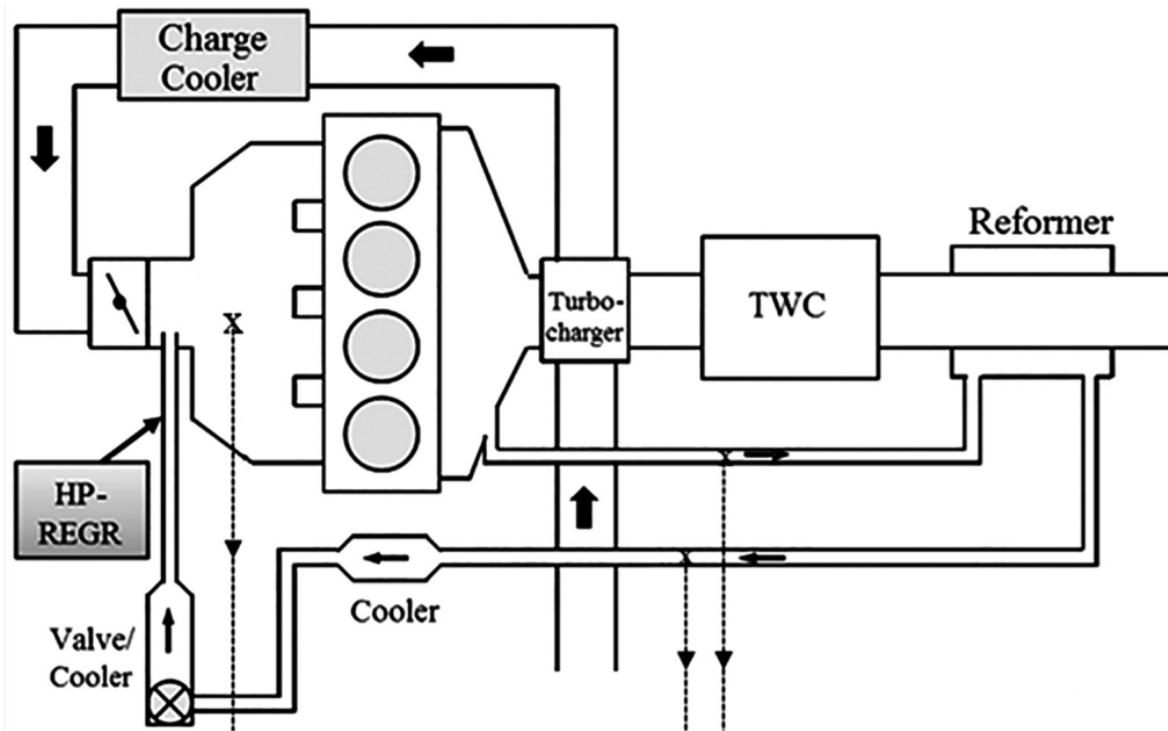
Figure 2.11. Schematic of a prototype of exhaust gas fuel reformer integrated with a modern, turbocharged, 4-cylinder gasoline direct injection engine from University of Birmingham [161].

Gukelberger et al. [163] demonstrated the water gas shift catalyst's capability of producing significant quantities of H2 integrated with DEGR system. The setup of the system is shown in Figure 2.12. However, the formulation was not stable in the exhaust operating environment, leading to an activity loss over a period of approximately 12 hours.
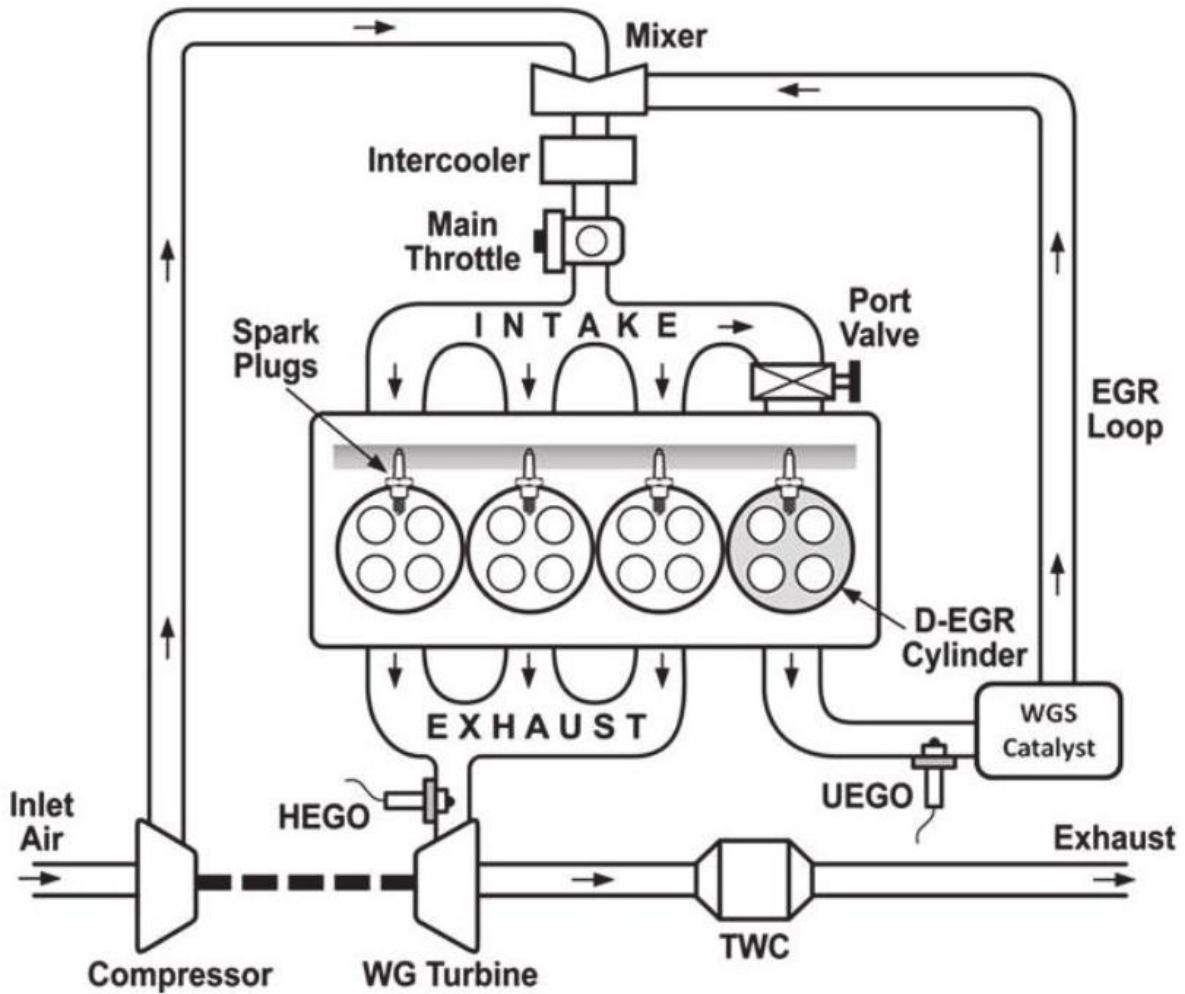
Figure 2.12. Schematic of Water-Gas-Shift Catalyst Reforming for a D-EGR Engine [163].

The primary reforming reactions for a given hydrocarbon fuel include partial oxidation (POx), steam reforming (SR), dry reforming, and corresponding water gas shift (WGS) reactions [162]. Partial oxidation is exothermic, while steam reforming is endothermic. Steam reforming can take advantage of the exhaust heat, which is beneficial for thermochemical recuperation (TCR). Dry reforming is significantly endothermic. POx produces heat when O_2 is available and drives further steam reforming when O_2 is not accessible. The heat of reaction of WGS is minimal, but WGS leads to a larger H_2/CO ratio.

Chapter 3. Fuel Effects on EGR Dilution Limit and Engine Efficiency

3.1 Introduction

Engine technology is evolving at a rapid pace to meet vehicle fuel economy and CO_2 emission targets worldwide. External cooled EGR is an attractive technology to consider because it offers known thermodynamic benefits while maintaining compatibility with conventional 3-way catalysts for emissions control.

The amount of EGR dilution is limited due to combustion instability issue. As EGR dilution increases, cycle-to-cycle variability increases, eventually leading to lower efficiency as reported by Alger et al. [26] and Stone et al. [66]. While there are some contributing factors to the instability, one major one is the large decrease in flame speed that occurs with EGR, as reported by Middleton et al. [164] and by Szybist and Splitter [50].

In this study, the EGR dilution tolerance is investigated in a multi-cylinder engine for two pure components: iso-octane, which has a relatively slow flame speed, and ethanol, which has a fast flame speed [165]–[167]. Additionally, Tier II certification gasoline is also included in the study. The comparisons are conducted at an early combustion phasing and a late combustion phasing condition to understand how the combustion process and cyclic stability changes with combustion phasing and with fuel type.

3.2 Methodology

The engine used in this study is a 2.0 L GM Ecotec LNF engine equipped with the production side-mounted DI fueling system. Engine geometry details are presented in Table 3.1. The

engine is operated in the stock configuration, with the combustion chamber geometry and camshaft profiles unchanged.

Table 3.1. Engine geometry.

Bore x Stroke [mm]	86 x 86
Conrod length [mm]	145.5
Compression ratio [-]	9.2:1
Fuel injection system	Direct injection, side-mounted

The engine is operated using a laboratory fueling system rather than the stock configuration. The fueling system uses a pneumatically-actuated positive displacement pump in conjunction with an electronic pressure regulator to provide fuel rail pressure. A constant fuel rail pressure of 100 bar is used throughout this study. A conditioning system is used to control the humidity of the intake combustion air to a dewpoint of 15°C.

The engine is equipped with an external cooled EGR loop with the flow rate controlled by an electromechanical valve. Cooled EGR mixes with fresh air upstream of an air heater, followed by the intake plenum and then the intake manifold. The EGR used in this study is not treated with an exhaust catalyst before being recirculated to the intake. This arrangement allows the intake manifold temperature to be held at a constant temperature of 50°C regardless of the EGR level. EGR is measured by a non-intrusive method that utilizes pressure-compensated wideband oxygen sensors in both the intake and exhaust.

A DRIVVEN engine controller with the Combustion Analysis Toolkit (DCAT) package is used to control the engine, to acquire crank-angle resolved data, and analyze combustion performance. Cylinder pressure data, heat release, and combustion analysis are collected for 300 fired cycles for each condition. Cylinder pressure in each cylinder is measured using a flush-mounted piezoelectric pressure transducer from Kistler (6125C). Fuel injection timing occurs during the intake stroke and is held constant at 280 CAD before top dead center firing (bTDCf). Spark timing is adjusted as-needed to achieve the desired combustion phasing and is trimmed for individual cylinders to match phasing. Spark dwell is held constant at 3.8 ms with the stock ignition coil to maintain constant ignition energy.

Engine fuel flow is measured with a Coriolis-based fuel flow meter, and engine coolant temperature is maintained at 90°C. The combustion emissions are monitored using a standard array of analyzers. NOx is measured using a heated chemiluminescence analyzer, CO and CO_2 are measured using infrared analyzers, oxygen is measured using a paramagnetic analyzer, and unburned hydrocarbon emissions (HC) are measured with a heated flame ionization detector.

Three fuels are used in this investigation to illuminate the fuel-specific differences on EGR tolerance. Two of these are pure-components: iso-octane and ethanol. The iso-octane is primary reference fuel (PRF) grade obtained from Haltermann Solutions and has a purity of 99.89%. The ethanol is non-denatured (200 proof) and is procured from Decon Labs. The gasoline is a low-sulfur Tier II certification gasoline, referred to as "gasoline" throughout this manuscript, and is obtained from Haltermann under the product name EEE-Lube Cert Gasoline.   The fuel properties are given in Table 3.2.

Table 3.2. Fuel Property

	ASTM Method	Isooctane	Ethanol	Gasoline
RON	D2699	100	109	97.0
MON	D2700	100	90	88.7
S (RON-MON)	N/A	0	19	8.3
C (wt%)	E191	84.21	52.17	86.32
H (wt%)	E191	15.79	13.04	13.28
O (wt%)	D4815	0	34.78	<0.01
HoV (kJ/kg)	N/A	308	840	305

External EGR sweeps are performed at engine load of 4 bar BMEP at an engine speed of 2000 rpm and with CA50 combustion phasing of 8 and 16 CAD aTDCf. EGR sweeps are conducted at increments of 5% EGR to the intake system. The EGR dilution is limited by the coefficient of variation (COV) of indicated mean effective pressure (IMEP) of 5%.

3.3 Results

3.3.1 Efficiency and Emission

Gross, net and brake thermal efficiency are shown as functions of EGR in Figure 3.1 for both advanced and retarded combustion phasing. Results in Figure 3.1 are for ethanol, though the trends are representative for all fuels. As EGR is initially increased, all efficiency metrics increase due to a combination of reduced pumping work, heat transfer, and increased γ, as discussed in the introduction. The efficiency decrease that occurs at the highest EGR levels is due to combustion instability and increased combustion duration. The efficiency of the condition with a late combustion phasing is lower because of the under-utilized engine expansion.

The trends observed for the gross indicated efficiency are not exactly mirrored in the net indicated efficiency and brake efficiency. Peak gross indicated efficiency is achieved at 20% and 15% EGR for the advanced and retarded combustion phasing conditions respectively. However, the net indicated efficiency and the brake efficiency both increase after the net indicated efficiency has been achieved. This is because there are competing effects of gross work, which begins to decline, and a continued reduction in pumping work with additional EGR.
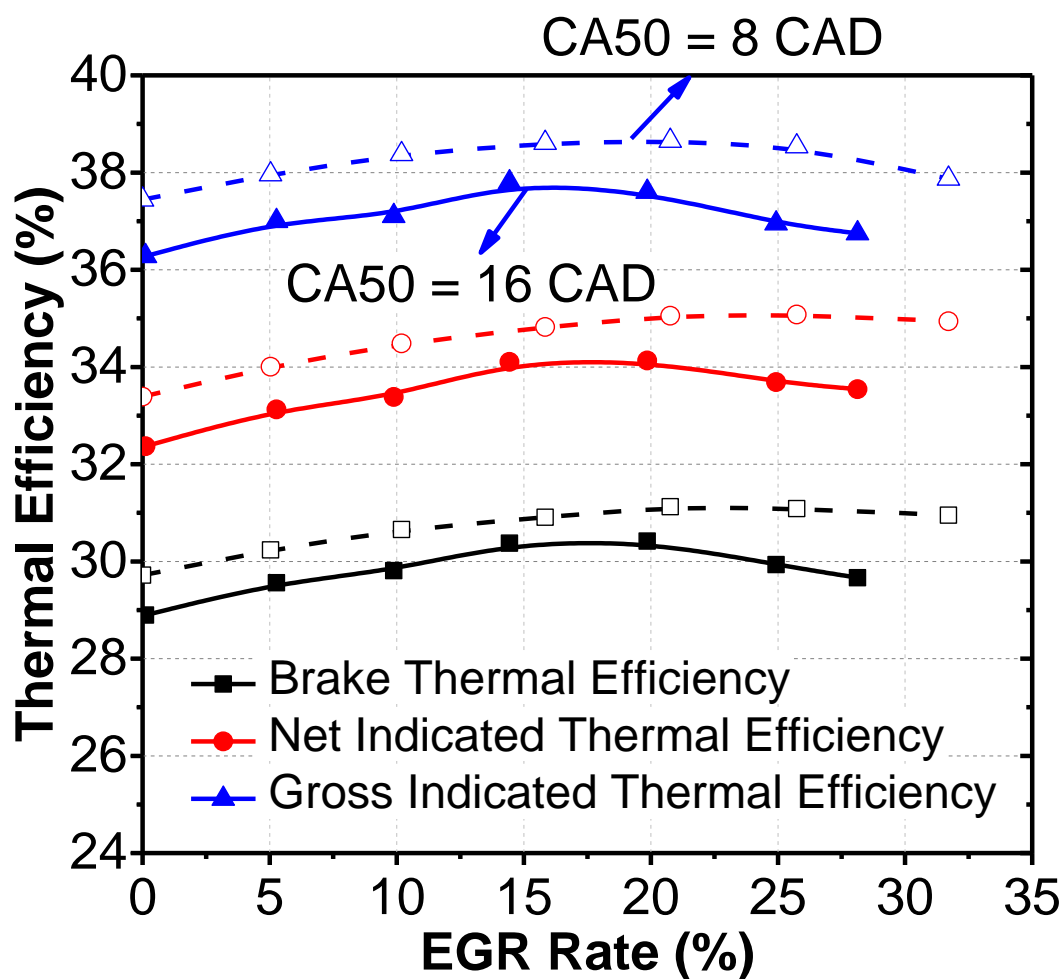
Figure 3.1. Thermal engine efficiency of ethanol as a function of EGR level and CA50 combustion phasing.

NO_x emissions are shown for ethanol in Figure 3.2, and the results are representative of the trends for all fuels. NO_x emissions decrease with the increase of EGR rate and the retarded combustion phasing, as expected because both higher EGR rate and retarded combustion phasing lead to lower combustion temperature. However, increasing the EGR from 0% to 25% reduces the NO_x emissions by a factor of about 10, which is a much larger effect than the effect of retarded combustion phasing.
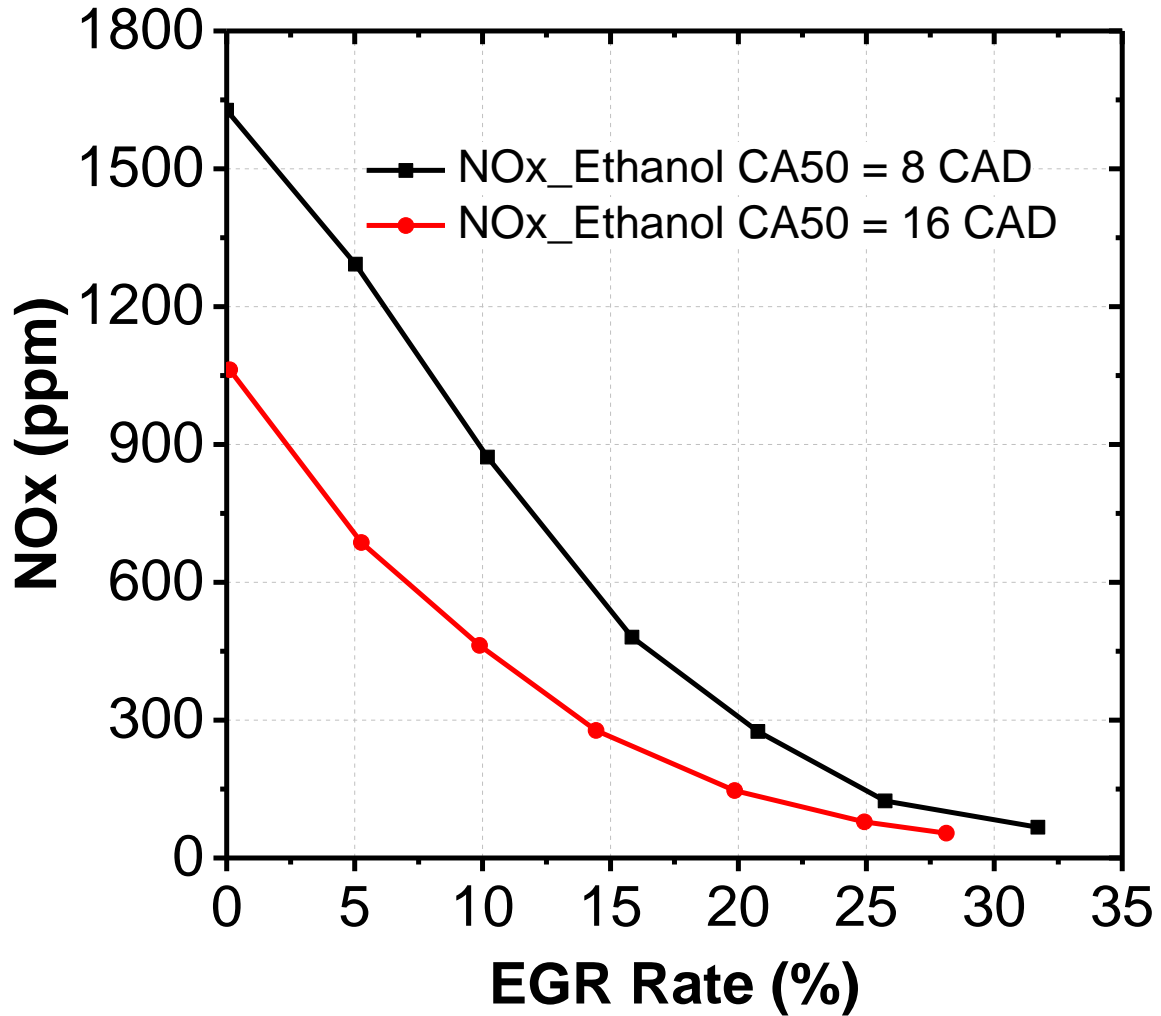
Figure 3.2. NO$_x$ emission of ethanol as a function of EGR level and CA50 combustion phasing.

3.3.2 Combustion Stability

The level of EGR that can be used is limited by the combustion stability. Combustion stability can be indicated by COV of IMEP. Figure 3.3 shows that both higher EGR and retarded phasing lead to higher COV of IMEP. For the early combustion phasing cases, COV of IMEP is nearly constant at EGR rates below 20%, and then dramatically increases to the dilution limit for early combustion phasing cases. For the late combustion phasing cases, COV of IMEP increases gradually with the increase of EGR rate. Fuel specific differences are also observed in Figure 3.3, with ethanol producing the lowest COV of IMEP for a given EGR rate and combustion phasing. This is the expected trend given the high flame speed of ethanol, and it is in agreement with previous literature reports [50].
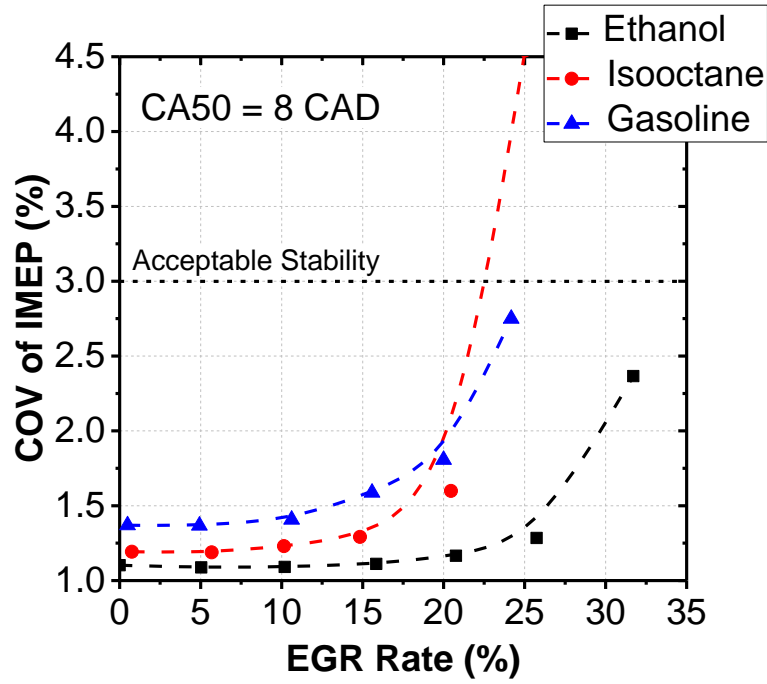
(a)
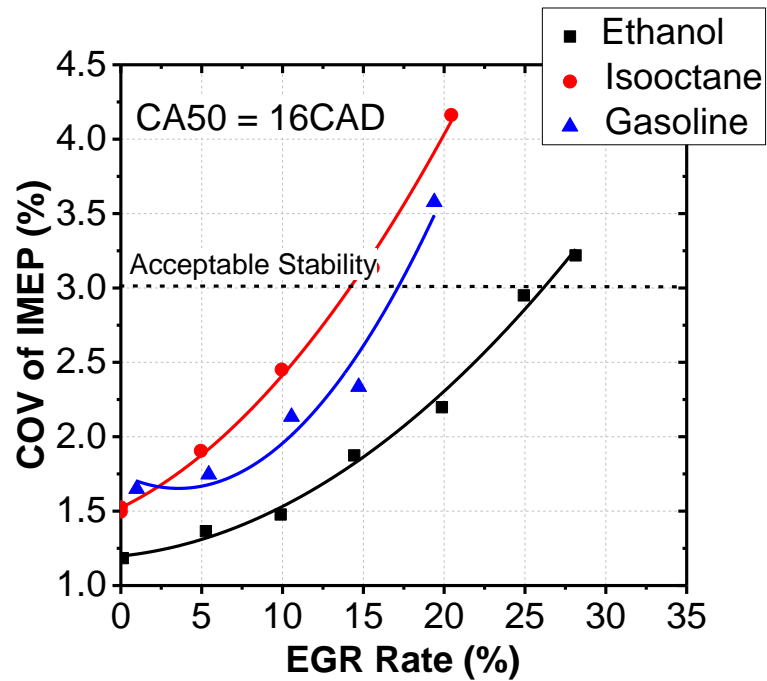
(b)

Figure 3.3. COV of IMEP as a function of EGR level of ethanol, isooctane, and gasoline while CA50 combustion phasing equals to 8 CAD (a) and 16 CAD (b).

As EGR increases, it is necessary to advance spark timing to maintain combustion phasing control as shown in Figure 3.4. Spark timing becomes less effective as a control method when it is highly advanced, as is necessary with high EGR rates. Once spark timing is more than 30 CAD bTDC, the amount of spark advance per percent EGR is much higher, as indicated by the non-linearity between spark timing and EGR in Figure 3.4. When spark timing is more advanced, the in-cylinder temperature is lower, which reduces flame speed. Also, the turbulence length scale is primarily a function of cylinder volume, with the length scale decreasing as cylinder volume decreases. The larger in-cylinder turbulence length scale when spark timing is more advanced leads to slower flame propagation. Also, the larger turbulence intensity at that moment is not beneficial for early flame kernel initiation and growth [1]. And if ignition timing is too advanced, it can lead to misfire [168]. Conversely, when spark timing occurs closer to TDC, spark timing is a much more effective control. Thus, there is a limited spark timing window available to compensate for the longer combustion duration that occurs as a result of high EGR rates.
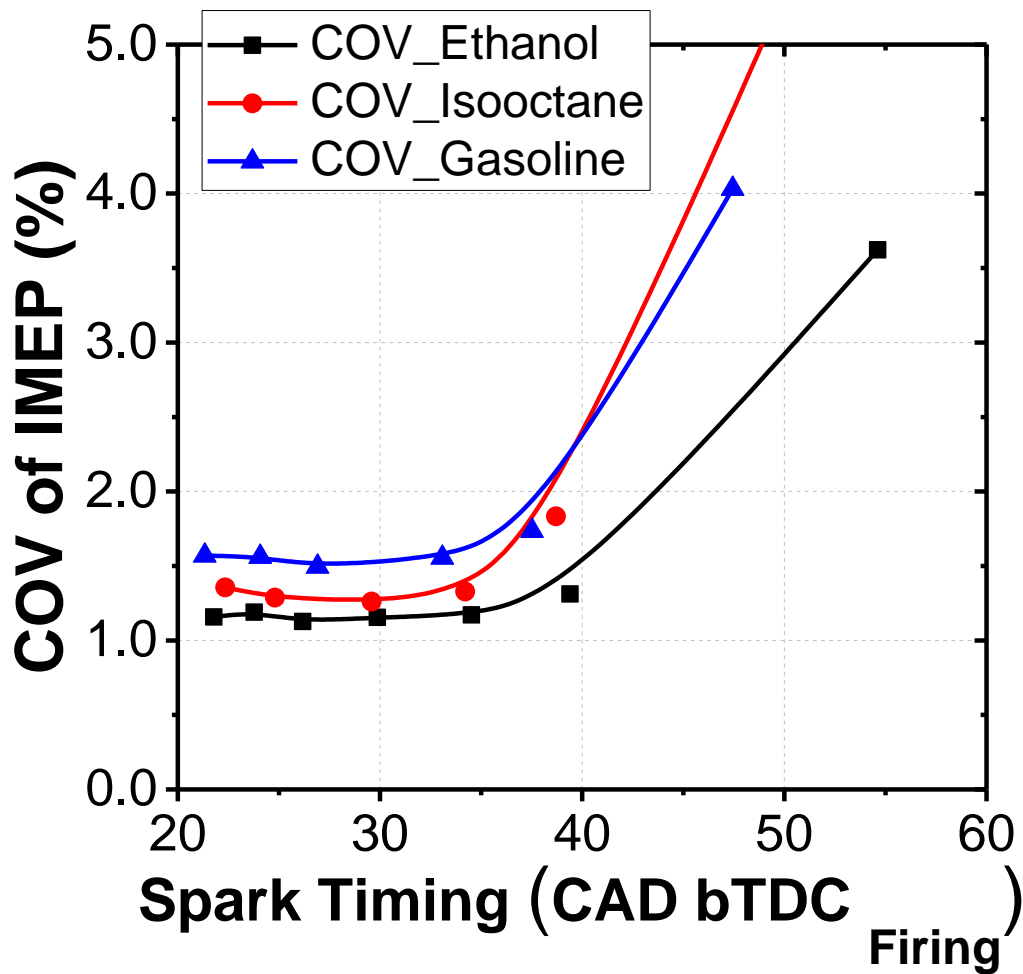
Figure 3.4. Spark timing as a function of EGR level and CA50 combustion phasing of ethanol, isooctane, and gasoline.

3.3.3 Combustion Duration

The COV of IMEP, discussed in Figure 3.3, is an indication of the cycle-to-cycle variability, although it fails to provide insight into where and how the combustion instabilities occur from a phenomenological standpoint. To provide additional insight into the instability, Figure 3.5 breaks the combustion event into three separate phases and illustrates the differences between early and late combustion phasing cases. Phase 1 is the spark timing to CA5 combustion phasing, which is indicative of the early flame kernel growth. Phase 2 is the CA5 to CA50 combustion duration, which is indicative of the turbulent flame propagation. Phase 3 is the CA50 to CA75 combustion duration, which is indicative of the late stages of

combustion after the turbulent flame in the near-wall area. Figure 3.5 shows that the duration for all phases of combustion increases with increasing EGR, as does the variability of the combustion events, indicated by the height of the box. The box plot and the distribution curve shown in Figure 3.5 are a representation of key values from summary statistics of combustion duration of 300 cycles for each condition. The boxes are determined by the 25th and 75th percentiles. The whiskers are determined by the 10th and 90th percentiles. In phase 1, the spark timing to CA5 duration is the longest phase of combustion, and it has the most variability and the strongest response to EGR. It is notable that both Phase 2 and Phase 3 respond linearly to EGR rate while Phase 1 shows a nonlinear trend. The cycle to cycle variation of combustion duration increases rapidly with the increase of EGR rate. Also, combustion phasing has little effect on the combustion duration of Phase 1 and Phase 3 for a given EGR level. However, as In-cylinder turbulence dominates phase 2, retarded combustion phasing hurts the combustion duration of Phase 2 and higher cycle to cycle variability of Phase 2.
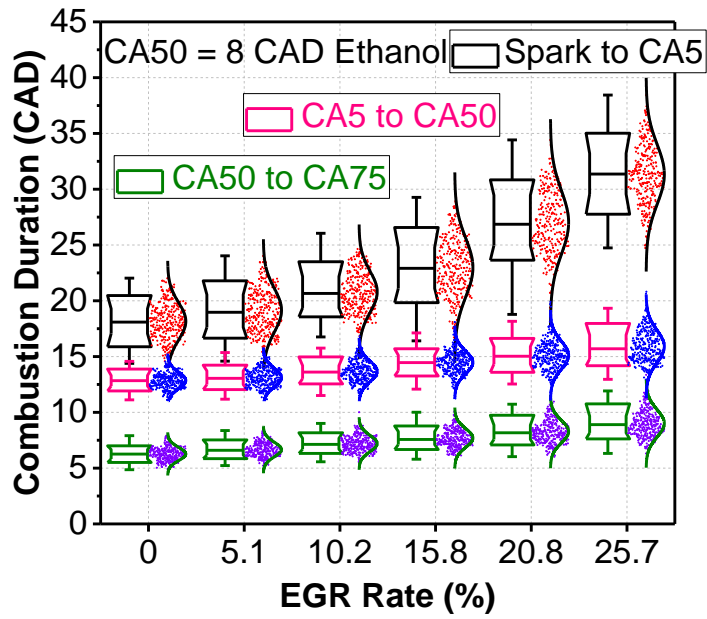
(a)
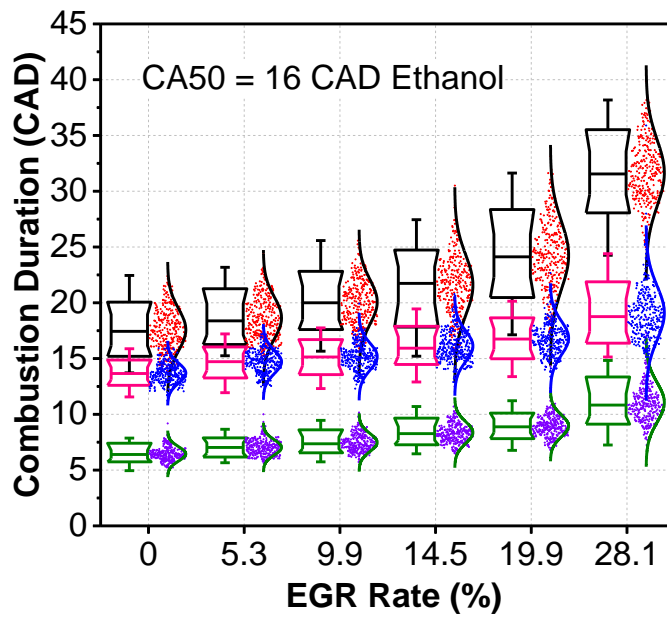
(b)

Figure 3.5. Box plot distributions of the spark-to-CA5, CA5-CA50, and CA50-CA75 distributions of ethanol for the entire 300 cycle averages as a function of EGR level while CA50 combustion phasing equals to 8 CAD and 16 CAD.

The difference between the combustion duration of Phase 1 and Phase 2 for early combustion phasing cases is larger than that of retarded combustion phasing cases. Combustion duration of Phase 2 is larger than that of Phase 1 for some cycles for retarded combustion phasing cases. Also, cycle to cycle variability of combustion duration of Phase 3 is much larger for retarded combustion phasing cases when EGR rate is above 20%, while cycle to cycle variability of the duration of Phase 3 is similar for early combustion phasing and retarded combustion phasing cases when EGR rate is below 20%.

Figure 3.5 illustrates the nature of the combustion instability for ethanol. While this is qualitatively similar for all fuels, Figure 3.6 and Figure 3.7 show the fuel-specific differences. As was previously highlighted in Figure 3.3, ethanol is the most dilution tolerant fuel, and coinciding with this, it also has the shortest duration of all fuels, regardless of EGR level and the portion of combustion. Interestingly, Figure 3.6 and Figure 3.7 show that the combustion stability limit occurs at approximately the same combustion duration for all fuels. This suggests that the combustion duration is responsible for the combustion instability, and the fuel type can affect the combustion duration, thereby influencing combustion stability. Also, critical combustion duration is affected by CA50 combustion phasing. For early combustion phasing cases, EGR rate mainly affects spark to CA5 while EGR largely affects both spark to CA5 and CA50 to CA90 for late phasing cases. The fuel type affects the combustion duration mainly during spark to CA5 period. Shorter spark to the CA5 duration for the late phasing can be attributed to the in-cylinder conditions that are more conducive to ignition. Namely, there is a higher in-cylinder temperature at late phasing, and the turbulence length scale is also smaller since in-cylinder turbulence is primarily a function of crank angle. Ozdor et al. [67] explain that the turbulent flame propagation starts when the flame kernel interacts with multiple turbulent eddies simultaneously, and a small turbulence lengths scale helps to transition into the turbulent flame propagation stage with a smaller flame kernel.
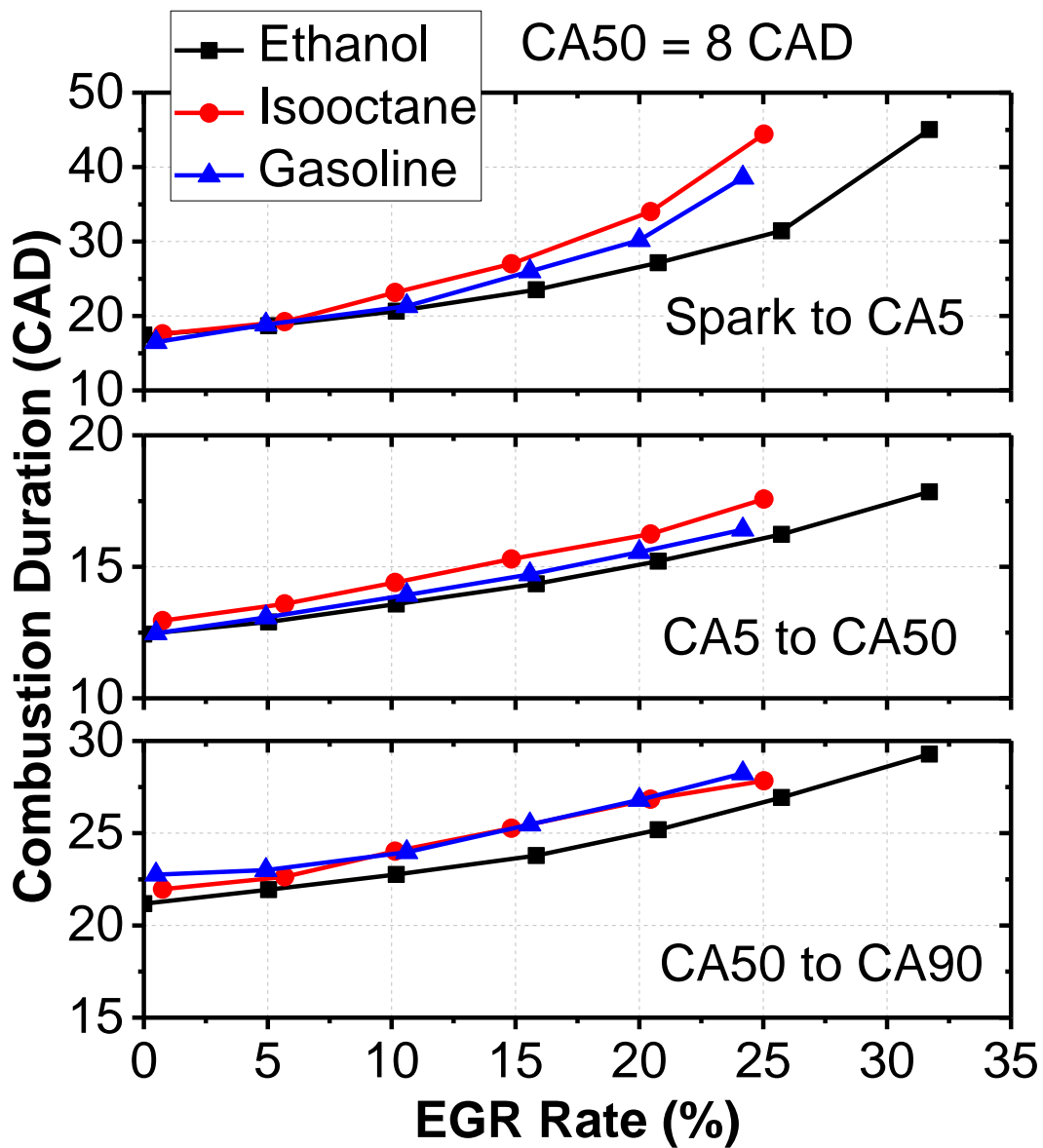
Figure 3.6. Combustion duration as a function of EGR level of ethanol, isooctane, and gasoline while CA50 combustion phasing equals to 8 CAD.
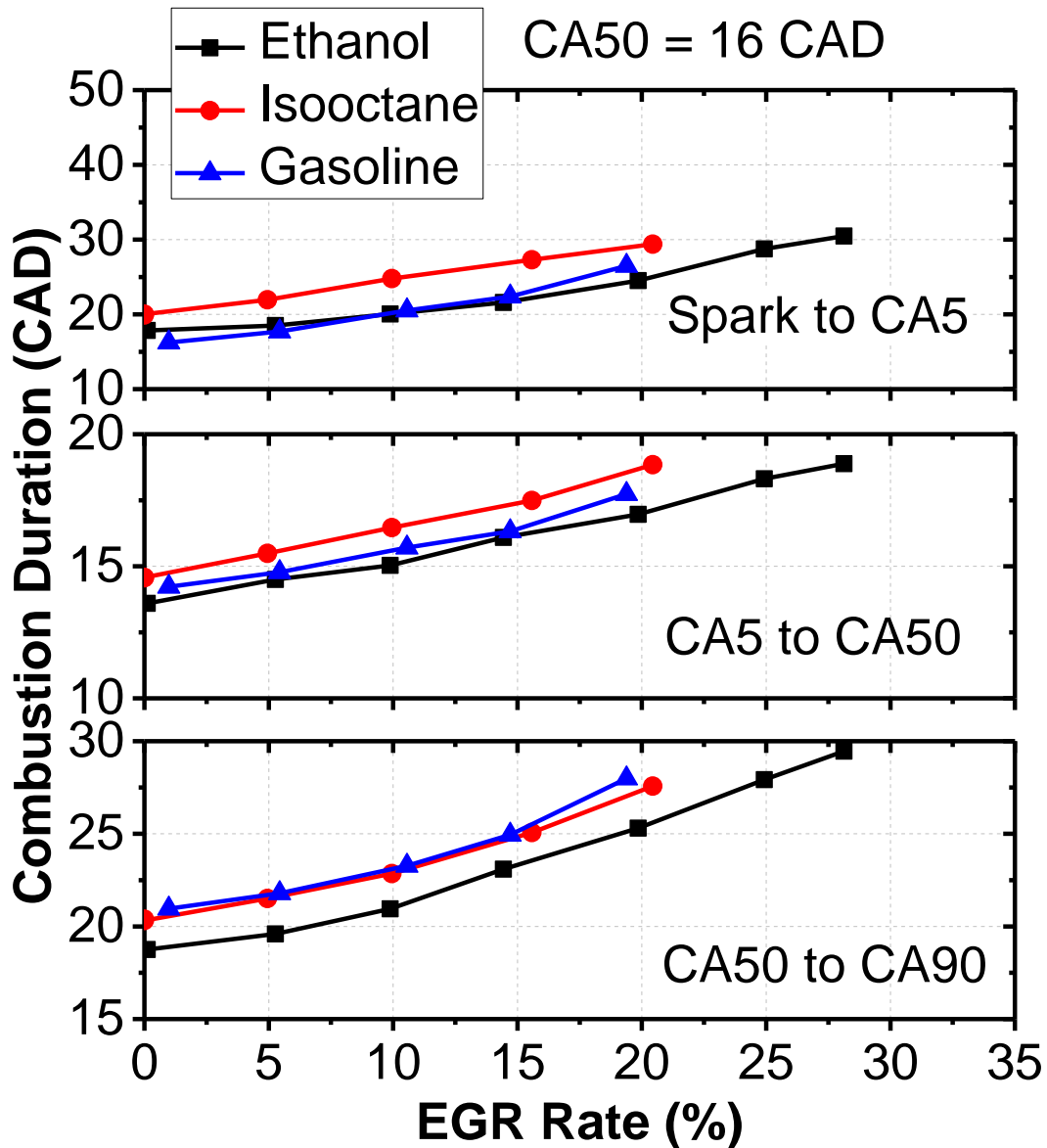
Figure 3.7. Combustion duration as a function of EGR level of ethanol, isooctane, and gasoline while CA50 combustion phasing equals to 16 CAD.

Figure 3.8 shows the standard deviation of combustion duration for each of the phases of combustion. The most significant fuel-specific differences are in Phase 1 duration. The fuel-specific differences for Phase 2 are attenuated significantly, and fuel-specific differences for the latter phase of combustion are nearly indistinguishable. Further, the standard deviation of Phase 2 and Phase 3 follows a linear trend as a function of the corresponding mean value of that combustion duration. Also, the difference in Phase 1 between different types of fuel is much larger than that of Phase 2. This is because Phase 1 is largely affected by the flame

speed of the specific fuel. Also, as the mean value of Phase 1 duration increases, the difference of standard deviation of spark to the CA5 duration between different fuels becomes larger. This is mainly because higher flame speed allows the flame kernel development to be faster, which makes the combustion more resilient to the stochastic cycle-to-cycle turbulence differences [27].
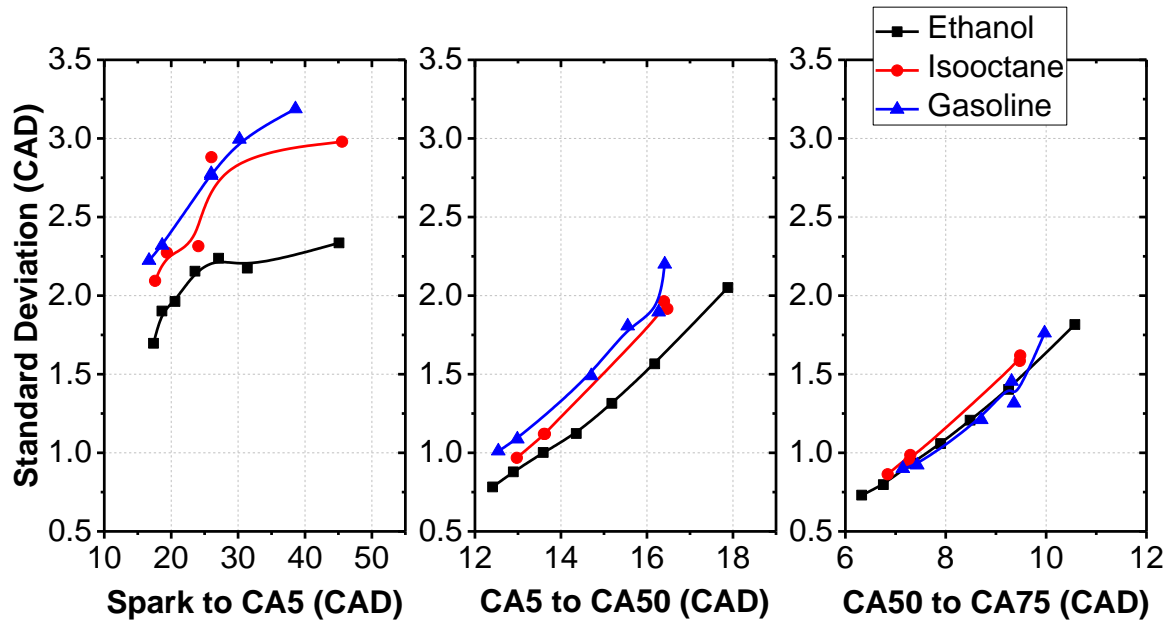
Figure 3.8. The standard deviation of combustion duration as a function of the mean value of combustion duration of ethanol, isooctane, and gasoline.

3.4 Conclusions

Ethanol gives the largest EGR tolerance at a given combustion phasing, engine load, and speed compared to isooctane and gasoline. The improved EGR dilution tolerance with ethanol is attributed to a faster flame speed.

COV of IMEP increases gradually with the increase of EGR rate for late combustion phasing cases. COV of IMEP is nearly constant at EGR rates below a certain level, and then dramatically increases to the dilution limit for early combustion phasing cases.

There is a limited spark timing window available to compensate for the longer combustion duration that occurs with high EGR rates.

The spark timing to CA5 duration is the longest phase of combustion, and it has the most variability and the strongest response to EGR.

Combustion stability limit occurs at approximately the same combustion duration for all fuels. Combustion duration is responsible for the combustion instability, and the fuel type can affect the combustion duration, thereby influencing combustion stability.

The standard deviation of CA5 to CA50 and CA50 to CA75 follows a linear trend as a function of the corresponding mean value of that combustion duration.

Chapter 4. Committed In-Cylinder Reformer Engine System

4.1 Introduction

Technical challenges need to be addressed for the implementation of EGR. There are several potential ways to extend the dilution limit of EGR. These include the use high-energy long spark systems as shown by Alger et al. [69], incorporation of different higher turbulence combustion chamber flows [70], and the addition of fuel reformate which primarily consists of hydrogen and CO into the intake manifold. Regarding the benefits of fuel reformate, Alger et al. found that the addition of 1% (vol) hydrogen could extend the EGR limit from 25% to over 50% for gasoline and from 20% to 28% for CNG [29]. Hydrogen addition increases combustion rate, allows retarded spark timing leading to lower NOx, and improves indicated efficiency, as shown by Conte et al. [72], D'Andrea et al. [73], Ji et al. [74] and Tahtouh et al. [75]. Conte and Bouloucho used a bottled blend of CO, H_2, and N_2 chosen to simulate the most likely output of a partially oxidative reformer suitable for Internal Combustion Engine applications [169]. They found that addition of hydrogen-rich gas allows the engine to run with EGR as high as 51%. In all conditions they used, a significant increase in engine efficiency and a substantial decrease of UHC and NO_x emissions were observed.

Investigations into the use of a non-catalytic in-cylinder reforming process are promising. Alger and Mangold proposed a concept that one cylinder is converted to operate under fuel-rich conditions to produce reformate with significant concentrations of H_2 and CO. The reformate is exhausted to the intake of the remaining cylinders and consumed in spark-ignited (SI) combustion [140]. Their SwRI D-EGR demonstrator shows an improved engine efficiency and fuel consumption of at least 10% across the performance map [142]. From the

energy analysis, it was found that increased NVO-period global equivalence ratio, either from lower NVO period oxygen concentrations or higher fueling rates, in general, led to a higher fraction of net recovered fuel energy, and work as heat losses were minimized [152]. These results indicate that an O_2 deficient operation approach may be a pathway toward a chemical reforming process that is not thermodynamically expensive, and may even enable thermodynamic recuperation.

The goal of the present study is to investigate the feasibility of in-cylinder reforming to achieve thermochemical recuperation and extended EGR dilution limits in SI Engines. In this research, an in-cylinder reforming technique in a multi-cylinder configuration, in which one of the engine cylinders acts as the reformer, is used. The reforming cylinder breathes in from the exhaust manifold and exhausts into the intake and requires input work from the crankshaft to the reforming cylinder rather than extracting from it. In this configuration, the advantageous fuel properties of reformate are utilized to determine if a sufficiently large efficiency benefit can be realized in the combustion cylinder to overcome the added friction and thermodynamic penalties associated with the reforming process.

4.2 Methodology

The engine used in this study is a highly modified GM Ecotec SI engine with the production side-mounted DI fueling system. Engine geometry details are presented in Table 4.1. The engine is re-configured such that the reforming cylinder breathes in from the exhaust manifold and exhausts into the intake manifold, as shown in Figure 4.1. A small research module hydraulic valve actuation (HVA) system from Sturman Industries is installed to enable fully variable valve actuation of cylinder 4, to accommodate the function of fuel reformer cylinder (cylinder 4). HVA system has the feasibility to achieve the TCR strategy and mimic the stock configuration of the engine. Accordingly, the cylinder head has been machined, disabling the functionality of the production cam of cylinder 4 and fuel pump systems, as shown in Figure 4.2. One of the stock pistons (compression ratio: 9.20:1) and the customized piston of cylinder 4 shown in Figure 4.3 (compression ratio: 11.85:1) were used during each part of the testing.

Table 4.1. Engine geometry.

Bore x Stroke [mm]	86 x 86
Conrod length [mm]	145.5
Compression ratio [-]	9.2:1 for cylinder 1-3, 9.2:1 or 12.9 for cylinder 4
Fuel injection system	Direct injection, side-mounted
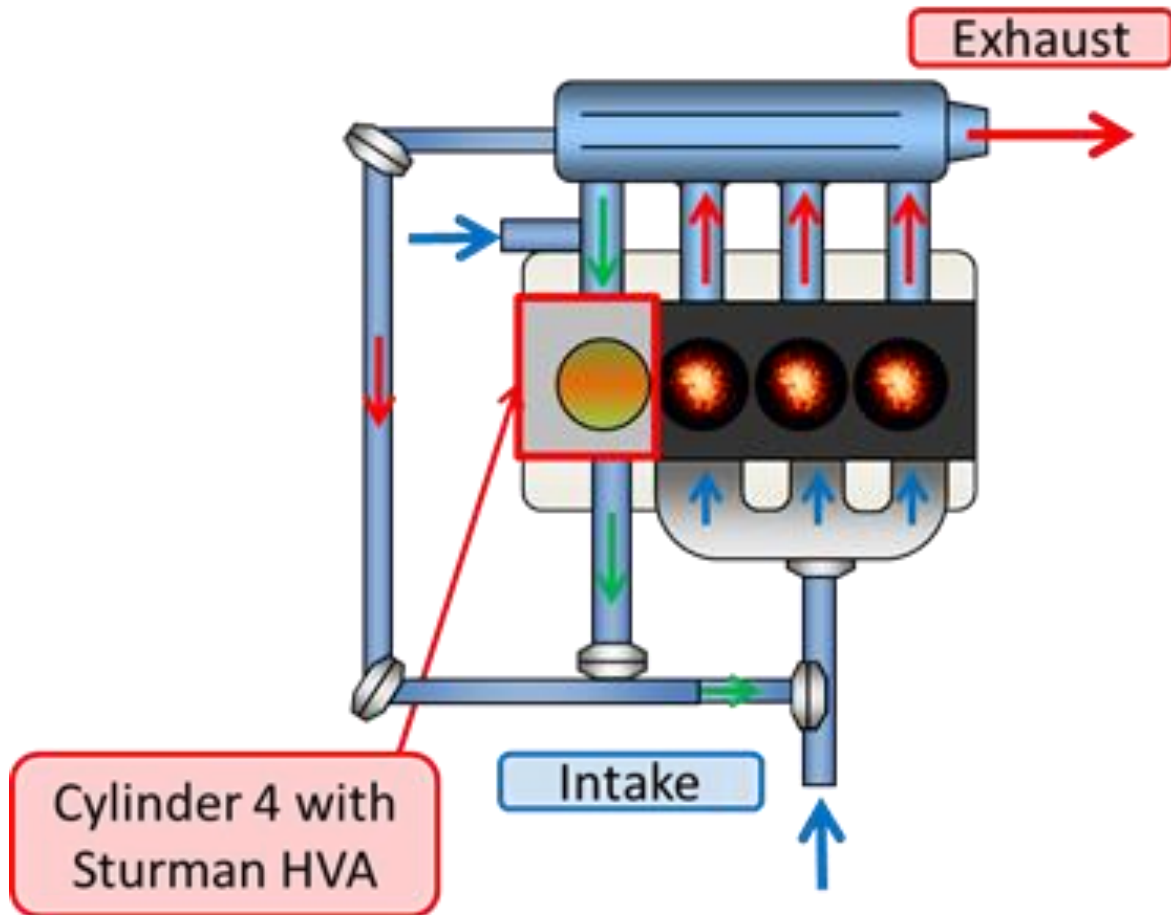
Figure 4.1. The layout of the in-cylinder reforming engine.
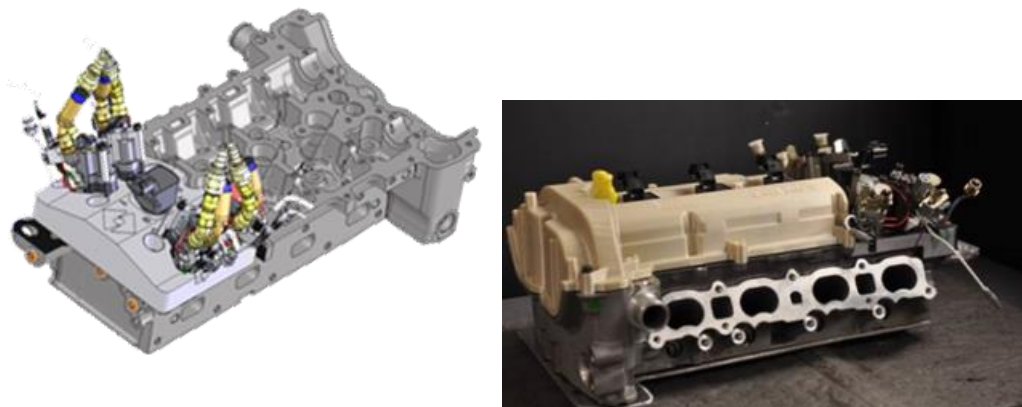
Figure 4.2. Modified cylinder head.

Figure 4.3. Stock piston and customized piston of cylinder 4.

A conditioning system is used to control the humidity of the intake combustion air to a dewpoint of 15°C. The engine is equipped with an external cooled EGR loop with the flow rate controlled by an electromechanical valve. Cooled EGR mixes with fresh air upstream of an air heater, followed by the intake plenum and then the intake manifold. The EGR used in this study is not treated with an exhaust catalyst before being recirculated to the intake. This arrangement allows the intake manifold temperature to be held at a constant temperature of 50°C regardless of the EGR level. EGR is measured using a non-intrusive method that utilizes pressure-compensated wideband oxygen sensors in both the intake and exhaust. Air is also metered to cylinder 4 using a mass air flow controller.

The engine is operated using a laboratory fueling system rather than the stock configuration. The fueling system uses a pneumatically-actuated positive displacement pump in conjunction with an electronic pressure regulator to provide fuel rail pressure. A constant fuel rail pressure of 79.3 bar is used throughout this study.

A DRIVVEN engine controller with the Combustion Analysis Toolkit (DCAT) package is used to control the engine and acquire crank-angle resolved data and to analyze combustion

performance at 1800 samples per revolution (0.2°CA resolution). Cylinder pressure data, heat release, and combustion analysis are collected for 300 fired cycles for each condition. The pressure in each cylinder is measured using a flush-mounted piezoelectric pressure transducer from Kistler (6125C). Spark timing is adjusted as needed to achieve the desired combustion phasing and is trimmed for individual cylinders to match phasing. Spark dwell is held constant at 3.8 ms with the stock ignition coil to maintain constant ignition energy.

Engine fuel flow is measured with a Coriolis-based fuel flow meter. Engine coolant temperature is maintained at 90°C. The combustion emissions are monitored using a standard array of analyzers. NO_x is measured using a heated chemiluminescence analyzer, CO and CO_2 are measured using infrared analyzers, oxygen is measured using a paramagnetic analyzer, and unburned hydrocarbon emissions (HC) are measured with a heated flame ionization detector. The SI combustion exhaust passes through heated sample lines and filters held at a constant temperature of 190°C before the emissions bench. All reformates from cylinder 4 except H_2 from the fuel-rich reforming event in cylinder 4 are measured using a Fourier Transform Infrared (FTIR) instrument from MKS. H_2 is measured using a magnetic sector capillary inlet mass spectrometer from VTI Instruments. The reformate gases are pulled through a heated filter and sample line at 190°C, and the FTIR sample cell is also heated to a constant 190°C.

The conditions maintained for sweeps of fuel injection durations, injection-timing settings, different compression ratio conditions, and EGR combinations are listed in Table 4.2.

Table 4.2. Constant Operating Conditions

Engine Speed (RPM)	2000
Brake Mean Effective Pressure (kPa)	400
Max Exhaust Valve Lift (mm)	9
Max Intake Valve Lift (mm)	9
DI Rail Pressure (bar)	77
Exhaust Lambda (-)	1
Intake Manifold Gas Temperature (°C)	49
Engine Coolant Temperature (°C)	86
Engine Oil Temperature ((°C)	95

Fuel used in this research is non-denatured (200 proof) ethanol procured from Decon Labs. Key fuel properties are listed in Table 4.3.

Table 4.3. Fuel Property

	ASTM Method	Ethanol
RON	D2699	109
MON	D2700	90
S (RON-MON)	N/A	19
C (wt%)	E191	52.17
H (wt%)	E191	13.04
O (wt%)	D4815	34.78
HoV (kJ/kg)	N/A	840

1. RON and MON of iso-octane are 100 by definition

2. Calculated from the molecular formula

4.3 Results and Discussion

The results section is divided into four subsections. The first subsection shows the effect of fuel injection duration and fuel injection timing in-cylinder reformate temperature on the fuel reforming process and engine performance, based on the testing results when the compression ratio of cylinder 4 is 9.2:1. The second subsection provides insight into the effect of compression ratio, oxygen concentration, and fuel concentration on the fuel reforming process and engine performance, based on the testing results when the compression ratio of cylinder 4 is 12.9:1. The third subsection presents the overall efficiency and combustion assessment of this strategy and this engine concept design by comparing with the conventional stock configuration and cylinder deactivation strategy. The fourth subsection describes the feasibility of feeding air to cylinder 4 by short-circuiting the exhaust of cylinder 2 (lean combustion) and cylinder 4.

4.3.1 Fuel Injection Duration

To investigate the effect of fuel injection duration into cylinder 4 on the fuel reforming process, the end of fuel injection of ethanol was swept while keeping the start of injection timing and valve timing constant.

Figure 4.4 shows an example of the engine operating under the in-cylinder reforming conditions when the compression ratio of all the cylinders is 9.2:1. The upper portion of the figure shows the cylinder pressure for cylinders 1-3 and depicts the conventional SI combustion process: the DI fueling system introduces the fuel during the intake stroke, and the cylinder contents are then compressed, expanded, and then exhausted. The lower portion of the figure depicts the in-cylinder reforming process, including valve lift traces from the HVA system. The cylinder breathes in the stoichiometric exhaust from cylinders 1-3 from the exhaust manifold while introducing the fuel with the GDI fueling system. The cylinder contents are then compressed without an ignition source and exhausted into the intake system.

Figure 4.4 also depicts the fuel injection command for a sweep of injected ethanol quantity. As the injected fuel mass into the reforming cylinder was adjusted, the fuel injected into cylinders 1-3 was also adjusted to maintain a constant BMEP of 400 kPa. Spark timing was adjusted to maintain a constant CA50 combustion phasing of 8 CA aTDCf.

Figure 4.5 shows the brake thermal efficiency and engine stability which is indicated by COV of IMEP of cylinder 1 as a function of fuel injection duration in cylinder 4. It has been shown that as the brake thermal efficiency increases, engine stability improves as the increase of injection duration. However, when the injection duration is larger than 1.6 ms, thermal efficiency starts to decrease while COV of IMEP stays at a small value.
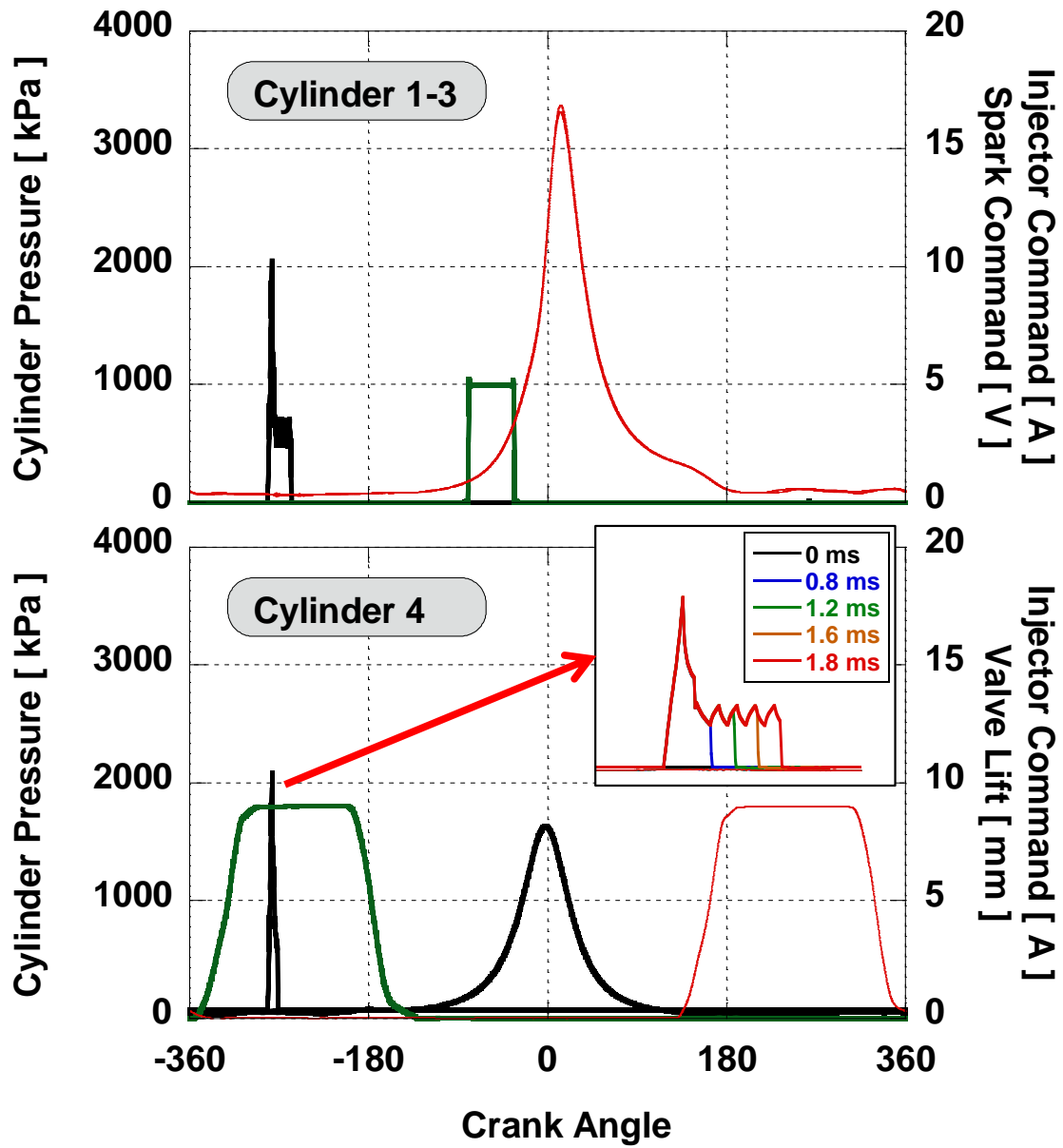
Figure 4.4. Representative cylinder pressure for in-cylinder reforming strategy with corresponding valve, spark and injection event schedule.
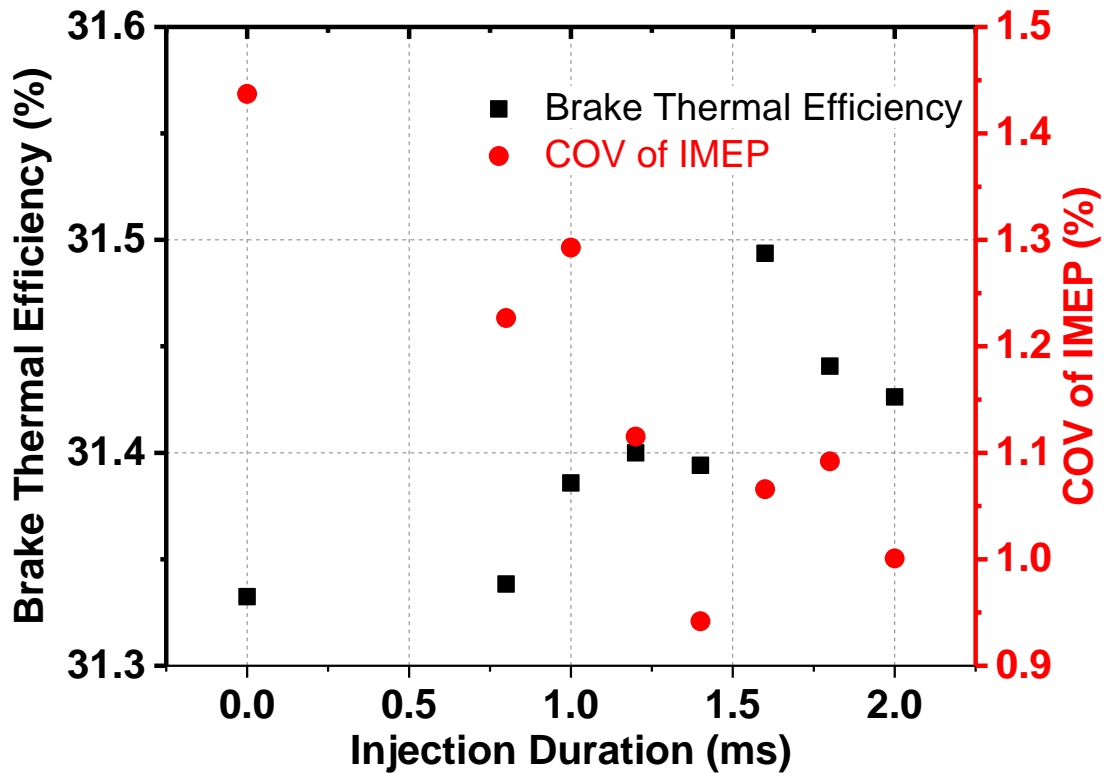
Figure 4.5. Brake thermal efficiency and COV of IMEP as a function of injection duration of ethanol.

Figure 4.6 shows the H_2 and CO concentrations as functions of injected fuel. While there is an initial increase in these products when no fuel is injected, the product concentration of these species is low. Even though hydrogen increases slightly with the increase of injection duration, the trend doesn't continue after a certain level of injection duration. While CO concentration is higher when fuel is injected into cylinder 4 compared to the case without fuel injection into cylinder 4, the CO concentration decreases as more fuel is injected into cylinder 4.

Figure 4.7 indicates the concentrations of major reformate species and remaining ethanol in the intake manifold while the fuel injection duration increases. As the amount of ethanol injected for the reforming process increases, the amount of ethanol that was measured in the intake manifold increases as well. Compared to a theoretical ethanol concentration for zero conversion, this figure shows that only a small fraction of the fuel is being converted to reformed products. This figure also illustrates that ethanol reforming yields significant

concentrations of acetaldehyde and ethylene. Acetaldehyde is not an equilibrium product, according to previous research. The concentration of acetaldehyde decreases significantly with the increase of injection duration, which mainly might be due to the charge cooling effect of evaporation of ethanol. Energy balance analysis of reforming products in the intake manifold as a function of injection duration is shown in Figure 4.8.
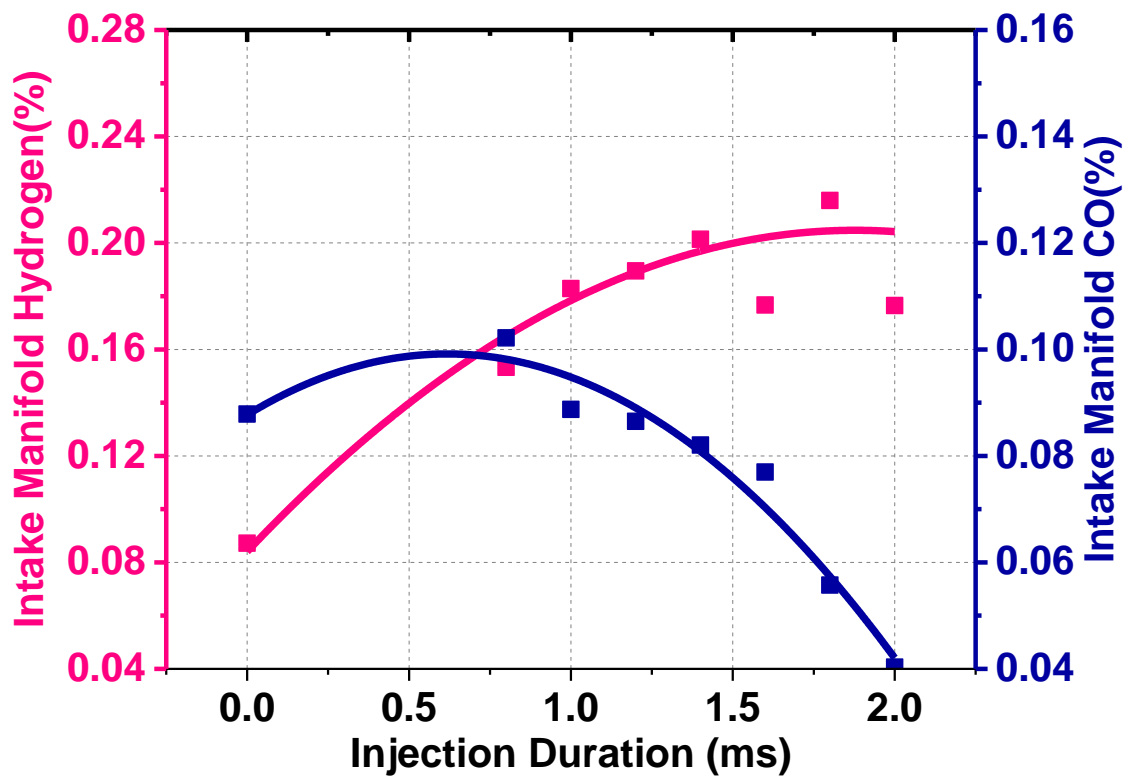
Figure 4.6. The concentration of hydrogen and CO in the intake manifold as a function of injection duration of ethanol.
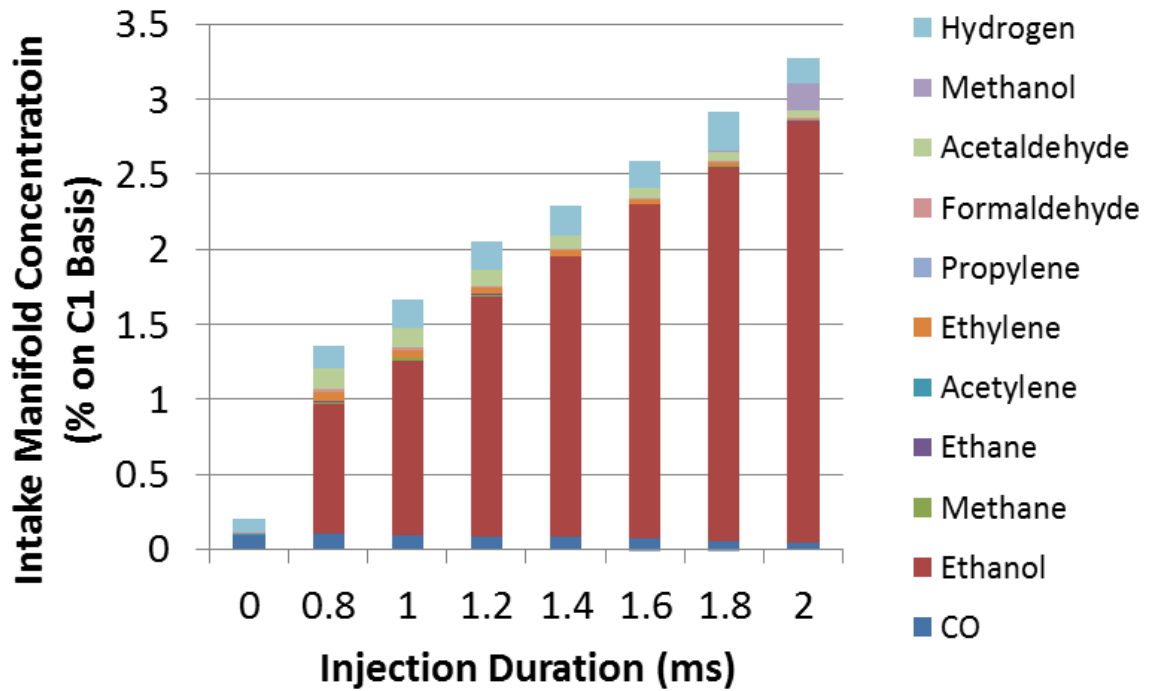
Figure 4.7. Speciation of reforming products in the intake manifold as a function of injection duration.
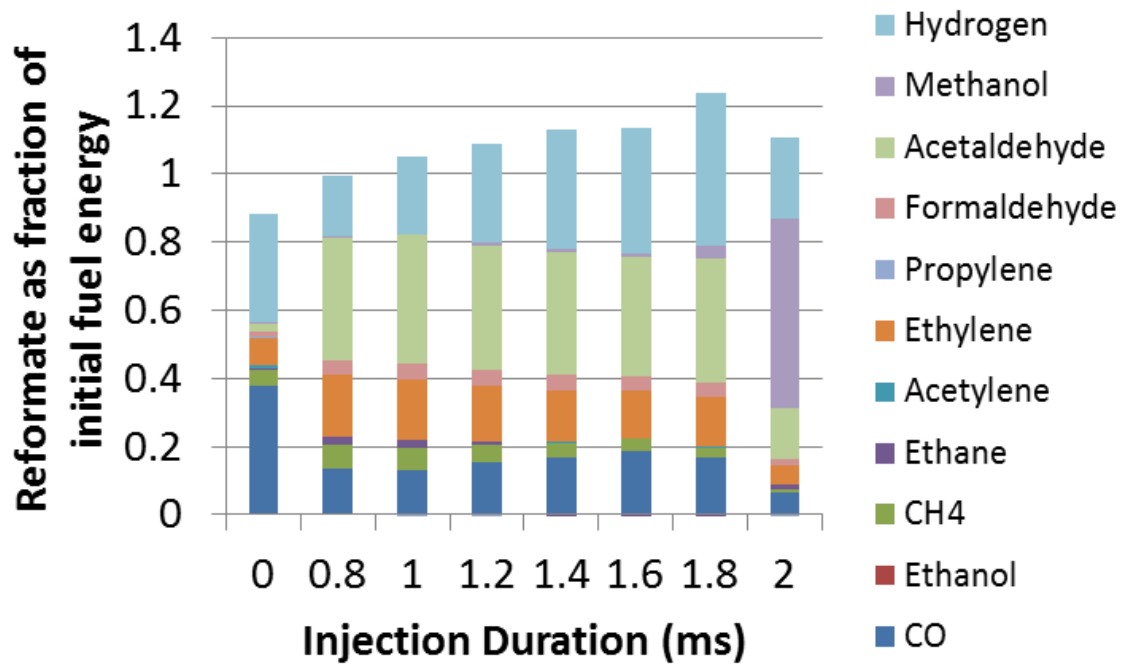
Figure 4.8. The energy balance of reforming products in the intake manifold as a function of injection duration of ethanol.

4.3.2 Fuel Injection Timing

In the previous section on the sweep of the fuel injection duration, the fuel was injected into the reforming cylinder while stoichiometric exhaust from the exhaust manifold was being inducted into the cylinder, akin to open-valve DI injection. This section explores the effect of fuel injection timing on the reforming event after the valve closing, as depicted in Figure 4.9. As in the previous section, engine load was maintained at a BMEP of 400 kPa, and CA50 combustion phasing for cylinders 1-3 was maintained constant at 8 CA aTDCf by adjusting spark timing, while the valve timing setting was constant.
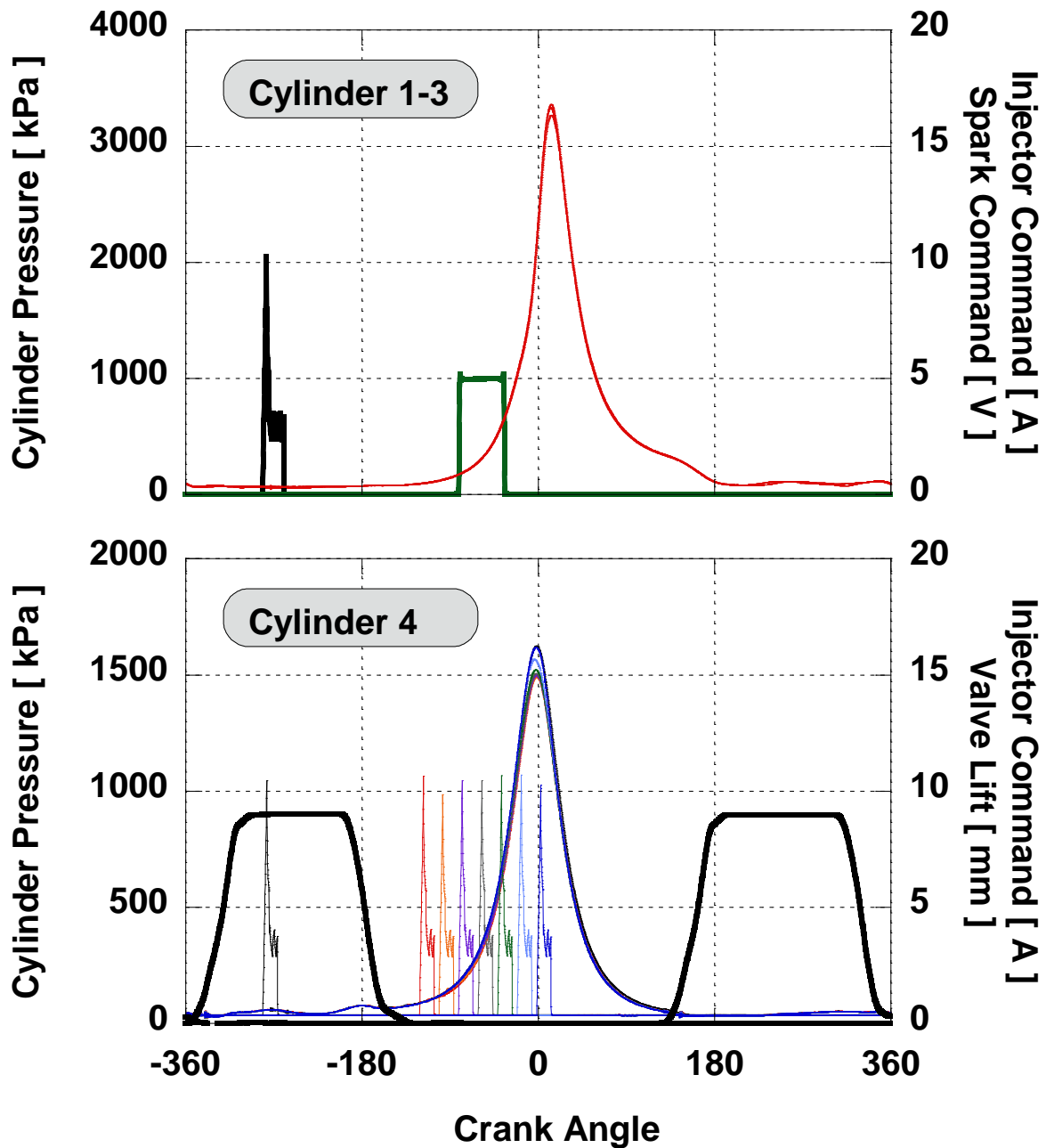
Figure 4.9. Representative cylinder pressure for in-cylinder reforming strategy with corresponding valve, spark and injection timing sweep.

Figure 4.10 shows the effect of injection timing on the brake thermal efficiency and COV of IMEP by comparing the operating conditions of fuel injection timing on the reforming event after the valve closing to the operating conditions with fuel injection right after the valve opening event. It can be observed that brake thermal efficiency is slightly higher when fuel is injected at -280 CAD after TDC firing, and COV of IMEP is not affected directly by injection timing.
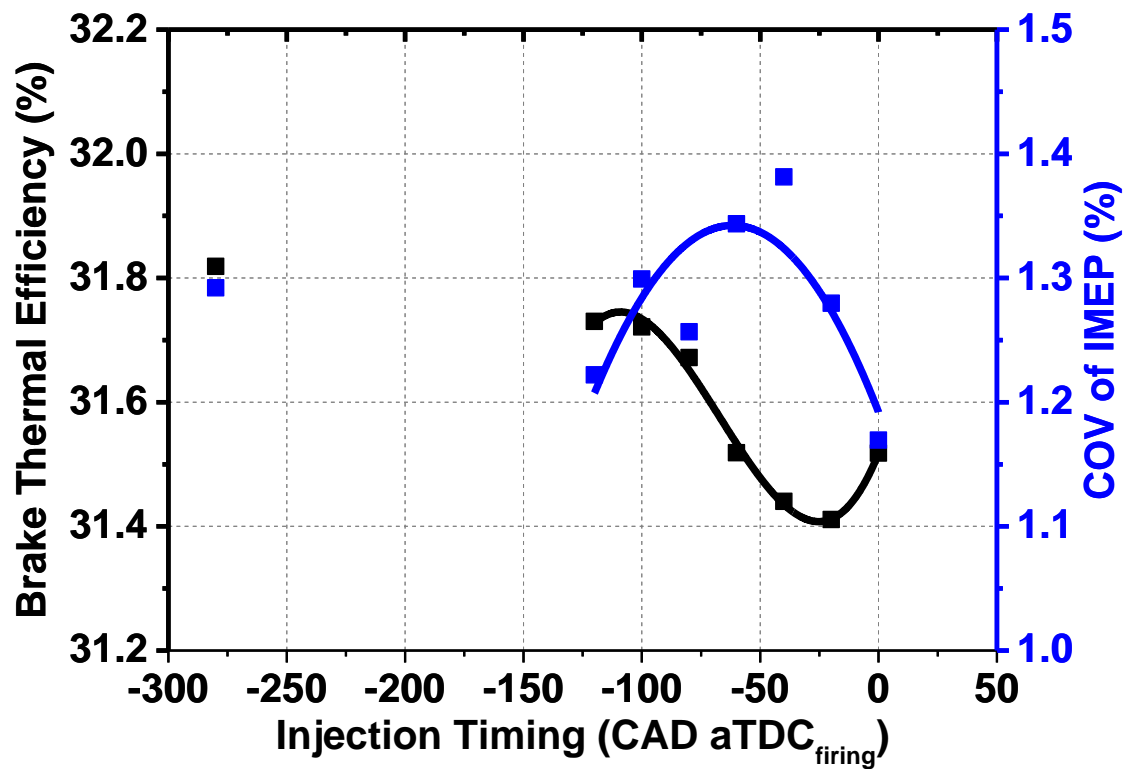
Figure 4.10. Brake thermal efficiency and COV of IMEP as a function of injection timing of ethanol.

Figure 4.11 shows that the effect of fuel injection timing on H_2 is not significant. Hydrogen concentration and CO concentration in the intake manifold are highest when fuel is injected at -280 CAD after TDC firing.
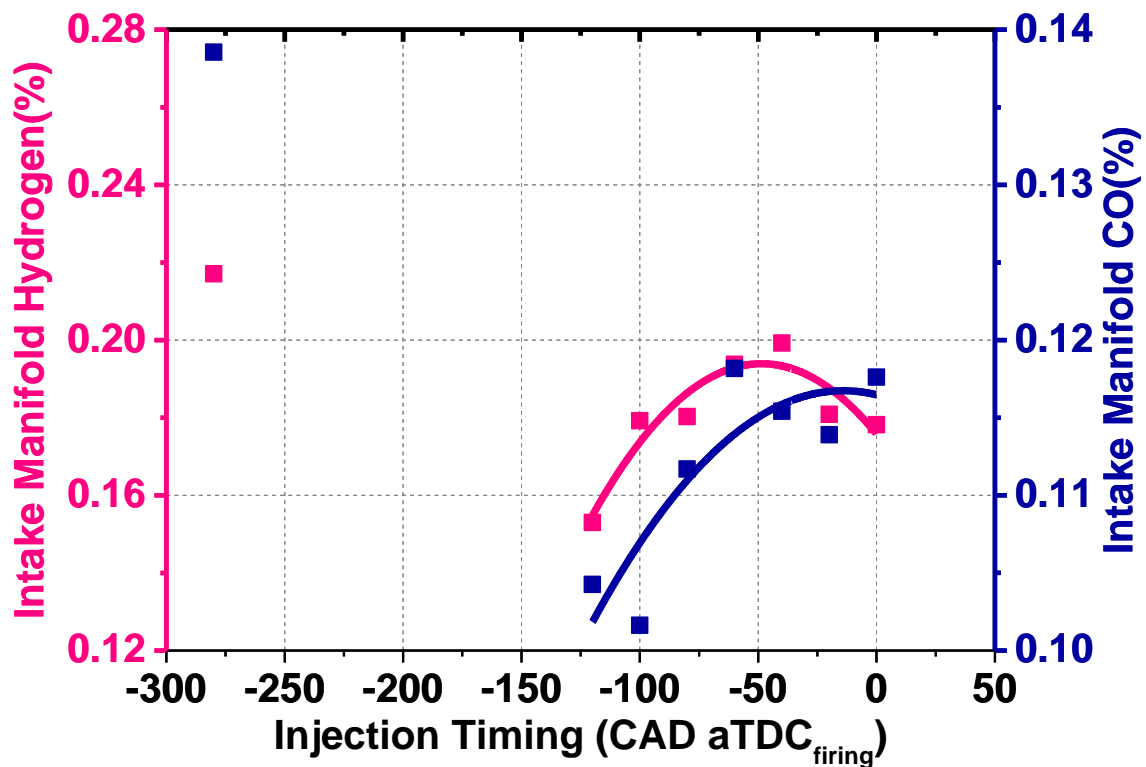
Figure 4.11. H_2 and CO concentration in the intake manifold as a function of injection timing of ethanol.

Figure 4.12 shows the speciation of reforming products in the intake manifold as a function of injection timing. Fuel conversion decreases and concentration of acetaldehyde decreases when the fuel injection timing is retarded closer to TDC of the compression event. Early injection timing is favorable for the fuel reforming process but still could not lead to a complete reforming process, which can be indicated by the concentration of acetaldehyde.

Figure 4.13 shows the energy balance analysis of reforming products in the intake manifold as a function of injection timing.
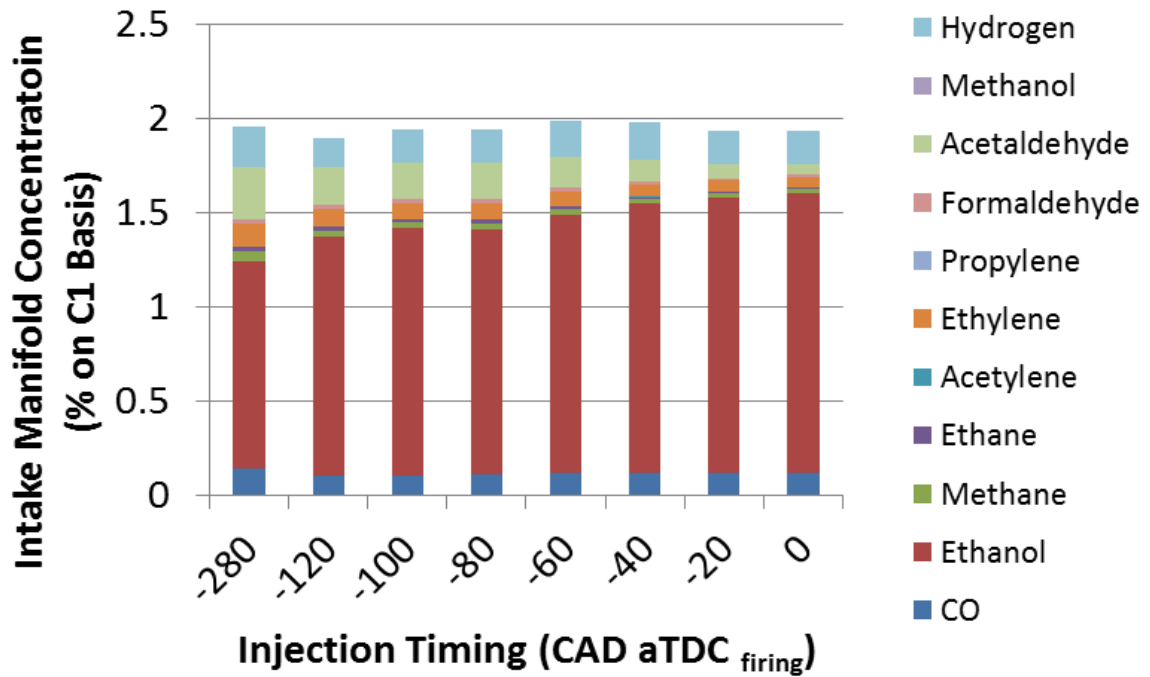
Figure 4.12. Speciation of reforming products in the intake manifold as a function of injection timing of ethanol.
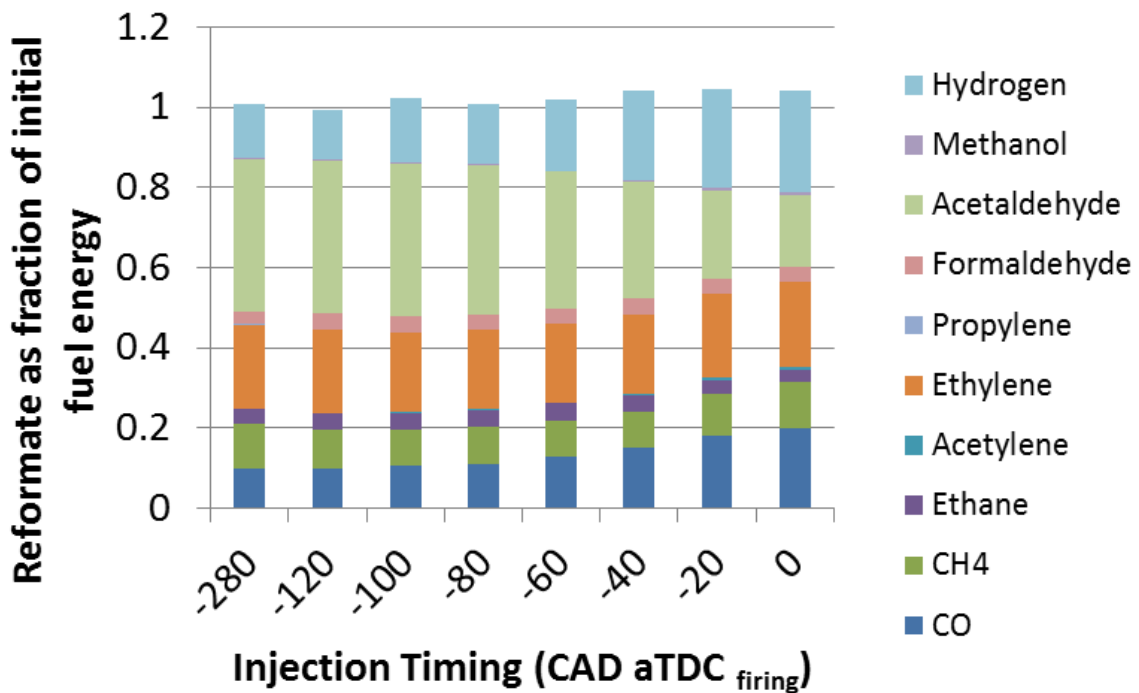
Figure 4.13. Energy balance analysis of reforming products in the intake manifold as a function of injection timing of ethanol.

4.3.3 In-Cylinder Reformate Temperature

The level of reforming activity shown in Figure 4.7 and Figure 4.11 was lower than initially expected based on the experience of previous work [151]. However, a closer examination of the present system can provide insight into the differences. In the previous work, compressed gases had been trapped in-cylinder and then recompressed using a 6-stroke engine cycle. As a result, the temperature decrease from heat transfer was modest because the timescale was short and the gas wasn't being moved past a valve or through a manifold, reducing the opportunities for convective heat transfer. This resulted in estimated peak cylinder temperatures during the recompression event of 1120-1200K.

In contrast, the current study uses exhaust produced in cylinders 1 through 3, routed through the production exhaust manifold, and then inducted into cylinder 4. In this process, the temperature decreases substantially. The temperature of the exhaust gas for cylinders 1-3 is 535°C when it enters the exhaust manifold, and by the time it is inducted into cylinder 4 the temperature has decreased to 419°C, representing a temperature drop of 116°C (shown in

Figure 4.14). This temperature drop occurs despite using heavy insulation and a heating tape on the exhaust manifold to minimize thermal losses, and it illustrates the difficulty in retaining thermal energy as the gas is moved from one cylinder to another. While it is possible that this can be partially addressed with an exhaust manifold designed to minimize heat losses, it will likely always be a significant source of thermal energy losses.
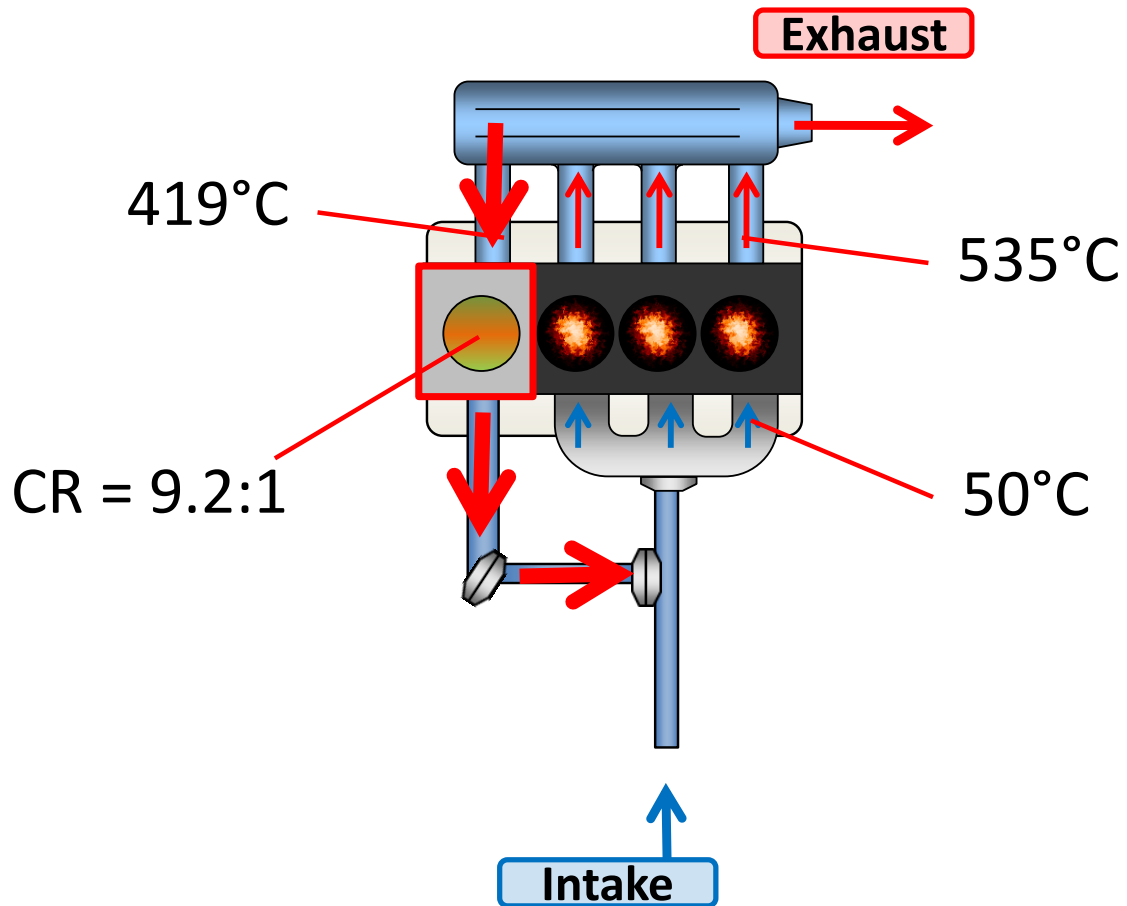
Figure 4.14. Diagram of thermal loss.

This heat loss, combined with using the OEM compression ratio piston of 9.2:1, leads to the much lower in-cylinder temperature. The peak in-cylinder temperature is less than 950 K. Ekoto et al. [152] showed the temperature and equivalence ratio conditions required to generate a significant concentration of reformate for each species. Their work shows that for all equivalence ratios, minimum temperatures between 1000 [152] and 1050K are required to generate significant amounts of reformed products (shown in Figure 4.15).
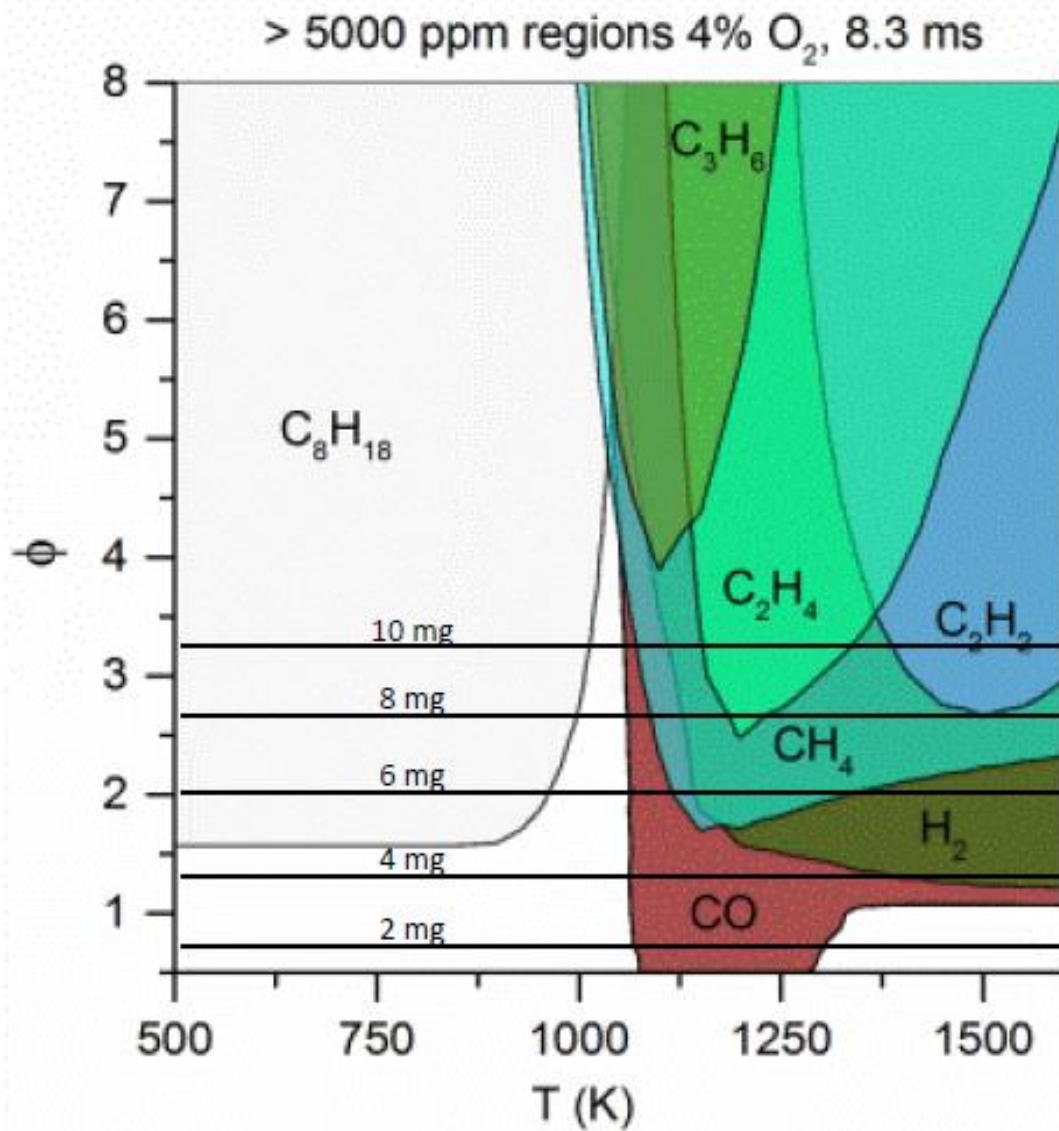
Figure 4.15. Reformate islands from Ekoto et al. [152].

Thus, in the following section, an attempt to increase the in-cylinder temperature is made through (1) increasing the compression ratio of cylinder 4 from 9.2:1 to 12.9:1, and (2) adding air injection into cylinder 4 so that exothermic combustion reactions can elevate the temperatures to drive the reforming reactions.

4.3.4 Compression Ratio

The effect of the compression ratio change in cylinder 4 is shown in Figure 4.16 for matched conditions for the two compression ratio configurations. The higher compression ratio produces a significantly higher cylinder pressure, 2400 kPa vs. 1600 kPa.
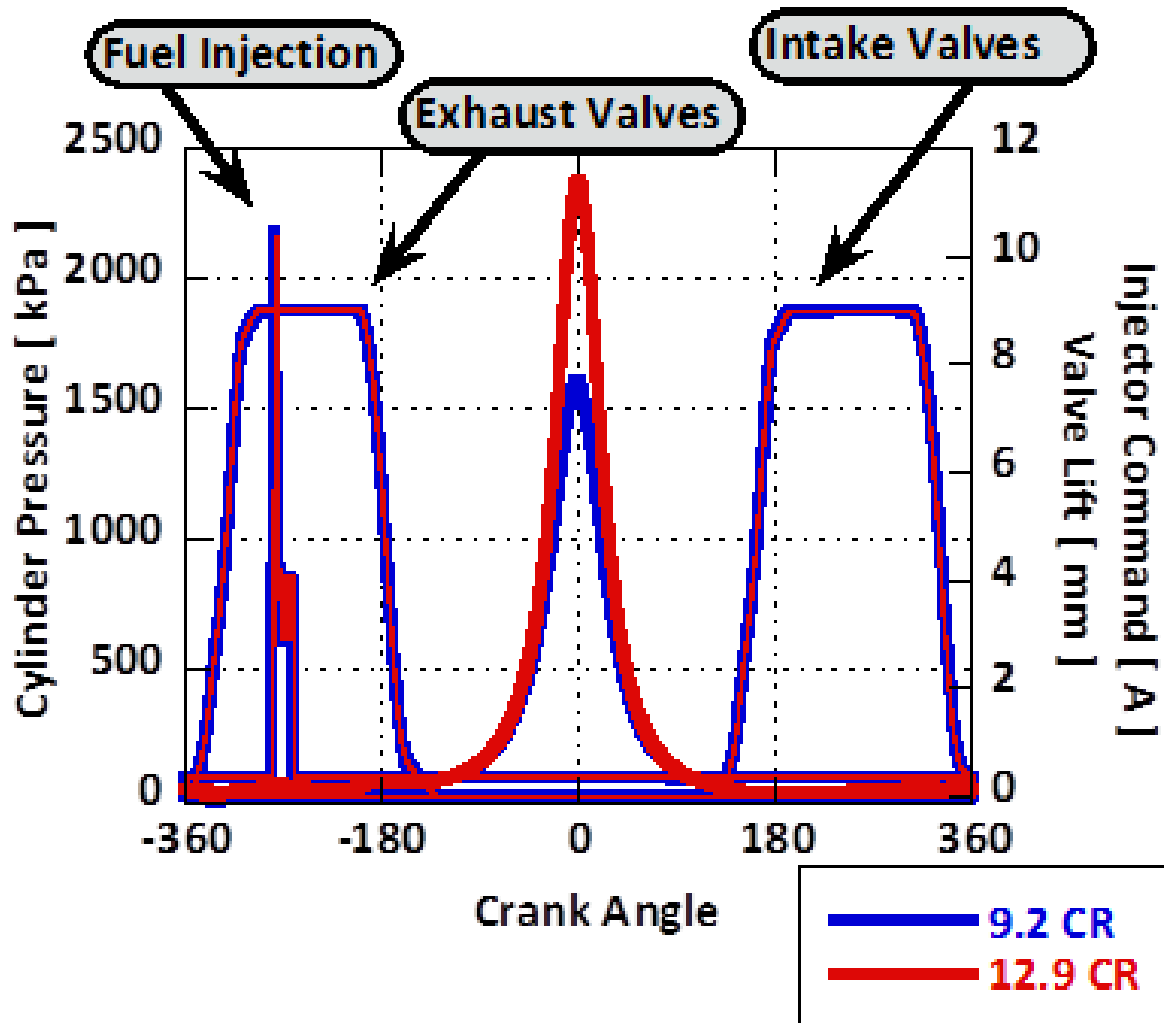
Figure 4.16. Pressure for cylinder 4 for matched in-cylinder reforming conditions for the two different compression ratio configurations.
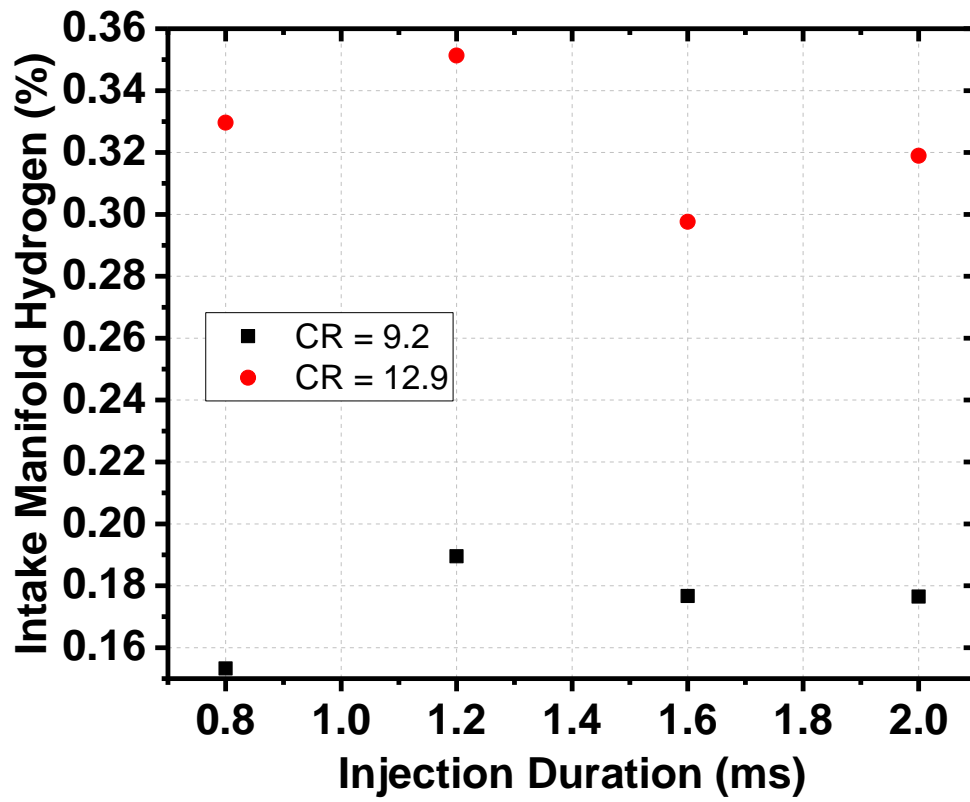
Figure 4.17. The concentration of hydrogen in the intake manifold with different compression ratios.
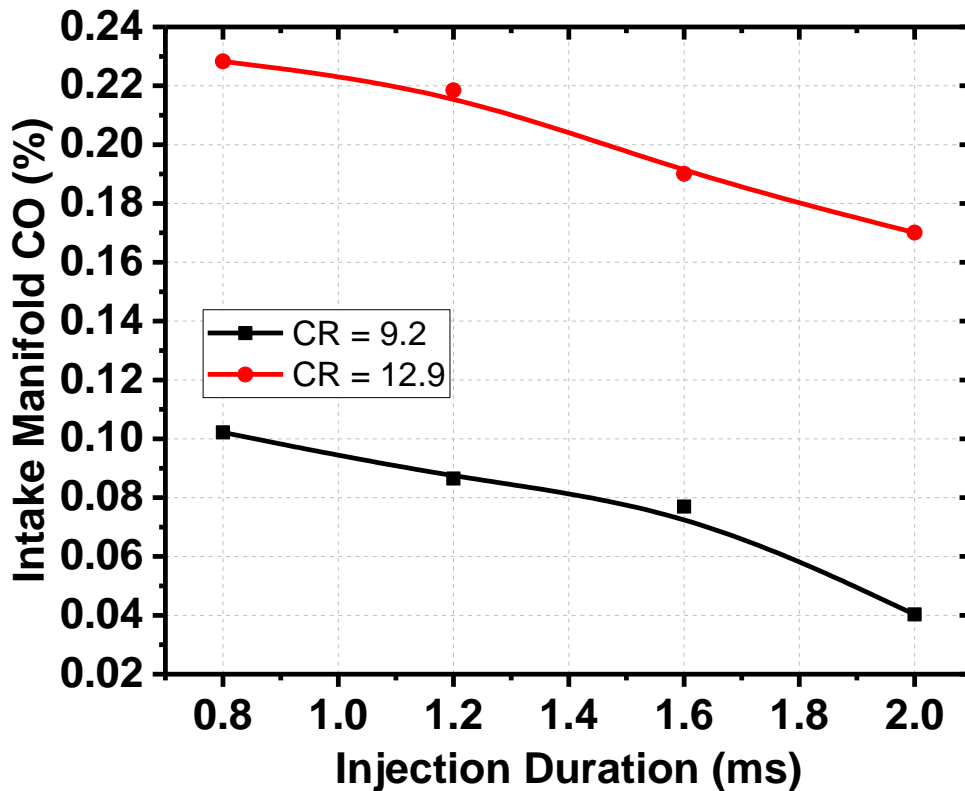
Figure 4.18. The concentration of CO in the intake manifold with different compression ratios.

This increase in temperature was smaller than what was expected based on the compression ratio increase, and it only resulted in a modest in-cylinder temperature increase, which leads to a slight increase of the concentration of H_2 and CO, as shown in Figure 4.17 and Figure 4.18. Increasing the compression ratio, however, did not have as large an effect on the in-cylinder temperature because doing this also increased the heat transfer losses.

4.3.5 Oxygen Concentration

Results from experiments show that fuel conversion and reformate yield increase dramatically with the addition of air into the reforming cylinder. As shown in Figure 4.19 and Figure 4.20, as the equivalence ratio in the reforming cylinder decreases, the concentrations of hydrogen and CO in the intake manifold increase significantly. However, other species such as acetaldehyde and ethylene decrease at the same time, shown in Figure 4.21, which indicates that acetaldehyde and ethylene are not favorable products with more air addition.

The amount of hydrogen, CO, and CH4 still are not sufficient even with relatively low equivalence ratio, so that the effect of oxygen concentration is minimal to change the thermal efficiency and combustion duration, as shown in Figure 4.22 and Figure 4.23.
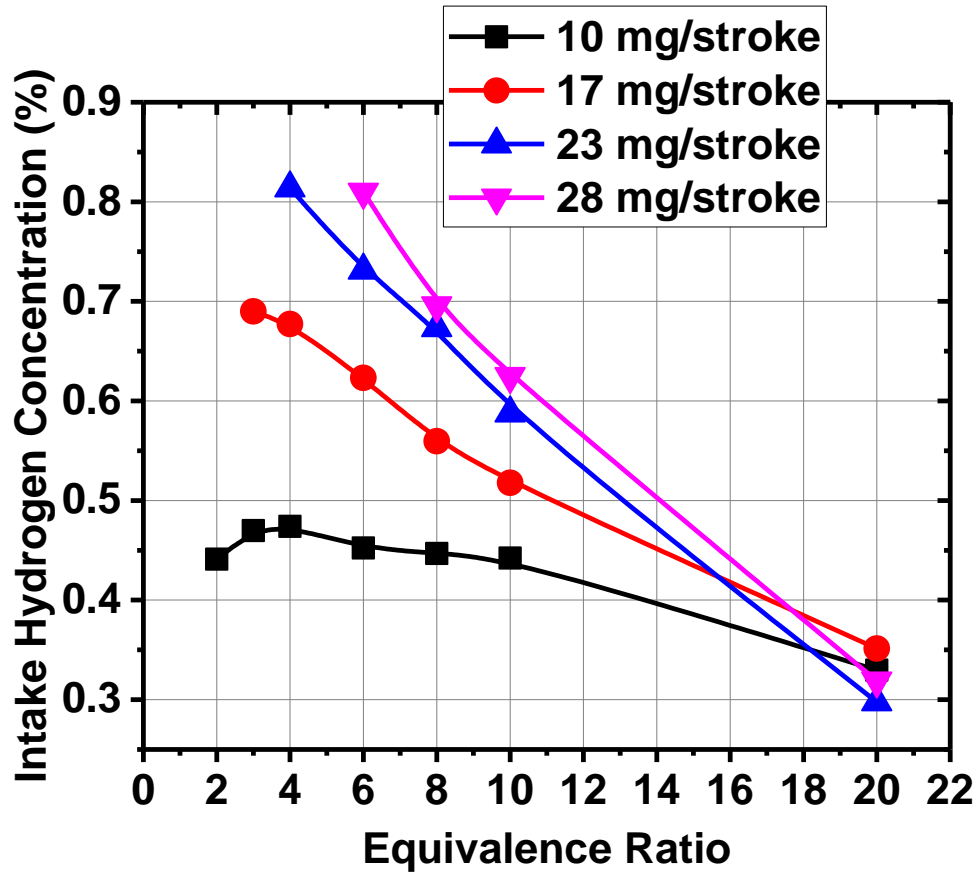
Figure 4.19. Intake hydrogen concentration as a function of equivalence ratio.
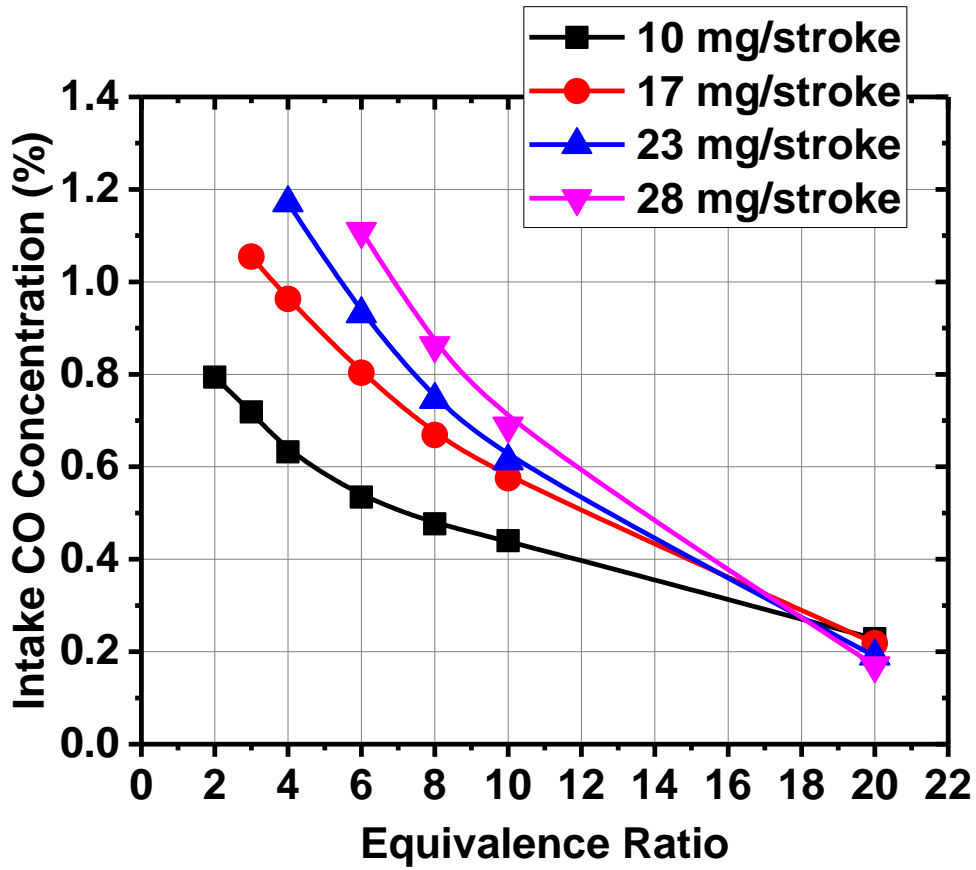
Figure 4.20. Intake CO concentration as a function of equivalence ratio.
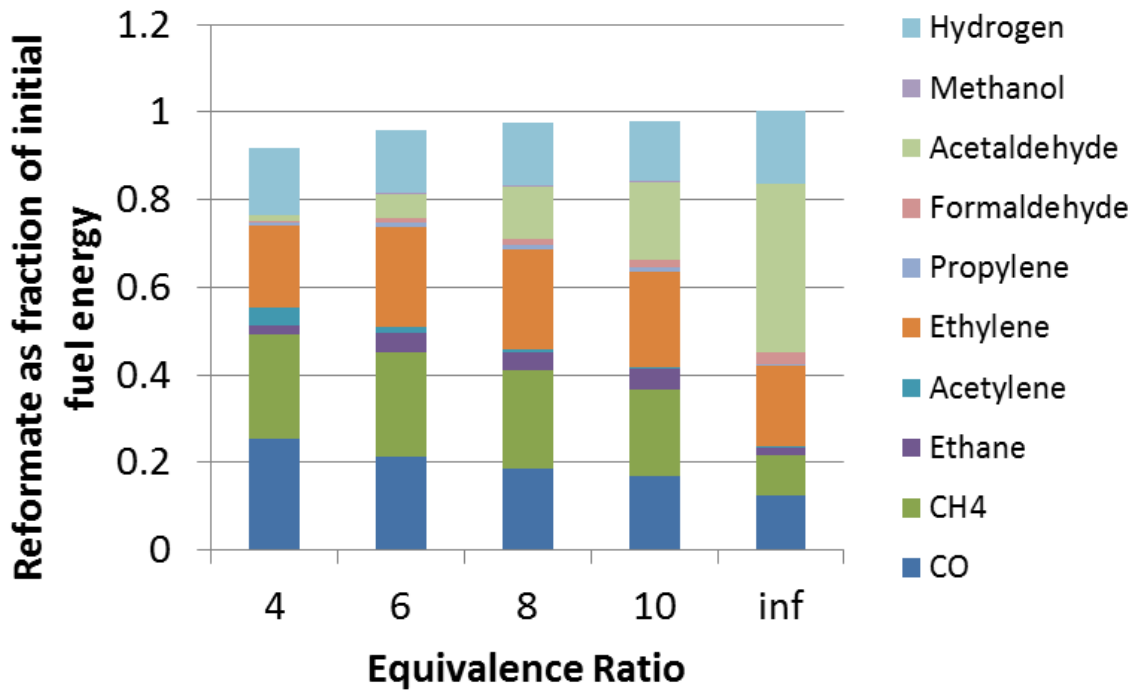
Figure 4.21. Reformate species concentration as a function of equivalence ratio.
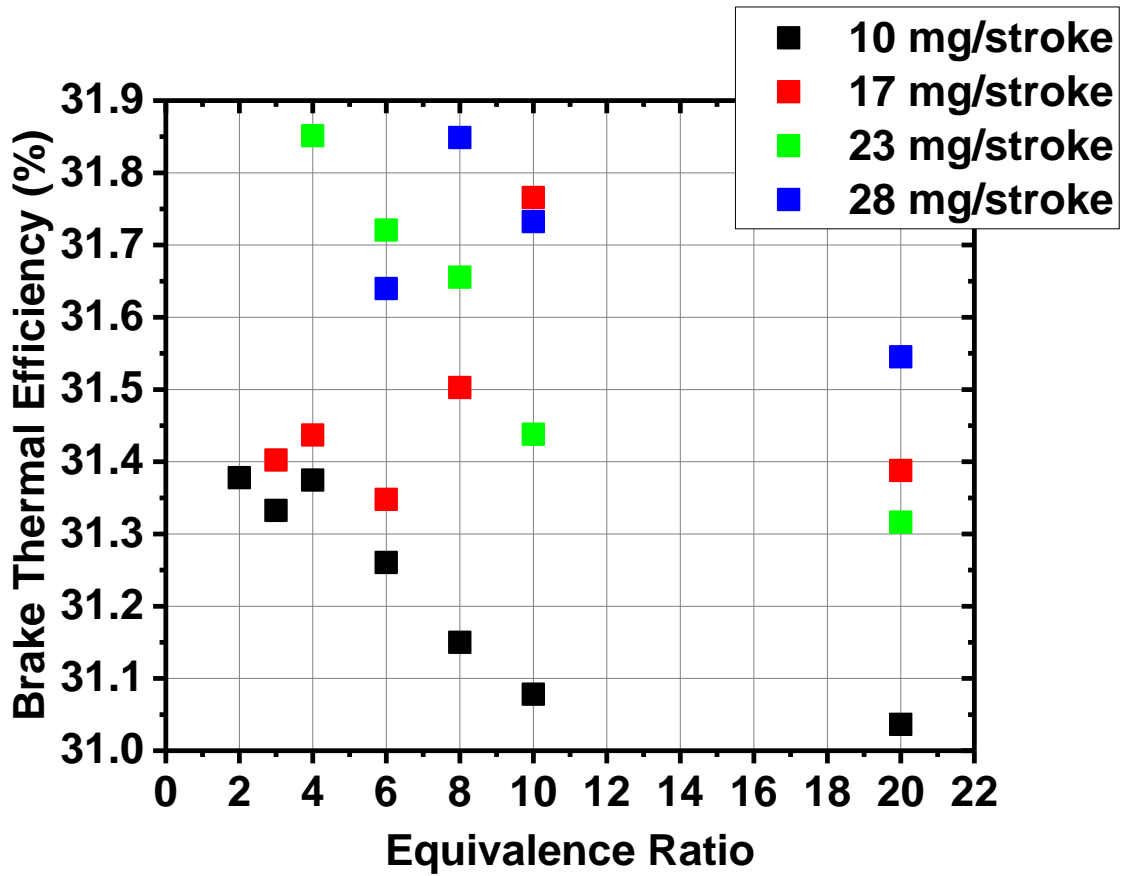
Figure 4.22. Brake thermal efficiency as a function of equivalence ratio.
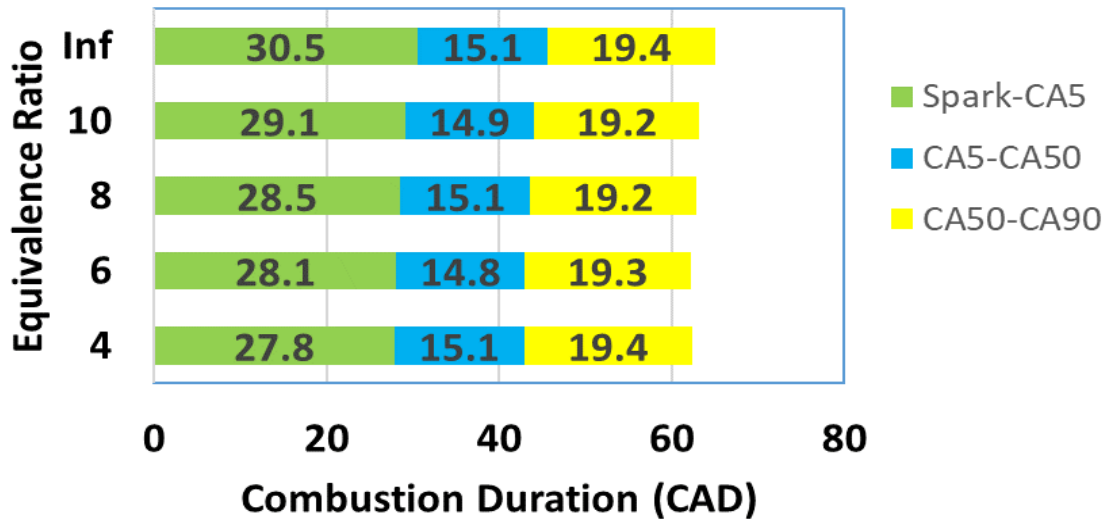
Figure 4.23. Combustion duration as a function of equivalence ratio.

4.3.6 Comprehensive Efficiency Analysis

Comparing the brake thermal efficiency of the best operating points for each sweep with that of conventional EGR and cylinder deactivation, it has been shown in Figure 4.24 that the efficiency increase of in-cylinder fuel reforming strategy can be attributed primarily to cylinder deactivation and EGR dilution rather than in-cylinder reforming.
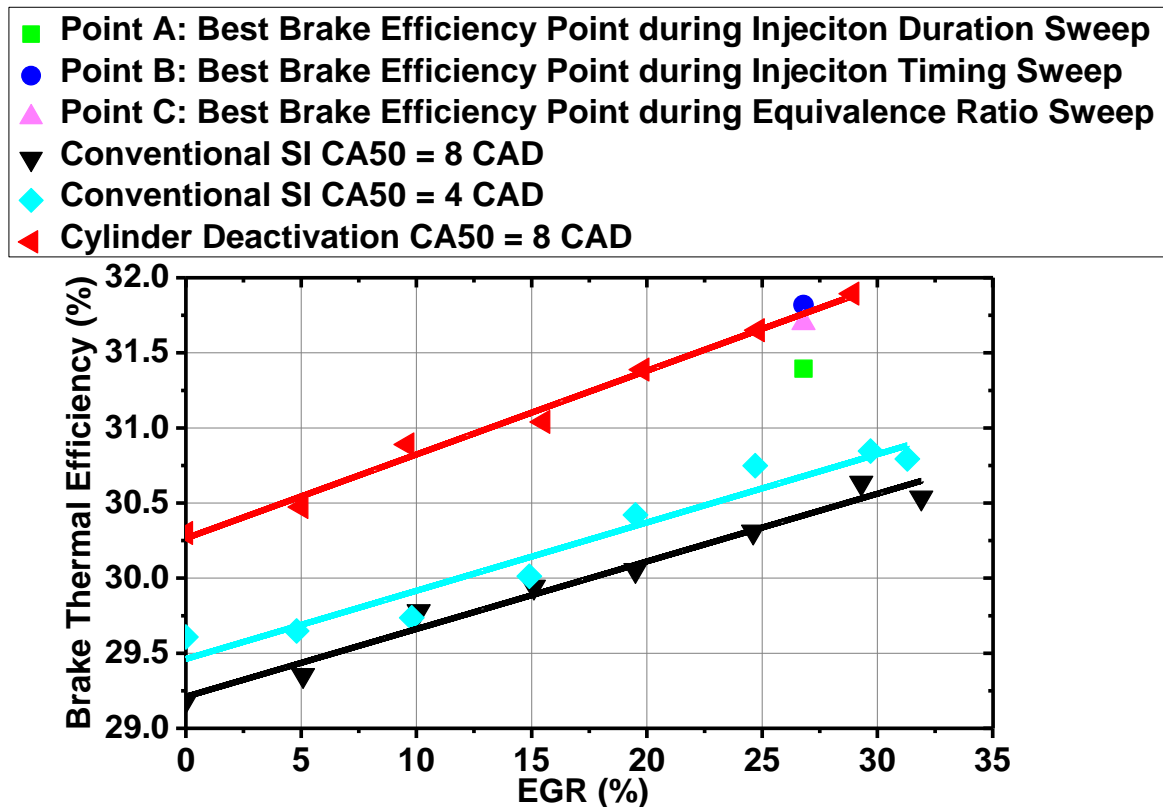
Figure 4.24. Comprehensive Efficiency Comparison of Conventional EGR, Cylinder Deactivation, and In-cylinder Fuel Reforming.

4.4 Conclusions

Low cylinder temperatures resulted in minimal fuel conversion with the in-cylinder reforming strategy of the ethanol. Despite low fuel conversion, brake thermal efficiency improvement of 8% is achieved through EGR and cylinder deactivation effects. Some oxygen in-cylinder helps fuel conversion, but the higher conversion of fuel into reformate did not result in higher brake thermal efficiency and dilution limit extension.

Chapter 5. Catalytic EGR-Loop Reforming Engine System

5.1 Introduction

Efficiency improvements in spark-ignited engines are desired as a way to meet increasingly challenging fuel economy and CO_2 emission regulations [4]. External cooled exhaust gas recirculation (EGR) provides known thermodynamic benefits while maintaining compatibility with conventional three-way catalysts for emissions control [24]. Caton [25] summarized the thermodynamic benefits of EGR, which include reduced pumping work at part-load conditions, decreased heat transfer due to lower cylinder temperature, and an increased ratio of specific heats. External EGR is also a proven way to decrease the knocking propensity for a given fuel, which can be used as the basis for additional increases in efficiency through more advanced combustion phasing or higher compression ratio [26]. Lastly, EGR reduces NO_x emissions over a broad range of speed and load conditions [27].

The amount of EGR dilution that can be used is limited due to cycle-to-cycle combustion instability, thereby limiting the potential efficiency benefit of EGR [28], [65]. The cause of the cyclic instability with EGR has been linked to a decrease in flame speed, which elongates the initial flame kernel development process, making it more susceptible to stochastic turbulence variation [61], [66], [170]. While several technologies unrelated to fuel reforming are being developed to extend the EGR dilution limit, including high-energy long-duration ignition systems [69] and incorporation of different higher turbulence combustion chamber flows [70], the focus of this work is to extend the EGR dilution limit by using the reformed products of the fuel to increase the EGR dilution tolerance.

The addition of the major products of fuel reforming, H_2 in particular, increases the combustion rate and can increase engine efficiency because of the shorter combustion duration [72]-[75], [165]–[168]. Alger et al. [29] reported that H_2 could also be used to extend the EGR dilution limit, with the addition of 1 vol % H_2 extending the EGR limit from 25% to more than 50% for gasoline and from 20% to 28% for compressed natural gas. Ivanič et al. [44] added reformate at levels of 15% and 30% gasoline energy equivalent in a single cylinder engine and found that, under part-load conditions, lean dilution can improve engine efficiency by as much as 12% while EGR dilution delivers 8% improvement.

Though there are many approaches to generating reformate on-board, they can generally be classified into two broad categories. The first category is where fuel is reformed in one or more cylinders in an engine using non-catalytic processes. This category includes the Dedicated EGR (D-EGR) strategy developed by Southwest Research Institute, which is the most advanced strategy in this category [140]. D-EGR uses fuel-rich combustion in one cylinder and recirculates its exhaust to the intake system, generating brake thermal efficiency as high as 42.5% [141] and demonstrating a vehicle-level fuel consumption decrease of more than 10% [144]. This category also includes injecting fuel during the negative valve overlap period for a homogeneous charge compression ignition engine to manipulate the fuel-air mixture auto-ignition propensity [141], [149], [169]–[172]. The second category of fuel reforming and the category of the present work is where a catalyst is used to reform the fuel outside of the engine cylinders [153]–[156], [173]–[176].

Catalytic reforming processes often use the sensible enthalpy in the exhaust to promote reforming reactions over the catalyst to improve the energetics of reforming [153]–[155], [173]. The range of possible combustion and reforming reactions that can occur has been presented by Ahmed and Krumpelt [182] and by Jamal and Wyszynski [173], [183] and is presented below for completeness using iso-octane as the starting fuel. Equation 5.1 below shows the reaction stoichiometry for the complete combustion of iso-octane, while Equation 5.2 defines equivalence ratio (Φ). For this manuscript, Φ refers to the O_2/Fuel ratio of complete combustion in Equation 5.1 relative to the actual O_2/Fuel ratio. Equation 5.3, Equation 5.4, and Equation 5.5 show the primary types of reactions that can occur in a

reformer, using iso-octane as an example fuel. When O_2 is present such that the molar O/C ratio is unity, partial oxidation (PO_x) occurs where the parent hydrocarbon is converted to CO and H_2, resulting in an exothermic process as shown in Equation 5.3. For an environment where O_2 is not sufficient but where H_2O is present, the resultant steam reforming reaction, shown in Equation 5.4, is highly endothermic and results in much higher concentrations of H_2. Ideally, the endothermic steam reforming reactions are driven by the sensible enthalpy in the exhaust, allowing for waste heat recovery through thermochemical recuperation (TCR) [101]. In this work, we studied reforming environments that contain an insufficient amount of O_2 to convert all of the fuel to CO and H_2 through Equation 5.3 and thus consist of a balance of POx, steam, and dry reforming processes.

Complete Combustion: $C_8H_{18} + 12.5\ O_2 \rightarrow 8\ CO_2 + 9\ H_2O$ (-5050.2 kJ/mol)   **Equation 5.1**
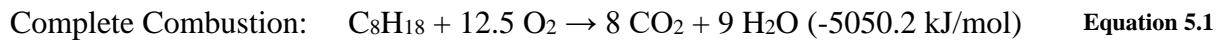
Equivalence Ratio: $$\Phi = \frac{\left(Fuel/O_2\right)}{\left(Fuel/O_2\right)_{Complete\ Combustion}}$$ **Equation 5.2**

POx Reforming: $C_8H_{18} + 4\ O_2 \rightarrow 8\ CO + 9\ H_2$ (-660.4 kJ/mol)   **Equation 5.3**

Steam Reforming: $C_8H_{18} + 8\ H_2O \rightarrow 8\ CO + 17\ H_2$ (+1,274.2 kJ/mol)   **Equation 5.4**

Dry Reforming: $C_8H_{18} + 8\ CO_2 \rightarrow 16\ CO + 9\ H_2$ (+1,603.8 kJ/mol)   **Equation 5.5**
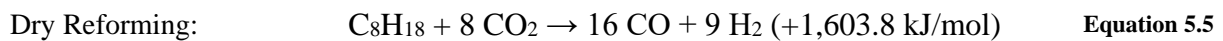
The work by Leung et al. [180] showed that, for ethanol, the steam reforming reaction (Equation 5.4) is very active at engine exhaust temperatures, converting nearly 100% of the fuel energy at 600°C. In contrast, dry reforming (Equation 5.5) produces less than 40% fuel conversion at the same temperature. This indicates that dry reforming is not the favored reaction pathway, likely due to the larger energy input required, especially at lower initial temperatures. Regardless of whether reforming takes place via the steam or dry reforming pathway, though, the product concentrations can equilibrate via the water-gas shift (WGS) reaction, shown in Equation 5.6.

WGS: $CO + H_2O \rightarrow CO_2 + H_2$ (-41 kJ/mol) **Equation 5.6**

It can be challenging to operate the engine and catalyst systems together, so that good performance of the catalytic reformer and engine are achieved simultaneously. Hwang et al. [160] integrated a reforming catalyst containing Rh and Pt into the exhaust manifold of a diesel engine. While they were able to produce high concentrations of H_2 (> 10%), the reforming system resulted in an overall engine efficiency decrease because the reformer catalyst equivalence ratio was too low ($\Phi_{catalyst}$ as low as 1.5), and the reforming process was too dependent on the exothermic reactions. In contrast, Ashida et al. [156] used a steam reforming catalyst (4 wt% Rh/Al_2O_3, La additive) in the EGR loop of a spark ignition engine without any additional O_2 ($\Phi_{catalyst}$ approaching ∞). They initially found high levels of fuel conversion and H_2 production, but the steam reforming catalyst began deactivating immediately, with a 35 ppm Sulfur fuel resulting in a 90% deactivation within 5 hours.

In this chapter, we characterize reformer catalyst performance over a range of $\Phi_{catalyst}$ conditions to find a balance between the PO_x reactions required for sustained catalyst activity and durability and the endothermic steam reforming reactions needed to minimize energy losses or to achieve TCR during reforming. This experimental study was conducted using a full-sized catalyst on a multi-cylinder engine but builds on previous bench flow reactor experiments conducted by Pihl et al. [184]. This chapter characterizes reformer performance and energetics using iso-octane with the EGR-loop reforming catalyst under a variety of operating conditions and the whole-engine performance, including EGR dilution tolerance, emissions, and brake thermal efficiency.

5.2 Methodology

5.2.1 Equilibrium Calculations

The limiting chemical equilibrium products were determined for a range of conditions in the reforming reactor using the equilibrium solver in ANSYS Chemkin-Pro 17.2. All of the 1,389 species in the Lawrence Livermore National Laboratory (LLNL) gasoline surrogate kinetic

mechanism (and their associated thermodynamic properties) were included, allowing the resulting products to be fully unconstrained [185]. A range of equivalence ratios was included, with the as-fed CO_2, O_2, H_2O, and N_2, and the parent fuel at varying concentrations. Two parent fuels representing different H/C ratios were considered for the calculations: iso-octane (H/C = 2.25) and toluene (H/C = 1.14). The calculations were performed for initial O_2 mole fractions ranging from 0.005 to 0.06 and for equivalence ratios from 3.0 to 10.0. Equilibrium calculations were conducted at initial temperatures of 500°C and 700°C.

5.2.2 Experimental Facility

The engine used in this study was a 2.0 L GM Ecotec LNF engine equipped with the production side-mounted direct injection fueling system. Engine geometry details are presented in Table 5.1. The combustion chamber geometry and camshaft profiles were unchanged from the stock configuration. The first part of the experiment focuses on the catalyst operation, and data presented here represent just one of the four cylinders operating and feeding the catalyst, referred to as cylinder 4. The second part of the experiment evaluates the full engine operation performance. The engine configuration shown in Figure 5.1 is used for reformer performance characteristics experiment. Primary fuel used in this research is isooctane and Tier II Lube Certificate fuel is also tested to verify the performance of this system design with a real fuel. The fuel properties of the primary reference fuel iso-octane and obtained from Haltermann and the comparison with other reference fuels are listed in Table 5.2.

Table 5.1. Engine geometry.

Bore × Stroke [mm]	86.0 × 86.0
Conrod length [mm]	145.5
Wrist pin offset toward expansion stroke[mm]	0.8
Compression ratio [-]	9.2/1
Fuel injection system	Direct injection, side-mounted, production injector with opposite linear wall directed six-hole spray pattern
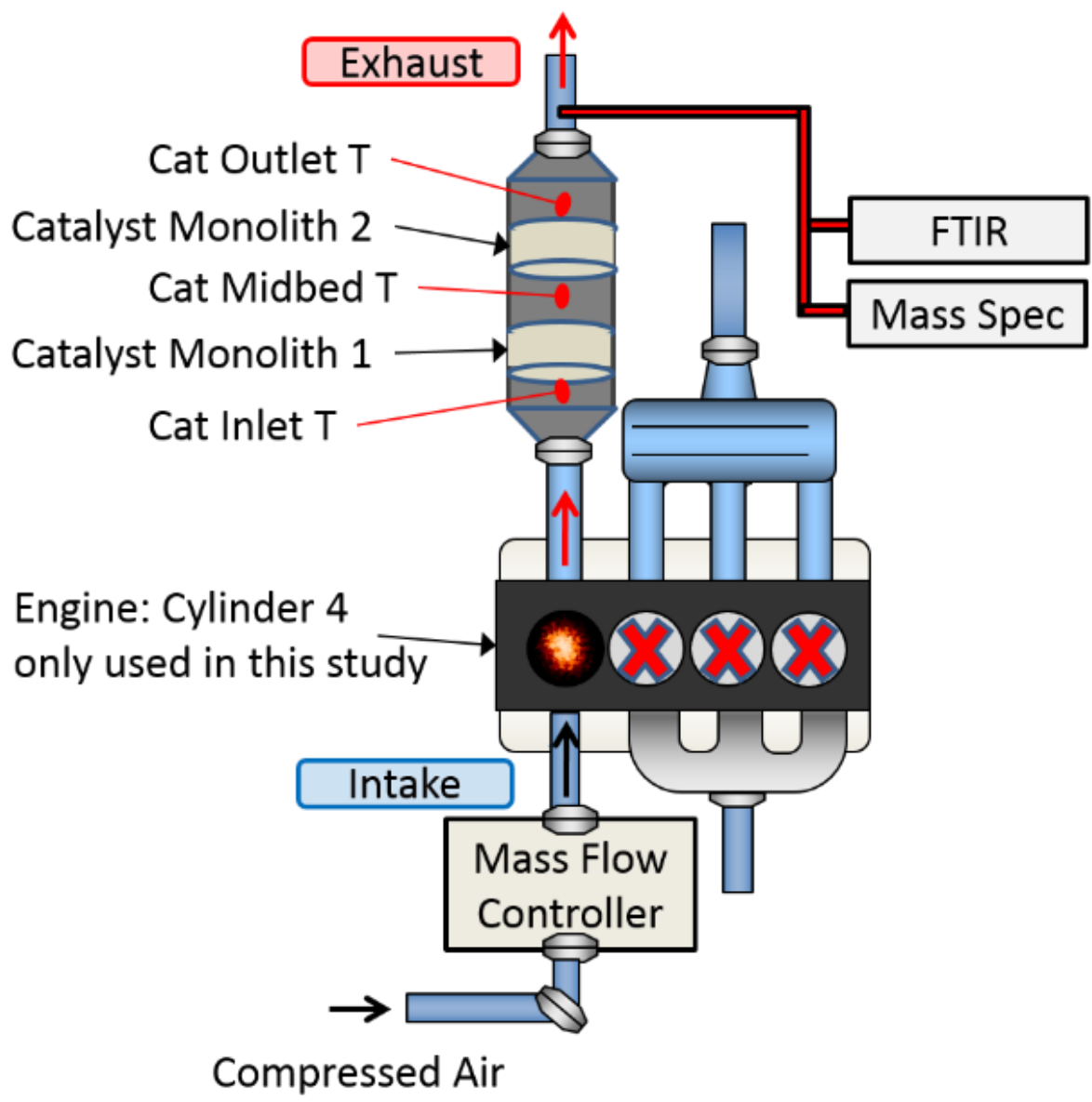
Figure 5.1. Schematic of the engine and test cell configuration for the catalyst-only experiments.

Table 5.2. Investigated Fuel Properties and Reference Fuel Specifications

	Iso-octane	Tier II Lube Cert Gasoline	Tier II Gasoline	Tier III Gasoline
RON	100	97	96.8	91.8
MON	100	88.7	88.6	84.2
S	0	8.3	8.3	88
Ethanol [%]	0	0	0	9.8
T10 [deg C]	99	52.2	52.2	54.6
T50 [deg C]	99	104.5	103.3	89.9
T90 [deg C]	99	156.7	155.6	157.8
Sulfur [ppm]	0	7	30	10.2
Carbon [wt %]	84.2	86.5	86.6	82.63
Hydrogen [wt%]	15.8	13.28	13.4	13.66
Oxygen [wt %]	0	<0.01	None Detected	3.71

To evaluate the full engine operation performance, two different configurations for the engine were used: a conventional EGR configuration and a catalytic EGR-loop reforming strategy configuration. All data were collected at an engine speed of 2,000 rpm, and a load of 4 bar brake mean effective pressure (BMEP). Further, all data were collected for CA50 combustion phasing, or the timing of 50% heat release, between 6 and 10 crank angle degrees (CAD) ATDC firing (ATDC$_f$) in each cylinder, which corresponds to maximum brake torque.

For the conventional EGR condition, which is shown in Figure 5.2a, the engine was equipped with an external cooled EGR loop with the flow rate controlled by an electromechanical valve. Cooled exhaust gas was mixed with fresh air upstream of an air heater. The recirculated exhaust gas in this study was not treated with an exhaust catalyst before being recirculated to the intake. This arrangement allowed the intake manifold to be held at a constant temperature of 52°C regardless of the EGR level. EGR was measured using nonintrusive pressure-compensated wideband oxygen sensors in both the intake and exhaust. This method has been described in Chapter 2 and is similar to that used in other investigations using conventional EGR [50].

The catalytic reforming strategy, which is shown in Figure 5.2b, presents an alternative engine operating strategy that has not been reported previously. A single isolated cylinder feeds the reforming catalyst and provides the entirety of the reformate-EGR mixture to the other three cylinders. The isolated cylinder, which will be referred to as cylinder 4, does not

have the ability to breathe the EGR-reformate mixture as the other cylinders do. However, because all of the cylinder 4 exhaust is used to feed the reforming catalyst and is recirculated to the other three cylinders, it is not necessary to maintain stoichiometric conditions in cylinder 4 to have a stoichiometric exhaust. In fact, to provide the catalyst with the proper feed for good performance, cylinder 4 is intentionally operated under non-stoichiometric conditions.
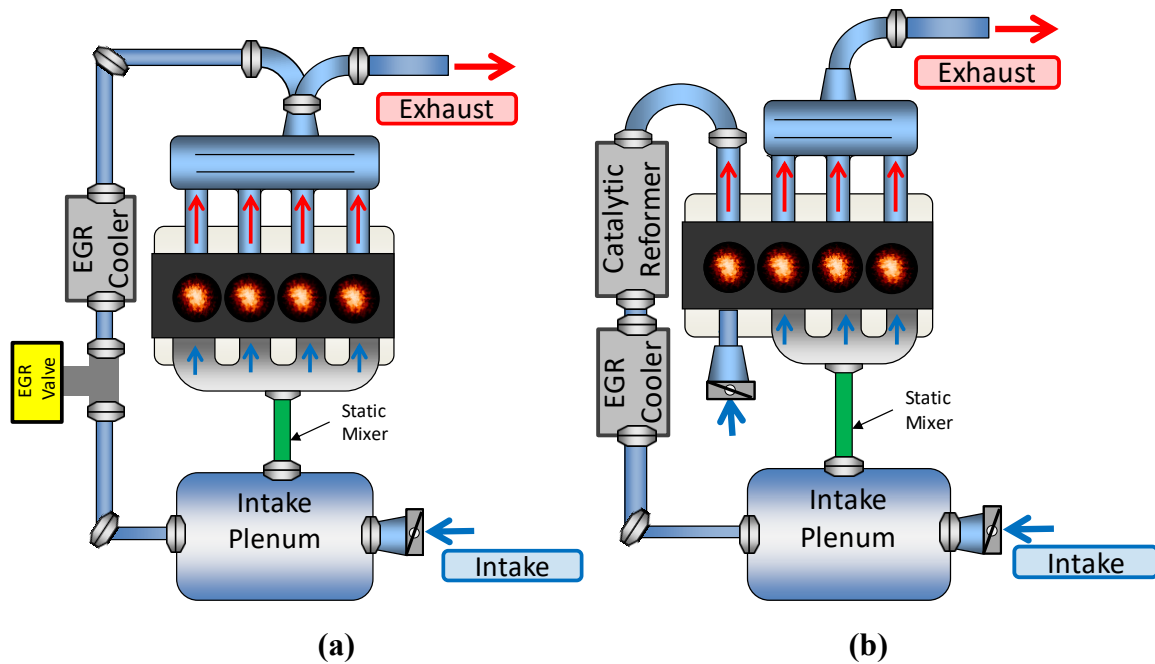
Figure 5.2. Schematic of the engine and test cell configuration for (a) the conventional EGR configuration and (b) the catalytic exhaust gas recirculation (EGR)–loop reforming strategy.

The engine was operated using laboratory fueling and air handling systems. A lift pump delivered fuel at 5 bar pressure through a Coriolis effect flow meter to the engine, where the cam-driven fuel pump was used to maintain a constant rail pressure of 100 bar throughout the experiment. The air for cylinder 4 was supplied using a mass flow controller. A Drivven engine controller with the Combustion Analysis Toolkit package was used to control the engine and acquire crank angle (CA)–resolved data. For each experimental condition, cylinder pressure, spark discharge, and camshaft position data were recorded at 0.2°CA resolution for 1,000 sequentially fired cycles. Cylinder pressure was measured using a flush-mounted piezoelectric pressure transducer from Kistler (6125C), and camshaft position was recorded from the production Hall-effect sensors. Start of fuel injection timing was

commanded during the intake stroke and was held constant at 280°CA before firing top dead center (TDC), and the start of post-injection was held constant at 150°CA after TDC. Engine coolant temperature was maintained at 90°C. Concentrations of water, CO2, CO, CH4, and iso-octane were measured using a MultiGas 2030HS Fourier transform infrared (FTIR) instrument from MKS Instruments. The FTIR was calibrated to detect up to 20% water using an 8-point calibration and 23% CO_2 using a 14-point calibration. Two different calibrations for CO were, with the low detection range being a 5000 ppm, 15-point calibration, and the high detection range being an 8%, 10-point calibration. The calibrated ranges for CH_4 was 3000ppm using a 14-point calibration, and for iso-octane, a 1000ppm range using a 5-point calibration was used. Hydrogen was measured using an ODYSSEY magnetic sector capillary-inlet mass spectrometer from VTI Instruments. A gas divider was used to verify that there was a linear response up to 10% H_2, thereafter a single-point calibration of 10% was used for daily calibration. Smoke emissions were monitored with a reflective filter smoke number instrument, but all smoke measurements registered a negligible filter smoke number (< 0.01). Thus the further discussion of smoke emissions is omitted.

The reforming catalyst was a pre-commercial 2 wt % Rh supported on Al_2O_3, which was synthesized and coated on a cordierite monolith substrate by Umicore Autocat USA. Rh is used because of its overall durability and sulfur tolerance [158]. Two cordierite catalyst monoliths were used in the experiment, each measuring 106 mm in diameter and 106 mm in depth, providing a total catalyst volume of 1.9 L. The catalyst cell density was 400 cells per square inch. The temperature was monitored at the catalyst inlet, between the two catalyst monoliths, and at the catalyst outlet, also shown in Figure 5.1.

5.2.3 Experimental Methodology for Reformer Characterization

The engine was operated in such a way as to provide the catalyst with a fuel-rich mixture that also contained oxygen. This was accomplished by operating the main combustion event in cylinder 4 fuel-lean and providing a post-injection of fuel near the exhaust valve opening timing. A schematic of the cylinder pressure and the fuel injection schedule for this strategy is shown in Figure 5.3. The main injection event was held constant throughout this study,

delivering 16 mg/injection event. Both the level of excess air and the post-injection fuel mass were variable.
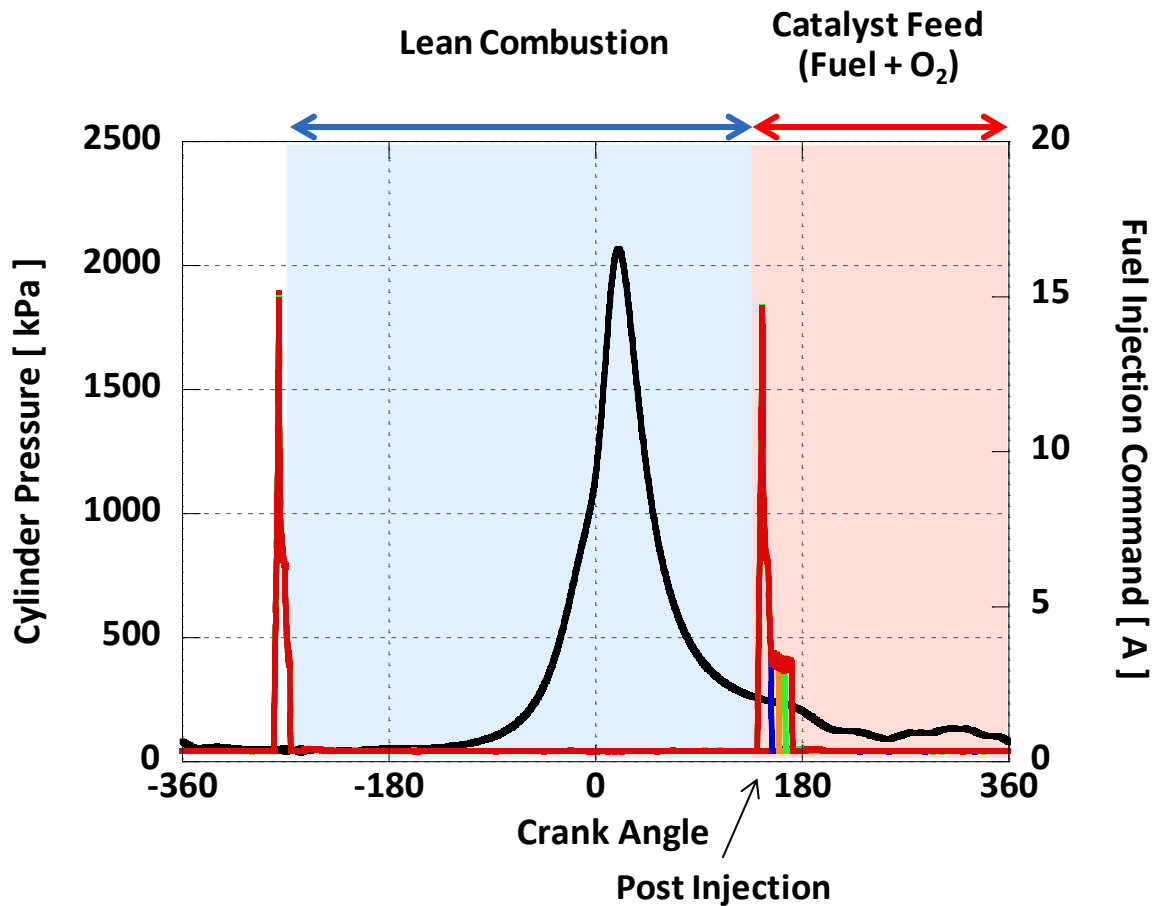
Figure 5.3. Cylinder pressure and fuel injection strategy for operation with catalyst reforming. Fuel-Lean combustion combined with a post-injection provides a fuel-rich catalyst with oxygen present.

The main combustion event was adjusted among four $\Phi_{combustion}$ conditions ($\Phi_{combustion} = 0.91$, 0.83, 0.77, and 0.71), resulting in four nominal oxygen flow rates to the catalyst ($\dot{m}_{O2} = 6.1$, 11.9, 17.5, and 23.3 g/min). A portion of the fuel that was delivered in the post-injection was not exhausted and sent to the catalyst, but rather was included in the trapped residuals and consumed in the subsequent combustion cycle. For the purpose of presenting results, that portion of fuel was neglected when calculating $\Phi_{combustion}$, $\dot{m}_{O2}$ and $\Phi_{catalyst}$. As a practical matter, though, the trapped residual fuel prevented us from precisely knowing the fuel energy and the composition being delivered to the reforming catalyst, effectively preventing elemental and energy balances to be conducted on the experimental results.

At each oxygen flow rate, the post-injection fuel was varied to yield an estimated $\Phi_{catalyst}$ ranging from 3.0 through 10.0. The minimum fuel delivered in the post-injection event was < 5 g/min, or about 10% of the fuel required by the remaining three cylinders to achieve 4.0 bar brake mean effective pressure (BMEP) at 2,000 rpm. The maximum fuel delivered in the post-injection was 66.6 g/min, or about 135% of the fuel required by the remaining three cylinders. Thus, this range of fuel flux over the catalyst, presented graphically in Figure 5.4, represents a wide operating range (note that the markers for conditions I, II, and III in Figure 5.4 are referred to in the Results section).
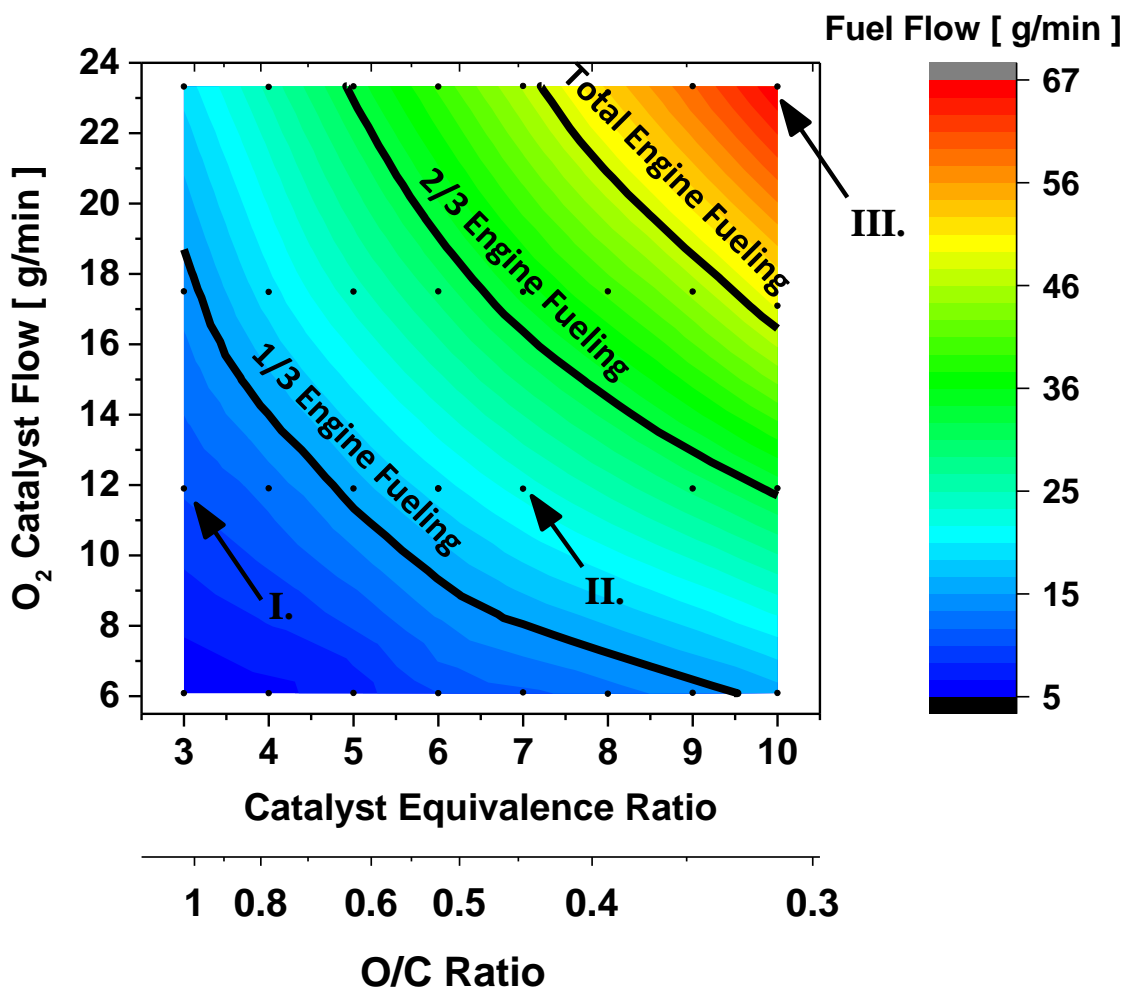
Figure 5.4. Fuel flow rate through the catalyst as a function of catalyst O_2 flow rate and catalyst.

We followed a systematic procedure at each experimental condition to ensure that if coking did occur, the catalyst was regenerated prior to the next condition. This procedure consisted of the following steps.

1. Operating the engine without the post-injection at the desired $\Phi_{combustion}$ and allowing the catalyst to thermally stabilize.

2. Once the catalyst stabilized, the data acquisition was started and allowed to run for about 1 min before the post-injection was started.

3. The post-injection was introduced, causing a step-change in $\Phi_{catalyst}$, and the system was allowed to operate under these conditions for about 7 min.

4. The air flow rate was reduced, and the post-injection was stopped at nearly simultaneous timing to produce $\Phi_{combustion} = 1.0$.

5. The $\Phi_{combustion}$ was gradually decreased by increasing the cylinder 4 air flow rate over the course of 5 min to allow any coke formed on the catalyst to be gradually oxidized, preventing a large and potentially damaging spike in temperature.

Throughout the chapter, the results from these conditions are presented in two ways: (a) the transient response to the step change in $\Phi_{catalyst}$ with the post-injection introduction and (b) the quasi-steady-state temperature profiles and species concentrations at the catalyst exit produced by the reforming process.

5.2.4 Experimental Methodology for Engine Performance Evaluation

While this full range of oxygen flow rates and the catalyst was investigated in the companion catalyst mapping investigation, it is noteworthy that only a portion of this operating map provided sufficient combustion stability in cylinders 1–3, as is discussed in the Results section.

While cylinder 4 was operated over the range of combustion described above, cylinders 1–3 were operated to maintain overall stoichiometric conditions in the exhaust to maintain compatibility with conventional three-way catalyst emissions control systems. As catalyst and

oxygen flow rate conditions changed, the amount of fuel energy contained in the EGR-reformate mixture also changed. Thus, the fueling rate in cylinders 1–3 was adjusted to maintain overall stoichiometric conditions and a constant brake load.

5.3 Results and Discussion

5.3.1 Energetics and Equilibrium Analysis

The energetics of the reforming process is dependent on the relative amount of steam vs. PO_x reforming, the H/C ratio of the fuel, and competing for equilibrium products. The energetics of the reforming process is dependent on the relative amount of steam vs. PO_x reforming, the H/C ratio of the fuel, and competing for equilibrium products. Equations 1 and 2 introduced the energetic differences of steam and PO_x reforming in the introduction of a single fuel. Figure 5.5 introduces the effect of H/C ratio by showing the ratio of product enthalpy to reactant enthalpy for a series of alkanes, olefins, and aromatics. The individual species enthalpy values were taken from Szybist et al. [152] and are referenced at a constant temperature and pressure condition and therefore do not consider sensible enthalpy effects. An enthalpy ratio less than unity represents a chemical energy loss during the reforming process, whereas an enthalpy ratio of greater than unity represents a chemical energy increase or TCR.

Figure 5.5 illustrates the limiting energetics when the reactions are constrained to either PO_x reforming or steam reforming only. PO_x reforming results in a chemical energy loss for all fuels, whereas steam reforming results in a chemical energy increase. The chemical energy loss for PO_x reforming decreases as the H/C ratio of the fuel increases. For example, methane (H/C = 4) experiences only a 4% energy loss whereas benzene (H/C = 1) experiences a 23% energy loss. The enthalpy ratio of steam reforming for all of the fuels considered shows a 15% to 25% chemical energy increase. Steam reforming shows some dependencies with regard to the H/C ratio but is overall not as sensitive to this factor. Interestingly, olefins have the lowest enthalpy reforming ratio for steam reforming.
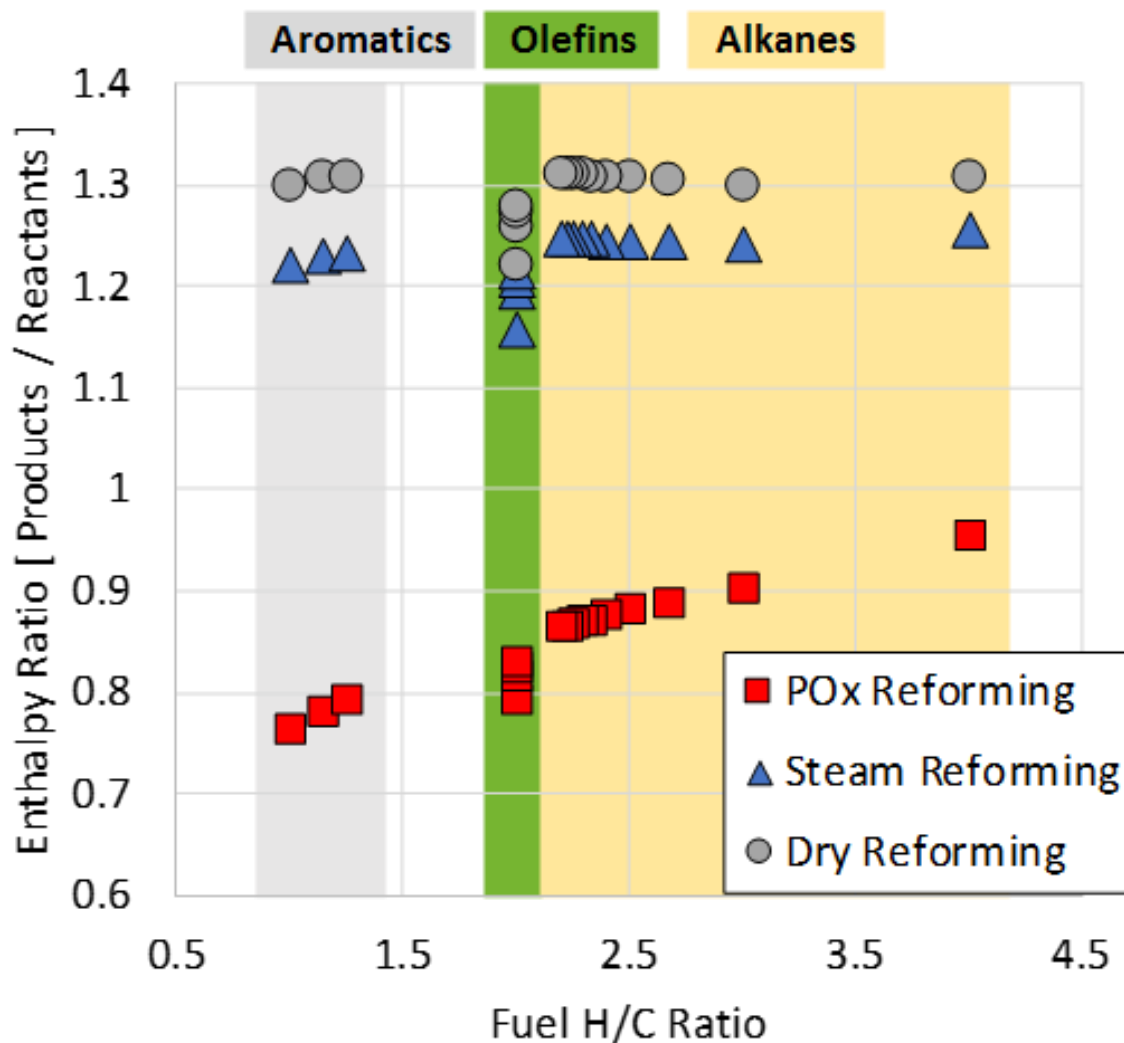
Figure 5.5. Enthalpy ratio of reforming as a function of the fuel H/C ratio for PO_x and steam reforming.

To understand the more complex realistic equilibrium product distributions, calculations were performed using CHEMKIN as described above with iso-octane and toluene over the range of initial temperatures, equivalence ratios, and oxygen concentrations investigated experimentally. These calculations considered all possible product species included in the LLNL gasoline kinetic mechanism. Iso-octane and toluene were chosen as initial reactants because they are commonly used in gasoline surrogates and because they have significantly different H/C ratios (iso-octane H/C = 2.25, toluene H/C = 1.14).

Figure 5.6 shows the calculated equilibrium reforming enthalpy ratios for two different initial temperatures, 500°C and 700°C, for both iso-octane and toluene. The reforming enthalpy ratios are presented as functions of $\Phi_{catalyst}$ of the mixture and the O_2 mole fraction. In addition to $\Phi_{catalyst}$, the abscissa is also labeled with the molar O/C ratio, as this is commonly used in describing reforming stoichiometry. First, it is notable that the enthalpy fraction is significantly higher for the higher starting temperature for both fuels, particularly for $\Phi > 5$. This indicates that the reforming energetics are enthalpy-limited at the high $\Phi_{catalyst}$. Steam reforming is highly endothermic and thus requires considerable initial sensible enthalpy to drive the equilibrium products to H_2 and CO. The enthalpy fraction results fall into two distinct operating regimes.

For $\Phi_{catalyst} < 5$, the enthalpy ratio is primarily a function of Φ, with very little dependence on the O_2 mole fraction. In this region, POx dominates, and fuel energy is consumed during the reforming process.

For $\Phi_{catalyst} > 5$, the enthalpy ratio becomes more dependent on the O_2 mole fraction, with higher O_2 mole fractions resulting in reduced enthalpy ratios. At these conditions, a higher O_2 mole fraction corresponds to a higher mole fraction of the fuel to maintain a constant $\Phi_{catalyst}$. As a result, more energy input is needed to drive the endothermic steam reforming reactions. At lower O_2 flow rates, the diluents carry sufficient sensible enthalpy to convert the fuel to H_2 and CO. At higher O_2 flow rates, the diluents make up a smaller fraction of the total and do not have sufficient sensible enthalpy. Thus, the higher the O_2 mole fraction, the higher the demand for energy input to drive the reaction toward the products with high chemical enthalpy: H_2 and CO.
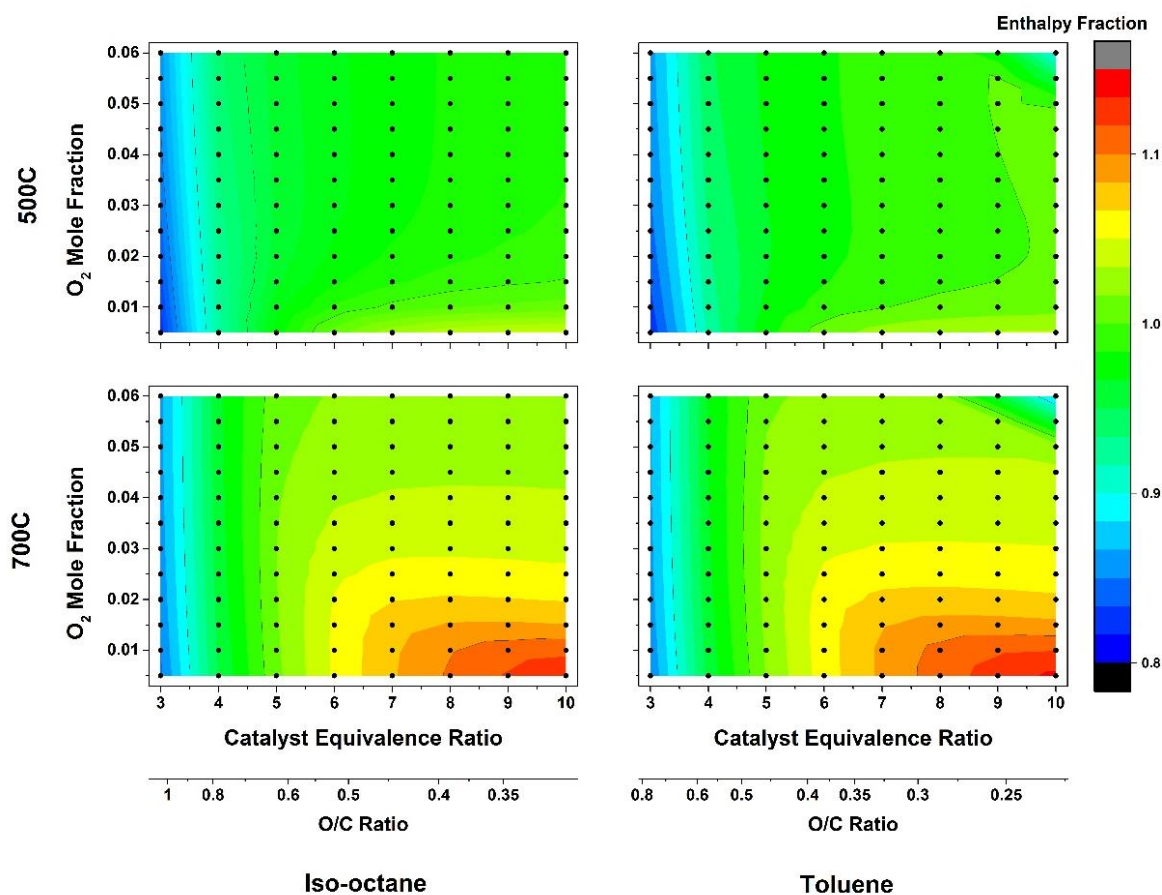
Figure 5.6. Enthalpy fraction of reforming products to the initial fuel with 500°C and 700°C for iso-octane and toluene.

From the above equilibrium modeling results, it is clear that the reforming products contain three major components: H_2, CO, and CH_4. The enthalpy fraction of each of these components relative to the reactant enthalpy is shown in Figure 5.6 for iso-octane at 700°C. The H_2 enthalpy fraction resembles the overall enthalpy fraction shown in Figure 5.8, exhibiting a maximum coincident with the overall enthalpy fraction maximum. The H_2 enthalpy accounts for anywhere from < 25% to > 75% of the initial fuel enthalpy. Relative to the other species, the CO enthalpy fraction shows only a small amount of variability over this range of conditions, accounting for 30%–50% of the total fuel energy. The CH_4 formation is highly dependent on the $\Phi_{catalyst}$ and oxygen mole fraction conditions. There is minimal CH_4 formation for a $\Phi_{catalyst}$ < 5, but substantial CH_4 at a $\Phi_{catalyst}$ > 5 at high O_2 concentrations. The CH_4 formation occurs in the region where the enthalpy balance becomes less favorable (Figure 5.6) and the H_2 concentration decreases (Figure 5.8). Thus, the enthalpy balance is

highest when H_2 and CO are formed, but CH_4 can also be a competing equilibrium product that degrades the enthalpy balance at high O_2 mole fraction concentrations.

Regardless of whether the initial reforming reactions are steam reforming (Equation 5.7) or dry reforming (Equation 5.8), WGS reactions will drive the system toward an equilibrium H_2/CO ratio. The H_2/CO ratio is a strong function of temperature, as shown in Figure 5.7 for a single starting condition ($\Phi_{catalyst} = 6$, O_2 mole fraction = 0.03). Thus, regardless of whether the initial mechanistic step is steam or dry reforming, WGS reactions will favor H_2 at low temperatures and favor CO at higher temperatures. It is interesting to note that the equilibrium H_2/CO ratio at 400°C is close to the H_2/CO ratio from steam reforming alone ($H_2/CO = 2.125$, as shown in Equation 5.9), and the H_2/CO ratio from dry reforming is asymptotically approached as the temperature exceeds 1400°C ($H_2/CO = 0.5$, Equation 5.10). The catalyst-out temperatures for the experimental portion of this study are all below 625°C.
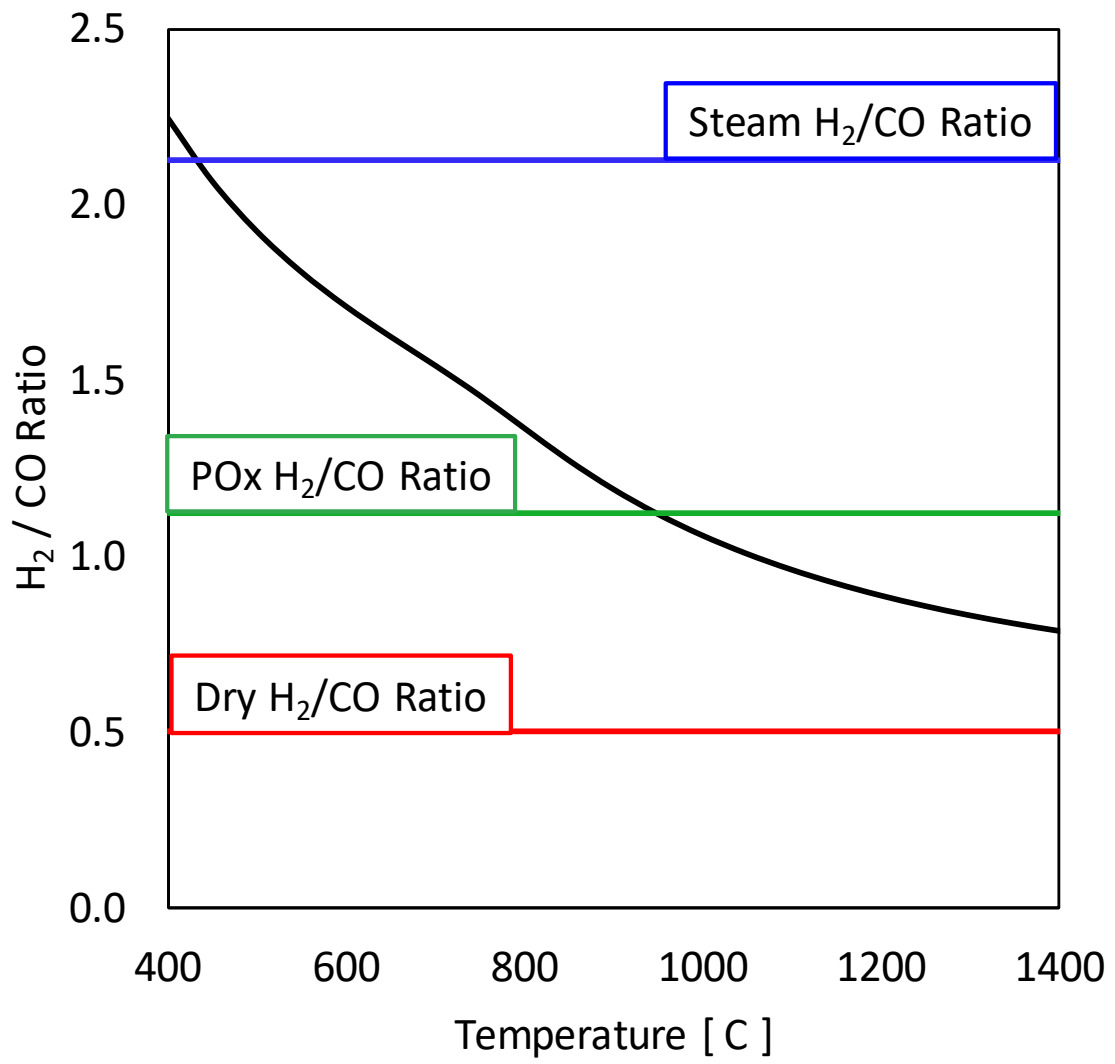
Figure 5.7. Equilibrium H_2/CO ratio as a function of temperature for initial conditions of $\Phi_{catalyst} = 6$, O_2 mole fraction = 0.03.
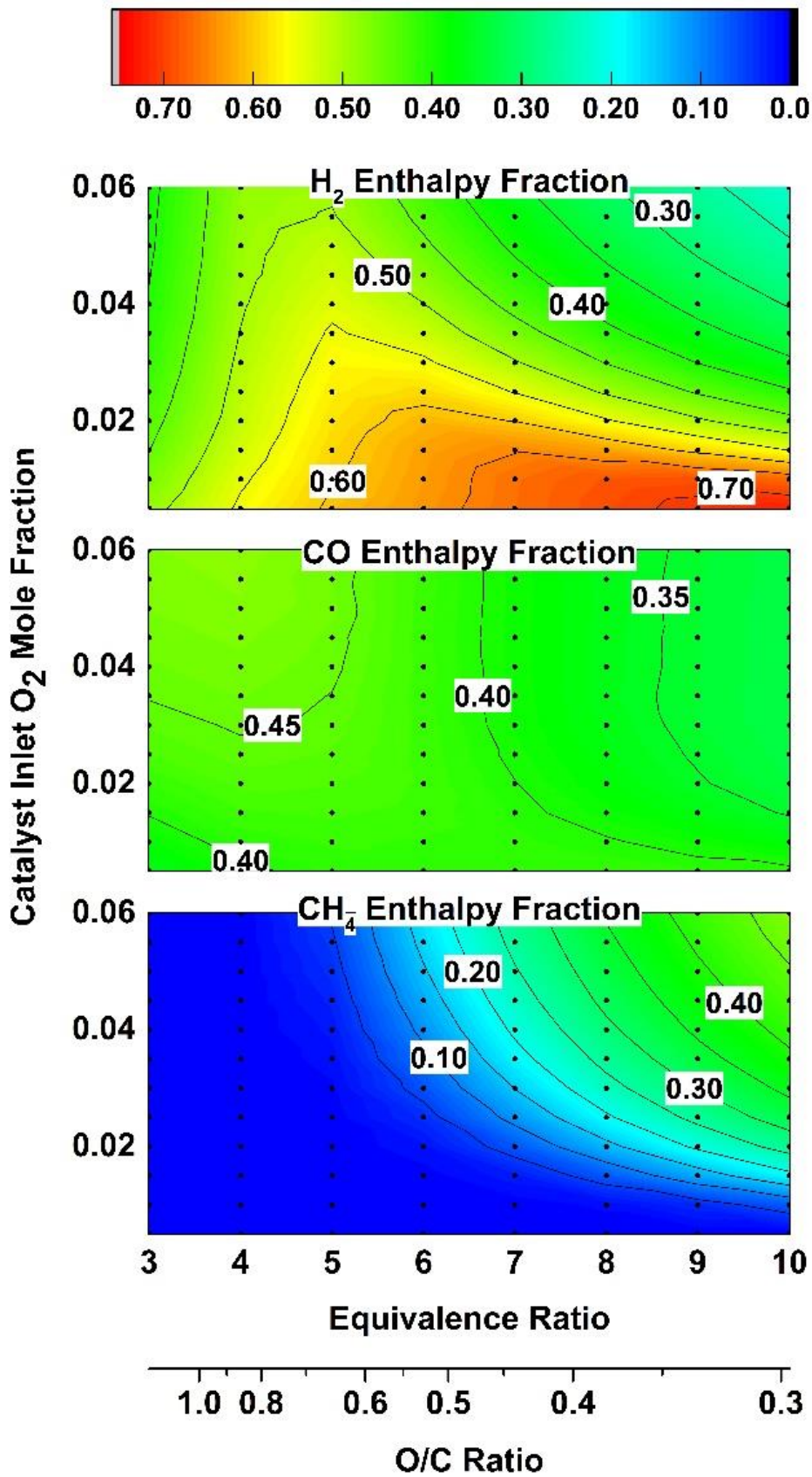
Figure 5.8. Enthalpy fraction of H_2 to the initial fuel with 700°C initial temperature for iso-octane.

Figure 5.6 shows that the reforming enthalpy ratio is highly dependent on the initial temperature for a $\Phi_{catalyst} > 5$, with higher temperatures resulting in a more favorable enthalpy balance.

Figure 5.8 shows that the less favorable enthalpy ratio can be attributed to the formation of CH_4. Increasing the initial temperature from 500°C to 700°C in Figure 5.9 results in a substantial decrease in CH_4 in this region, though significant concentrations of CH_4 persist.
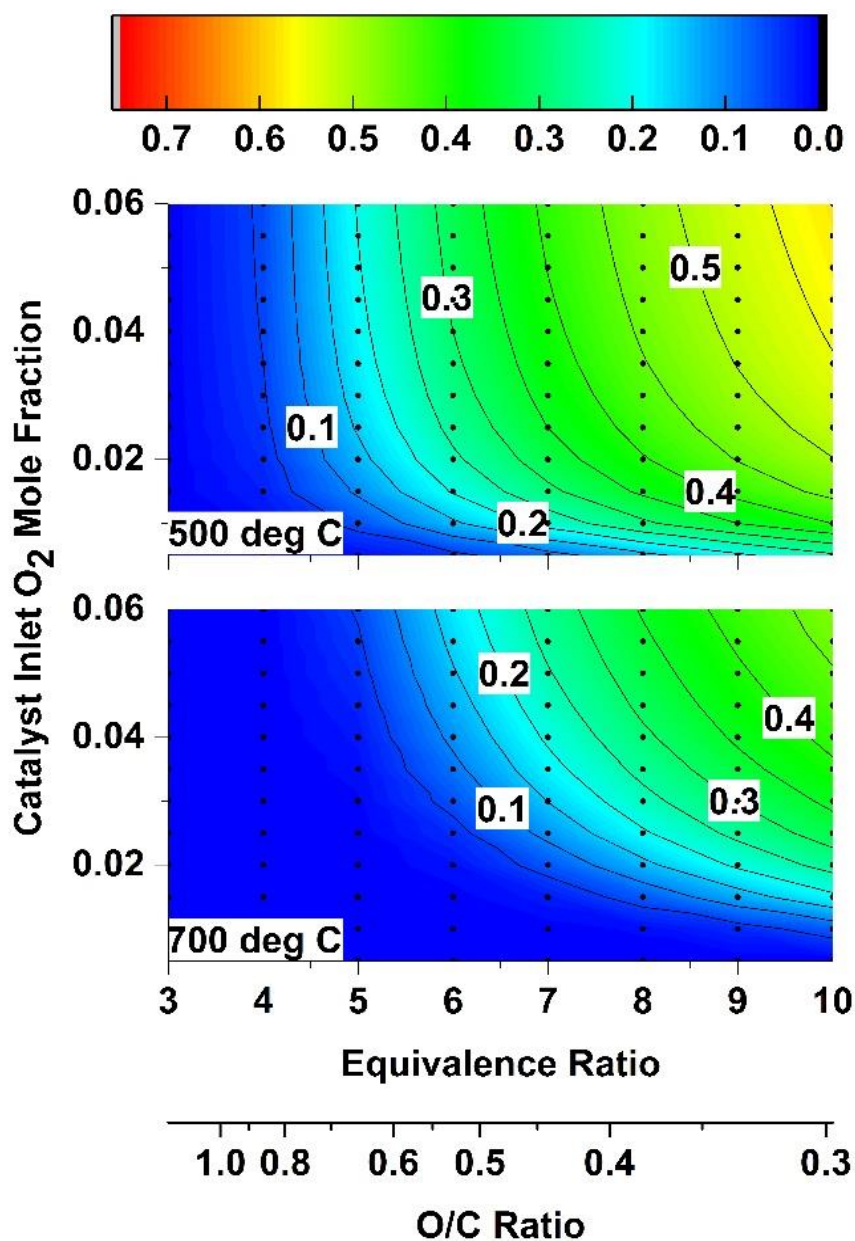
Figure 5.9. CH_4 equilibrium mole fraction with 500°C (top) and 700°C (bottom) initial temperature for iso-octane.

In summary, the equilibrium calculations reveal reforming products should be highly dependent on the initial temperature, $\Phi_{catalyst}$, O_2 mole concentration, and H/C ratio of the fuel. The most favorable energetics occur at a high $\Phi_{catalyst}$ with low O_2 mole fraction so that the diluent gases carry a sufficient sensible enthalpy to drive the endothermic steam reforming processes, thus avoiding the less favorable CH_4 formation. However, equilibrium calculations are based solely on thermodynamics and do not account for the actual reaction rates or the selectivity that may occur over the catalyst. In an engine environment, the timescale of reaction is limited by the size of catalyst and gas flow rate so that the products can differ from equilibrium results, and the reaction pathways over the catalyst may not reflect equilibrium. Furthermore, there can be substantial gradients in the catalyst temperature under realistic operating conditions, so the favored equilibrium products can vary significantly as a function of position within the catalyst monolith. Nonetheless, an equilibrium calculation allows us to set expectations for the energetics of the reforming reactions.

5.3.2 Achieving Quasi-Steady-State Reforming

The experimental procedure used to provide fuel to the catalyst as described in the experimental methodology section, where the post-injection to provide the fuel to the catalyst is introduced as a step-change. The catalyst does not immediately achieve a steady-state condition, but instead comes to a quasi-steady-state condition over several minutes as the catalyst achieves thermal equilibrium. The path to achieving quasi-steady-state operating conditions can vary significantly depending on the O_2 flow rate and $\Phi_{catalyst}$. Thus, the purpose of this section is to describe the transient response of the catalyst to the fueling step-change in an effort to understand the reforming process in more detail. It should be noted that the transients observed here are not intended to simulate vehicle operation, but rather to provide a better phenomenological understanding. The more realistic transient operation will be a focus of future work.

The actual reforming catalyst performance was measured at each of the O_2 flow rate and $\Phi_{catalyst}$ combinations shown in Figure 5.4. Each operating condition started with the lean operation ($\Phi_{combustion} < 1$) to set the O_2 flow rate, followed by the introduction of the

post-injection, causing a step-change in the $\Phi_{catalyst}$. With the step-change in $\Phi_{catalyst}$, it takes several minutes for the catalyst to achieve a quasi-steady-state condition. This section highlights the transient response of the catalyst to a step-change in $\Phi_{catalyst}$ at conditions I, II, and III, which are indicated in Figure 5.4.

The condition I, shown in Figure 5.10 is at an O_2 catalyst flow rate of 12 g/min and $\Phi_{catalyst} = 3$. When the fuel is introduced via post-injection, there is a slow increase in the catalyst mid-bed and outlet temperature, indicating that this is an exothermic process. The catalyst outlet temperature reaches a steady value after about 4 min of post-injection fueling. The CO_2 and H_2O concentrations do not change significantly with the introduction of the post-injection. There is a step-change increase in the H_2 and CO concentrations, from near zero to about 5% CO and 7%–8% H_2. Additionally, CH_4 is formed at a concentration of 1,000 ppm. Nearly all of the input iso-octane is converted across the catalyst, with < 200 ppm iso-octane measured at the catalyst output.
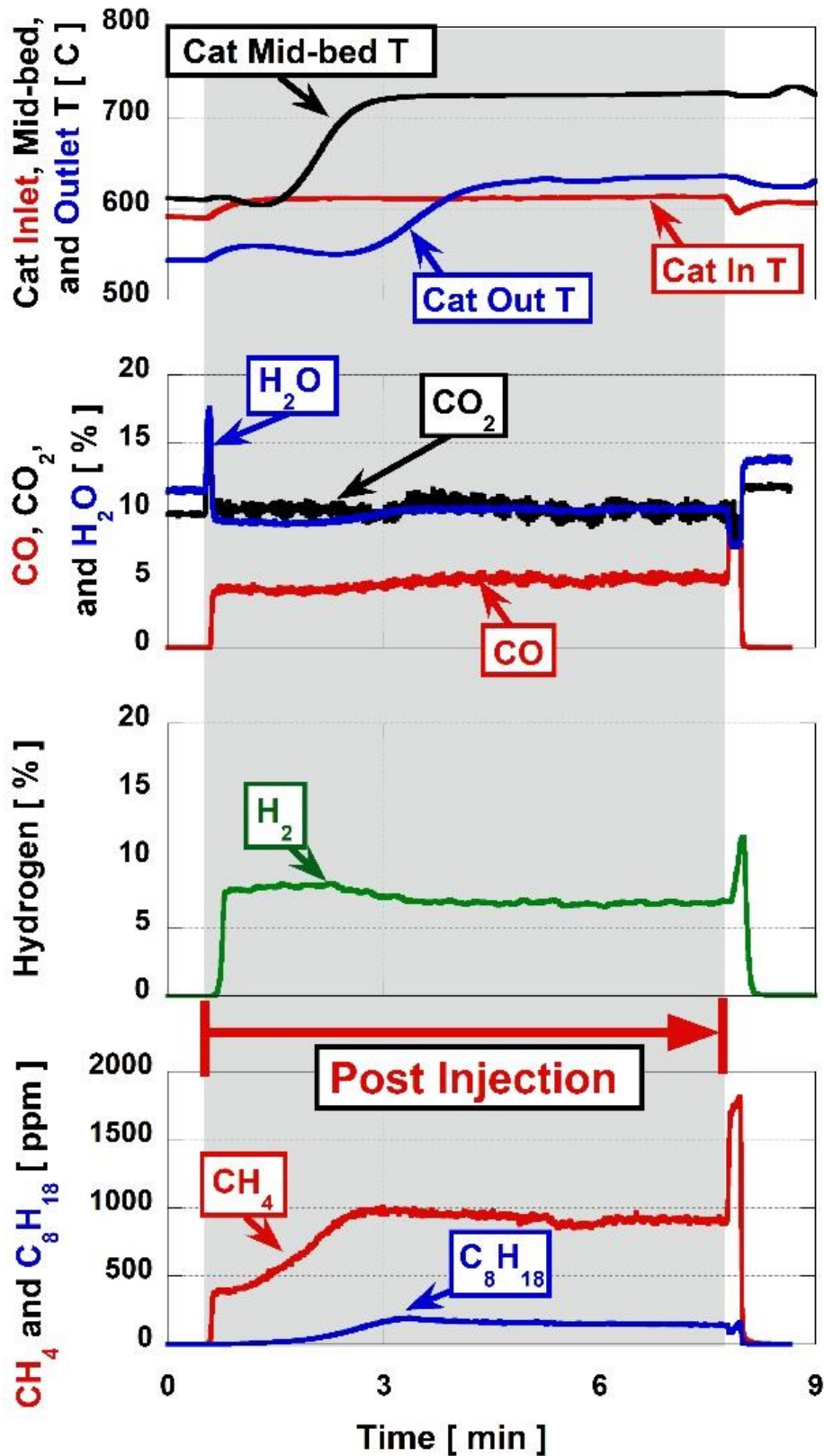
Figure 5.10. Transient response of the exit concentrations of catalytic reforming products and the monolith temperature profile at an O_2 catalyst flow rate of 12 g/min and $\Phi_{catalyst} = 3$ (The condition I in Figure 5.4).

Condition II in Figure 5.4 also uses an O_2 catalyst flow rate of 12 g/min, but at a richer condition, $\Phi_{catalyst} = 7$, and is shown in Figure 5.11. In contrast to the condition I, where the mid-bed and outlet temperatures increased as a function of time, each of these temperatures decrease by more than 100°C within 2 min of the initiation of the post-injection. A decrease in temperature is indicative of the endothermic steam reforming process. Also, indicative of steam reforming is the lower H_2O concentration and the higher H_2 concentration compared to condition I. The H_2O concentration decreases from about 12% before the post-injection to about 5% during the post-injection, indicating that it is being consumed in the catalyst as a reactant during steam reforming, and the concentration of H_2 is 13%–15%, about double the concentration of condition I. Taken together, the trends associated with CO, CH_4, and iso-octane reveal an interesting behavior. There is a spike in CO and CH_4 immediately after the post-injection is introduced, with more than 10% CO and 1.5% CH_4. The initial spike slowly decreases as the iso-octane concentration at the catalyst outlet increases, while simultaneously the catalyst-out temperature decreases. This demonstrates that as the catalyst temperature decreases, the fuel conversion decreases, once again demonstrating that the reforming process is enthalpy limited. The H_2 concentration remaining nearly constant despite large transient changes in the other species indicates that the H_2 concentration alone is not a complete descriptor of the reforming process.
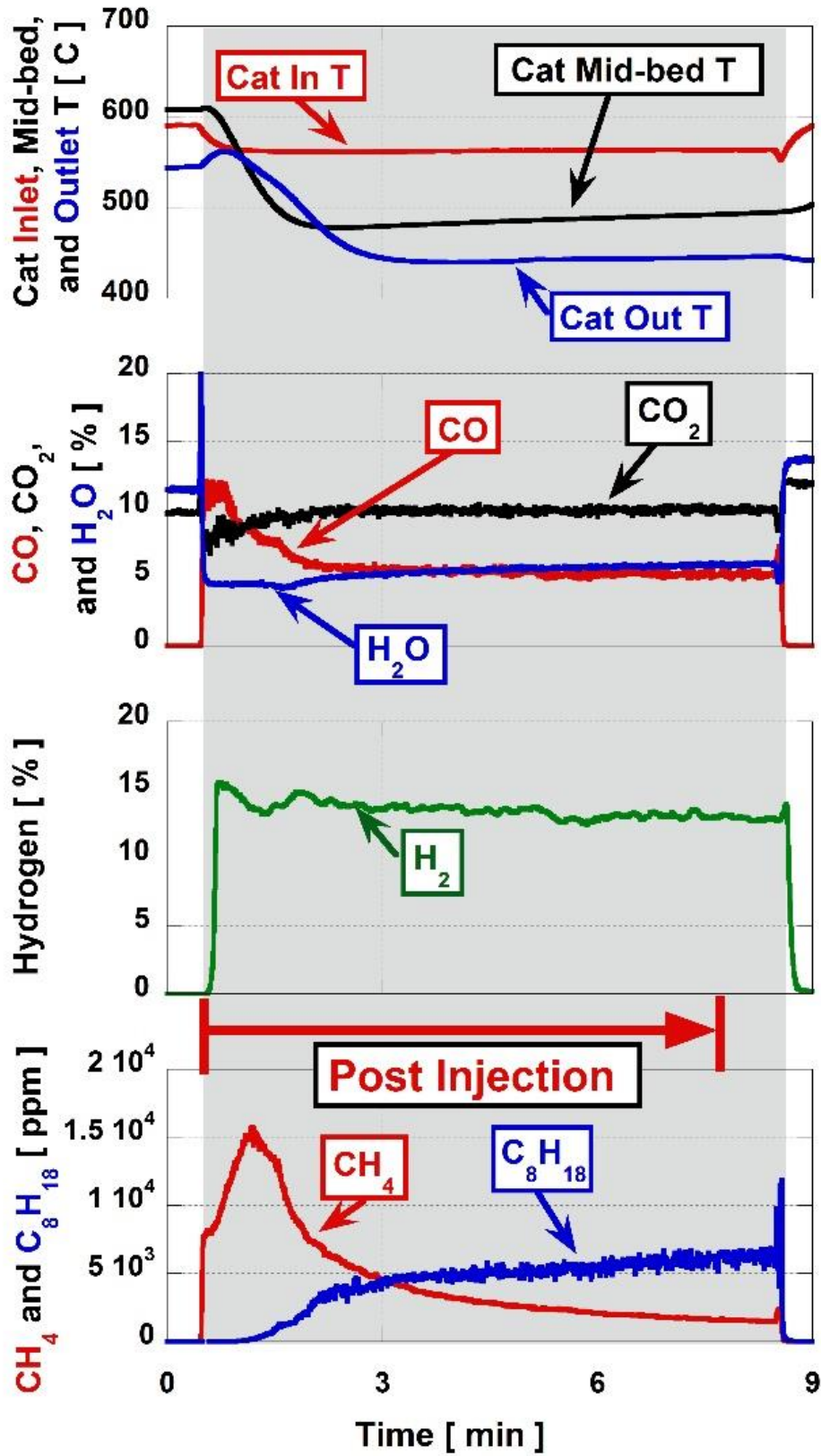
Figure 5.11. Transient response of the exit concentration of catalytic reforming products and monolith temperature profile at an O_2 catalyst flow rate of 12 g/min and $\Phi_{catalyst} = 7$ (condition II in Figure 5.4).

The transient response at condition III in Figure 5.4, shown in Figure 5.12, is at an O_2 flow rate of 23 g/min and $\Phi_{catalyst} = 10$. As with condition II, there is a decrease in the mid-bed and outlet temperatures of more than 100°C that occurs within 2 min of the introduction of the post-injection. When the post-injection initially occurs, there is a spike in the CO, H_2, and CH_4 concentrations, followed by a rapid decline. Concurrently, there is an initial large decrease in H_2O concentration, down to less than 2%, followed by an increase in its concentration. These concentration spikes then decrease as the catalyst outlet temperature decreases. It is believed that after the initial spike occurred, there was also an increase in the iso-octane concentration. However, the FTIR analyzer became saturated, and reliable measurement of iso-octane at this condition was not possible with the measurement techniques used for this experiment.
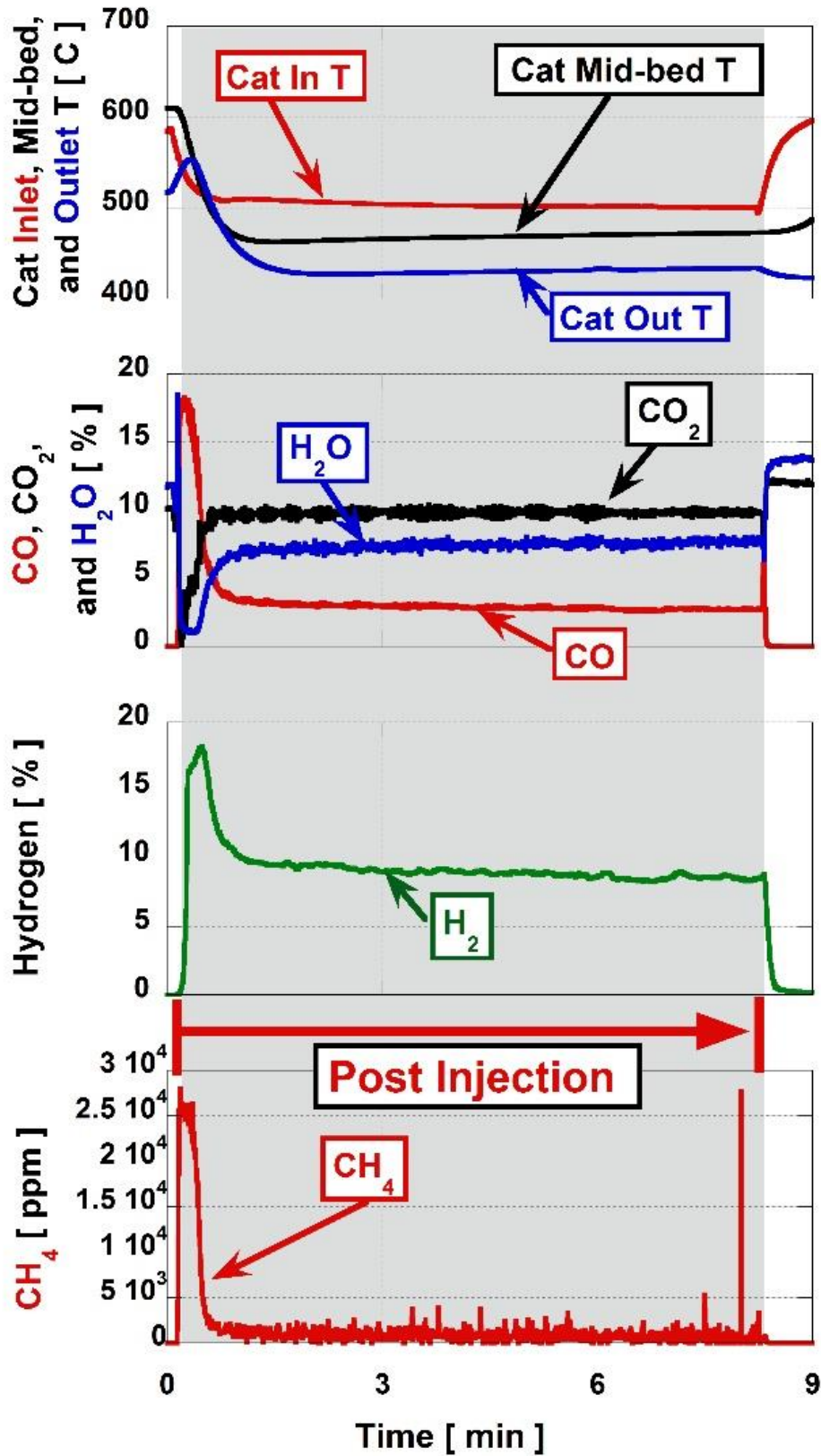
Figure 5.12. Transient response of the exit concentration of catalytic reforming products and the monolith temperature profile at an O_2 catalyst flow rate of 23 g/min and $\Phi_{catalyst} = 10$ (condition III in Figure 5.4).

Thus, it is clear that the catalyst performance is dependent on the O_2 flow rate and $\Phi_{catalyst}$ condition. The performance can range from being exothermic at the lowest $\Phi_{catalyst}$ investigated to being enthalpy-limited with a significant amount of unconverted fuel at the highest $\Phi_{catalyst}$. For the next section, the quasi-steady-state operation of the catalyst is compared at the various operating conditions. This considers only the data where the catalyst outlet temperature is within 10°C of the final temperature.

5.3.3 Quasi-Steady-State Performance of Catalytic EGR-Loop Reformer

Based on the equilibrium calculations described above, the major energy-containing reforming products are H_2, CO, and CH_4. The concentrations of each of these products are shown as functions of O_2 flow rate and $\Phi_{catalyst}$ in Figure 5.13 through Figure 5.15 As illustrated in the previous section, steady-state reforming products are highly dependent on operating conditions, and Figure 5.13 shows that the catalyst-out H_2 concentration ranges from 4% to 15%. The highest H_2 concentrations occur for $4 < \Phi_{catalyst} < 7$, and for O_2 flow rates of 12 g/min and higher. For $\Phi_{catalyst} > 7$, steam reforming dominates but fuel conversion is enthalpy limited, so overall H_2 production is low. For $\Phi_{catalyst} < 4$, there is too much air, and there is a shift to more complete oxidation, leading to water generation rather than H_2 production. Figure 5.14 shows that the peak in CO concentration largely mirrors the H_2 concentration, with the exception that the peak CO occurs at slightly leaner conditions: $3.5 < \Phi_{catalyst} < 5.5$.
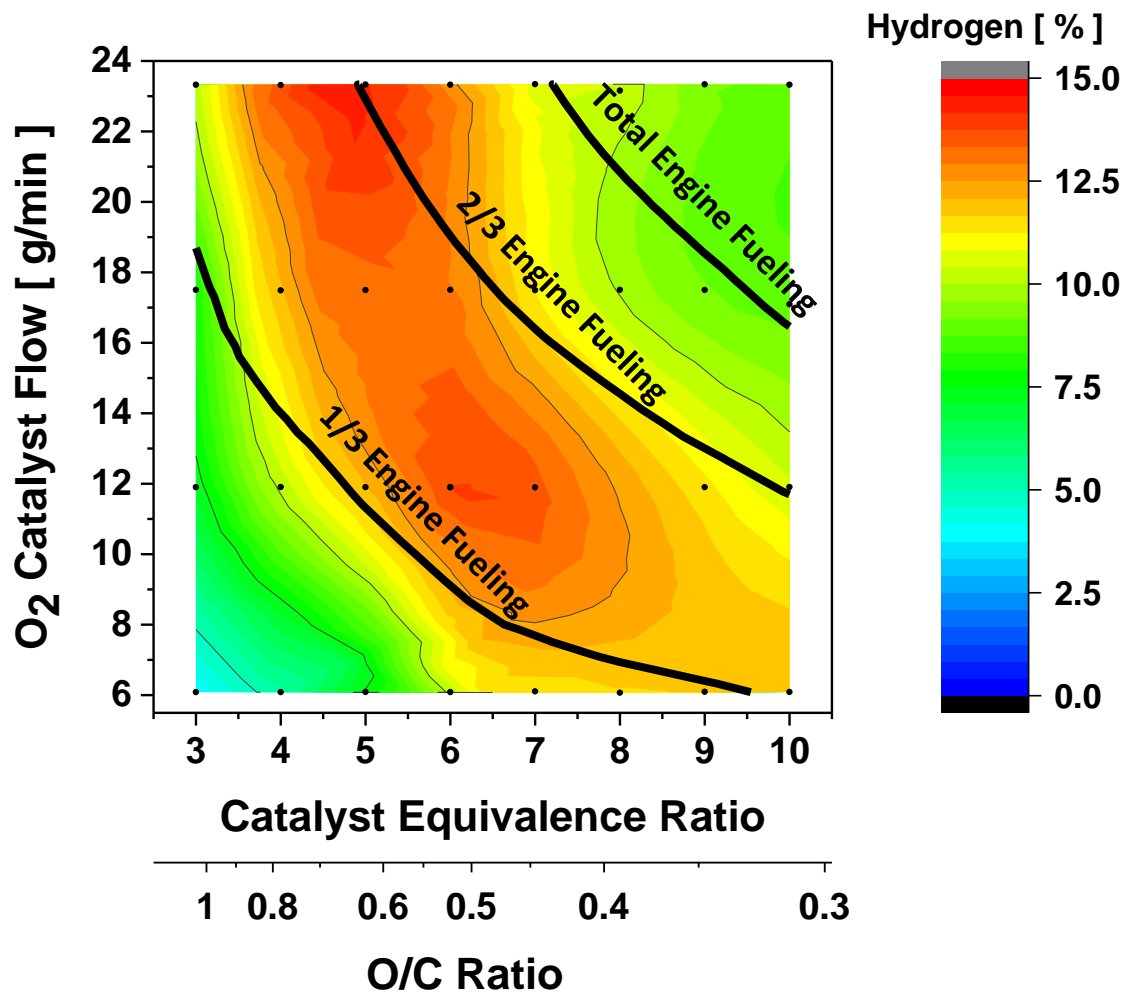
Figure 5.13. H_2 concentrations at the outlet of the catalyst as functions of $\Phi_{catalyst}$ and O_2 flow into the catalyst.
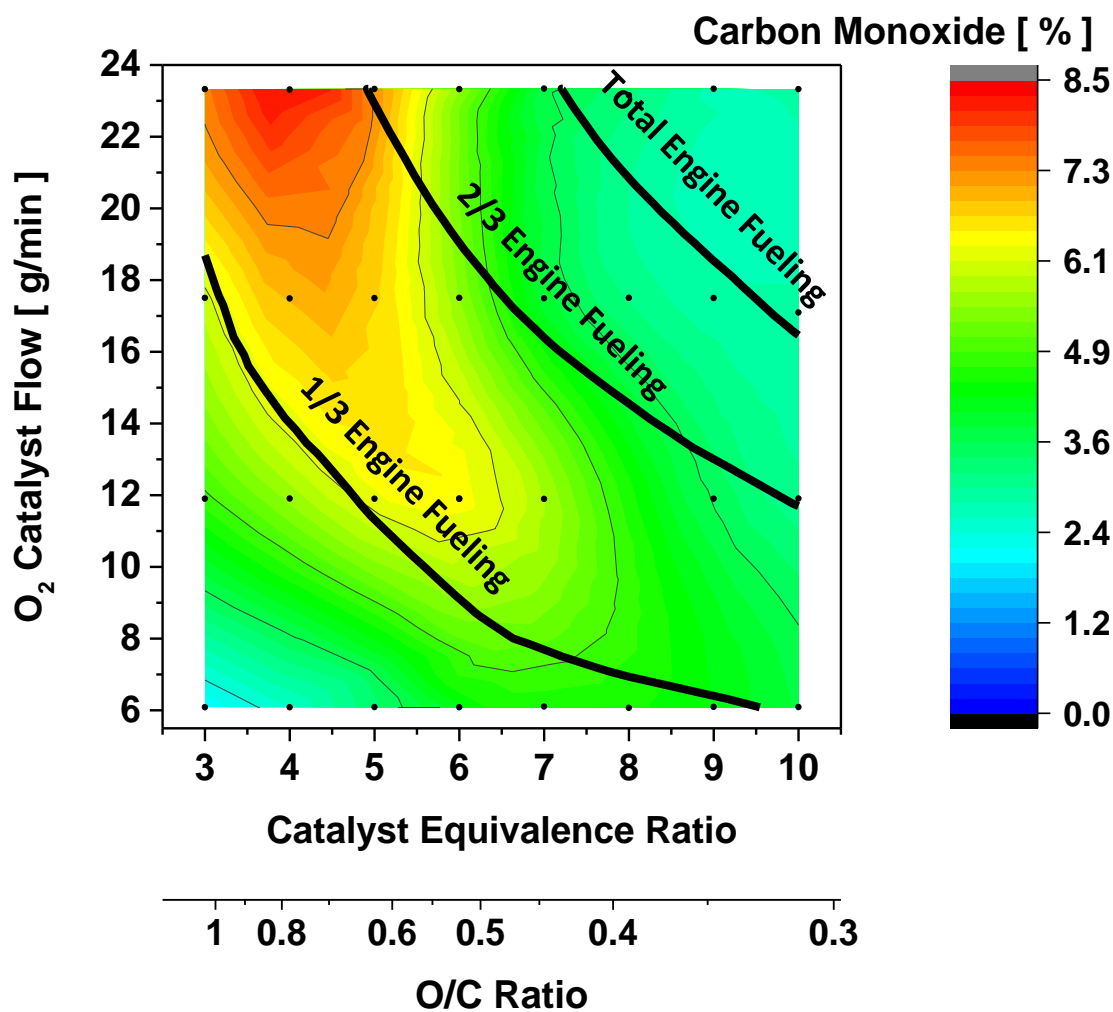
Figure 5.14. Carbon monoxide concentrations at the outlet of the catalyst as functions of $\Phi_{catalyst}$ and O_2 flow into the catalyst.

Figure 5.15 reveals that the CH_4 concentrations are low (about 300 ppm) for much of the experimental space investigated, but there is a high-magnitude band where catalyst-out CH_4 was measured to be in excess of 10,000 ppm. Initially, this finding seems to be counter to the equilibrium modeling findings where CH_4 was found to be highest at the highest O_2 mole fractions and highest $\Phi_{catalyst}$. It is worth noting, though, that equilibrium calculations do not consider the timescales required to achieve equilibrium, nor do they consider whether the catalyst is an effective means of achieving equilibrium at all temperatures considered. There is only a short amount of time for reactions to occur in the catalyst (residence time < 100 ms, space velocity of 37,000 h^{-1}), and as previously established in the Energetics and Equilibrium Analysis section, the high $\Phi_{catalyst}$ and high O_2 flow rate conditions are the most

enthalpy-limited. If the endothermic reactions cause a sufficient temperature decrease, the catalyst activity will cease, and the CH_4 concentrations will not reach equilibrium.
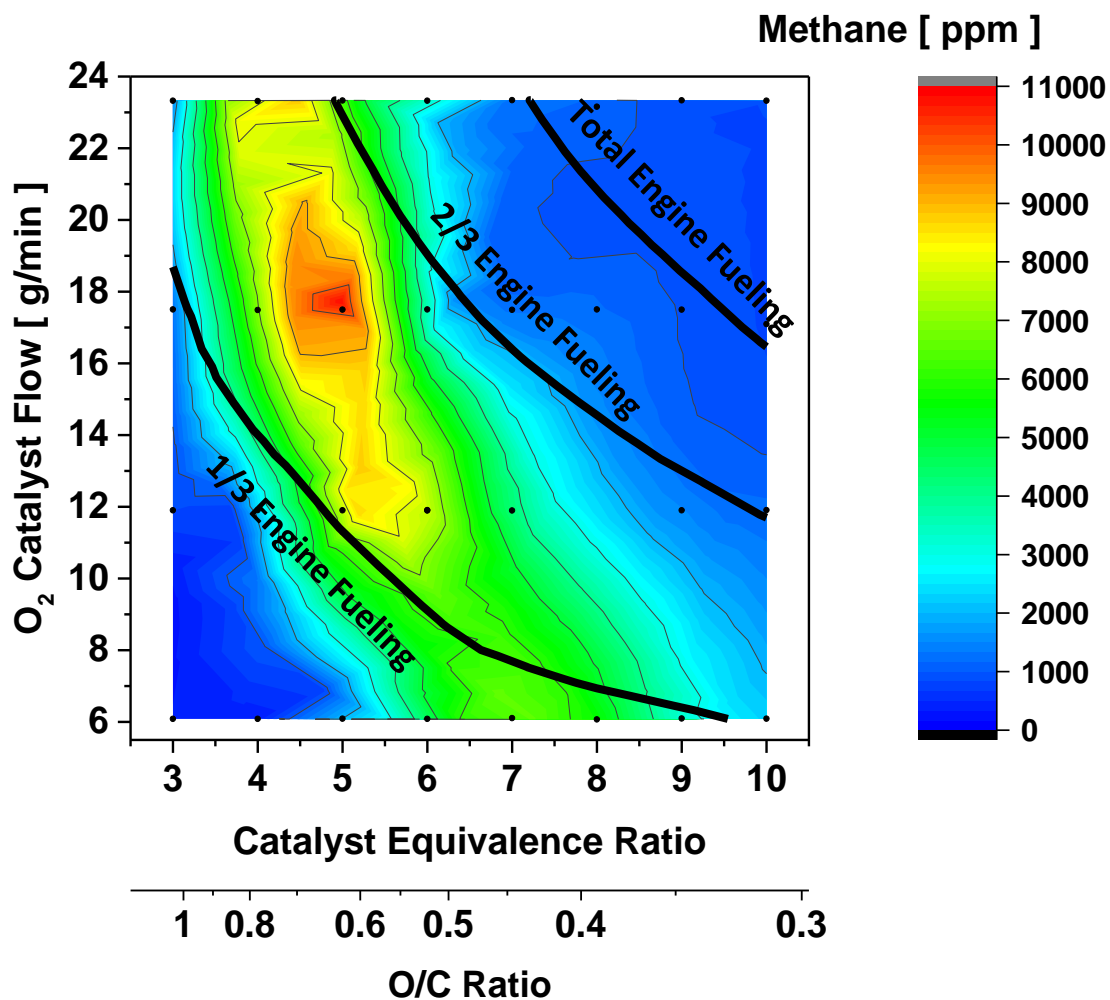
Figure 5.15. CH_4 concentrations at the outlet of the catalyst as functions of $\Phi_{catalyst}$ and O_2 flow into the catalyst.

Figure 5.16 shows the catalyst-out water concentration over the experimental space investigated. The water concentration contour plot is, in many ways, the inverse of that for H_2 concentration in Figure 5.13. Instead of the maximum in H_2 concentration, there is a minimum in water concentration for $4 < \Phi_{catalyst} < 7$ and for O_2 flow rates of 12 g/min and higher. Low water concentration is an indication that water is being consumed in the catalyst.
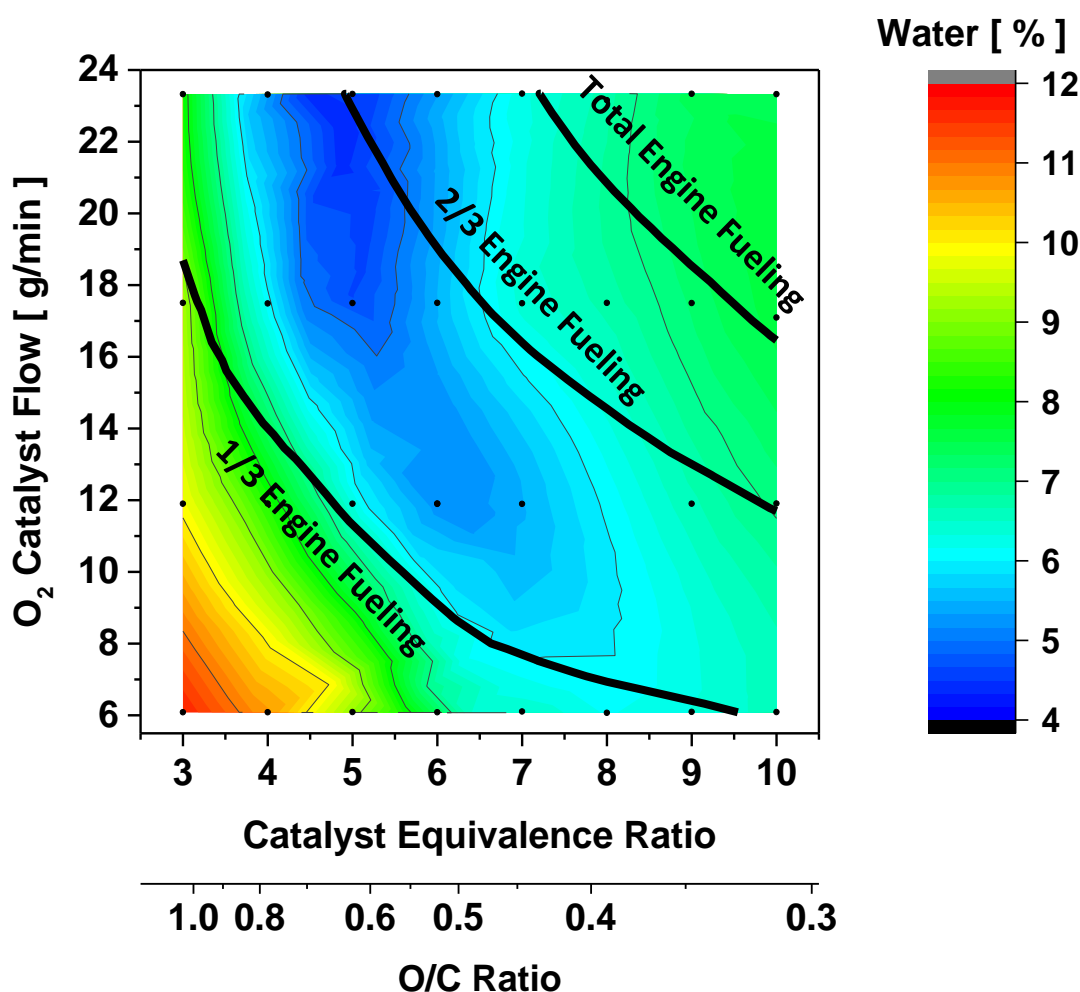
Figure 5.16. H$_2$O concentrations at the outlet of the catalyst with a sweep of equivalence ratio in the catalyst and O$_2$ flow rate into the catalyst.

Water consumption can occur in two ways: steam reforming and the WGS reaction. Further insight into the type of chemistry occurring over the catalyst can be gained by investigating the H$_2$/CO ratio, shown in Figure 5.17. For iso-octane, the H$_2$/CO$_{POx}$ = 1.125, and H$_2$/CO$_{Steam}$ = 2.125. Figure 5.18 shows that for all conditions investigated the H$_2$/CO > H$_2$/CO$_{POx}$, and for Φ > 5.5, H$_2$/CO > H$_2$/CO$_{Steam}$. This is an indication that WGS chemistry does occur and plays an important role in increasing the overall H$_2$/CO ratio at some conditions. Interestingly, the highest H$_2$/CO ratios, which indicate more WGS chemistry, occur at the highest $\Phi_{catalyst}$ conditions rather than where the highest H$_2$ yields and the lowest H$_2$O concentrations are observed.
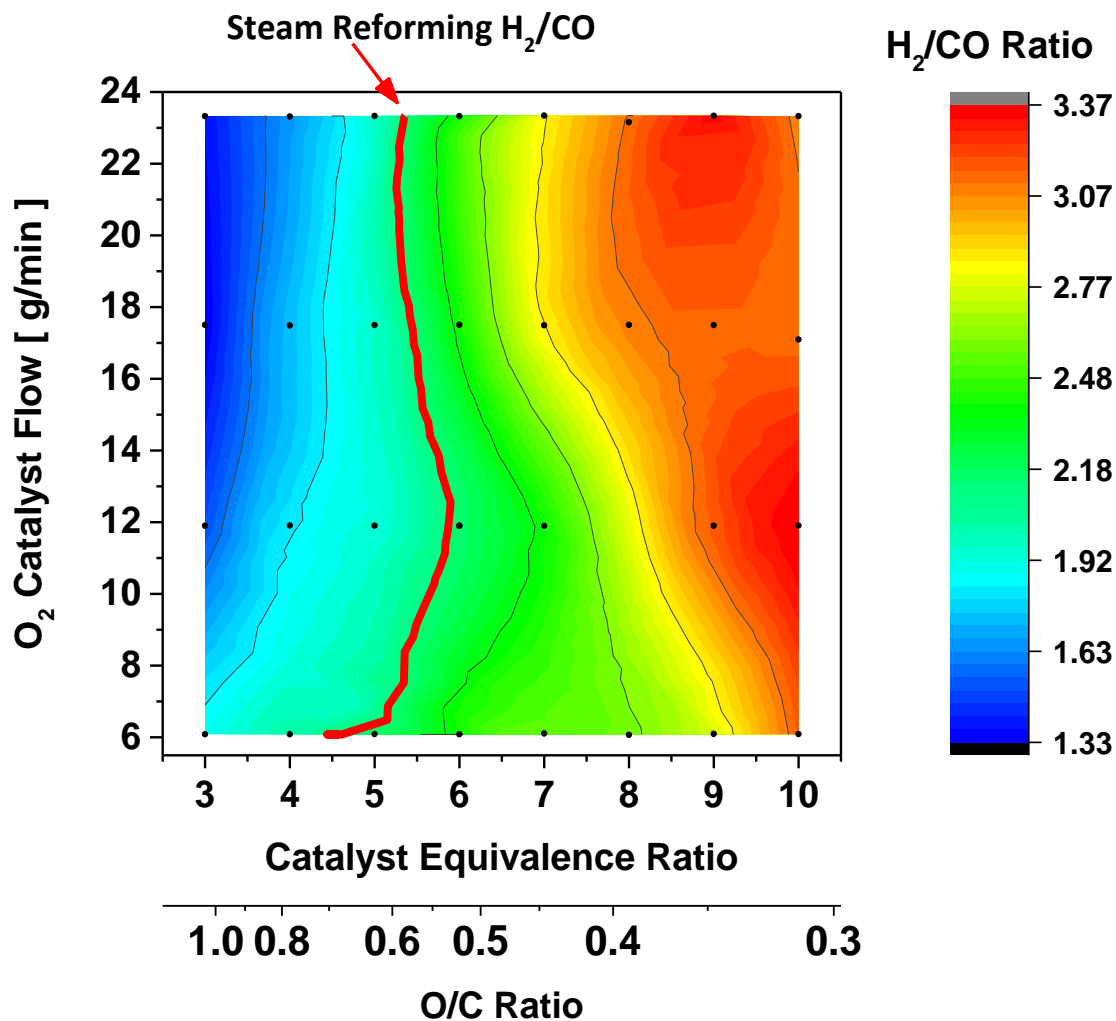
Figure 5.17. H2/CO at the outlet of the catalyst with a sweep of equivalence ratio in the catalyst and O2 flow rate into the catalyst.

Because the production of H_2 in the WGS reaction is slightly exothermic, Le Chatelier's principle suggests that a lower temperature will favor H_2 production. Figure 5.18 shows the H_2/CO ratio as a function of catalyst-out temperature. Interestingly, all of the O_2 flow rate conditions collapse to show a very similar trend: when the exhaust temperature is below about 475°C, the H_2/CO ratio is higher than what would be expected from steam reforming alone. Thus, while WGS chemistry is present and it does shift the H_2/CO ratio, it plays a greater role at low catalyst temperatures and high $\Phi_{catalyst}$, where the reforming activity is low.
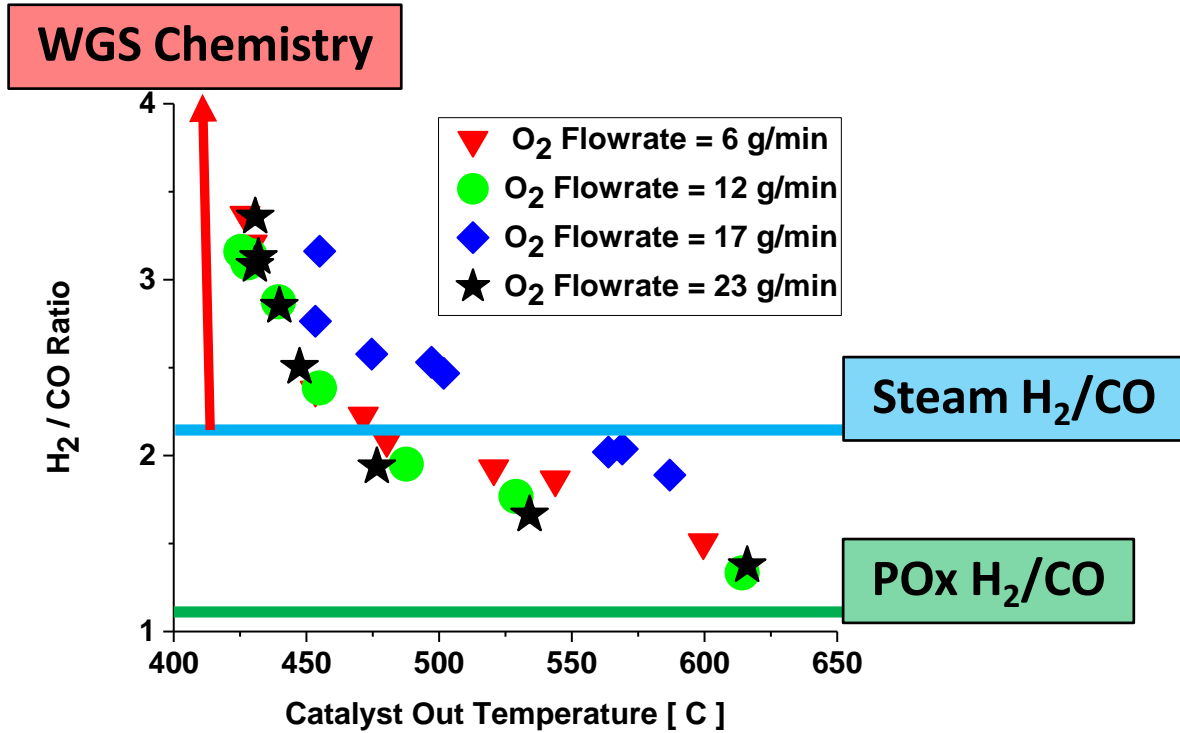
Figure 5.18. Correlation of H_2/CO ratio and the catalyst-out temperature with a sweep of equivalence ratio in the catalyst and O_2 flow rate into the catalyst. (POx = partial oxidation; WGS = water-gas shift.)

5.3.4 Thermal Analysis of the Catalyst

Figure 5.10 through Figure 5.12 illustrated that the catalyst mid-bed temperatures could either increase or decrease, depending on the dominant chemistry. Figure 5.19 (a) and (b) show the temperature change across the first and second catalyst monoliths to provide a more direct indication of the type of chemistry that occurs under the conditions investigated. Over the first catalyst monolith, Figure 5.19(a), there is a temperature increase for $\Phi_{catalyst} < 4$ indicating exothermic chemistry, and there is a temperature decrease for $\Phi_{catalyst} > 5$ indicating endothermic chemistry. The second catalyst monolith, Figure 5.19(b), does not show any signs of exothermic chemistry. In contrast to the first catalyst monolith, the greatest temperature decreases are for the lowest $\Phi_{catalyst}$, and the highest $\Phi_{catalyst}$ shows very little temperature change. This can again be attributed to enthalpy-limited chemistry. At a low $\Phi_{catalyst}$, the mid-bed temperature is sufficiently high to drive endothermic reactions in the second catalyst monolith. However, at a high $\Phi_{catalyst}$, all of the endothermic chemistry in the

first catalyst monolith has already decreased the temperature significantly so that there is very little activity in the second catalyst monolith.
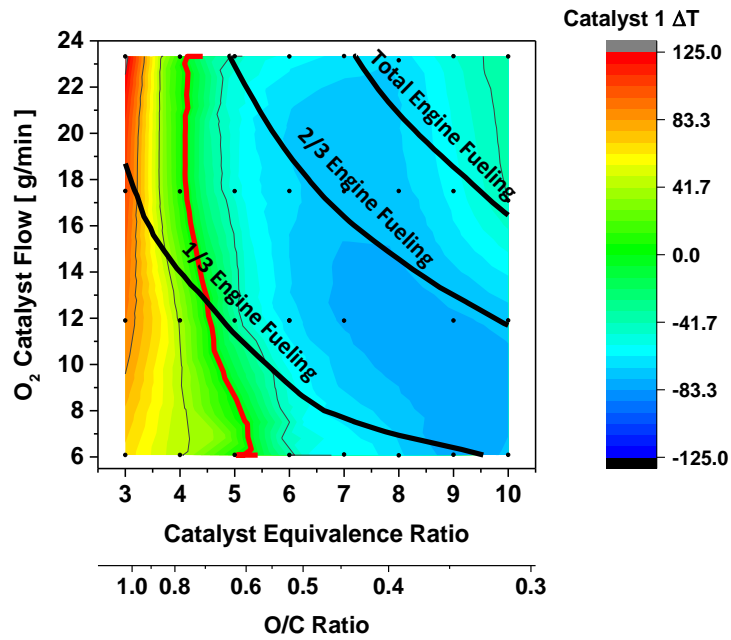
(a)
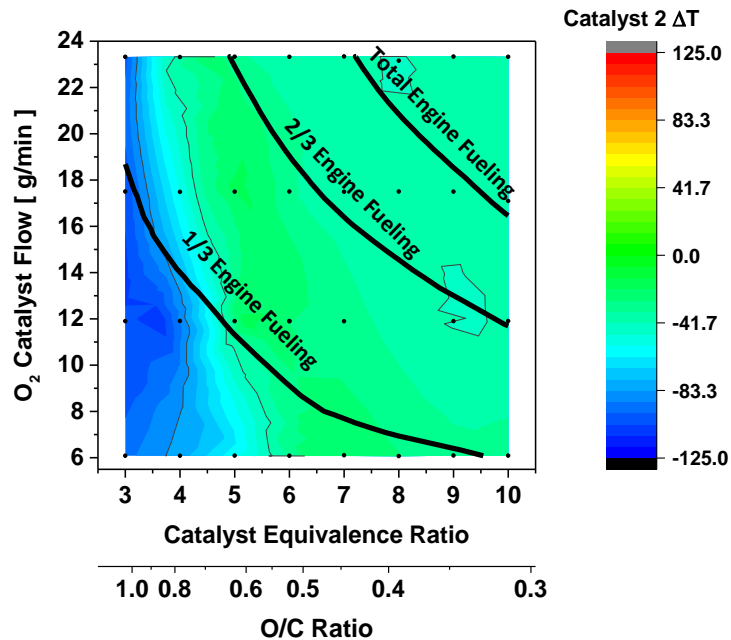
(b)

Figure 5.19. Temperature change in the first and second catalyst: (a) mid-bed temperature minus inlet temperature and (b) outlet temperature minus mid-bed temperature.

5.3.5 Effect of Exhaust Gas Recirculation Dilution on Baseline Engine

To assess the effects of reformate on the combustion process relative to conventional EGR, baseline experiments using conventional EGR were conducted with the same experimental engine. Figure 5.20 illustrates how the heat release rate changes with increasing amounts of EGR. Note that the CA50 combustion phasing was held constant at 8 CAD ATDC$_f$, necessitating that the spark timing is advanced as EGR was added. The peak heat release rate drops by more than 35% at the highest EGR concentration, and the combustion duration increases correspondingly. The increase in the combustion duration with EGR is shown in Figure 5.21, where the timing of the spark, 5% mass fraction burned (CA05), 50% mass fraction burned (CA50), and 85% mass fraction burned (CA85) are indicated. While most portions of the combustion process elongate with increasing EGR, the interval between the spark and CA05 increases the most, which is consistent with previous findings [50]. Figure 5.22 shows the spark-to-CA05 duration and the coefficient of variation (COV) of the indicated mean effective pressure (IMEP), which is a metric of combustion stability. Combustion is stable for all EGR concentrations below 25% (COV < 3%), corresponding to spark-to-CA05 durations shorter than 40 CAD. Combustion instability increases dramatically at higher EGR concentrations, where spark-to-CA05 durations are longer than 40 CAD. The increased instability is a direct result of the reduced laminar flame speed with EGR, causing the initial flame kernel growth to be longer and making the process more susceptible to stochastic turbulence variations [50][67].
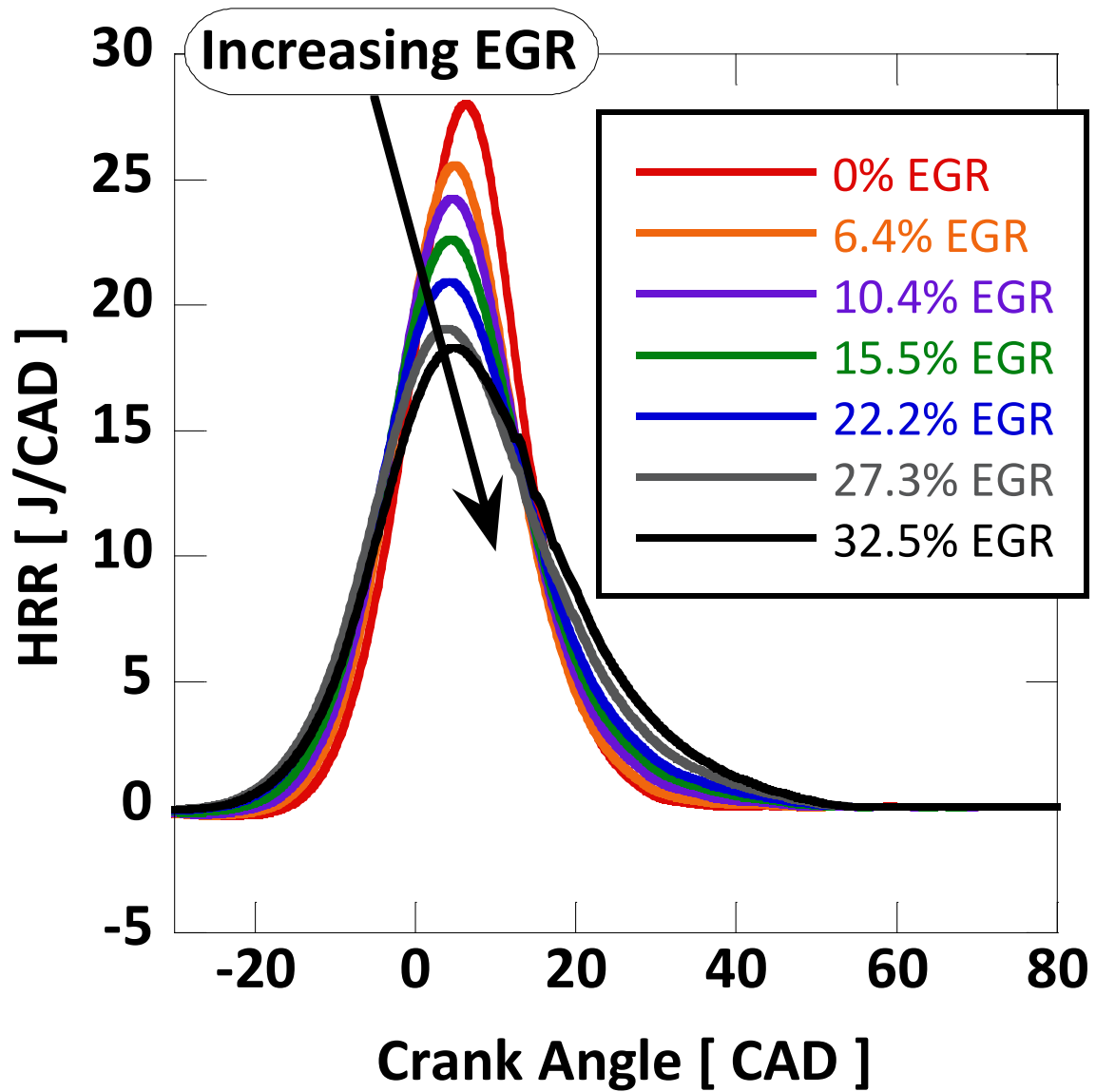
Figure 5.20. Baseline heat release rate as a function of crank angle with different exhaust gas recirculation (EGR) rates. (HRR = heat release rate; CAD = crank angle degrees.)
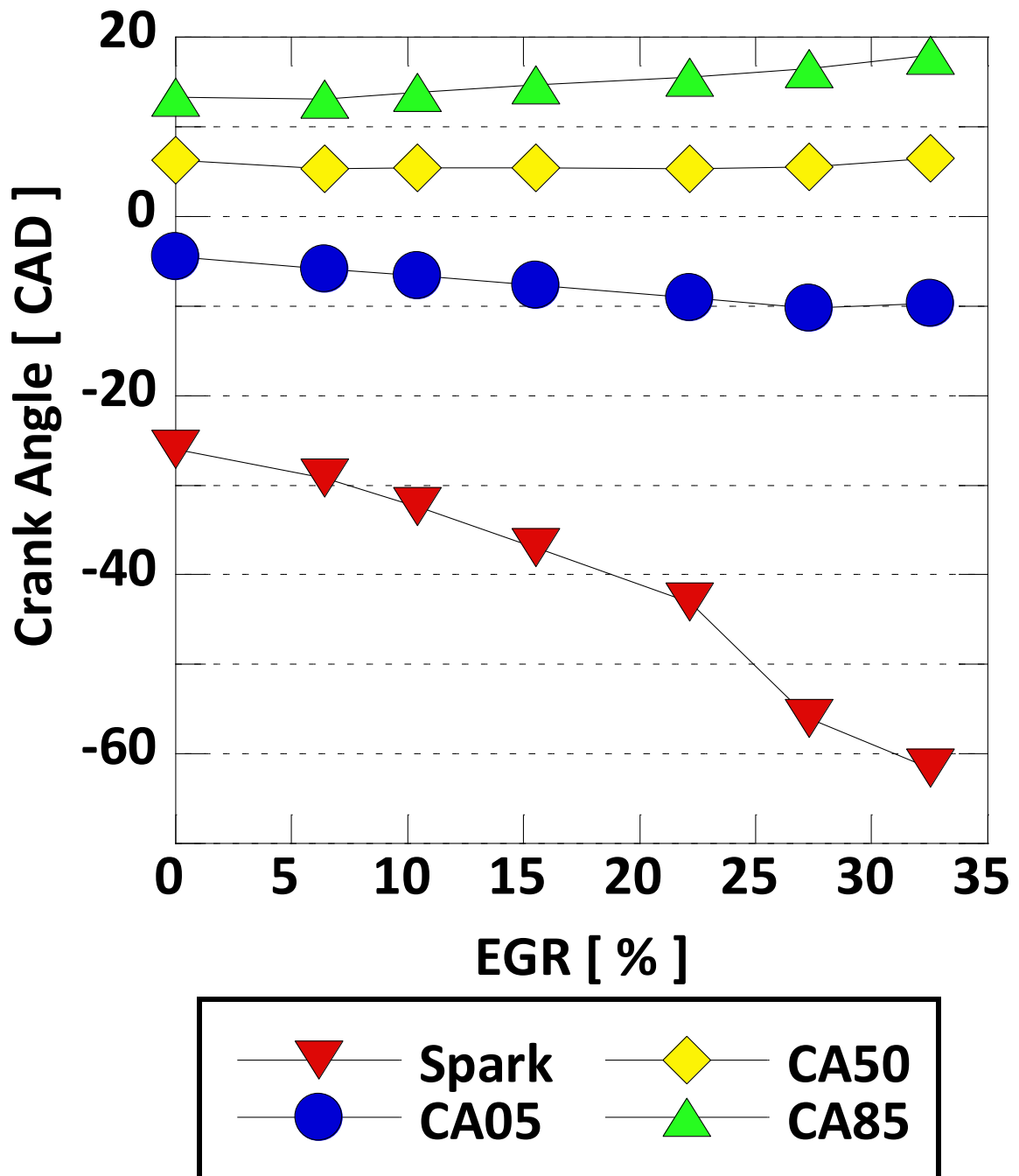
Figure 5.21. Baseline timing of the combustion process as exhaust gas recirculation (EGR) is increased. Note that CA50 (crank angle at which 50% of the mass fraction has burned) combustion phasing is held nearly constant.
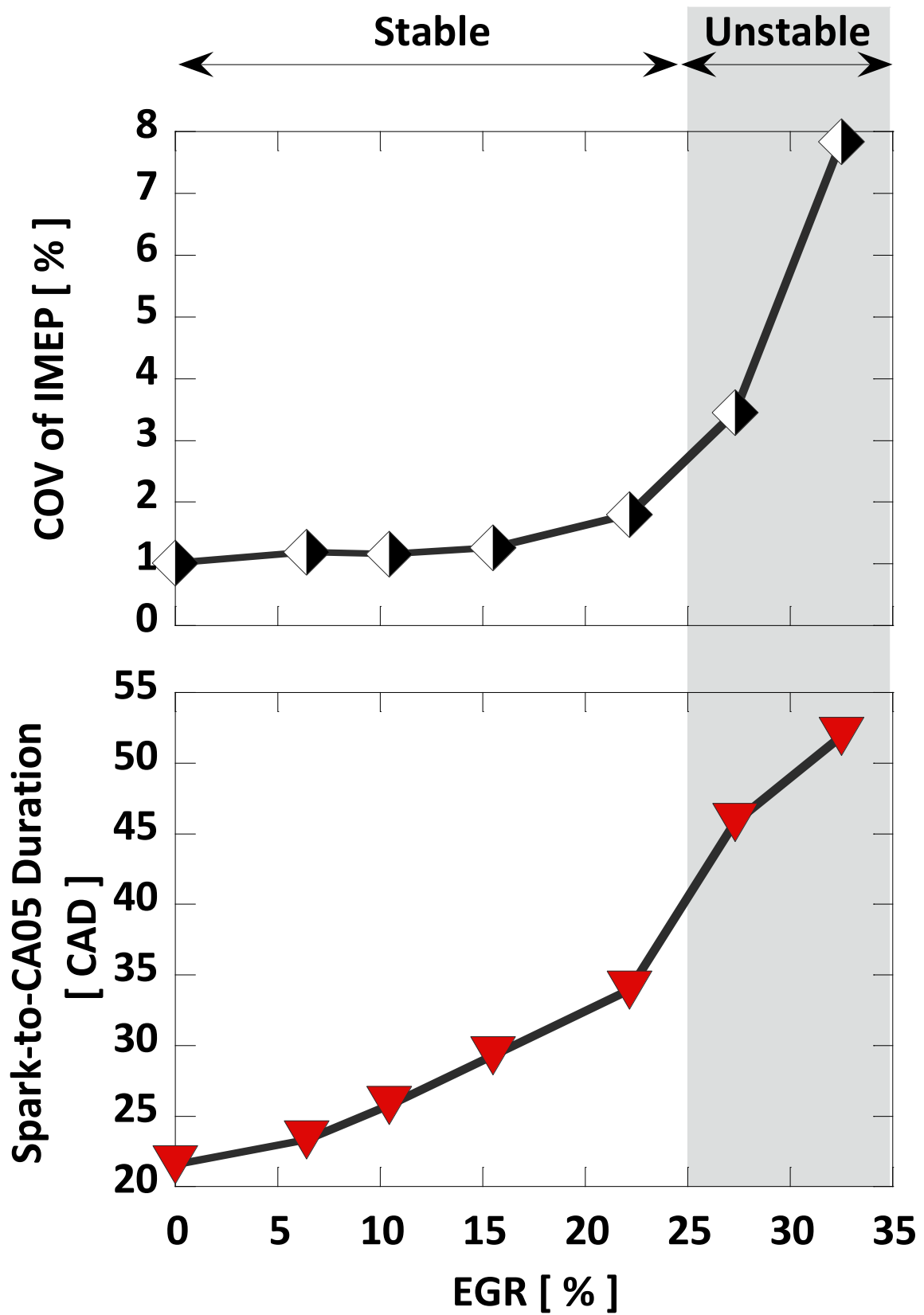
Figure 5.22. Baseline combustion stability as indicated by the COV of IMEP and spark-to-CA05 duration as a function of EGR.

The brake thermal efficiency with conventional EGR is shown in Figure 5.23. Initially, efficiency increases with EGR, but it reaches a maximum value and begins to decline due to increased combustion duration and decreased combustion stability. This is consistent with previous studies on the subject [26], [66], [170]. In the following sections, highly dilute combustion with reformate is compared to this baseline performance trend with conventionally cooled EGR.
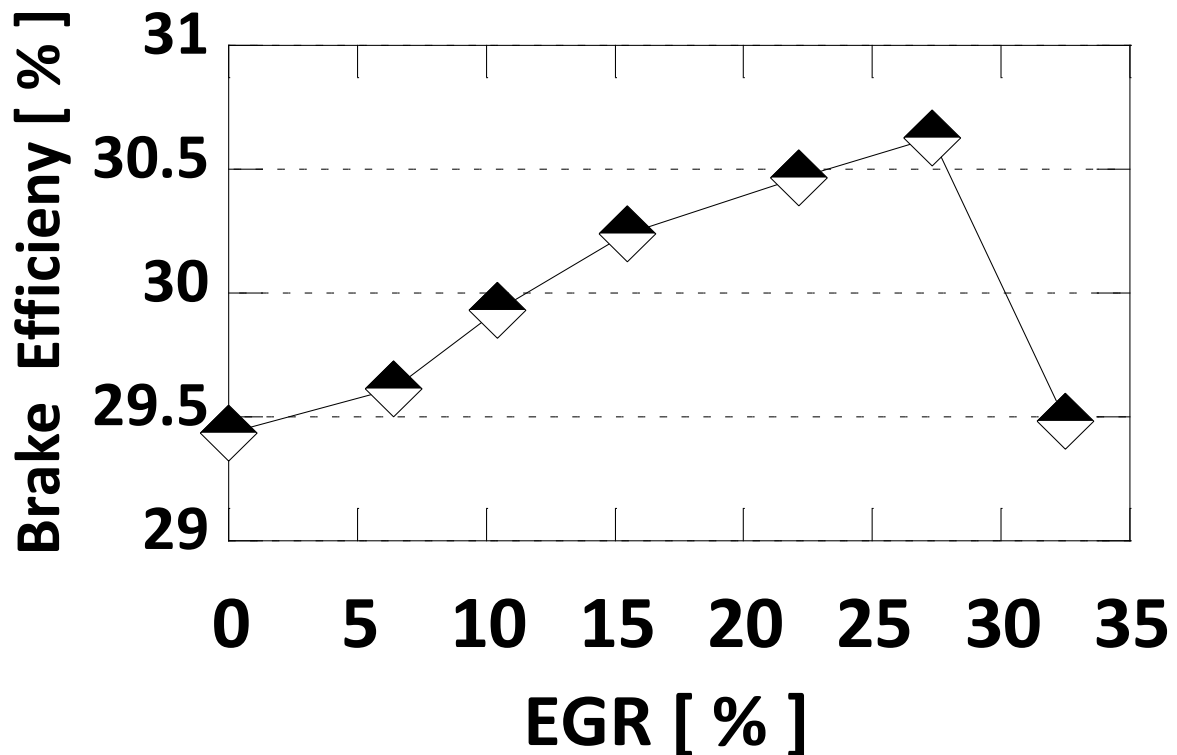
Figure 5.23. Baseline engine brake efficiency as a function of exhaust gas recirculation (EGR) rates.

5.3.6 Catalytic Reforming Operating Limits and EGR Estimation

That range of operating conditions was reduced during multi-cylinder engine operation because the engine was only operated under relatively stable conditions. The engine became unstable when H_2 production from the reforming catalyst decreased, likely due to reduced flame speed. Figure 5.24 compares the operable range of oxygen flow rates and $\Phi_{catalyst}$ from the catalyst mapping to the full engine experiments. Note that the catalyst-out concentrations

of H_2 translate to H_2 concentrations in the intake manifold of up to 5% as reformate is mixed with incoming air.
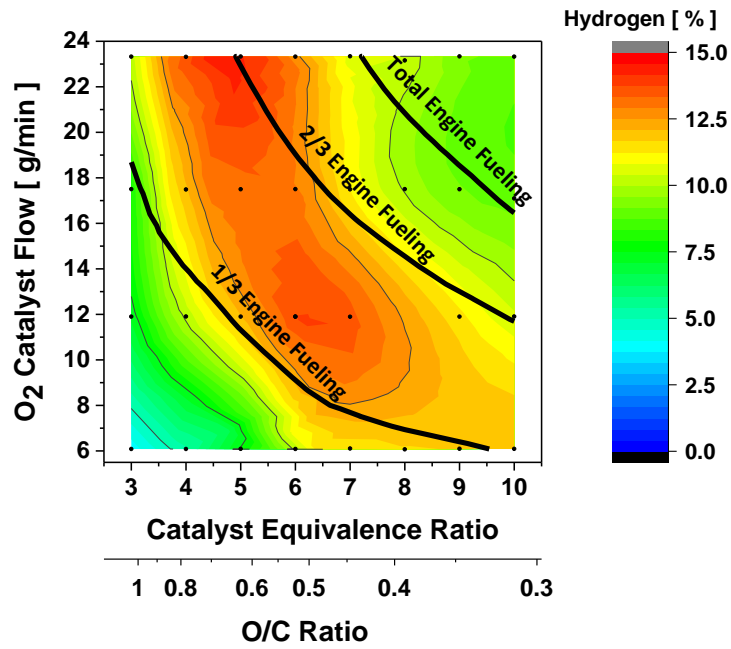
(a)
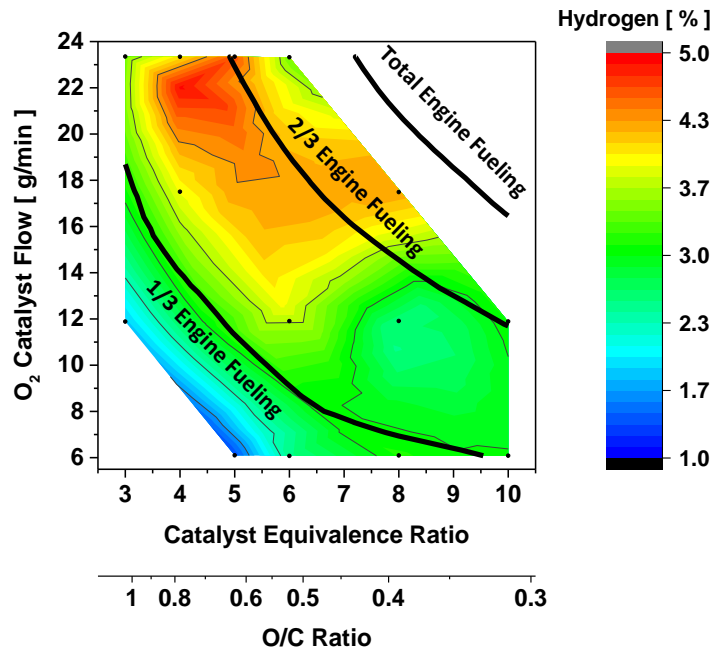
(b)

Figure 5.24. H_2 concentration as a function of oxygen catalyst flow and $\Phi_{catalyst}$ at the catalyst inlet for (a) catalyst-out concentration from the catalyst mapping study [58] and (b) intake manifold concentration for the multi-cylinder experiments.

For catalytic reforming conditions, the reformate stream contains a significant portion of the fuel energy for the combustion event, and therefore it is not exhaust gas per se. However, the effective EGR rate from a pumping perspective can be estimated. Figure 5.25 shows a contour plot of the intake manifold pressure for the catalytic fuel reforming strategy. The intake manifold pressure for this operating condition (2,000 rpm, 4 bar BMEP) varies between 65 and 70 kPa, with the highest intake manifold pressures corresponding to high oxygen catalyst flow and coincident with the highest levels of H_2 formation in Figure 5.24. For comparison, Figure 5.26 shows that intake manifold pressure increases linearly with conventional EGR from 48 kPa to 60 kPa. By extrapolating this trend to the manifold pressures observed for the catalytic reforming strategy, it can be determined that the catalytic reforming strategy is operating at an equivalent of 45%–55% EGR from a volumetric perspective.
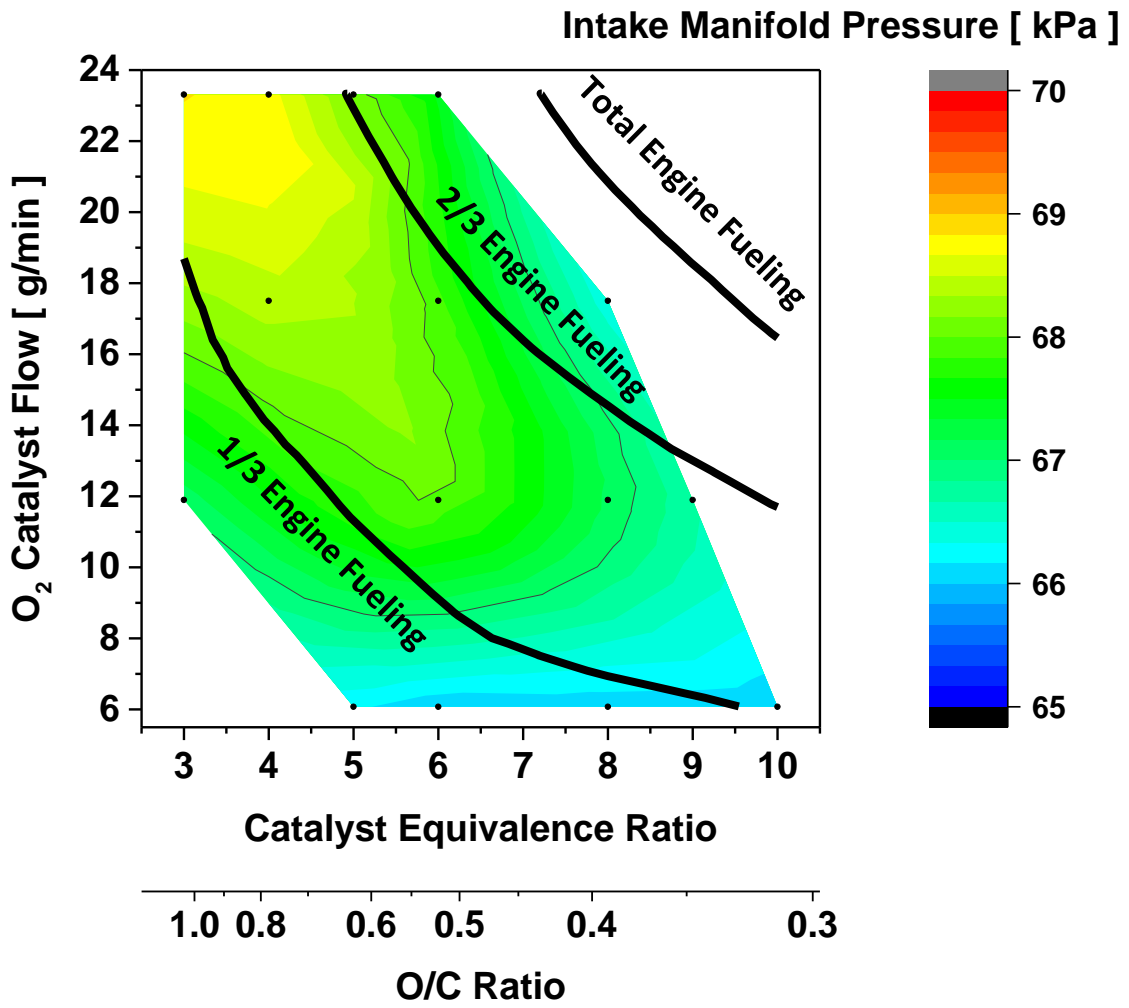
Figure 5.25. Intake manifold pressure for the catalytic reforming strategy as a function of oxygen catalyst flow and $\Phi_{catalyst}$ at the catalyst inlet.
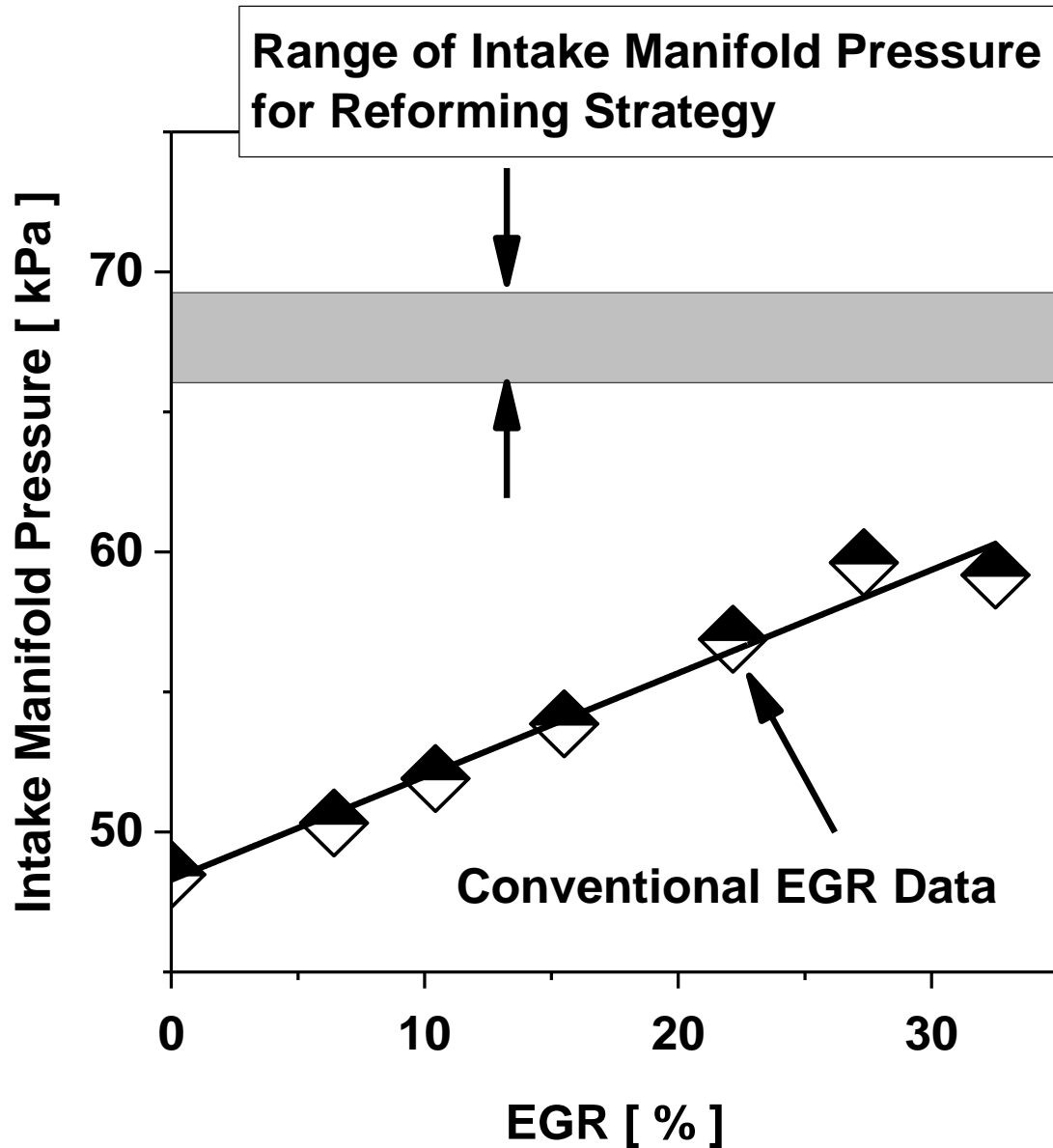
Figure 5.26. Intake manifold pressure as a function of conventional exhaust gas recirculation (EGR) operation.

The manifold pressure determines the thermodynamic expense of moving air into and out of the cylinder, which is quantified as the pumping mean effective pressure (PMEP). PMEP, shown in Figure 5.27 as a function of the manifold pressure for both the conventional EGR and reforming strategies, demonstrates a nearly linear dependence on intake manifold pressure regardless of operating strategy. Relative to the baseline operating condition without EGR (PMEP = −60 kPa), the catalytic reforming strategy can reduce the pumping work by more than 40% [PMEP = (−35 ± 3) kPa].
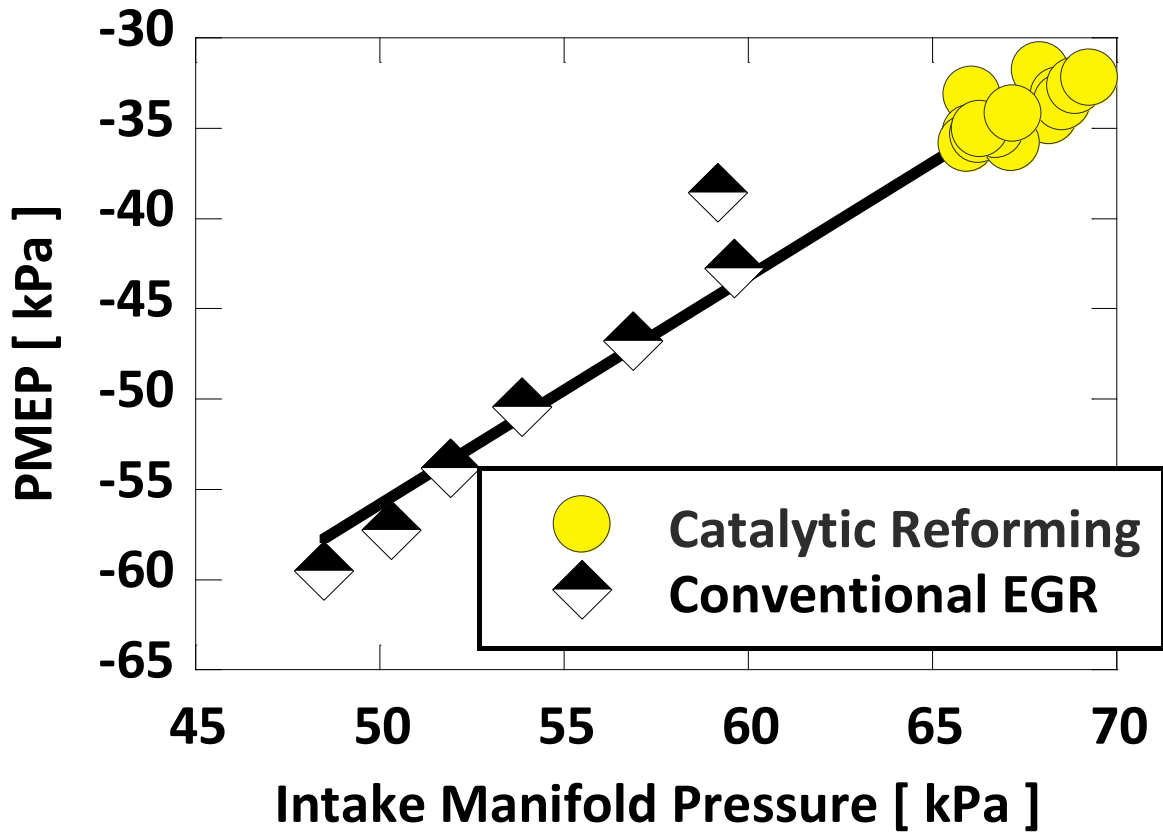
Figure 5.27. Pumping mean effective pressure (PMEP) as a function of intake manifold pressure for conventional exhaust gas recirculation (EGR) and catalytic reforming.

Cylinder 4, the engine cylinder that is feeding the reformer, is operating with an isolated intake manifold and can be at a different pressure than the manifold for cylinders 1-3. This cylinder operates fuel-lean in order to provide the required O_2 to the reforming catalyst. Figure 5.28 compares the intake manifold pressure of cylinder 4 vs. the intake manifold pressure of cylinders 1-3. The intake manifold pressure of cylinders 1-3 falls in a narrow range between 66 and 69 kPa, while the intake manifold pressure of cylinder 4 varies over a much larger range, from 63 to 81 kPa. Thus, the intake pressure for cylinder 4 can be higher or lower than cylinders 1-3. The intake pressure of cylinder 4 is dependent on $\dot{m}_{O2}$ to the catalyst, which is controlled by how lean the engine operates.
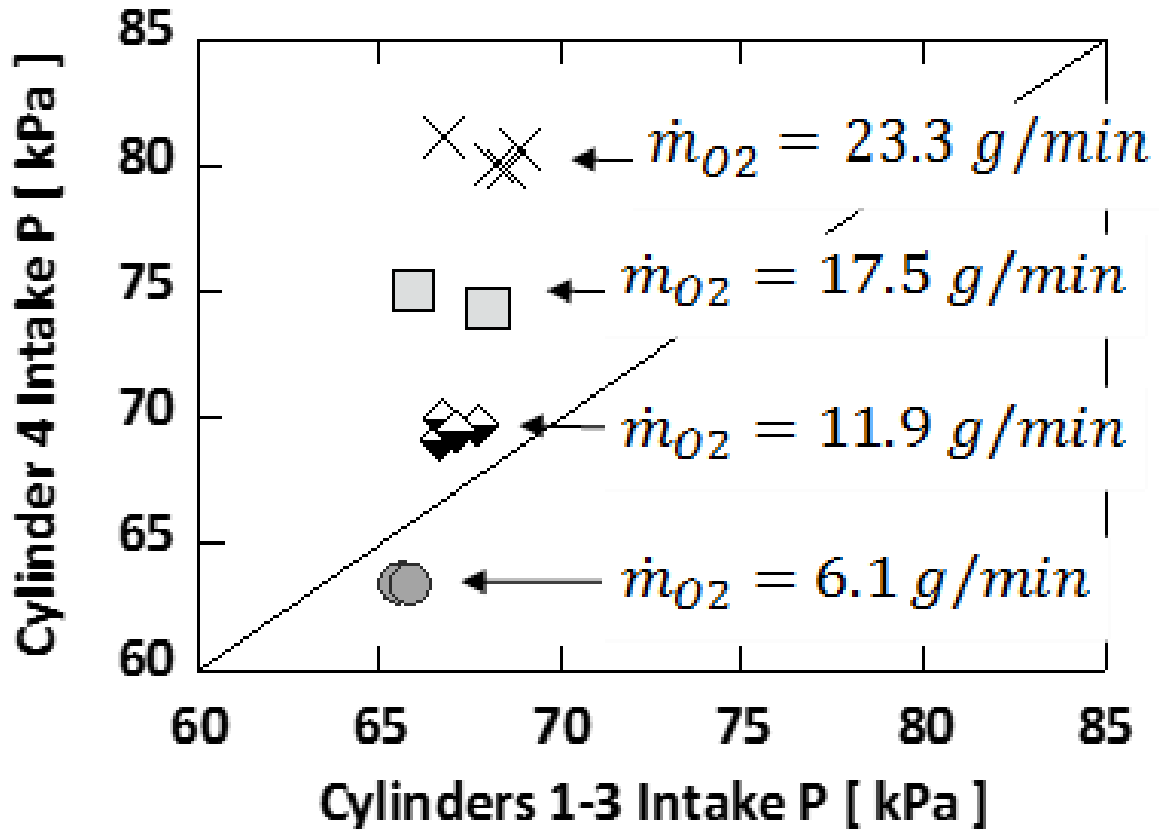
Figure 5.28. Intake manifold pressure for cylinder 4 vs. the intake manifold pressure for cylinders 1-3.

5.3.7 Combustion Duration and Stability Analysis

Figure 5.29 shows the spark-to-CA05 duration as a function of oxygen catalyst flow and $\Phi_{catalyst}$ for the catalytic reforming strategy. The spark-to-CA05 duration is representative of the early flame kernel development time, and it was shown in Figure 5.21 that this combustion interval exhibits the largest increase with the presence of conventional EGR. The spark-to-CA05 duration for the catalytic reforming strategy is less than 30 CAD for a significant portion of the oxygen catalyst flow, and $\Phi_{catalyst}$ domain investigated, including a number of operating points where the spark-to-CA05 duration is less than 25 CAD. It can be seen in Figure 5.21 that, for the conventional EGR cases, combustion became unstable (COV of IMEP > 3%) when the spark-to-CA05 duration was greater than 40 CAD.
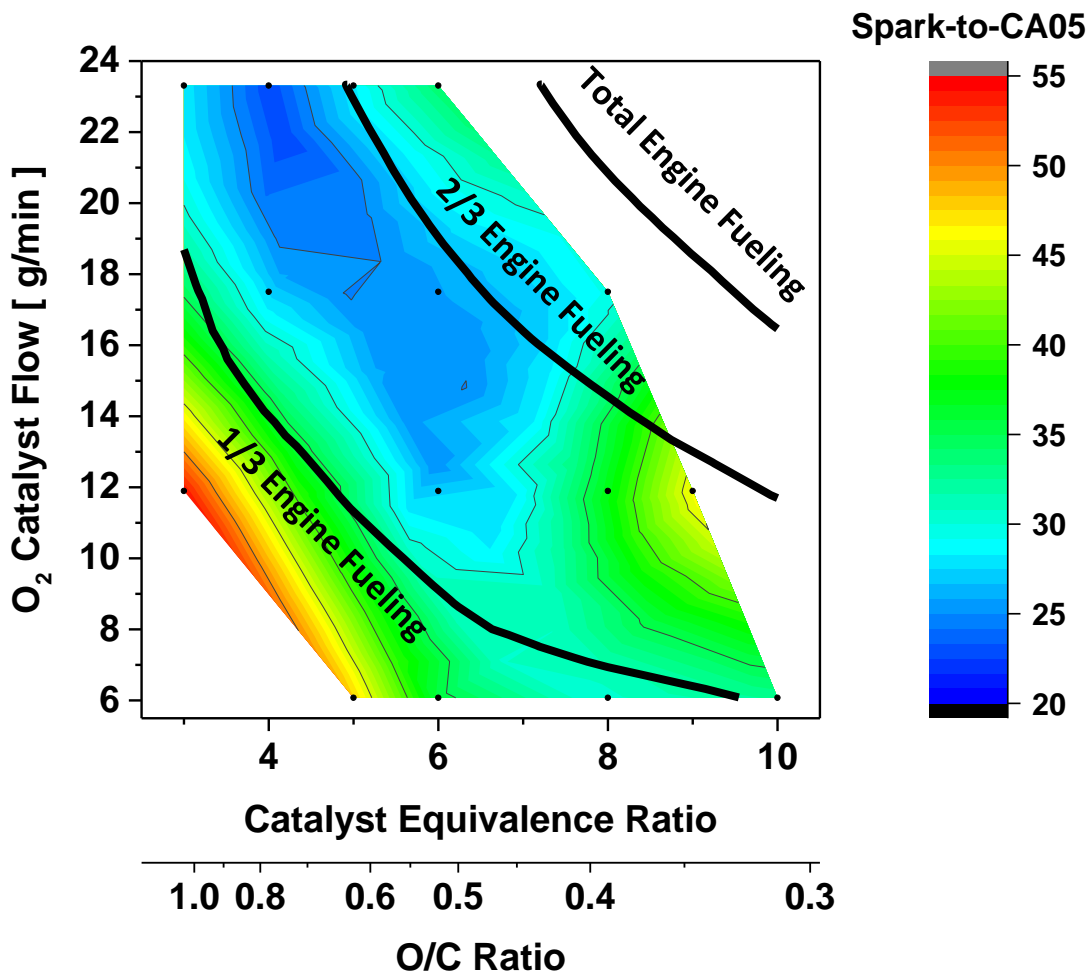
Figure 5.29. Spark-to-CA05 duration as a function of oxygen catalyst flow and $\Phi_{catalyst}$ at the catalyst intake for reforming conditions.

Figure 5.30 shows the COV of IMEP as a function of the spark-to-CA05 duration for both the catalytic reforming strategy and the conventional EGR strategy. It can be seen that, with the exception of two outliers, the conventional EGR and the catalytic reforming strategy show the same trend: combustion instability begins when the spark-to-CA05 duration is greater than 40 CAD at this speed and load condition. This finding confirms that the mechanism by which reformate extends the dilution limit is by accelerating the initial portion of combustion through a faster flame speed.
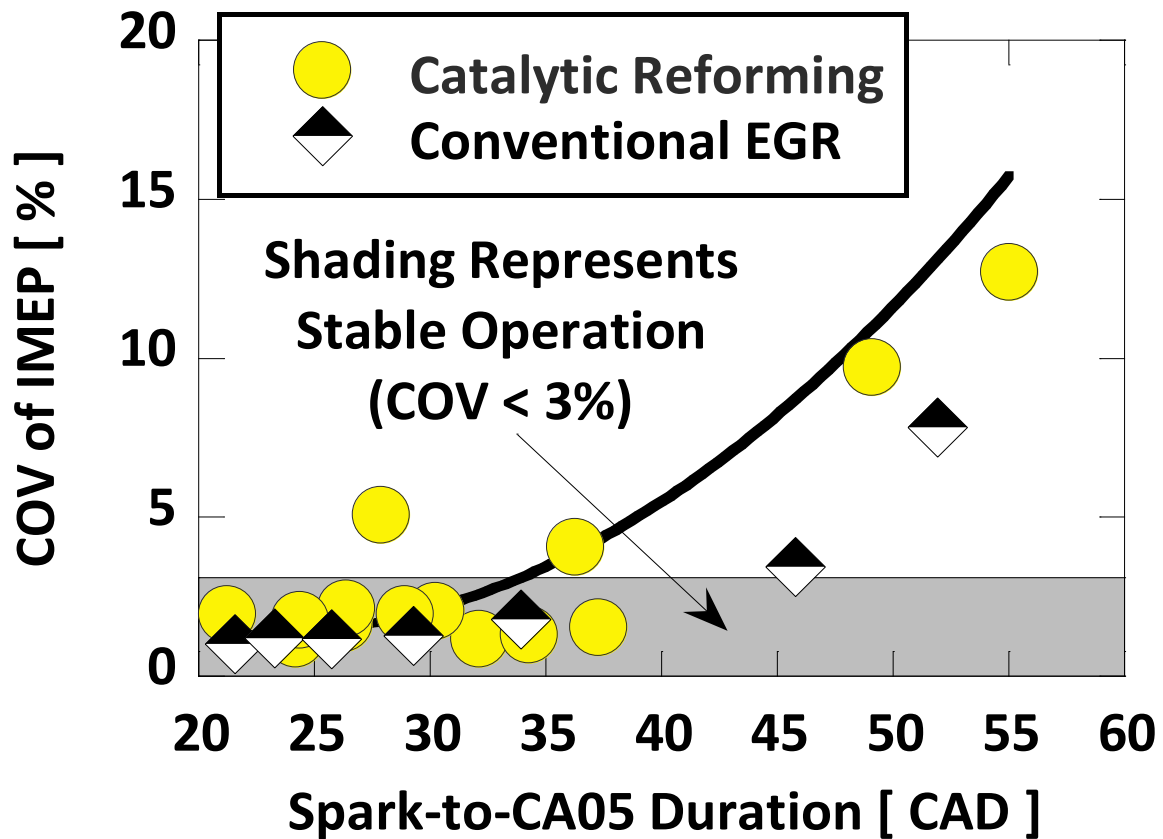
Figure 5.30. Combustion stability as quantified by the coefficient of variation (COV) of the indicated mean effective pressure (IMEP) as a function of the spark-to-CA05 duration for both conventional exhaust gas recirculation (EGR) and the catalytic reforming strategy.

5.3.8 Brake Efficiency

A plot of brake efficiency as a function of O_2 catalyst flow and $\Phi_{catalyst}$ is shown in Figure 5.31 for the catalytic reforming strategy. At this engine operating condition, 2,000 rpm and 4 bar BMEP with stoichiometric exhaust, the maximum brake efficiency was as high as 32.1%. The peak efficiency occurs for an oxygen flow rate of 12 g/min and $\Phi_{catalyst} = 6$. This condition is a lower oxygen flow rate than where the minimum spark-to-CA05 (Figure 5.29) and the maximum H_2 concentration (Figure 5.24) occur. However, according to the energetics of reforming were examined in the section 5.3.1, it was found that minimizing the oxygen flow rate while still providing sufficient catalyst activity maximizes the TCR of the reforming process.
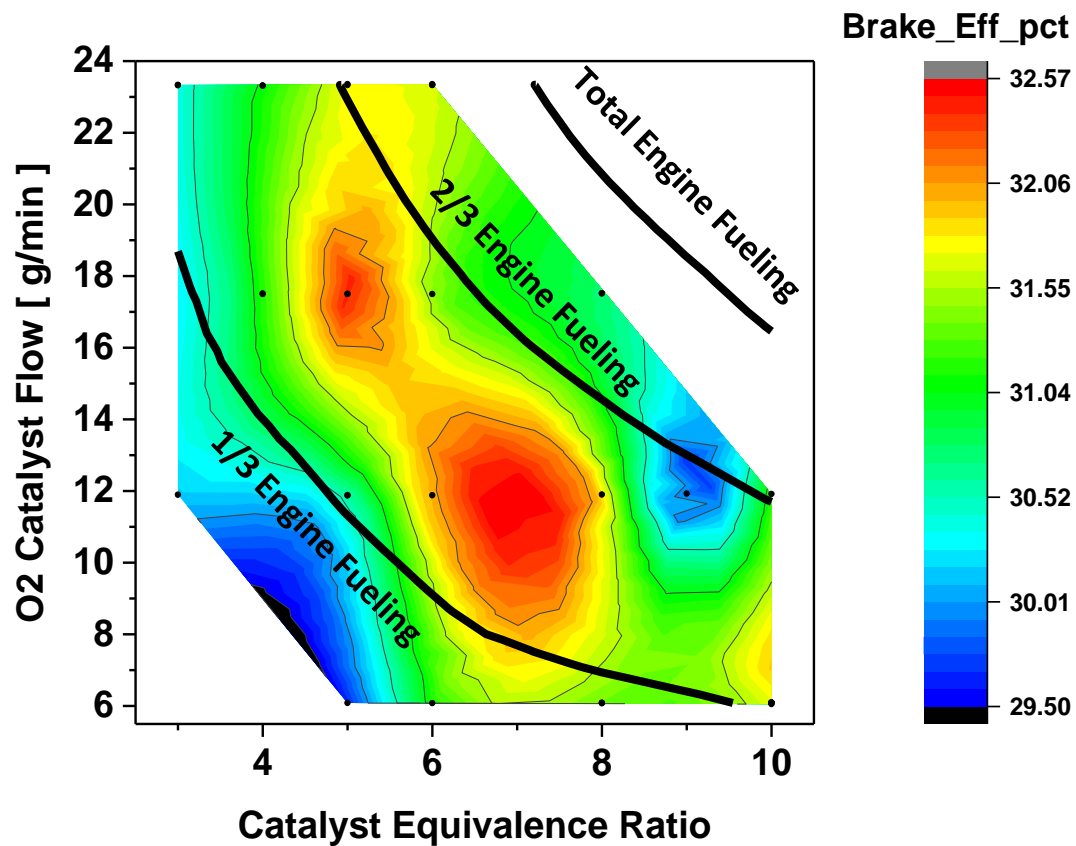
Figure 5.31. Brake thermal efficiency as a function of oxygen catalyst flow and $\Phi_{catalyst}$ at the catalyst inlet.

Figure 5.32 shows brake thermal efficiency for both conventional EGR and the catalytic reforming strategy as a function of the intake manifold pressure. Relative to the baseline engine condition without EGR, the brake thermal efficiency increased from 29.5% to 32.1%, which is equivalent to a fuel consumption decrease of 8.3% (brake specific fuel consumption decrease from 276.1 to 253.1 g/kWh). It is noteworthy that all of the parametric conditions investigated with the reforming strategy have a better brake thermal efficiency than the baseline operating condition without EGR. This is due, in large part, to the reduction of pumping work at such a high dilution level at this part-load engine condition, as shown in Figure 5.27. This efficiency improvement demonstrates that extending the dilution limit through catalytic reforming can produce a substantial increase in the brake efficiency of a multi-cylinder engine.
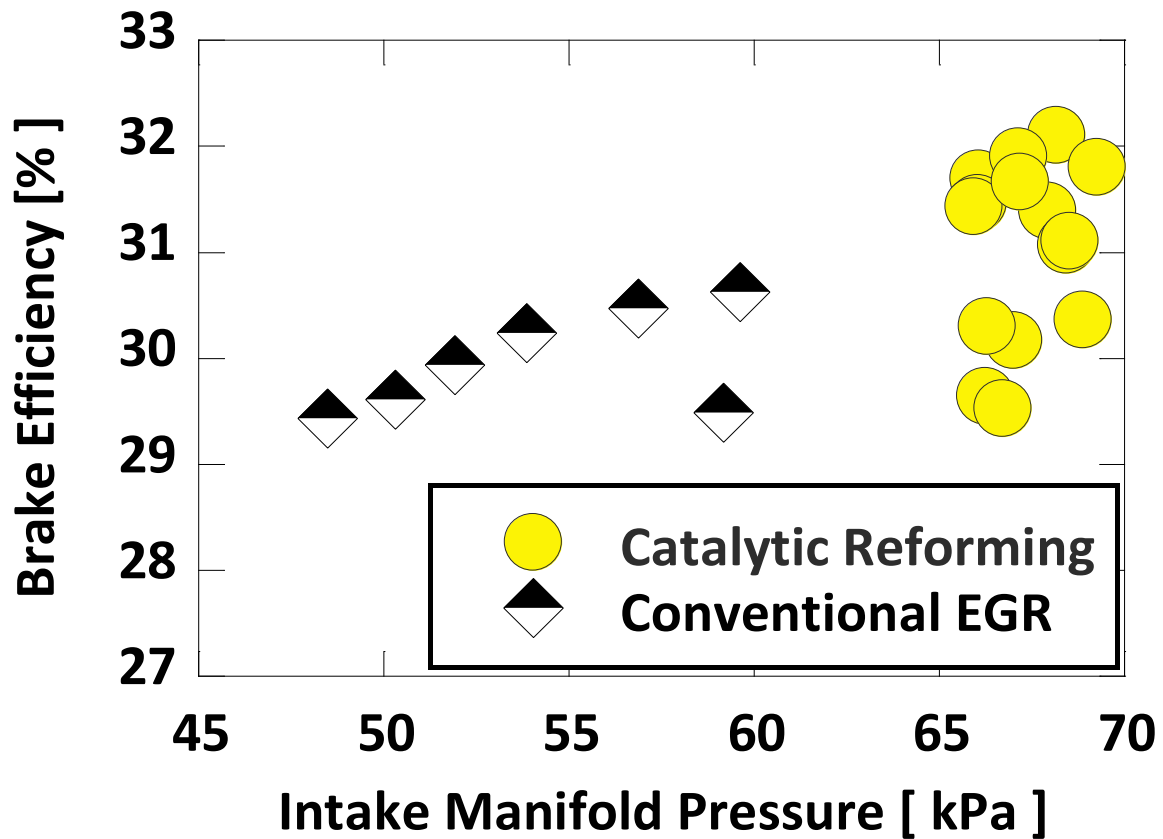
Figure 5.32. Brake thermal efficiency as a function of intake manifold pressure for conventional exhaust gas recirculation (EGR) and the catalytic reforming strategy.

It is emphasized that the efficiency increase observed here with the catalytic reforming strategy was achieved without any optimization of the engine geometry or optimization of the catalyst, and there is a reason to believe that significant optimization is possible. EGR has been shown to be an effective knock suppressant [26] that could allow a substantial increase in the engine compression ratio, which could increase engine efficiency. Further, this engine uses a square combustion chamber geometry (stroke = bore), whereas newer engines that are highly tolerant of EGR dilution are under-square (stroke > bore). An under-square geometry increases the mean piston speed and by extension the in-cylinder turbulence, which scales with mean piston speed [186]. Higher turbulence shortens the combustion duration, which increases efficiency. Finally, no attempt was made to optimize the fuel injection timing or targeting. This engine used a side-mounted fuel injector, making it possible that fuel spray impingement on the cylinder wall occurred. Thus, with further development focused on the

compression ratio, stroke-to-bore ratio, and fuel injection processes, additional efficiency improvements could be realized.

5.3.9 Effects of Fuel on the Catalytic Fuel Conversion and Engine Efficiency

When the fuel of isooctane is replaced by gasoline, CO concentration is similar as shown in Figure 5.34, but H_2 concentration is reduced as shown in Figure 5.33. Reduction of H_2 is due to the reduction of H/C ratio of the fuel compared to that of isooctane and higher sulfur which leads to the less effectiveness of the catalyst. Brake thermal efficiency performance is an improvement over the baseline, but diminished relative to iso-octane.
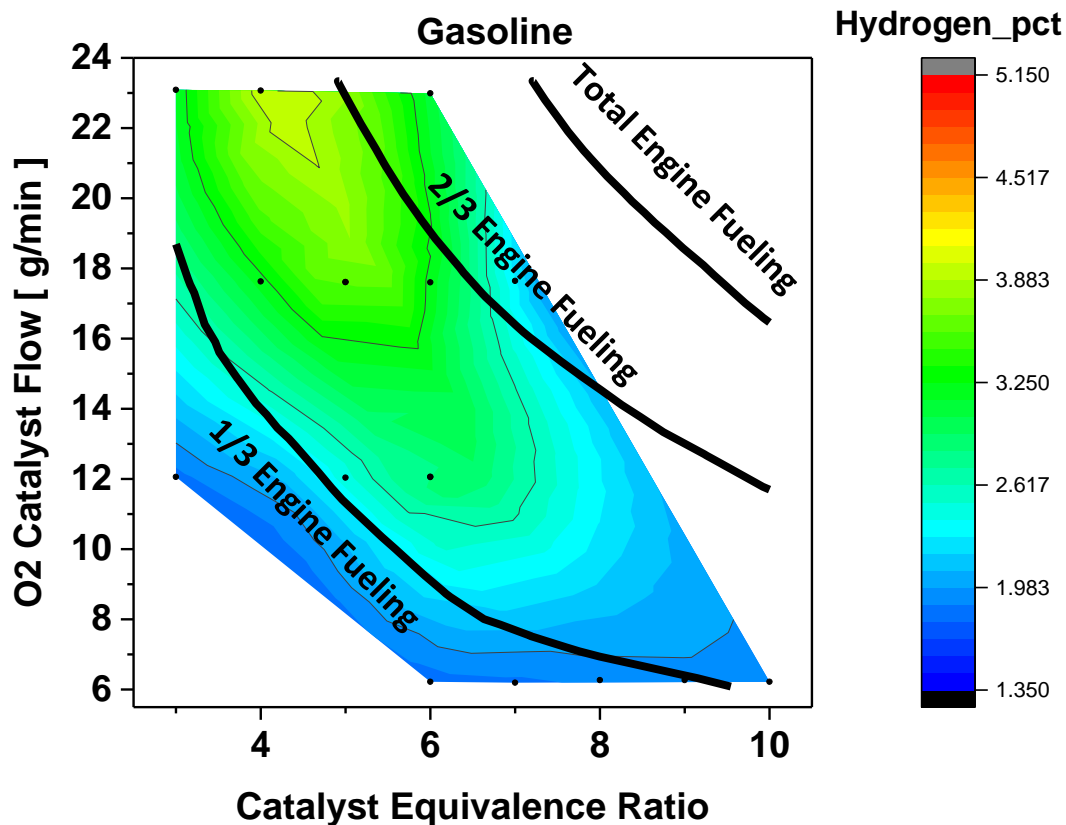
Figure 5.33. H_2 concentration as a function of oxygen catalyst flow and $\Phi_{catalyst}$ at the catalyst inlet with gasoline fuel.
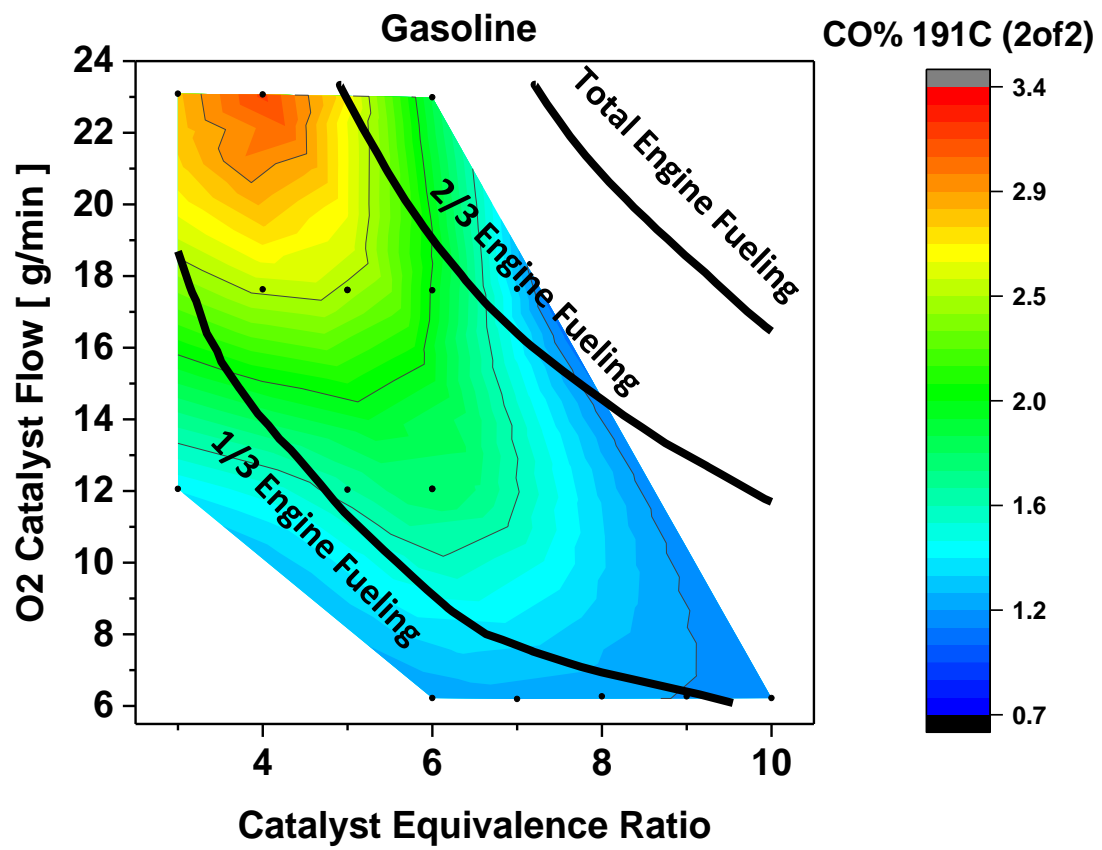
Figure 5.34. CO concentration as a function of oxygen catalyst flow and $\Phi_{catalyst}$ at the catalyst inlet with gasoline fuel.
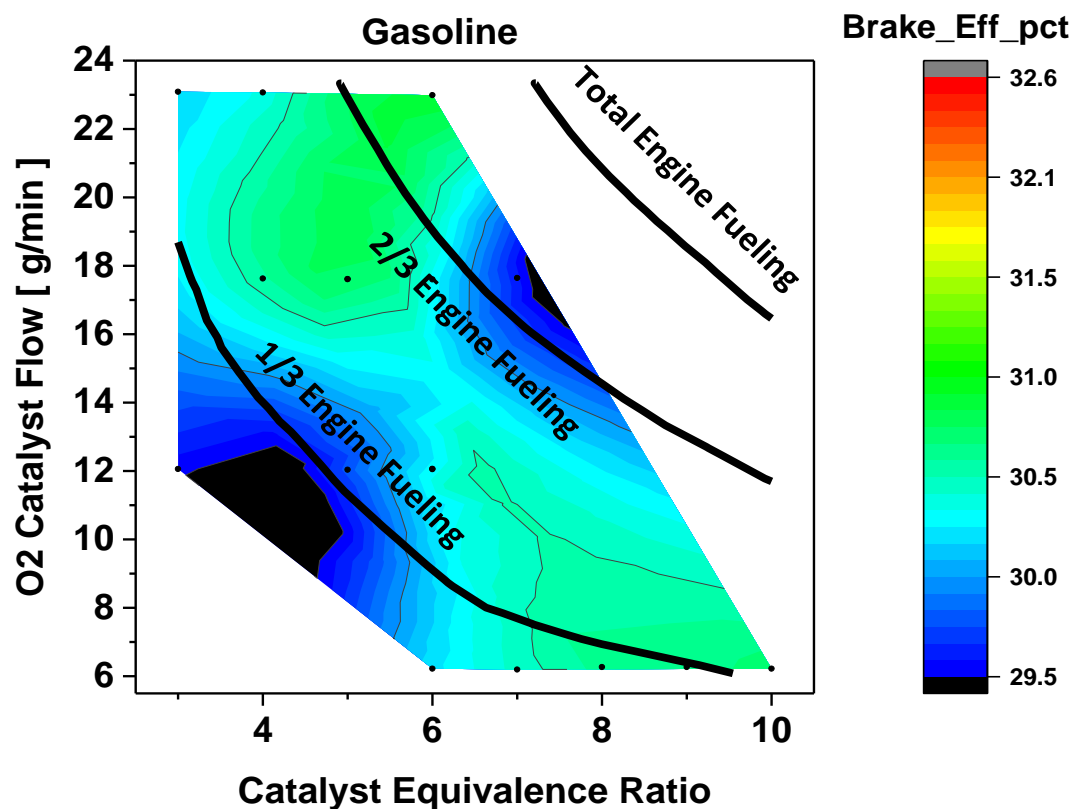
Figure 5.35. Brake thermal efficiency as a function of oxygen catalyst flow and $\Phi_{catalyst}$ at the catalyst inlet with gasoline fuel.

5.4 Conclusions

A combination of equilibrium calculations and fuel reforming on an engine were used to characterize catalytic reforming behavior and energetics over a range of $\Phi_{catalyst}$ and O_2 concentration conditions. Calculations of the reaction energetics provided insight into the desirable conditions from a thermodynamic standpoint. From an ideal standpoint, the highest levels of TCR are possible for the highest catalyst equivalence ratio. However, steam reforming is highly endothermic, and the system becomes enthalpy limited, resulting in the production of CH_4 as a reforming product rather than H_2 and CO, which are more favorable from an energetics standpoint.

Experimental results illustrated that high concentrations of H_2 and CO could be formed over the catalyst at quasi-steady-state conditions, with as much as 15 vol % H_2 at the catalyst outlet. There was a range of $\Phi_{catalyst}$ and O_2 flow rate conditions with which to achieve

maximum reforming performance. The best performance was found for $4 < \Phi_{catalyst} < 7$. Under these conditions, the H_2 and CO yield were highest, and measurements showed a significant amount of water consumption over the catalyst, confirming the presence of steam reforming reactions. Thermal analyses of the catalyst indicate that the reactions can be either endothermic or exothermic and also show that the majority of the reactions occur in the first catalyst monolith, indicating that higher space velocities are possible.

The engine experiments described here demonstrate the potential benefits of EGR-loop reforming for combustion stability and brake efficiency. Specifically, we found that the catalytic reforming strategy could produce intake manifold H_2 concentrations as high as 5% at the 2,000 rpm and 4 bar BMEP condition investigated. The reforming strategy also introduced a high level of dilution in the engine, equivalent to 45%–55% EGR. However, despite the high level of dilution, the strategy resulted in good combustion stability. A combined analysis of both the conventional EGR and the reformate-assisted combustion shows that combustion stability problems occur when the spark-to-CA05 duration exceeds 40°CA. With the high flame speed components in the reformate, namely H_2, this threshold was not exceeded for large parts of the reforming conditions investigated.

The brake thermal efficiency for the multi-cylinder engine was increased substantially with EGR-loop reforming, thereby decreasing fuel consumption by more than 8%. This efficiency improvement was achieved while maintaining stoichiometric engine exhaust, meaning that this technology should be compatible with conventional three-way emissions control technology for gasoline engines. We expect that additional efficiency increases should be possible by combining EGR-loop reforming with other engine hardware and operating strategies that enhance the positive impacts of reformate on the combustion profile.

Chapter 6. Fuel Reforming by Fuel Injection during Negative Valve Overlap

6.1 Introduction

Increasing fuel economy and emission control requirements motivate the development of advanced combustion strategies. The spark ignition (SI) engine offers considerable benefits over the compression ignition engine in terms of cost and tailpipe emissions but suffers in comparison in terms of efficiency [1]. Advanced gasoline combustion modes such as homogeneous charge compression ignition (HCCI) and spark assisted compression ignition (SACI) are possible enablers of improved fuel economy for gasoline engines [187]. An engine operating in such modes has the potential for higher fuel economy and lower emissions compared to traditional engines [5]. But control of ignition and combustion in HCCI and SACI pose significant challenges [188]. HCCI and SACI combustion modes also have reduced engine load range compared with conventional SI operation, where HCCI and SACI are constrained at low loads by dilute flammability limits and at high loads by in-cylinder pressure restrictions [189]. Furthermore, the conventional after-treatment device, the three-way catalyst (TWC), requires stoichiometric conditions in the exhaust stream to operate effectively [190]. In HCCI operating mode, as the air to fuel ratio becomes lean, the high conversion efficiency of the TWC can only be maintained for short periods of time as the TWC becomes saturated with oxygen [191].

The use of cooled EGR and stoichiometric fuel/air composition has been demonstrated in a gasoline direct injection (GDI) SI engine to substantially improve fuel consumption and reduce emissions over a broad range of speed and load conditions [27]. The benefits were attributed to dilute combustion and reduced throttling loss[27], but cooled EGR can cause

slower rates of flame propagation, decreased engine stability and even lead to misfire [70]. The improvement in EGR tolerance at low load conditions is an important enabler for high dilution engines.

Negative valve overlap (NVO), which is a common way of controlling HCCI combustion phasing, incorporates early exhaust valve closing (EVC) and late intake valve opening (IVO) in order to retain internal residual gases [147], [148], [192], [193]. NVO provides thermal and dilution advantages compared to external EGR strategies. Additionally, because the residuals are recompressed (reheated), NVO can enable reaction or reformation of fuel during the NVO period [149]. The effects of reformed gases include charge heating, dilution (reduced oxygen concentrations), increased heat capacity, changed chemical reactivity, and increased stratification. Reactions and heat release accompanying NVO fuel injection can change the temperature and composition of the charge prior to the main combustion, which can be used to control ignition, rate of pressure rise, peak pressure, combustion noise, misfire, and emissions [150].

There are a few studies that have focused on the fuel reforming chemistry and improving standard operating conditions using NVO. The research focused on NVO fuel reforming chemistry has indicated the reforming process under low-O_2 conditions produces substantial concentrations of H_2, CO, methane, and other short-chain hydrocarbon species [151]. The amount of fuel reforming can be controlled by injection timing and the ratio of split fuel injection [194]. Increased global equivalence ratio in the NVO-period led to a greater fraction of net recovered fuel energy and work as heat losses were minimized (based on energy analysis) [152]. Klinkert [195] provides new insights into how boost pressure and other operating parameters in an NVO HCCI engine impact the maximum attainable load and combustion phasing limits.

Fuel injection during NVO of SI engine operation has the potential to extend the dilution limit while retaining the advantages of SI operation with respect to combustion phasing control, and potentially reducing emissions. The goal of this study is to quantify the combustion and emissions benefits of dilute SI combustion with fuel injection during NVO

and to investigate the effectiveness of this strategy towards extending the low load dilution limit of SI combustion without changing the engine structure significantly.

6.2 Methodology

The study was performed using a 2.0 L in-line four-cylinder engine based on the General Motors "Ecotec LNF" platform. The engine used stock connecting rods, crank, and block, and a custom cylinder head and custom pistons (AVL designed), which increased compression ratio from 9.25 to 11.7. The compression ratio was increased to enable to the engine to operate in HCCI, SACI, and SI combustion modes. Only the SI mode of operation was used in this study.

The cylinder head incorporated 4 valves/cylinder, Denso electric intake and exhaust camshaft phasers for variable valve timing (VVT), and a variable valve lift (VVL) mechanism for camshaft lobe switching. 100 crank angle degrees (CAD) of camshaft phasing authority allowed varying degrees of NVO to trap varying amounts of residual gas.

The head used a central-mounted direct injection fuel injection system using Bosch HDEV5 6-hole injectors. Piston crown design included a shallow bowl and valve cut-outs to work with the fuel injector placement in the custom head. Piston pin offset was 0.8 mm.

A high-pressure EGR system was added to move exhaust gas from the turbine inlet, through an EGR cooler, to the intake manifold just upstream of the intake air throttle. The EGR cooler used engine coolant to maintain the EGR temperature at approximately 100°C. Key engine specifications are summarized in Table 6.1. For this study, only the low lift camshaft lobes were used, and the valve lift profiles are provided in Figure 6.1.

Table 6.1. Engine specifications

Displacement Volume (L)	2.0
Number of Cylinders	4
Valves per Cylinder	4
Bore (mm)	86.0
Stroke (mm)	86.0
Connecting Rod Length (mm)	145.5
Compression Ratio	11.7:1
Valvetrain	DOHC dual independent VVT/VVL
Injection Type	Direct (spray-guided)
Injector Location	Central
Turbocharger	Borg Warner K04 Twin-Scroll
External EGR Layout	High pressure
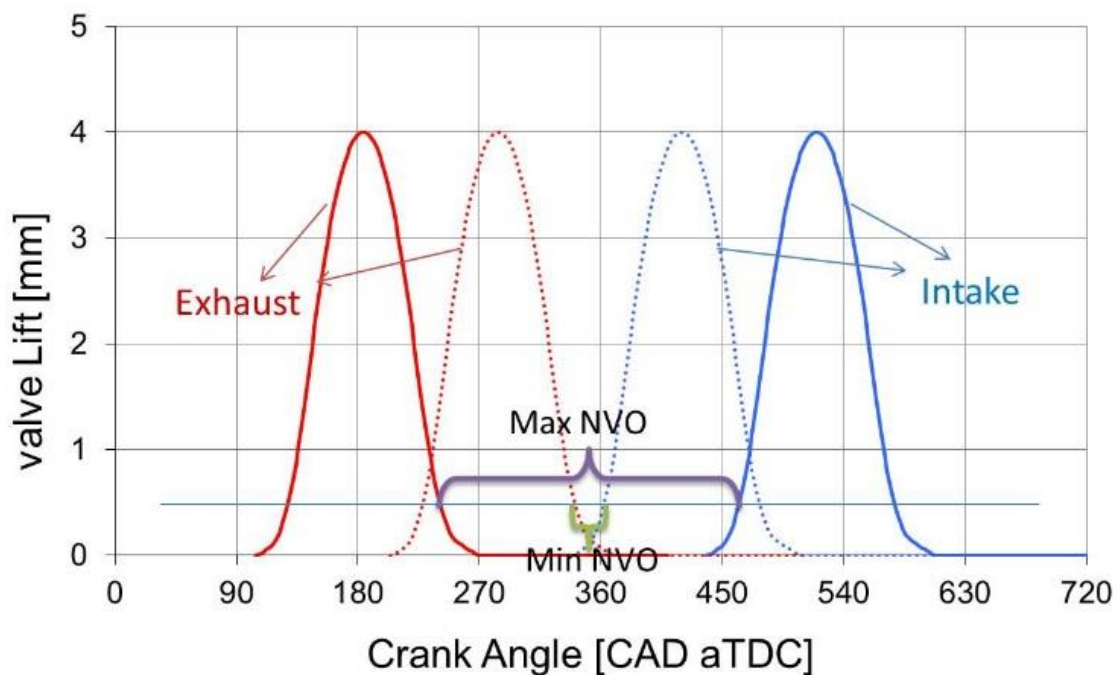
Figure 6.1. Valve lift profiles.

Engine control was via a Bosch MED17.3.2 ECU and ETAS ES910.3 prototyping interface. An AVL AC dynamometer system was used to maintain engine speed and measure engine load. The pressure in each cylinder was measured using Kistler 6125C pressure transducers. Engine-out oxygen was measured with a Bosch LSU4.9 wide range oxygen sensor and an ETAS LA4 lambda module. The fuel utilized in this study was premium grade consumer

pump gasoline containing 10% ethanol. The fuel specifications shown in Table 6.2 are estimated from previous batches of the same fuel analyzed by Paragon Laboratories (Livonia, MI).

Table 6.2. Fuel specifications

Fuel type	BP Premium 93 octane (E10)
H/C atomic ratio	1.991
Stoichiometric air-fuel ratio (mass basis)	14.02
Lower heating value (MJ/kg)	41.94
RON/MON/AKI/Sensitivity	99.4/91.3/95.4/8.1
Density at 15.56ºC (g/ml)	0.7113
Saturates/olefins/aromatics (by volume)	83.0/0.9/6.0
Molar composition C/H/O	1/2.217/0.0377
Ethanol content (by volume %)	10.02
Vapor pressure (psi)	12.34 DVPE (ASTM)

External EGR molar fraction was determined from the molar ratio of intake CO_2 to exhaust CO_2. Intake and exhaust CO_2 concentrations were measured with an AVL SESAM i60 using infrared analyzers for measuring intake (NDIR) and exhaust (FTIR) CO_2. The estimated repeatability was 0.53% for the NDIR measurements, 0.35% for the FTIR measurements, and 0.65% for the EGR calculation.

As this study focuses on low load dilution limit extension, 1800 rpm and 3 bar BMEP was selected as the test point for evaluating the effects of SOI and NVO. All the fuel is injected in the NVO period. This operating point is frequently visited during the FTP-75 drive cycle for a representative US passenger car [196]. The NVO period was set symmetrically about top dead center (TDC) gas exchange.

The first set of experiments was conducted to investigate how SOI during NVO affects SI combustion phasing and emissions. The engine was operated at 1800 RPM, 3 bar BMEP, air-fuel ratio (mass basis) = 14.02 (lambda =1), NVO = 80 CAD (at a reference valve lift of 0.5 mm), and spark timing = 54 CAD before top dead center (bTDC). A baseline SOI of 300 CAD bTDC firing was selected because this is the fuel injection timing of this speed/load point of the production version of the engine without NVO.

At the baseline SOI, the combustion stability limit (defined as when the coefficient of variation (COV) of the indicated mean effective pressure (IMEP) reaches or exceeds 4%) for external EGR was 10% molar fraction of the total fuel and air charge. Speed, fueling rate, lambda, NVO, spark timing, and external EGR molar fraction were then held constant, while SOI was advanced from 300 to 420 CAD bTDC firing in increments of 20 CAD. The engine operating conditions for the SOI study are summarized in Table 6.3. Some end gas auto-ignition was considered acceptable as long as knocking/ringing was below acceptable standards (e.g. maximum pressure rise rates below 3 bar/CAD).

Table 6.3. Engine operating conditions for SOI investigation

Actuator	Value
Engine Speed	1800 RPM
BMEP	3 bar
Air-fuel ratio (mass basis)	14.02
EVC (reference lift = 0.5 mm)	40 CAD bTDC gas exchange (400 CAD bTDC firing)
IVO (reference lift = 0.5 mm)	40 CAD aTDC gas exchange (320 CAD bTDC firing)
NVO	80 CAD
Fuel Injection Pressure	100 bar
Start of Injection	300 to 420 CAD bTDC firing
Spark Timing	54 CAD bTDC firing
External EGR dilution	~10%
COV	<4%
Average Pressure Rise Rate	<3 bar/ CAD

The second set of experiments was conducted to investigate how SOI during NVO affects the dilution limit (defined by COV of IMEP as described earlier), heat release rate, fuel efficiency, cycle to cycle variation, and emissions. As in the first set of experiments, the engine was maintained at 1800 RPM, 3 bar BMEP, and air-fuel ratio (mass basis) =14.02 (lambda =1). For NVO of 50, 80, 100 CAD, SOI was set to 300, 360, and 380 CAD bTDC firing. At each of these points, spark timing was adjusted to allow maximum external EGR while COV was maintained below 4%. Engine operating conditions for these experiments are summarized in Table 6.4.

Table 6.4. Engine operating conditions for dilution limit investigation

Actuator	Value
Engine Speed	1800 RPM
BMEP	3 bar
Air-fuel ratio (mass basis)	14.02
EVC (reference lift = 0.5 mm)	25, 40, 50 CAD bTDC gas exchange (385, 400, 410 CAD bTDC firing)
IVO (reference lift = 0.5 mm)	25, 40, 50 CAD aTDC gas exchange (335, 320, 310 CAD bTDC firing)
Fuel Injection Pressure	100 bar
Start of Injection	300, 360, 380 CAD bTDC firing
Spark Timing	Set to allow maximum external EGR
EGR dilution	Increased until COV reached 4%
COV of IMEP	<4%
Average Pressure Rise Rate	<3 bar/ CAD

The rate of heat release analysis and residual estimation was performed using three pressure analysis (TPA) in GT Power (Gamma Technologies) [197]. With this analysis, crank-angle based intake, exhaust and cylinder pressures are used in conjunction with cylinder head port flow data and intake and exhaust valve lift profiles to determine the crank angle based contents of the cylinder (air flow, residual content and fuel quantity) at the start of combustion [198]. The TPA method in G-T power was used to calculate the fraction of internal EGR. This model uses intake, exhaust and cylinder dynamic pressures as boundary conditions of each pipe inlet and outlet. The in-cylinder thermodynamic state is calculated using instantaneous mass flow rates through the intake and exhaust ports and the cylinder pressure measurement, and by solving the equation of state for an ideal gas. Several assumptions are applied for this analysis including that the ideal gas model is valid; losses in the pipes are negligible (isentropic flow); the intake gas is a homogeneous stoichiometric mixture, and complete combustion occurs. Mixing at the valve ports by backflow is not considered. The conservation of mass (flow rate basis) and momentum equations in the form of the method of characteristics were solved along the pipe length. The mode cycle (the most frequently occurring) for peak pressure out of 300 cycles of pressure data was chosen for the heat release analysis using TPA with GT power. Firstly, the cycles were grouped by peak

pressure after rounding the peak pressure to two significant figures. Then the group that has the mode peak pressure was found out, and the first cycle in that group was picked to perform the heat release. The Woschni heat transfer correlation [199] was used.

6.3 Results and Discussion

6.3.1 Start of Injection Investigation

The rate of heat release profiles for different SOI timings with NVO = 80 CAD are shown in Figure 6.2. For cases with SOI from 300 CAD bTDC to 380 CAD bTDC, the heat release analysis shows distinct regions of flame propagation followed by rapid auto-ignition of the remaining charge. Auto-ignition is promoted by higher compression ratio and increased gas temperature from the use of NVO. For SOI more advanced than 380 CAD bTDC, the data indicate weak and late combustion conditions exist. The maximum of the second derivative of the rate of heat release was used to determine the time of rapid auto-ignition of the remaining charge and calculate the flame propagation burn fraction [200].
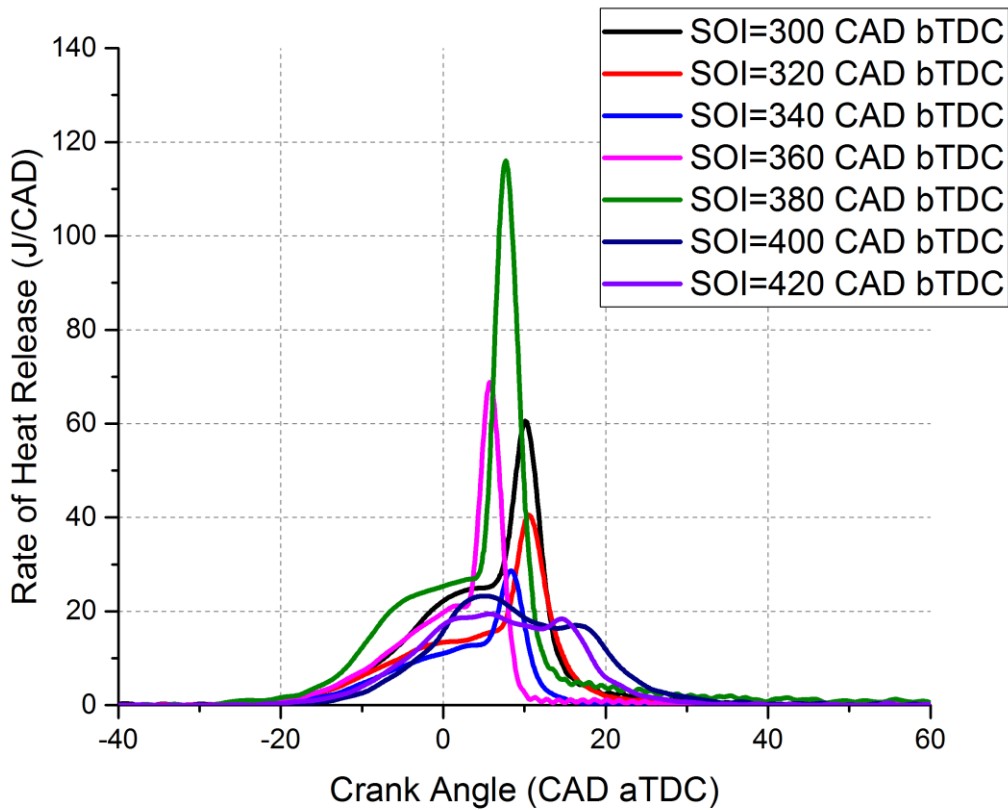
Figure 6.2 Heat release rate profiles for NVO = 80 CAD and various SOI timings.

The results in Figure 6.2 show SOI strongly affects the rate of heat release, with the maximum rate of heat release occurring for SOI = 380 CAD bTDC. Earlier and later SOI timing decreases the maximum rate of heat release. As stated earlier, previous research has shown the fuel reforming process under low O_2 conditions produces substantial concentrations of H_2, CO, methane, and other short-chain hydrocarbon species [151], and these species can increase the rate of flame propagation and the rate of heat release. As the fuel is injected earlier, there is more time available for the fuel reforming process which contributes to the higher rate of heat release. However, when fuel is injected at the beginning or before NVO period, the data resemble conventional spark-ignited combustion. Early SOI causes the gamma (i.e., the ratio of the specific heats) during NVO compression to be lower (due to the lower ratio of specific heats for gasoline), so the temperature at TDC is reduced. This may reduce NVO reaction, resulting in lower IVC temperature and fewer radicals, which reduces the amount of the charge consumed by auto-ignition.

The results for CA50, the crank angle at which 50% of the total apparent heat release occurs, and the burn fraction of flame propagation for the SOI study are plotted in Figure 6.3. CA50 is advanced from 8.9 to 5.6 CAD bTDC by advancing SOI from 300 to 380 CAD. The burn fraction of flame propagation also decreases with advancing fuel injection timing. The method for calculating flame propagation fraction is not valid for early SOI (400 and 420 CAD bTDC) because there is no significant increase in the heat release for these cases. The error bars in the figures represent the standard deviation for all engine cycles analyzed for each test condition, where a minimum of 300 cycles was considered for each operating condition.

From Figure 6.4, it can be seen that varying SOI from 300 to 420 CAD causes a maximum variation in BMEP of less than 5%. Figure 6.4 includes the results for maximum pressure rise rate, and the data show (expectedly) the maximum pressure rise rate correlates with the results for maximum rate of heat release presented in Figure 6.2. The constant BMEP also indicates there is little change in volumetric efficiency.

NVO fuel injection can improve combustion stability by affecting the species produced during NVO fuel reforming, improving the chemical reactivity of the charge, and increasing charge temperature [149]. The results for combustion stability (COV of IMEP) for the SOI study are presented in Figure 6.5. When SOI is advanced from 300 to 380 CAD bTDC, COV of IMEP is reduced from 3.9% to 1.5%. COV of IMEP increases again as SOI is further advanced, indicating there is an optimum SOI in terms of engine stability. The auto-ignition variability is lower than flame propagation variability which leads to lower overall variability when more auto-ignition is present. The results for BSFC are also presented in Figure 6.5, and show SOI has little effect on fuel consumption for the conditions studied. Also, when fuel is injected before or at the beginning of NVO, the results indicate no measurable fuel flows into the exhaust if the fuel is injected into the cylinder while the exhaust valve is still open.

Emissions data are shown in Figure 6.6. When SOI is advanced, exhaust CO decreases monotonically from 7282 ppm to 6480 ppm, which may be due to a less stratified charge

during NVO period caused by advanced fuel injection timing. Also shown in Figure 6.6 is that NOx is maximized for SOI timings between 380 and 400 CAD bTDC, which coincides with the SOI timings that produce the maximum ROHR.
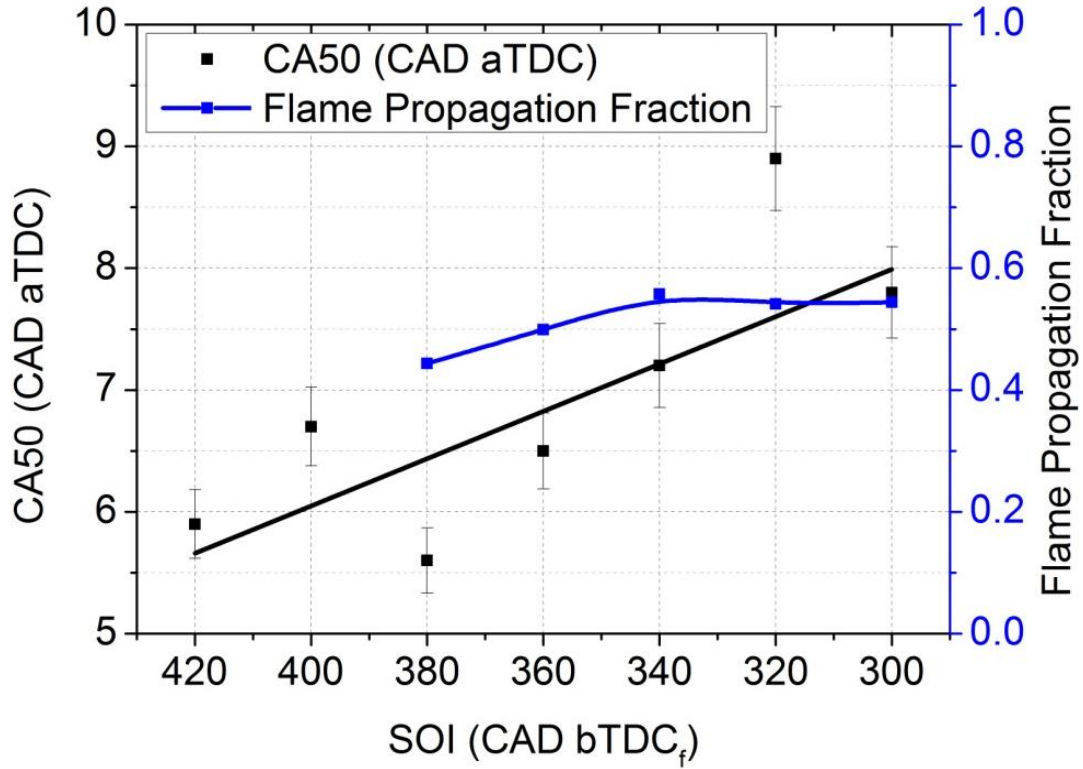
Figure 6.3. CA50 and fraction of flame propagation at NVO = 80 CAD as a function of SOI timing.
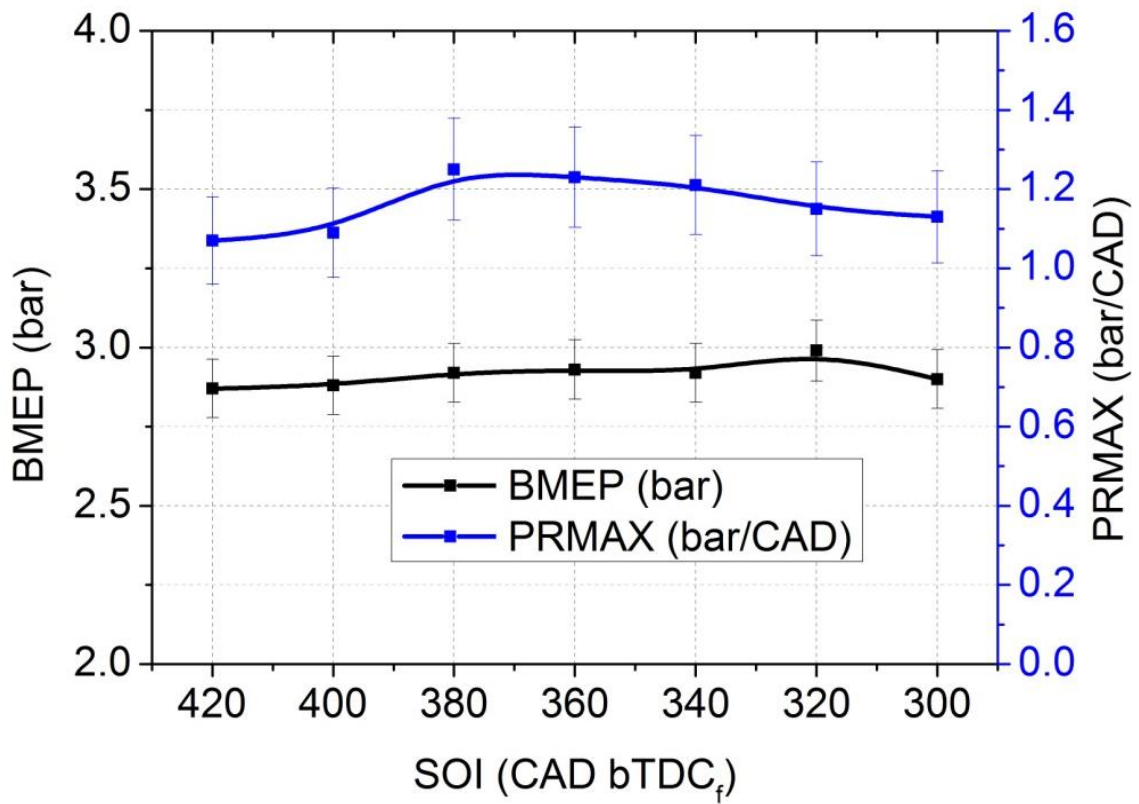
Figure 6.4. BMEP and maximum pressure rise rate at NVO = 80 CAD as a function of SOI timing.
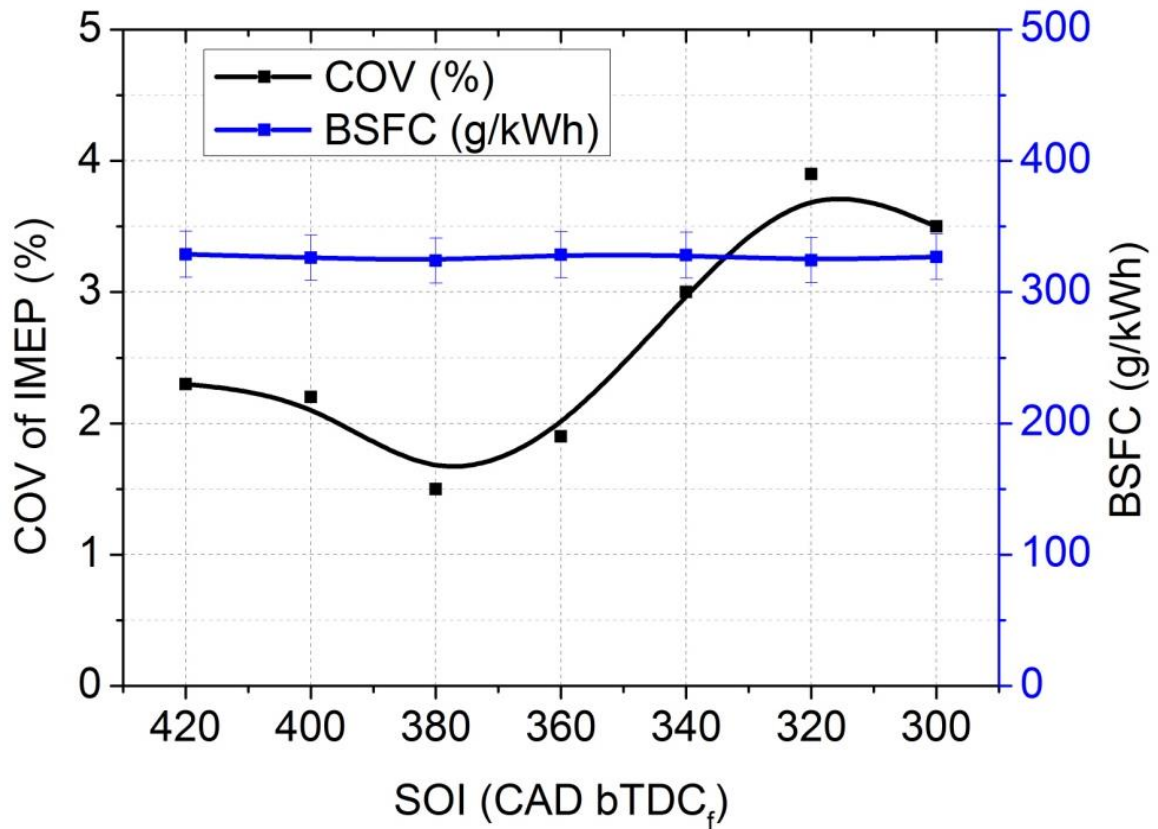
Figure 6.5. COV of IMEP and BSFC at NVO = 80 CAD as a function of SOI timing.
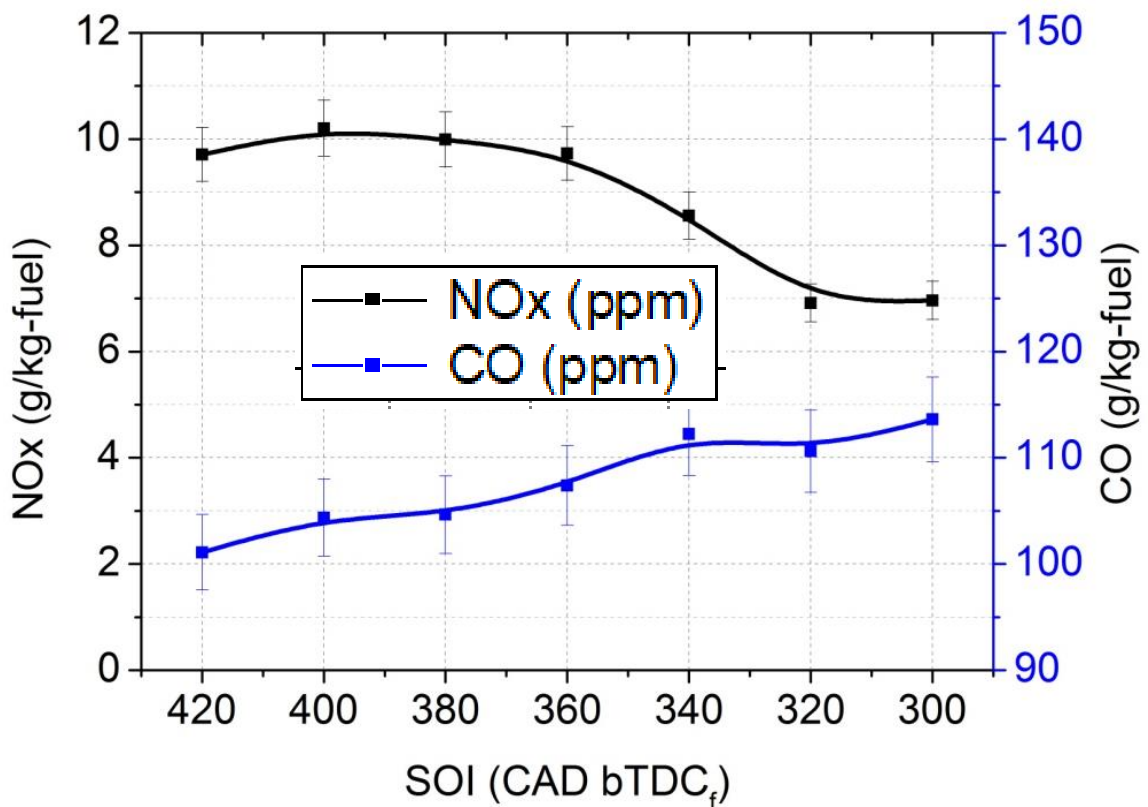
Figure 6.6. CO and NO$_x$ emissions at NVO = 80 CAD and various SOI timings.

6.3.2 Dilution Limit Investigation

In the previous section, operating conditions for NVO = 80 CAD, SOI of 360 and 380 CAD bTDC were shown to have the lowest COV of IMEP, which suggests the most significant potential for extending the dilution limit. In this section, additional NVO and SOI settings are investigated while operating the engine at its dilution limit by adjusting spark timing to allow maximum external EGR without exceeding 4% COV of IMEP.

Figure 6.7 shows rate of heat release profiles for the engine operated at its dilution limit with different NVO and SOI settings. The data indicate an NVO duration of 50 CAD avoids auto-ignition due to low internal EGR and low NVO temperatures. As seen in the previous section, an NVO duration of 80 CAD results in a significant fraction of the charge being consumed by auto-ignition when fuel is injected during the NVO period. When fuel is injected after the NVO period for NVO = 80 CAD, the heat release rate is greatly reduced. An NVO duration of 100 CAD causes the autoignition event to occur for every SOI condition studied, due to the large amount of internal EGR. The large fraction of autoignition associated with an NVO duration of 100 CAD also causes a high-pressure rise rate, as shown in Figure 6.8. Overall, Figure 6.8 shows higher NVO duration leads to higher maximum pressure rise rates.

The dilution limit data presented in Figure 6.8 also show CA50 can be adjusted to 7 CAD aTDC without misfire or excessive pressure rise rate (i.e., pressure rise rates higher than 3 bar/degree) using an NVO duration of 80 CAD and fuel injection around the middle of the NVO period. This operating condition also coincides with the lowest BSFC for all NVO durations studied as seen in Figure 6.9. Figure 6.9 also shows the total EGR molar fraction (internal and external EGR) at the dilution limit. When fuel is injected during the NVO period, a larger NVO duration allows higher tolerance to EGR. However, when fuel is injected after the NVO period, the EGR tolerance at the dilution limit with NVO duration of 100 CAD is slightly lower than that of 80 CAD due to the lack of fuel reforming process. Comparison of the results with the baseline dilution limit of this engine of 10% external EGR (same camshaft, same compression ratio, same custom piston and cylinder head) without

NVO proves the effectiveness of the strategy of fuel injection during NVO to extend the low load dilution limit of spark ignition combustion.
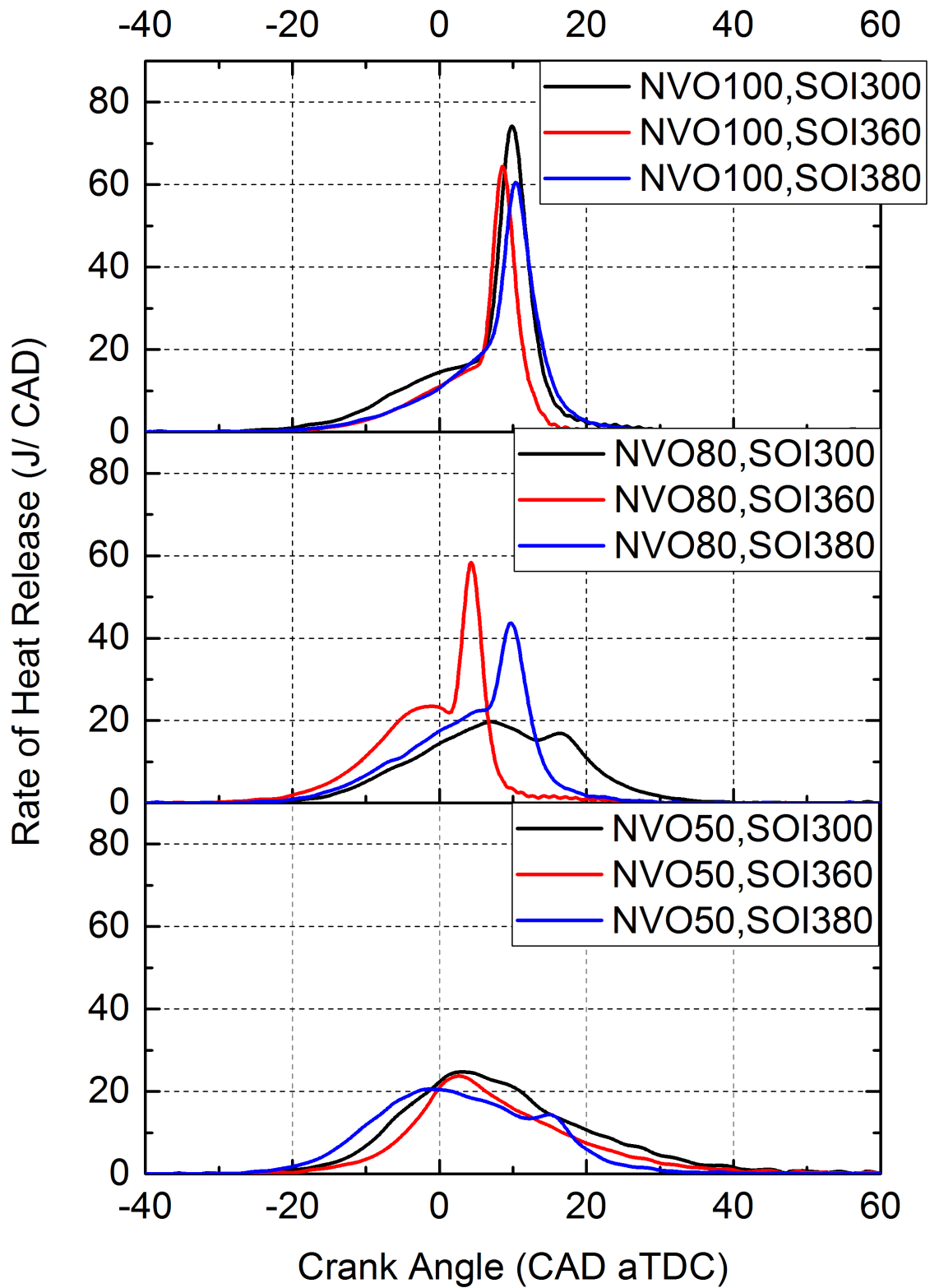
Figure 6.7. Heat release rate profiles at dilution limit conditions.
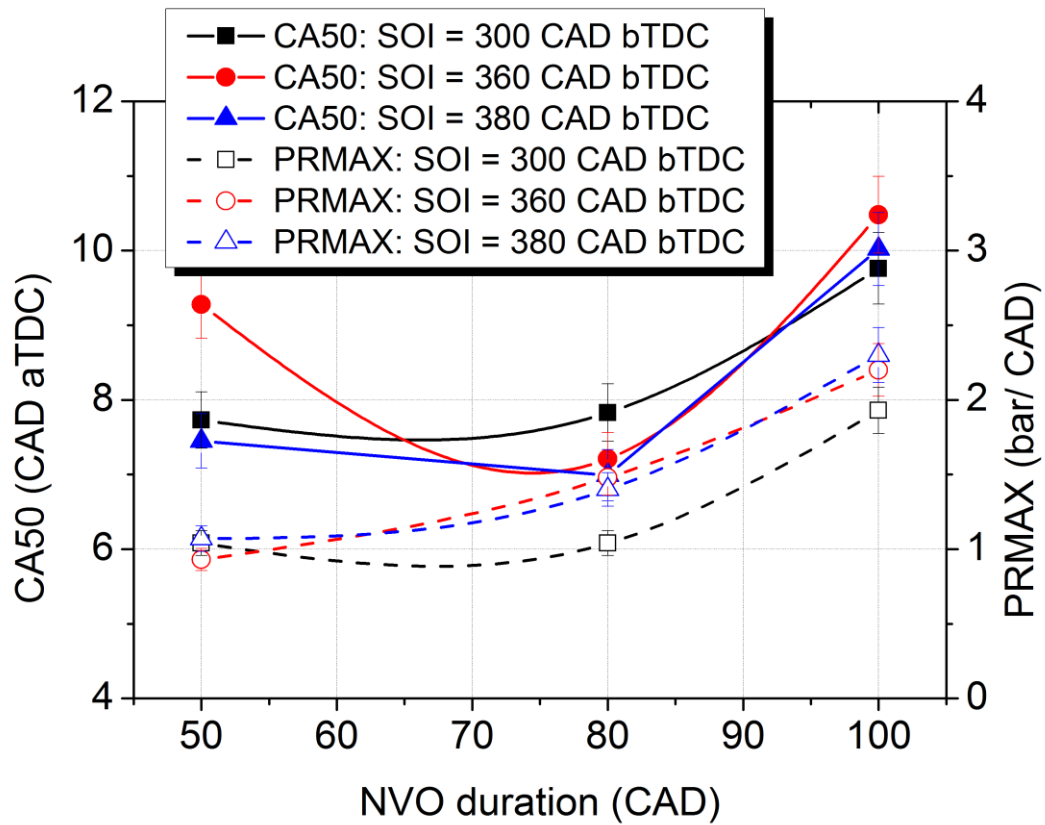
Figure 6.8. CA50 and maximum pressure rise rate at dilution limit conditions.
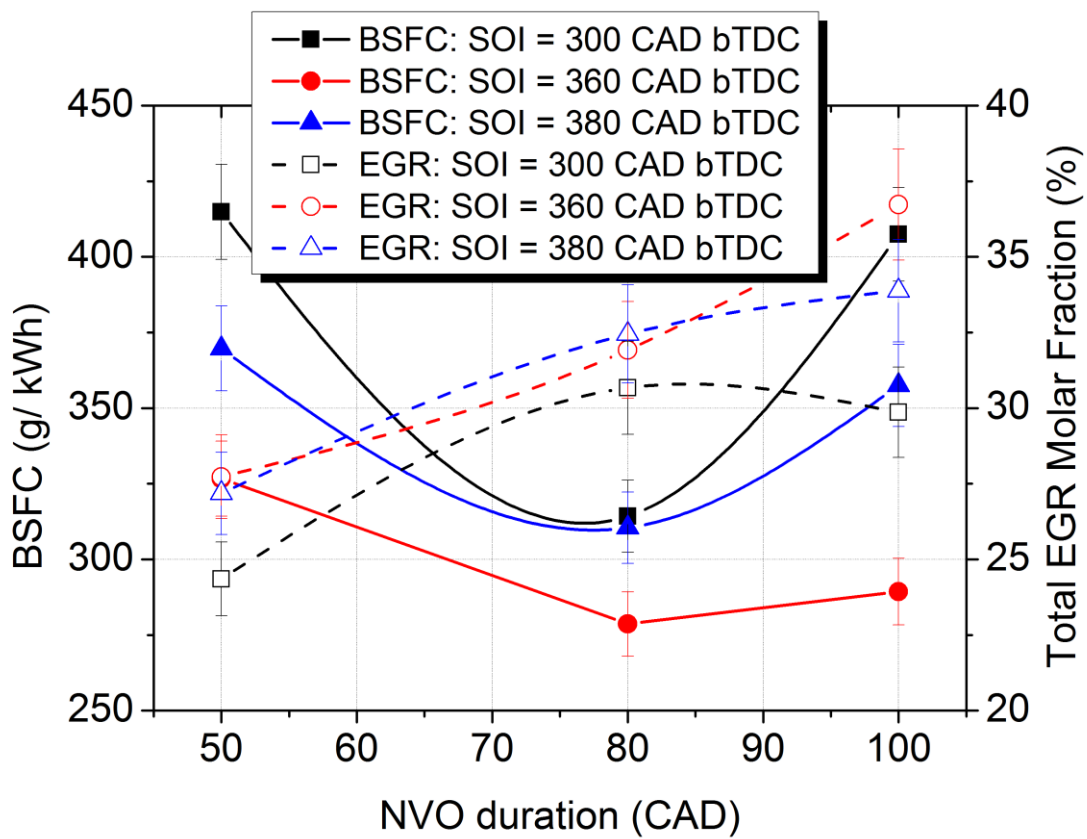
Figure 6.9. BSFC and total EGR molar fraction at dilution limit conditions.

Internal EGR molar fraction increases with increasing NVO duration, while the tolerated external EGR molar faction decreases with increasing NVO duration as shown in Figure 6.10. Higher external EGR leads to lower pumping losses, while higher internal EGR contributes to greater fuel reforming and more retained heat in the cylinder. When fuel is injected during the NVO period, external EGR tolerance is higher compared with operating conditions when fuel is injected after the NVO period.

Different combinations of internal EGR and external EGR lead to different maximum heat release rates with different phasing which affect the thermal efficiency. Too much internal EGR can lead to knock, while too much external EGR can lead to the misfire. Both outcomes also lead to higher COV, which limits optimization for BSFC. The data of Figure 6.9 and Figure 6.10 indicate a combination of internal EGR, external EGR and fuel injection near the middle of the NVO duration contribute to optimal fuel efficiency. Specifically, the lowest BSFC of 278.7 g/ kWh was recorded for SOI timing in the middle of the NVO duration of 80 CAD. The production version of the General Motors Ecotec LNF engine with the same displacement has been tested as the baseline engine and the operating condition with best fuel efficiency that we could calibrate to is BSFC of 314.2 g/kWh without EGR and with compression ratio of 9.25 at the same speed and load condition (1800 RPM and 3 bar BMEP). The efficiency improvement of this fuel injection strategy and the high EGR with high compression ratio is around 11% compared to LNF baseline engine. So the results of the current study demonstrate the strategy of fuel injection during the NVO period with EGR, and high compression ratio leads to the fuel efficiency improvement and dilution limit extension.
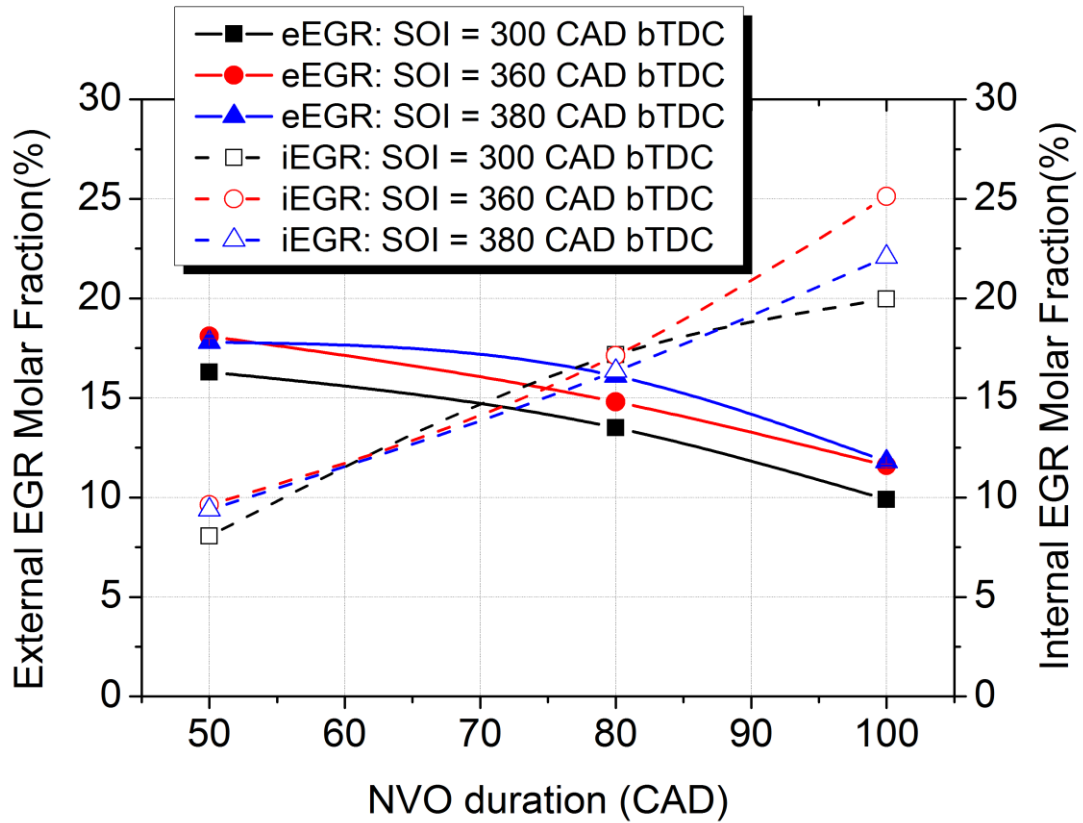
Figure 6.10. External EGR and internal EGR at dilution limit conditions.

The CO and NO_x emissions at the dilution limit conditions are shown in Figure 6.11. Both CO and NO_x concentration decrease as NVO is increased. Comparing the baseline case of SOI = 300 CAD bTDC and NVO = 50 CAD of this modified engine, with the optimized case of SOI = 360 CAD bTDC and NVO = 80 CAD, CO is reduced from 5100 to 3865 ppm, and NO_x is reduced from 350 to 281 ppm. The CO and NO_x emissions for the stock production version of the General Motors Ecotec LNF engine (which does not use external EGR) at the same speed/load condition are 3230 ppm and 986 ppm, respectively.
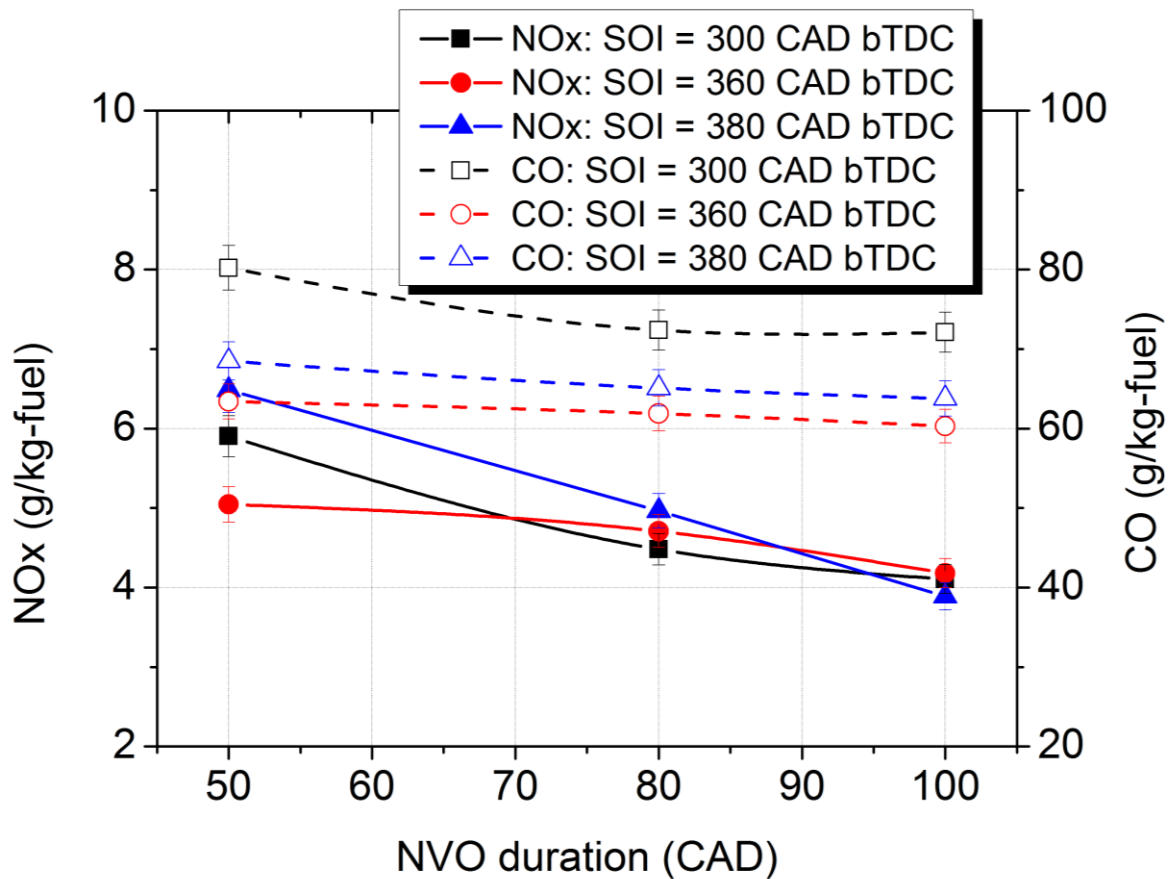
Figure 6.11. CO and NOx emission at dilution limit conditions.

6.4 Conclusions

This study quantified the effects of fuel injection during NVO on combustion, dilution limit, fuel efficiency, and engine-out emissions as a function of external EGR, SOI during NVO, and NVO duration. When other settings are fixed, SOI during NVO strongly affects the rate of heat release. The data indicate a transition from operating conditions consistent with flame propagation followed by rapid auto-ignition of the remaining charge to weak auto-ignition and then to conventional spark-ignited combustion as SOI was advanced. Phasing of CA50 advanced and the fraction of charge consumed by flame propagation decreased with advanced fuel injection timing. An optimum time for SOI in terms of engine stability (based on COV of IMEP) was observed. When SOI was advanced, CO levels in the exhaust decreased monotonically while NOx levels increased with advanced SOI and were highest for SOI timings between 360 and 380 CAD bTDC, which coincided with the SOI timings that

produced the highest rate of heat release. SOI of 360 and 380 CAD bTDC were shown to have the lowest COV of IMEP, suggesting the greatest potential for extending the dilution limit.

At dilution limit conditions, when fuel was injected during the NVO period, larger NVO duration led to higher tolerance to total EGR. Internal EGR mole fraction increased with the increase of NVO duration while the tolerated external EGR mole faction decreased with the increase of NVO duration. When fuel was injected during the NVO period, EGR tolerance is higher compared to operating conditions when fuel was injected after the NVO period. The results show 80 CAD of NVO with SOI at TDC allowed for the addition of 32% total EGR and resulted in the best BSFC. Higher total EGR mole fractions did not lead to even lower BSFC. CO and NOx concentrations decreased as NVO duration increased.

This study demonstrated that fuel injection during NVO could extend the dilution limit of SI engine operation. The amount of internal EGR, external EGR, and timing of fuel injection provide parameters for optimizing fuel efficiency. Furthermore, fuel injection during NVO was shown to improve BSFC and reduce the NOx emissions compared with baseline SI operating conditions. Thus, fuel injection during NVO has been shown to be a powerful means to improve SI engine performance while maintaining stoichiometric operation to enable effective three-way catalyst after treatment. A challenge of this operating strategy is the need for control of valve open timing and duration. If camshaft phasing is made with no change in camshaft duration, EVO and IVC will be affected when the NVO period is changed, and this can have adverse effects. Engine stability also has to be closely monitored.

Chapter 7. Comparison of Different Fuel Reforming Strategies

7.1 Overview of Different Fuel Reforming Integrated ICE Systems

With the literature review of other fuel reforming strategies described in Chapter 2 and the detailed explanation and verification of the development of three fuel reforming strategies demonstrated in this thesis (Chapter 4 to Chapter 6), one might ask how to choose the suitable fuel reforming strategy for an integrated engine system with high fuel economy and how to design a fuel reforming system that leads to higher fuel economy.

This is a very complex question to answer due to the combination of factors for the feasibility of a specific technology, such as cost-effectiveness, packaging issues, and durability of components, which are critical to the reliability of a system and quality control. In addition, all the research on fuel reforming integrated engine systems published by other researchers and proposed in this thesis involve several sub-systems have different response lags. Control algorithms to achieve effective powertrain control, especially during transient operating conditions, need to be developed and verified. More importantly, the interferences and effects of a fuel reforming system with other systems in the vehicle, such as after-treatment systems and the turbocharger, need to be considered. These systems are also significantly important to the fuel economy of powertrain systems. Last but not least, the on-board fuel reforming integrated engine systems are not yet in production, so the data for the public concerning the parameters and performances at different operating conditions of the developing technologies is very limited. This makes it difficult to be very fair and quantitative in comparing various fuel reforming ICE systems.

Table 7.1. Comparison of Key Characters and Parameters of Different Fuel Reforming Integrated ICE Systems

FUEL REFORMING ENGINE SYSTEM	FUEL TYPE	ENGINE TYPE	CATALYST	THERMAL EFFICIENCY IMPROVEMENT (%)	PEAK HYDROGEN CONCENTRATION (%)	LAMBDA	COMPRESSION RATIO	EGR RATE (%)	COMMENTS
DEDICATED EGR FROM SWRI [144]	Gasoline	Stoichiometric SI	None	13% (compared to Regal Premium baseline with CR =11.2)	1% Intake	1 (0.71-0.77 for D-EGR cylinder)	11.7	25%	Fuel economy improvement by 13% for City MPG, and 9% for Highway MPG
NVO FUEL INJECTION*	Gasoline (E10)	Stoichiometric SI	None	11% (compared to LNF baseline with CR = 9.2, ~4% from EGR addition, ~5% from CR)	N/A	1	11.7	35%	1800 rpm, 3 bar BMEP
COMMITTED IN-CYLINDER* REFORMER	Ethanol	Stoichiometric SI	None	8%	0.8% Intake	1 (1.0-1.4 for reforming cylinder)	9.2 (12.9 for reforming cylinder)	~25%	2000 rpm, 4 bar BMEP
E85 REFORMING SYSTEM FROM AVL [159]	Ethanol (E85)	Stoichiometric SI	Copper-plated nickel sponge	10%	N/A	1	12	N/A%	1500 rpm, 2.6 BMEP
CATALYTIC EGR-LOOP* REFORMING	Isooctane or Gasoline	Stoichiometric SI	Pre-commercial 2 wt % Rh supported on Al_2O_3	More than 8% with larger potential	15% outlet of the reformer, 5% Intake	1 (1.1-1.4 for reforming cylinder)	9.2	45-55%	2000 rpm, 4 bar BMEP
DUAL FUEL ON-BOARD REFORMING FROM UMN [160]	ULSD Diesel	CI	Catalyst containing Rh and Pt	Negative	12% outlet of the reformer	Highly lean	16.5	N/A%	1500 rpm, 4 bar BMEP; 2000 rpm, 5 bar BMEP

ON-BOARD THERMOCHEMICAL ENERGY RECOVERY TECHNOLOGY FROM U OF BIRMINGHAM [161]	Gasoline	Stoichiometric SI	Ceria-Zirconia–Alumina loaded with 3.3% Platinum/1.7% Rhodium	8% for high-temperature condition and 4% for low-temperature condition	Up to 7.3%	1	N/A	26%	2100 rpm, 35 Nm; 3000 rpm, 50 Nm; 2100 rpm, 105 Nm
BASELINE	Gasoline	Stoichiometric SI	None	4%	0%	1	9.2	25%	2000 rpm, 4 bar BMEP

*Fuel reforming systems marked by red color shown in column 1 are the systems developed in this thesis.

Table 7.1 provides a comparison of different fuel reforming systems, which are proposed by researchers that are leading the development of fuel reforming integrated engine systems, and the systems developed in this thesis (marked by red color). "N/A" shown in this table indicates that the specific information is not available. The key characteristics and parameters include the fuel type used for the fuel reforming process, the engine type (specifically SI or CI), catalyst formulation (if the system is a catalytic reforming system), thermal efficiency improvement of the integrated system compared to the baseline without fuel reforming, and peak hydrogen concentration that the reforming system could produce. The lambda in the cylinders for both normal cylinders and reforming cylinders, the compression ratio for both normal cylinders and reforming cylinders, and EGR rate in the system are also provided.

In terms of the comparison of the three strategies proposed in this thesis, catalytic EGR loop reforming provided more than 8% efficiency improvement and high H_2 concentration. The potential for further efficiency improvements, such as increases of compression ratio and cylinder balance, makes it even more promising. In addition, the space required to install this system is similar to that of a cooled EGR loop system, which has been widely used in vehicles. However, a catalytic reformer requires additional cost, and the payback period for the customers' needs to be evaluated. Additionally, the relatively low sulfur tolerance (7 ppm) of the catalyst causes a little concern for implementing this technology with Tier III gasoline (10 ppm). The development of the powertrain control of the startup and transient operating conditions is also critical for this implementation.

The strategy of NVO fuel injection needs to be implemented together with high compression ratio, variable valve timing, and variable valve duration capability, and cooled EGR loop setup. Considering the wide use of dual independent cam phasers and relatively high compression ratio, such as in Buick Regal which is powered by 2.0 turbocharged GM LHU installed with dual independent cam phasers and 11.2:1 compression ratio, this strategy is relatively easier to adapt. It mainly requires efforts on engine calibration, even though the efficiency benefit is relatively small.

The committed in-cylinder reformer is capable of improving thermal efficiency. However, the benefits come mainly from cylinder deactivation and EGR instead of dilution limit extension and shortening of combustion duration. This method is not recommended to be promoted before the technical challenges are addressed.

When we evaluate the performance of different fuel reforming systems, the following key factors are identified to significantly influence the performance of the fuel reforming integrated engine systems.

7.2 Key Factors of Performance of Fuel Reforming Integrated Engine Systems

7.2.1 Non-Catalytic Reaction vs. Catalytic Reaction

It can be seen from Table 7.1 that the catalytic reforming systems produce much higher peak hydrogen concentrations than the non-catalytic in-cylinder reforming systems. Ekoho et al. [152] also showed that for all equivalence ratios, minimum temperatures between 1000 and 1050K are required to generate significant amounts of reformed products (shown in Figure 4.15) without a catalyst.

To understand the possible homogenous reactions without the catalyst in the catalytic EGR-loop reforming system, ignition delay calculations were performed. The calculations were done using CHEMKIN closed homogeneous batch reactor with iso-octane over the range of initial temperatures (750 K to 900 K), and the species concentration which corresponds to the equivalence ratios, and oxygen concentrations investigated experimentally in Chapter 5 of the exhaust products before entering the reformer. LLNL gasoline kinetic mechanism was used. The ignition delay times of those operating conditions are much larger than the residence time of catalytic reformer (<100 ms), which indicates that it is difficult to have a big contribution of homogeneous reactions without heat from exothermic reactions.

However, the D-EGR with a small concentration of hydrogen (around 1%) also contributes to the significant improvement of thermal efficiency.

7.2.2 Spark Ignited Gasoline System vs. Compression Ignited Diesel System

Exhaust from a CI diesel system normally contains a much higher concentration of oxygen compared to exhaust from a traditional SI gasoline system. When the oxygen concentration is high, the EGR fuel reforming process involves a large portion of partial oxidation reaction which produces hydrogen but consumes energy as well. That might be the primary reason why the dual fuel diesel thermal integrated diesel reforming system [160] (Figure 2.10) has a negative effect on the thermal efficiency of the engine system even though a high percentage of hydrogen is produced.

The compression ratio difference between SI gasoline system and CI diesel system also leads to different in-cylinder temperatures after the compression process for in-cylinder reforming and difference in exhaust temperatures, which have an impact on the reforming process.

7.2.3 Fuel Properties

C/H ratio of fuel changes the reaction heat as well as the H_2 fraction of reforming products so that the performance of reforming system would be affected. Sulfur content in the fuel is an issue because of catalyst poisoning for catalytic reforming process. Simulation of alcohol steam reforming processes confirmed that use of methanol as a primary fuel allowed effective reforming at low temperatures of approximately 570 K compared with 1000-1100 K for ethanol [201].

7.2.4 Engine Operating Conditions

Different engine operating conditions change exhaust temperature and sometimes even exhaust composition so that the fuel reforming process is affected. Fennell et al. [161]

showed that their catalytic fuel reforming engine system (Figure 2.11) could improve fuel consumption up to 8% for high-temperature conditions and 4% for low-temperature conditions.

7.3 Conclusions

Several significant factors need to be considered to design efficient integrated fuel reforming systems. The most important ones are 1. whether to include the catalyst to generate reformates, 2. which type of engine is used (gasoline engine or diesel engine), 3. fuel properties used for main combustion and fuel reforming, and 4. the operating conditions of the engines and vehicles.

In many cases, reformate generation can incur a significant fuel penalty. Ideally, one might expect the highest levels of thermochemical recuperation for the highest catalyst equivalence ratios. However, reforming under these conditions is highly endothermic, and the available enthalpy for reforming is constrained. Efficient energy management such as the fraction of the partial oxidation reaction and endothermic reactions over the whole integrated systems with the different engine operating conditions is necessary. In addition, issues which might occur during the transient conditions of powertrain systems and cold start conditions need to be addressed before the application of integrated fuel reforming engine systems.

Chapter 8. Conclusions and Future Work

8.1 Conclusions

In conclusion, the objectives of this research study have been satisfied in the successful development of improved efficiency and dilution limit extension in gasoline-fueled spark-ignited combustion engine systems enabled by fuel reforming strategies while keeping the capability of using current mature stoichiometric after-treatment systems. More specifically, the research study has contributed the following knowledge to the engineering community:

- There is a limited spark timing window available to compensate for the longer combustion duration that occurs as a result of high EGR rates. Combustion stability limit occurs at approximately the same combustion duration for all fuels. Combustion duration is responsible for combustion instability, and the fuel type can affect the combustion duration, thereby influencing combustion stability.

- The concept and the system to use one cylinder to serve as a committed fuel reformer without spark ignition to make use of the exhaust heat by breathing in the exhaust from other cylinders is first proposed and demonstrated. The introduction of small amounts of oxygen during the committed in-cylinder reforming activities proved to be effective at increasing the fuel conversion. However, even the highest fuel conversion rates achieved were ineffective at increasing the EGR dilution tolerance in the remaining cylinders. The thermal efficiency improvement of 8% from this strategy is mainly due to cylinder deactivation and EGR addition.

- The unique EGR-Loop reforming system, in which the entirety of the exhaust from one of the cylinders (cylinder 4 has an isolated intake and exhaust manifold) is fed directly to the reforming catalyst, which then feeds into the intake for cylinders 1-3 is designed. In the engine experiment, this is accomplished by operating the main combustion event in cylinder 4 fuel-lean, but then using a post-injection when the exhaust valve opens to feed the catalyst the appropriate mixture. This novel design opens up a new method to control the amount of fuel reforming and the fraction of partial oxidation reforming and steam reforming by adjusting the lambda value of cylinder 4 to resolve the problem of enthalpy limit. In addition, the post-injection strategy to provide fuel to the fuel reformer eliminates the need for a port fuel injector which is commonly used by other catalytic reforming research.

- The catalytic reforming process was successfully applied to the engine. Experiments on the engine demonstrated H_2 and CO production over a wide range of reforming conditions. There is a maximum in H_2 production that approaches 15% at equivalence ratios between 5 and 7 and with high oxygen flow rate. The ways to balance the tradeoff of the hydrogen reformates concentration and thermal recuperation for the integrated system are also found.

- A significant increase in engine efficiency was achieved with the catalytic reforming process. Over the baseline case, brake thermal efficiency was increased leading to more than 8% reduction in fuel consumption. Higher compression ratio capability of the engine system, provided by the high tolerance of EGR from high H_2 concentration from fuel reforming, and energy balance optimization provide huge space for larger thermal efficiency improvement.

- The special design of the catalytic reforming testing system enables separate testing for the characteristics of the catalyst performance and overall engine performance, which can be referred as a systematic way to test different types of the catalyst with the purpose of catalytic reforming. Also, the systematic procedure proposed at each experimental condition to ensure the regeneration of any possible coking and

consistency of data, and to avoid the overheating of the catalyst during the regeneration events provides a good reference to other researchers working on catalytic fuel reforming.

- The fuel injection strategy during NVO period is combined with VVT and high compression ratio and provides 11% fuel efficiency improvement over baseline with normal compression ratio and no EGR. This research implements NVO fuel injection strategy for stoichiometric SI combustion while other NVO fuel injection research mainly focused on HCCI combustion and SACI combustion.

8.2 Suggestions for Future Work

The opportunities to investigate fuel reforming integrated engine systems or other types of powertrain systems is tremendous. I would be happy to offer some suggestions for follow-up studies related to the major topics of this thesis.

1. Test the strategies of catalytic EGR-loop reforming and fuel injection during NVO period over a large range of operating conditions, such as turbo-charged condition and idling condition to observe the effects of operating conditions on the performance of catalytic reforming.

2. Understand the reaction mechanism and reaction dynamics of the catalytic fuel reforming process especially to design a better catalytic reformer and to adjust the input parameters in a more thermodynamically favorable way.

3. Generate models to predict the hydrogen production rate of the catalytic reforming according to exhaust temperature, oxygen concentration, and fuel concentration, providing models for powertrain control of catalytic reforming integrated engine systems.

4. Investigate the synergy of the fuel reforming integrated engine systems with the hybrid powertrain systems to improve the overall vehicle efficiency.

5. Explore other possible catalyst formulations to get new catalyst formulation with a higher tolerance of sulfur. Development in this direction might also enhance the application of fuel reforming integrated engine systems for the application of distributed power generation in marine areas.

BIBLIOGRAPHY

[1]   J. B. Heywood, *Internal combustion engine fundamentals*. Mcgraw-hill New York, 1988.

[2]   A. Alagumalai, "Internal combustion engines: Progress and prospects," *Renewable and Sustainable Energy Reviews*, vol. 38. pp. 561–571, 2014.

[3]   A. M. K. P. Taylor, "Science review of internal combustion engines," *Energy Policy*, vol. 36, no. 12, pp. 4657–4667, 2008.

[4]   D. Splitter, A. Pawlowski, and R. Wagner, "A Historical Analysis of the Co-evolution of Gasoline Octane Number and Spark-Ignition Engines," *Front. Mech. Eng.*, vol. 1, no. 16, p. 16, Jan. 2016.

[5]   G. A. Lavoie, E. Ortiz-Soto, A. Babajimopoulos, J. B. Martz, and D. N. Assanis, "Thermodynamic sweet spot for high-efficiency, dilute, boosted gasoline engines," *Int. J. Engine Res.*, vol. 14, no. 3, pp. 260–278, Jun. 2013.

[6]   D. E. Foster, "Low Temperature Combustion – A Thermodynamic Pathway to High Efficiency Engines," in *Advancing Technology for America's Transportation*, 2012.

[7]   P. Smith and W. K. Cheng, "Assessing the Loss Mechanisms Associated with Engine Downsizing, Boosting and Compression Ratio Change," in *SAE Technical Paper*, 2013, no. 2013-01–0929.

[8]   R. C. Costa and J. R. Sodré, "Compression ratio effects on an ethanol/gasoline fuelled engine performance," *Appl. Therm. Eng.*, vol. 31, no. 2–3, pp. 278–283, 2011.

[9]   L. Bollini Braga, J. L. Silveira, M. Evaristo Da Silva, E. B. Machin, D. T. Pedroso, C. E. Tuna, L. B. Braga, J. L. Silveira, M. Evaristo Da Silva, E. B. Machin, D. T. Pedroso, and C. E. Tuna, "Comparative analysis between a PEM fuel cell and an internal combustion engine driving an electricity generator: Technical, economical and ecological aspects," *Appl. Therm. Eng.*, vol. 63, no. 1, pp. 354–361, 2014.

[10]   U.S. Energy Information Administration, "Annual Energy Outlook 2017 with projections to 2050," 2017.

[11]   P. M. Cox, R. A. Betts, C. D. Jones, S. A. Spall, and I. J. Totterdell, "Acceleration of global warming due to carbon-cycle feedbacks in a coupled climate model.," *Nature*, vol. 408, no. 6809, pp. 184–187, Nov. 2000.

[12]   S. Solomon, G.-K. Plattner, R. Knutti, and P. Friedlingstein, "Irreversible climate change due to carbon dioxide emissions.," *Proc. Natl. Acad. Sci. U. S. A.*, vol. 106, no. 6, pp. 1704–9, Feb. 2009.

[13]   J. D. Shakun, P. U. Clark, F. He, S. A. Marcott, A. C. Mix, Z. Liu, B. Otto-Bliesner, A. Schmittner, and E. Bard, "Global warming preceded by increasing carbon dioxide concentrations during the last deglaciation," *Nature*, vol. 484, no. 7392, pp. 49–54, Apr. 2012.

[14]   U.S. Environmental Protection Agency, "EPA and NHTSA Set Standards to Reduce Greenhouse Gases and Improve Fuel Economy for Model Years 2017-2025 Cars and Light Trucks," 2012.

[15]   "Table 4-23: Average Fuel Efficiency of U.S. Light Duty Vehicles | Bureau of Transportation Statistics." [Online]. Available: https://www.rita.dot.gov/bts/sites/rita.dot.gov.bts/files/publications/national_transportation_statistics/html/table_04_23.html. [Accessed: 25-Oct-2017].

[16]   E. P. A. (EPA) National Science Center for Environmental Publications (NSCEP), "Final Determination on the Appropriateness of the Model Year 2022-2025 Light-Duty Vehicle Greenhouse Gas Emissions Standards under the Midterm Evaluation." [Online]. Available: https://nepis.epa.gov/Exe/ZyNET.exe/P100QQ91.TXT?ZyActionD=ZyDocument&Client=EPA&Index=2011+Thru+2015&Docs=&Query=&Time=&EndTime=&SearchMethod=1&TocRestrict=n&Toc=&TocEntry=&QField=&QFieldYear=&QFieldMonth=&QFieldDay=&IntQFieldOp=0&ExtQFieldOp=0&XmlQuery=. [Accessed: 13-Nov-2017].

[17]   "The U.S. Department of Energy's Vehicle Technologies Office Advanced Combustion Systems and Fuels." [Online]. Available: https://energy.gov/eere/vehicles/advanced-combustion-systems-and-fuels. [Accessed: 26-Oct-2017].

[18]   G. T. Kalghatgi and Society of Automotive Engineers, *Fuel/engine interactions*. SAE International in United States, 2013.

[19]   S. Chu and A. Majumdar, "Opportunities and challenges for a sustainable energy future," *Nature*, vol. 488, no. 7411, pp. 294–303, 2012.

[20]   G. T. Kalghatgi, "Developments in internal combustion engines and implications for combustion science and future transport fuels," *Proc. Combust. Inst.*, vol. 35, no. 1, pp. 101–115, 2015.

[21]   B. Bilgin, P. Magne, P. Malysz, Y. Yang, V. Pantelic, M. Preindl, A. Korobkine, W. Jiang, M. Lawford, and A. Emadi, "Making the Case for Electrified Transportation," *IEEE Trans. Transp. Electrif.*, vol. 1, no. 1, pp. 4–17, Jun. 2015.

[22]   J. N. Barkenbus, "Eco-driving: An overlooked climate change initiative," *Energy Policy*, vol. 38, no. 2, pp. 762–769, 2010.

[23]   "New 2.5-liter Direct-injection, Inline 4-cylinder Gasoline Engine | TOYOTA Global Newsroom." [Online]. Available: http://newsroom.toyota.co.jp/en/powertrain/engine/. [Accessed: 26-Oct-2017].

[24]   T. Alger, T. Chauvet, and Z. Dimitrova, "Synergies between High EGR Operation and GDI Systems," *SAE Int. J. Engines*, vol. 1, no. 1, pp. 2008-01–0134, Apr. 2008.

[25] J. A. Caton, "A Comparison of Lean Operation and Exhaust Gas Recirculation: Thermodynamic Reasons for the Increases of Efficiency," in *SAE Technical Paper*, 2013, no. 2013-01–0266.

[26] T. Alger, B. Mangold, C. Roberts, and J. Gingrich, "The Interaction of Fuel Anti-Knock Index and Cooled EGR on Engine Performance and Efficiency," *SAE Int. J. Engines*, vol. 5, no. 3, pp. 2012-01–1149, Apr. 2012.

[27] M. Tabata, T. Yamamoto, and T. Fukube, "Improving NOx and Fuel Economy for Mixture Injected SI Engine with EGR," in *SAE Technical Paper*, 1995, no. 950684.

[28] B. C. Kaul, C. E. A. Finney, R. M. Wagner, and M. L. Edwards, "Effects of External EGR Loop on Cycle-to-Cycle Dynamics of Dilute SI Combustion," *SAE Int. J. Engines*, vol. 7, no. 2, pp. 2014-01–1236, Apr. 2014.

[29] T. Alger, J. Gingrich, and B. Mangold, "The Effect of Hydrogen Enrichment on EGR Tolerance in Spark Ignited Engines," in *SAE Technical Paper*, 2007, no. 2007-01–0475.

[30] D. Agarwal, S. K. Singh, and A. K. Agarwal, "Effect of Exhaust Gas Recirculation (EGR) on performance, emissions, deposits and durability of a constant speed compression ignition engine," *Appl. Energy*, vol. 88, no. 8, pp. 2900–2907, 2011.

[31] R. Banerjee, S. Roy, and P. K. Bose, "Hydrogen-EGR synergy as a promising pathway to meet the PM-NO$_x$-BSFC trade-off contingencies of the diesel engine: A comprehensive review," *International Journal of Hydrogen Energy*, vol. 40, no. 37. pp. 12824–12847, 2015.

[32] A. Maiboom, X. Tauzia, and J. F. Hétet, "Influence of EGR unequal distribution from cylinder to cylinder on NOx-PM trade-off of a HSDI automotive Diesel engine," *Appl. Therm. Eng.*, vol. 29, no. 10, pp. 2043–2050, 2009.

[33] D. A. Pierpont, D. T. Montgomery, and R. D. Reitz, "Reducing Particulate and NOx Using Multiple Injections and EGR in a D.I. Diesel," in *SAE Technical Paper*, 1995, no. 950217.

[34] S. Jafarmadar, "Multidimensional modeling of the effect of EGR (exhaust gas recirculation) mass fraction on exergy terms in an indirect injection diesel engine," *Energy*, vol. 66, pp. 305–313, Mar. 2014.

[35] N. Ladommatos, S. M. Abdelhalim, H. Zhao, and Z. Hu, "Effects of EGR on Heat Release in Diesel Combustion," in *SAE Technical Paper*, 1998, no. 980184.

[36] Y. A. Levendis, I. Pavlatos, and R. F. Abrams, "Control of Diesel Soot, Hydrocarbon and NOx Emissions with a Particulate Trap and EGR," in *SAE Technical Paper*, 1994, no. 940460.

[37] A. Maiboom, X. Tauzia, and J.-F. Hétet, "Experimental study of various effects of exhaust gas recirculation (EGR) on combustion and emissions of an automotive direct injection diesel engine," *Energy*, vol. 33, no. 1, pp. 22–34, 2008.

[38] M. Ghazikhani, M. E. Feyz, and A. Joharchi, "Experimental investigation of the Exhaust Gas Recirculation effects on irreversibility and Brake Specific Fuel

Consumption of indirect injection diesel engines," *Appl. Therm. Eng.*, vol. 30, no. 13, pp. 1711–1718, 2010.

[39] N. Ladommatos, S. Abdelhalim, H. Zhao, and Z. Hu, "The dilution, chemical, and thermal effects of exhaust gas recirculation on diesel engine emissions - Part 4: effects of carbon dioxide and water vapour.," in *SAE Technical Paper*, 1998, no. 971660.

[40] N. Ladommatos, S. M. Abdelhalim, H. Zhao, and Z. Hu, "The effects of carbon dioxide in exhaust gas recirculation on diesel engine emissions," *Proc. Inst. Mech. Eng. Part D J. Automob. Eng.*, vol. 212, no. 1, pp. 25–42, 1998.

[41] M. Zheng, G. T. Reader, and J. G. Hawley, "Diesel engine exhaust gas recirculation - A review on advanced and novel concepts," *Energy Convers. Manag.*, vol. 45, no. 6, pp. 883–900, 2004.

[42] M. Dong, G. Chen, M. Xu, C. Daniels, and V. Corp, "A Preliminary CFD Investigation of In-Cylinder Stratified EGR for Spark Ignition Engines Reprinted From : Engine Modeling Techniques : SI and Diesel," in *SAE Technical Paper*, 2002, no. 2002-01–1734.

[43] D. B. Roth, P. Keller, and M. Becker, "Requirements of External EGR Systems for Dual Cam Phaser Turbo GDI Engines," in *SAE Technical Paper*, 2010, no. 2010-01–0588.

[44] Ž. Ivanič, F. Ayala, J. Goldwitz, and J. B. Heywood, "Effects of Hydrogen Enhancement on Efficiency and NOx Emissions of Lean and EGR-Diluted Mixtures in a SI Engine," in *SAE Technical Paper*, 2005, no. 2005-01–0253.

[45] I. Saanum, M. Bysveen, P. Tunestål, and B. Johansson, "Lean burn versus stoichiometric operation with EGR and 3-way catalyst of an engine fueled with natural gas and hydrogen enriched natural gas," in *SAE Technical Paper*, 2007, no. 2007-01–0015.

[46] T. Li, D. Wu, and M. Xu, "Thermodynamic analysis of EGR effects on the first and second law efficiencies of a boosted spark-ignited direct-injection gasoline engine," *Energy Convers. Manag.*, vol. 70, pp. 130–138, 2013.

[47] B. Grandin and H.-E. Ångström, "Replacing Fuel Enrichment in a Turbo Charged SI Engine: Lean Burn or Cooled EGR," in *SAE Technical Paper*, 1999, no. 1999-01–3505.

[48] H. Blank, H. Dismon, M. W. Kochs, M. Sanders, and J. E. Golden, "EGR and Air Management for Direct Injection Gasoline Engines," in *SAE Technical Paper*, 2002, no. 2002-01–0707.

[49] B. Grandin, H.-E. Angstroem, P. Stalhammar, and E. Olofsson, "Knock suppression in a turbocharged SI engine by using cooled EGR," in *SAE Technical Papers*, 1998, no. 982476.

[50] J. P. Szybist and D. Splitter, "Effects of Fuel Composition on EGR Dilution Tolerance in Spark Ignited Engines," *SAE Int. J. Engines*, vol. 9, no. 2, pp. 2016-01–0715, Apr. 2016.

[51] J. Hacohen, S. J. Ashcroft, and M. R. Belmont, "Lean Burn Versus EGR S . I . Engine," in *SAE Technical Paper*, 1995, no. 951902.

[52] M. Fathi, R. K. Saray, and M. D. Checkel, "The influence of Exhaust Gas Recirculation (EGR) on combustion and emissions of n-heptane/natural gas fueled Homogeneous Charge Compression Ignition (HCCI) engines," *Appl. Energy*, vol. 88, no. 12, pp. 4719–4724, 2011.

[53] S. Potteau, P. Lutz, S. Leroux, S. Moroz, and E. Tomas, "Cooled EGR for a turbo SI engine to reduce knocking and fuel consumption," in *SAE Technical Paper*, 2007, no. 2007-01–3978.

[54] L. Francqueville and J.-B. Michel, "On the Effects of EGR on Spark-Ignited Gasoline Combustion at High Load," *SAE Int. J. Engines*, vol. 7, no. 4, pp. 2014-01–2628, 2014.

[55] B. Huang, E. Hu, Z. Huang, J. Zheng, B. Liu, and D. Jiang, "Cycle-by-cycle variations in a spark ignition engine fueled with natural gas-hydrogen blends combined with EGR," *Int. J. Hydrogen Energy*, vol. 34, no. 19, pp. 8405–8414, 2009.

[56] F. Sarikoc, M. Kettner, A. Velji, U. Spicher, A. Krause, and A. Elsaesser, "Potential of Reducing the NOX Emissions in a Spray Guided DI Gasoline Engine by Stratified Exhaust Gas Recirculation (EGR)," in *SAE Technical Paper*, 2006, no. 2006-01–1261.

[57] G. Fontana and E. Galloni, "Variable valve timing for fuel economy improvement in a small spark-ignition engine," *Appl. Energy*, vol. 86, no. 1, pp. 96–105, 2009.

[58] H. Wei, T. Zhu, G. Shu, L. Tan, and Y. Wang, "Gasoline engine exhaust gas recirculation - A review," *Appl. Energy*, vol. 99, pp. 534–544, 2012.

[59] K. Al-Qurashi, A. D. Lueking, and A. L. Boehman, "The deconvolution of the thermal, dilution, and chemical effects of exhaust gas recirculation (EGR) on the reactivity of engine and flame soot," *Combust. Flame*, vol. 158, no. 9, pp. 1696–1704, 2011.

[60] T. Jacobs, D. Assanis, and Z. Filipi, "The Impact of Exhaust Gas Recirculation on Performance and Emissions of a Heavy-Duty Diesel Engine," in *SAE Technical Paper*, 2003, no. 2003-01–1068.

[61] Y. Duchaussoy, A. Lefebvre, R. Bonetto, and S. A. Renault, "Dilution Interest on Turbocharged SI Engine Combustion," in *SAE Technical Paper*, 2003, no. 2003-01–0629.

[62] B. Hoepke, S. Jannsen, E. Kasseris, and W. K. Cheng, "EGR Effects on Boosted SI Engine Operation and Knock Integral Correlation," *SAE Int. J. Engines*, vol. 5, no. 2, pp. 2012-01–0707, Apr. 2012.

[63] D. A. Splitter and J. P. Szybist, "Experimental investigation of spark-ignited combustion with high-octane biofuels and EGR. 1. Engine load range and downsize downspeed opportunity," *Energy and Fuels*, vol. 28, no. 2, pp. 1418–1431, Feb. 2014.

[64] J. P. Szybist, S. W. Wagnon, D. Splitter, W. J. Pitz, and M. Mehl, "The Reduced Effectiveness of EGR to Mitigate Knock at High Loads in Boosted SI Engines," *SAE Int. J. Engines*, vol. 10, no. 5, pp. 2017-24–0061, 2017.

[65]   A. Cairns, H. Blaxill, and G. Irlam, "Exhaust Gas Recirculation for Improved Part and Full Load Fuel Economy in a Turbocharged Gasoline Engine," in *SAE Technical Paper*, 2006, no. 2006-01–0047.

[66]   C. R. Stone, A. G. Brown, and P. Beckwith, "Cycle-by-cycle variations in spark ignition engine combustion-part ii: Modelling of flame kernel displacements as a cause of cycle-by-cycle variations," in *SAE Technical Paper*, 1996, no. 960613.

[67]   N. Ozdor, M. Dulger, and E. Sher, "Cyclic Variability in Spark Ignition Engines A Literature Survey," in *SAE Technical Paper*, 1994, no. 940987.

[68]   J. Sevik, T. Wallner, M. Pamminger, R. Scarcelli, D. Singleton, and J. Sanders, "Extending Lean and Exhaust Gas Recirculation-Dilute Operating Limits of a Modern Gasoline Direct-Injection Engine Using a Low-Energy Transient Plasma Ignition System," *J. Eng. Gas Turbines Power*, vol. 138, no. 11, p. 112807, May 2016.

[69]   T. Alger, J. Gingrich, B. Mangold, and C. Roberts, "A Continuous Discharge Ignition System for EGR Limit Extension in SI Engines," *SAE Int. J. Engines*, vol. 4, no. 1, pp. 2011-01–0661, Apr. 2011.

[70]   J. Wheeler, D. Polovina, S. Ramanathan, K. Roth, D. Manning, and J. Stein, "Increasing EGR Tolerance using High Tumble in a Modern GTDI Engine for Improved Low-Speed Performance," in *SAE Technical Paper*, 2013, no. 2013-01–1123.

[71]   M. Xu, G. Chen, C. Daniels, and M. Dong, "Numerical study on swirl-type high-dilution stratified EGR combustion system," in *SAE Technical Paper*, 2000, no. 2000-01–1949.

[72]   E. Conte and K. Boulouchos, "Hydrogen-Enhanced Gasoline Stratified Combustion in SI-DI Engines," *J. Eng. Gas Turbines Power*, vol. 130, no. 2, Mar. 2008.

[73]   T. D'Andrea, P. F. Henshaw, and D. S.-K. Ting, "The addition of hydrogen to a gasoline-fuelled SI engine," *Int. J. Hydrogen Energy*, vol. 29, no. 14, pp. 1541–1552, Nov. 2004.

[74]   C. Ji and S. Wang, "Effect of hydrogen addition on combustion and emissions performance of a spark ignition gasoline engine at lean conditions," *Int. J. Hydrogen Energy*, vol. 34, no. 18, pp. 7823–7834, Sep. 2009.

[75]   T. Tahtouh, F. Halter, E. Samson, and C. Mounaïm-Rousselle, "Effects of hydrogen addition under lean and diluted conditions on combustion characteristics and emissions in a spark-ignition engine," *Int. J. Engine Res.*, vol. 12, no. 5, pp. 466–483, Oct. 2011.

[76]   C. Sprouse and C. Depcik, "Review of organic Rankine cycles for internal combustion engine exhaust waste heat recovery," *Applied Thermal Engineering*, vol. 51, no. 1–2. Pergamon, pp. 711–722, 01-Mar-2013.

[77]   X. Liang, X. Wang, G. Shu, H. Wei, H. Tian, and X. Wang, "A review and selection of engine waste heat recovery technologies using analytic hierarchy process and grey relational analysis," *International Journal of Energy Research*, vol. 39, no. 4. pp. 453–471, 25-Mar-2015.

[78] R. Saidur, M. Rezaei, W. K. Muzammil, M. H. Hassan, S. Paria, and M. Hasanuzzaman, "Technologies to recover exhaust heat from internal combustion engines," *Renew. Sustain. Energy Rev.*, vol. 16, no. 8, pp. 5649–5659, 2012.

[79] H. Teng, G. Regner, and C. Cowland, "Waste Heat Recovery of Heavy-Duty Diesel Engines by Organic Rankine Cycle Part I: Hybrid Energy System of Diesel and Rankine Engines," in *SAE Technical Paper*, 2007, no. 2007-01–0537.

[80] D. A. Arias, T. A. Shedd, and R. K. Jester, "Theoretical Analysis of Waste Heat Recovery from an Internal Combustion Engine in a Hybrid Vehicle," in *SAE Technical Paper*, 2006, no. 2006-01–1605.

[81] G. A. Longo, A. Gasparella, and C. Zilio, "Analysis of an absorption machine driven by the heat recovery on an I.C. reciprocating engine," *Int. J. Energy Res.*, vol. 29, no. 8, pp. 711–722, 2005.

[82] T. Endo, S. Kawajiri, Y. Kojima, K. Takahashi, T. Baba, S. Ibaraki, T. Takahashi, and M. Shinohara, "Study on Maximizing Exergy in Automotive Engines," in *SAE Technical Paper*, 2007, no. 2007-01–0257.

[83] M. Tahani, S. Javan, and M. Biglari, "A comprehensive study on waste heat recovery from internal combustion engines using organic rankine cycle," *Therm. Sci.*, vol. 17, no. 2, pp. 611–624, 2013.

[84] Z. Peng, T. Wang, Y. He, X. Yang, and L. Lu, "Analysis of environmental and economic benefits of integrated Exhaust Energy Recovery (EER) for vehicles," *Appl. Energy*, vol. 105, pp. 238–243, May 2013.

[85] C. O. Katsanos, D. T. Hountalas, and E. G. Pariotis, "Thermodynamic analysis of a Rankine cycle applied on a diesel truck engine using steam and organic medium," in *Energy Conversion and Management*, 2012, vol. 60, pp. 68–76.

[86] Y. R. Li, J. N. Wang, M. T. Du, S. Y. Wu, C. Liu, and J. L. Xu, "Effect of pinch point temperature difference on cost-effective performance of organic Rankine cycle," *Int. J. Energy Res.*, vol. 37, no. 15, pp. 1952–1962, Sep. 2013.

[87] M. Ryms, T. Pyś, and E. Klugmann-Radziemska, "Adapting the pinch point analysis to improve the ORC design process," *Int. J. Energy Res.*, vol. 38, no. 1, pp. 29–40, Jan. 2014.

[88] P. J. Mago, K. K. Srinivasan, L. M. Chamra, and C. Somayaji, "An examination of exergy destruction in organic Rankine cycles," *Int. J. Energy Res.*, vol. 32, no. 10, pp. 926–938, Aug. 2008.

[89] H. Teng, G. Regner, and C. Cowland, "Achieving High Engine Efficiency for Heavy-Duty Diesel Engines by Waste Heat Recovery Using Supercritical Organic-Fluid Rankine Cycle," in *SAE Technical Paper*, 2006, no. 2006-01–3522.

[90] E. W. Miller, T. J. Hendricks, and R. B. Peterson, "Modeling energy recovery using thermoelectric conversion integrated with an organic rankine bottoming cycle," *J. Electron. Mater.*, vol. 38, no. 7, pp. 1206–1213, Jul. 2009.

[91] I. Vaja and A. Gambarotta, "Internal Combustion Engine (ICE) bottoming with

Organic Rankine Cycles (ORCs)," *Energy*, vol. 35, no. 2, pp. 1084–1093, Feb. 2010.

[92] V. Dolz, R. Novella, A. García, and J. Sánchez, "HD Diesel engine equipped with a bottoming Rankine cycle as a waste heat recovery system. Part 1: Study and analysis of the waste heat energy," *Appl. Therm. Eng.*, vol. 36, no. 1, pp. 269–278, Apr. 2012.

[93] D. T. Hountalas, G. C. Mavropoulos, C. Katsanos, and W. Knecht, "Improvement of bottoming cycle efficiency and heat rejection for HD truck applications by utilization of EGR and CAC heat," *Energy Convers. Manag.*, vol. 53, no. 1, pp. 19–32, Jan. 2012.

[94] S. Zhu, K. Deng, and S. Qu, "Energy and exergy analyses of a bottoming rankine cycle for engine exhaust heat recovery," *Energy*, vol. 58, pp. 448–457, Sep. 2013.

[95] R. El Chammas, D. Clodic, R. El Chammas, and D. Clodic, "Combined Cycle for Hybrid Vehicles," in *SAE Technical Paper*, 2005, no. 2005-01–1171.

[96] A. Boretti, "Recovery of exhaust and coolant heat with R245fa organic Rankine cycles in a hybrid passenger car with a naturally aspirated gasoline engine," *Appl. Therm. Eng.*, vol. 36, no. 1, pp. 73–77, Apr. 2012.

[97] A. A. Boretti, "Transient operation of internal combustion engines with Rankine waste heat recovery systems," *Appl. Therm. Eng.*, vol. 48, pp. 18–23, Dec. 2012.

[98] O. Badr, P. W. O'Callaghan, and S. D. Probert, "Rankine-cycle systems for harnessing power from low-grade energy sources," *Appl. Energy*, vol. 36, no. 4, pp. 263–292, Jan. 1990.

[99] M. Kadota and K. Yamamoto, "Advanced Transient Simulation on Hybrid Vehicle Using Rankine Cycle System," *SAE Int. J. Engines*, vol. 1, no. 1, pp. 240–247, Apr. 2008.

[100] F. A. DiBella, L. R. DiNanno, and M. D. Koplow, "Laboratory and On-Highway Testing of Diesel Organic Rankine Compound Long-Haul Vehicle Engine," in *SAE Technical Paper*, 1983, no. 830122.

[101] V. K. Chakravarthy, C. S. Daw, J. A. Pihl, and J. C. Conklin, "Study of the theoretical potential of thermochemical exhaust heat recuperation for internal combustion engines," *Energy and Fuels*, vol. 24, no. 3, pp. 1529–1537, Mar. 2010.

[102] M. He, X. Zhang, K. Zeng, and K. Gao, "A combined thermodynamic cycle used for waste heat recovery of internal combustion engine," *Energy*, vol. 36, no. 12, pp. 6821–6829, Dec. 2011.

[103] G. J. Snyder and E. S. Toberer, "Complex thermoelectric materials," *Nat. Mater.*, vol. 7, no. 2, pp. 105–114, Feb. 2008.

[104] R. K. Stobart, A. Wijewardane, and C. Allen, "The Potential for Thermo-electric Devices in Passenger Car Applications," in *SAE Technical Paper*, 2010, no. 2010-01–0833.

[105] A. Patyk, "Thermoelectric generators for efficiency improvement of power generation by motor generators - Environmental and economic perspectives," *Appl. Energy*, vol. 102, pp. 1448–1457, Feb. 2013.

[106] C.-C. Weng and M.-J. Huang, "A simulation study of automotive waste heat recovery using a thermoelectric power generator," *Int. J. Therm. Sci.*, vol. 71, pp. 302–309, Sep. 2013.

[107] Y. Y. Hsiao, W. C. Chang, and S. L. Chen, "A mathematic model of thermoelectric module with applications on waste heat recovery from automobile engine," *Energy*, vol. 35, no. 3, pp. 1447–1454, Mar. 2010.

[108] X. Gou, S. Yang, H. Xiao, and Q. Ou, "A dynamic model for thermoelectric generator applied in waste heat recovery," *Energy*, vol. 52, pp. 201–209, Apr. 2013.

[109] X. Niu, J. Yu, and S. Wang, "Experimental study on low-temperature waste heat thermoelectric generator," *J. Power Sources*, vol. 188, no. 2, pp. 621–626, Mar. 2009.

[110] Q. E. Hussain, D. R. Brigham, and C. W. Maranville, "Thermoelectric Exhaust Heat Recovery for Hybrid Vehicles," *SAE Int. J. Engines*, vol. 2, no. 1, pp. 1132–1142, Apr. 2009.

[111] C. T. Hsu, G. Y. Huang, H. S. Chu, B. Yu, and D. J. Yao, "Experiments and simulations on low-temperature waste heat harvesting system by thermoelectric power generators," *Appl. Energy*, vol. 88, no. 4, pp. 1291–1297, Apr. 2011.

[112] M. A. Karri, E. F. Thacher, and B. T. Helenbrook, "Exhaust energy conversion by thermoelectric generator: Two case studies," *Energy Convers. Manag.*, vol. 52, no. 3, pp. 1596–1611, Mar. 2011.

[113] X. Zhang, K. T. Chau, C. C. Chan, and S. Gao, "An automotive thermoelectric-photovoltaic hybrid energy system," in *2010 IEEE Vehicle Power and Propulsion Conference*, 2010, pp. 1–5.

[114] M. Mori, T. Yamagami, N. Oda, M. Hattori, M. Sorazawa, and T. Haraguchi, "Current Possibilities of Thermoelectric Technology Relative to Fuel Economy," 2009.

[115] X. Zhang and K. T. Chau, "An automotive thermoelectric-photovoltaic hybrid energy system using maximum power point tracking," *Energy Convers. Manag.*, vol. 52, no. 1, pp. 641–647, Jan. 2011.

[116] A. E. Teo Sheng Jye, A. Pesiridis, and S. Rajoo, "Effects of Mechanical Turbo Compounding on a Turbocharged Diesel Engine," in *SAE Technical Paper*, 2013, no. 2013-01–0103.

[117] M. Algrain, "Controlling an Electric Turbo Compound System for Exhaust Gas Energy Recovery in a Diesel Engine," in *2005 IEEE International Conference on Electro Information Technology*, 2005, pp. 1–6.

[118] C. O. Katsanos, D. T. Hountalas, and T. C. Zannis, "Simulation of a heavy-duty diesel engine with electrical turbocompounding system using operating charts for turbocharger components and power turbine," *Energy Convers. Manag.*, vol. 76, pp. 712–724, Dec. 2013.

[119] U. Hopmann, "Diesel Engine Waste Heat Recovery Utilizing Electric Turbocompound Technology," 2004.

[120] D. T. Hountalas, C. Katsanos, and V. T. Lamaris, "Recovering energy from the diesel

engine exhaust using mechanical and electrical turbocompounding," in *SAE Technical Paper*, 2007, no. 2007-01–1563.

[121] a G. Stefanopoulou, I. Kolmanovsky, and J. S. Freudenberg, "Control of variable geometry turbocharged diesel engines for reduced emissions," *IEEE Trans. Control Syst. Technol.*, vol. 3, no. 4, pp. 733–745, Jul. 2000.

[122] W. Bandel, G. K. Fraidl, P. E. Kapus, H. Sikinger, and C. N. Cowland, "The Turbocharged GDI Engine: Boosted Synergies for High Fuel Economy Plus Ultra-low Emission," in *SAE Technical Paper*, 2006, no. 2006-01–1266.

[123] D. Petitjean, L. Bernardini, C. Middlemass, and S. M. Shahed, "Advanced gasoline engine turbocharging technology for fuel economy improvements," in *SAE Technical Paper*, 2004, no. 2004-01–0988.

[124] Z. Filipi, Y. Wang, and D. N. Assanis, "Effect of Variable Geometry Turbine (VGT) on Diesel Engine and Vehicle System Transient Response," in *SAE Technical Paper*, 2001, no. 2001-01–1247.

[125] J. Andersen, E. Karlsson, and A. Gawell, "Variable Turbine Geometry on SI Engines," in *SAE Technical Paper*, 2006, no. 2006-01–0020.

[126] A. Pesiridis, *Automotive exhaust emissions and energy recovery*. 2014.

[127] N. Terdich, R. F. Martinez-Botas, A. Romagnoli, and A. Pesiridis, "Mild Hybridization Via Electrification of the Air System: Electrically Assisted and Variable Geometry Turbocharging Impact on an Off-Road Diesel Engine," *J. Eng. Gas Turbines Power*, vol. 136, no. 3, p. 31703, Mar. 2013.

[128] S. Matsuo, E. Ikeda, Y. Ito, and H. Nishiura, "The New Toyota Inline 4 Cylinder 1 . 8L ESTEC 2ZR-FXE Gasoline Engine for Hybrid Car," in *SAE Technical Paper*, 2016, no. 2016-01–0684.

[129] M. hakariya, T. Toda, and M. Sakai, "The New Toyota Inline 4-Cylinder 2.5L Gasoline Engine," in *SAE Technical Paper*, 2017, no. 2017-01–1021.

[130] Y. . Zhang, D. . Jesch, J. Oakley, and J. Ghandhi, "High resolution in-cylinder scalar field measurements during the compression and expansion strokes," in *SAE Technical Paper*, 2013, no. 2013-01–0567.

[131] K. D. Huang, S. C. Tzeng, and W. C. Chang, "Energy-saving hybrid vehicle using a pneumatic-power system," *Appl. Energy*, vol. 81, no. 1, pp. 1–18, May 2005.

[132] P. Brejaud, A. Charlet, Y. Chamaillard, A. Ivanco, and P. Higelin, "Pneumatic-Combustion Hybrid Engine: A Study of the Effect of the Valvetrain Sophistication on Pneumatic Modes," *Oil Gas Sci. Technol. – Rev. l'Institut Français du Pétrole*, vol. 65, no. 1, pp. 27–37, Jan. 2010.

[133] K. D. Huang and S. C. Tzeng, "Development of a hybrid pneumatic-power vehicle," *Appl. Energy*, vol. 80, no. 1, pp. 47–59, Jan. 2005.

[134] P. Higelin, A. Charlet, and Y. Chamaillard, "Thermodynamic simulation of a hybrid pneumatic-combustion engine concept," *Int. J. Appl. Thermodyn.*, vol. 5, no. 1, pp. 1–11, 2002.

[135] P. L. Chen and J. Xu, "Analysis on Hybrid Effects of Parallel Pneumatic Hybrid Vehicle," *Appl. Mech. Mater.*, vol. 246–247, pp. 103–107, Dec. 2012.

[136] Leonard H Dyer, "Internal-combustion engine," US1339176 A, 1915.

[137] R. C. Tibbs and Robert C. Tibbs, "Six cycle combustion and fluid vaporization engine," US3964263 A, 31-Dec-1974.

[138] Gregory J. Larsen, "Engine with a six-stroke cycle, variable compression ratio, and constant stroke," US4736715 A, 1985.

[139] J. C. Conklin and J. P. Szybist, "A highly efficient six-stroke internal combustion engine cycle with water injection for in-cylinder exhaust heat recovery," *Energy*, vol. 35, no. 4, pp. 1658–1664, Apr. 2010.

[140] T. Alger and B. Mangold, "Dedicated EGR : A New Concept in High Efficiency Engines," in *SAE Technical Paper*, 2009, no. 2009-01–0694.

[141] T. Alger, M. Walls, C. Chadwell, S. Joo, B. Denton, K. Kleinow, and D. Robertson, "The Interaction between Fuel Anti-Knock Index and Reformation Ratio in an Engine Equipped with Dedicated EGR," *SAE Int. J. Engines*, vol. 9, no. 2, pp. 786–795, Apr. 2016.

[142] C. Chadwell, T. Alger, J. Zuehl, and R. Gukelberger, "A Demonstration of Dedicated EGR on a 2.0 L GDI Engine," *SAE Int. J. Engines*, vol. 7, no. 1, pp. 2014-01–1190, Apr. 2014.

[143] J. Sarlashkar, S. Rengarajan, and R. Roecker, "Transient Control of a Dedicated EGR Engine," in *SAE Technical Paper*, 2016, no. 2016-01–0616.

[144] D. Robertson, C. Chadwell, T. Alger, J. Zuehl, R. Gukelberger, B. Denton, and I. Smith, "Dedicated EGR Vehicle Demonstration," *SAE Int. J. Engines*, vol. 10, no. 3, pp. 2017-01–0648, Mar. 2017.

[145] V. B. Kalaskar, R. Gukelberger, B. Denton, and T. Briggs, "The Impact of Engine Operating Conditions on Reformate Production in a D-EGR Engine," in *SAE Technical Paper*, 2017, no. 2017-01–0684.

[146] B. Denton, C. Chadwell, R. Gukelberger, and T. Alger, "Design and Implementation of a D-EGR® Mixer for Improved Dilution and Reformate Distribution," *SAE Int. J. Engines*, vol. 10, no. 3, pp. 2017-01–0647, 2017.

[147] H. H. Song and C. F. Edwards, "Optimization of Recompression Reaction for Low-Load Operation of Residual-Effected HCCI," in *SAE Technical Paper*, 2008, no. 2008-01–0016.

[148] D. Law, D. Kemp, J. Allen, G. Kirkpatrick, and T. Copland, "Controlled Combustion in an IC-Engine with a Fully Variable Valve Train," in *SAE Technical Paper*, 2001, no. 2001-01–0251.

[149] R. P. Fitzgerald and R. Steeper, "Thermal and Chemical Effects of NVO Fuel Injection on HCCI Combustion," *SAE Int. J. Engines*, vol. 3, no. 1, pp. 2010-01–0164, Apr. 2010.

[150] J. Waldman, D. Nitz, T. Aroonsrisopon, D. E. Foster, and M. Iida, "Experimental Investigation into the Effects of Direct Fuel Injection During the Negative Valve Overlap Period in an Gasoline Fueled HCCI Engine," in *SAE Technical Paper*, 2007, no. 2007-01–0219.

[151] J. P. Szybist, R. R. Steeper, D. Splitter, V. B. Kalaskar, J. Pihl, and C. Daw, "Negative Valve Overlap Reforming Chemistry in Low-Oxygen Environments," *SAE Int. J. Engines*, vol. 7, no. 1, pp. 2014-01–1188, Apr. 2014.

[152] I. Ekoto, B. Peterson, J. Szybist, and W. Northrop, "Analysis of Thermal and Chemical Effects on Negative Valve Overlap Period Energy Recovery for Low-Temperature Gasoline Combustion," *SAE Int. J. Engines*, vol. 8, no. 5, pp. 2015-24–2451, Sep. 2015.

[153] V. B. Kalaskar, J. P. Szybist, D. a Splitter, J. a Pihl, and C. S. Daw, "In-cylinder Reaction Chemistry and Kinetics during Negative Valve Overlap Fuel Injection Under Low-Oxygen Conditions," in *Poceedings of the ASME 2013 Internal Combustion Engine Division Fall Technical Conference*, 2013, p. ICEF2013-19230.

[154] N. Edwards, S. R. Ellis, J. C. Frost, S. E. Golunski, A. N. J. Van Keulen, N. G. Lindewald, and J. G. Reinkingh, "On-board hydrogen generation for transport applications: The HotSpot^{TM} methanol processor," *J. Power Sources*, vol. 71, no. 1–2, pp. 123–128, Mar. 1998.

[155] A. Tsolakis, A. Megaritis, and M. L. Wyszynski, "Application of Exhaust Gas Fuel Reforming in Compression Ignition Engines Fueled by Diesel and Biodiesel Fuel Mixtures," *Energy and Fuels*, vol. 17, no. 6, pp. 1464–1473, 2003.

[156] K. Ashida, H. Maeda, T. Araki, M. Hoshino, K. Hiraya, T. Izumi, M. Yasuoka, H. Maeda, T. Araki, K. Hiraya, and M. Yasuoka, "Study of an On-board Fuel Reformer and Hydrogen-Added EGR Combustion in a Gasoline Engine," in *SAE International Journal of Fuels and Lubricants*, 2015, vol. 8, no. 2, pp. 2015-01–0902.

[157] J. E. Kirwan, A. A. Quader, and M. J. Grieve, "Fast Start-Up On-Board Gasoline Reformer for Near Zero Emissions in Spark-Ignition Engines Reprinted From : SI Combustion and Flow Diagnostics," in *SAE Technical Paper*, 2002, no. 2002-01–1011.

[158] J. E. Kirwan, A. A. Quader, M. J. Grieve, K. M. Rahmoeller, KapilaWadumesthrige, and G. B. Fisher., "On-Board Reformer Development for Low Emissions in Spark-Ignition Engines," in *Proceedings of the Global Powertrain Congress*, 2002.

[159] J. Fowler, D. Morgenstern, E. Sall, and M. E. Veinbergs, "Integration of an E85 Reforming System into a Vehicle- Ready Package and Project Results," in *SAE Technical Paper*, 2014, no. 2014-01–1191.

[160] J. Hwang, X. Li, and W. Northrop, "Exploration of Dual Fuel Diesel Engine Operation with On-Board Fuel Reforming," in *SAE Technical Paper*, 2017, no. 2017-01–0757.

[161] D. Fennell, J. M. Herreros Arellano, A. Tsolakis, M. Wyszynski, K. Cockle, J. Pignon, and P. Millington, "On-board thermochemical energy recovery technology for low carbon clean gasoline direct injection engine powered vehicles," *Proc. Inst. Mech. Eng. Part D J. Automob. Eng.*, p. 95440701772670, Sep. 2017.

[162] D. Fennell, J. Herreros, A. Tsolakis, K. Cockle, J. Pignon, and P. Millington, "Thermochemical recovery technology for improved modern engine fuel economy – part 1: analysis of a prototype exhaust gas fuel reformer," *RSC Adv.*, vol. 5, no. 44, pp. 35252–35261, Apr. 2015.

[163] R. Gukelberger, G. Bartley, J. Gingrich, T. Alger, S. Almaraz, J. Buckingham, and C. Henry, "Water-Gas-Shift Catalyst Development and Optimization for a D-EGR ®Engine," in *SAE Technical Paper*, 2015, no. 2015-01–1968.

[164] J. B. Martz, R. J. Middleton, G. A. Lavoie, A. Babajimopoulos, and D. N. Assanis, "A computational study and correlation of premixed isooctane-air laminar reaction front properties under spark ignited and spark assisted compression ignition engine conditions," *Combust. Flame*, vol. 158, no. 6, pp. 1089–1096, Jun. 2011.

[165] J. E. Anderson, D. M. Dicicco, J. M. Ginder, U. Kramer, T. G. Leone, H. E. Raney-Pablo, and T. J. Wallington, "High octane number ethanol-gasoline blends: Quantifying the potential benefits in the United States," *Fuel*, vol. 97, pp. 585–594, 2012.

[166] L. Sileghem, V. A. Alekseev, J. Vancoillie, K. M. Van Geem, E. J. K. Nilsson, S. Verhelst, and A. A. Konnov, "Laminar burning velocity of gasoline and the gasoline surrogate components iso-octane, n-heptane and toluene," *Fuel*, vol. 112, pp. 355–365, Oct. 2013.

[167] G. M. Chupka, E. Christensen, L. Fouts, T. L. Alleman, M. A. Ratcliff, and R. L. McCormick, "Heat of Vaporization Measurements for Ethanol Blends Up To 50 Volume Percent in Several Hydrocarbon Blendstocks and Implications for Knock in SI Engines," *SAE Int. J. Fuels Lubr.*, vol. 8, no. 2, pp. 2015-01–0763, Apr. 2015.

[168] A. A. Quader, "What Limits Lean Operation in Spark Ignition Engines-Flame Initiation or Propagation?," in *SAE Technical Paper*, 1976, no. 760760.

[169] E. Conte and K. Boulouchos, "Influence of Hydrogen-Rich-Gas Addition on Combustion, Pollutant Formation and Efficiency of an IC-SI Engine," in *SAE Technical Paper*, 2004, no. 2004-01–0972.

[170] Y. Chang and J. P. Szybist, "Fuel Effects on Combustion with EGR Dilution in Spark Ignited Engine," in *Central States Meeting of the Combustion Institute, Knoxville, TN, USA,* 2016.

[171] S. Allenby, W.-C. C. Chang, A. Megaritis, M. L. Wyszyński, and M. L. Wyszy??ski, "Hydrogen enrichment: a way to maintain combustion stability in a natural gas fuelled engine with exhaust gas recirculation, the potential of fuel reforming," *Proc. Inst. Mech. Eng. Part D J. Automob. Eng.*, vol. 215, no. 3, pp. 405–418, Mar. 2001.

[172] D. Fennell, J. Herreros, and A. Tsolakis, "Improving gasoline direct injection (GDI) engine efficiency and emissions with hydrogen from exhaust gas fuel reforming," *Int. J. Hydrogen Energy*, vol. 39, no. 10, pp. 5153–5162, Mar. 2014.

[173] Y. Jamal and M. L. Wyszynski, "On-board generation of hydrogen-rich gaseous fuels-a review," *Int. J. Hydrogen Energy*, vol. 19, no. 7, pp. 557–572, 1994.

[174] Y. Chang, M. Wooldridge, and S. V. Bohac, "Extending the Dilution Limit of Spark Ignition Combustion via Fuel Injection during Negative Valve Overlap," in *SAE Technical Paper*, 2016, no. 2016-01–0671.

[175] V. B. Kalaskar, J. P. Szybist, D. a Splitter, J. a Pihl, and C. S. Daw, "Valve Overlap Fuel Injection Under Low-Oxygen Conditions," in *Internal Combustion Engine Fall Technical Conference*, 2013, pp. 2013–19230.

[176] T. Urushihara, K. Hiraya, A. Kakuhou, and T. Itoh, "Expansion of HCCI operating region by the combination of direct fuel injection, negative valve overlap and internal fuel reformation," in *SAE Technical Paper*, 2003, no. 2003-01–0749.

[177] A. W. Berntsson and I. Denbratt, "Optical Study of HCCI Combustion using NVO and an SI Stratified Charge," in *SAE Technical Paper*, 2007, no. 2007-24–12.

[178] J. C. Wheeler, R. A. Stein, D. A. Morgenstern, E. D. Sall, and J. W. Taylor, "Low-temperature Ethanol Reforming: A Multi-cylinder Engine Demonstration," in *SAE Technical Paper*, 2011, no. 2011-01–0142.

[179] S. R. Gomes, N. Bion, G. Blanchard, S. Rousseau, V. Bellière-Baca, V. Harlé, D. Duprez, and F. Epron, "Thermodynamic and experimental studies of catalytic reforming of exhaust gas recirculation in gasoline engines," *Appl. Catal. B Environ.*, vol. 102, no. 1–2, pp. 44–53, Feb. 2011.

[180] P. Leung, A. Tsolakis, J. Rodríguez-Fernández, and S. Golunski, "Raising the fuel heating value and recovering exhaust heat by on-board oxidative reforming of bioethanol," *Energy Environ. Sci.*, vol. 3, no. 6, p. 780, Jun. 2010.

[181] D. Fennell, J. M. Herreros, A. Tsolakis, H. Xu, K. Cockle, and P. Millington, "GDI Engine Performance and Emissions with Reformed Exhaust Gas Recirculation (REGR)," in *SAE Technical Paper*, 2013, no. 2013-01–0537.

[182] S. Ahmed and M. Krumpelt, "Hydrogen from hydrocarbon fuels for fuel cells," *Int. J. Hydrogen Energy*, vol. 26, no. 4, pp. 291–301, Apr. 2001.

[183] Y. Jamal and M. L. Wyszynski, "On-board generation of hydrogen-rich gaseous fuels—a review," *Int. J. Hydrogen Energy*, vol. 19, no. 7, pp. 557–572, Jul. 1994.

[184] D. W. Brookshear, J. A. Pihl, and J. P. Szybist, "Catalytic Steam and Partial Oxidation Reforming of Liquid Fuels for Application in Improving the Efficiency of Internal Combustion Engines," *Energy and Fuels*, 2018.

[185] M. Mehl, W. J. Pitz, C. K. Westbrook, and H. J. Curran, "Kinetic modeling of gasoline surrogate components and mixtures under engine conditions," *Proc. Combust. Inst.*, vol. 33, no. 1, pp. 193–200, Jan. 2011.

[186] Y. . Zhang, D. . Jesch, J. Oakley, and J. Ghandhi, "High resolution in-cylinder scalar field measurements during the compression and expansion strokes," in *SAE Technical Paper*, 2013, no. 2013-01–0567.

[187] L. Manofsky, J. Vavra, D. N. Assanis, and A. Babajimopoulos, "Bridging the Gap between HCCI and SI: Spark-Assisted Compression Ignition," in *SAE Technical Paper*, 2011, no. 2011-01–1179.

[188] R. M. Wagner, K. D. Edwards, C. S. Daw, J. B. Green, and B. G. Bunting, "On the Nature of Cyclic Dispersion in Spark Assisted HCCI Combustion," in *SAE Technical Paper*, 2006, no. 2006-01–0418.

[189] Z. Wang, J.-X. Wang, S.-J. Shuai, G.-H. Tian, X. An, and Q.-J. Ma, "Study of the Effect of Spark Ignition on Gasoline HCCI Combustion," *Proc. Inst. Mech. Eng. Part D J. Automob. Eng.*, vol. 220, no. 6, pp. 817–825, 2006.

[190] E. P. Brandt and J. W. Grizzle, "Dynamic modeling of a three-way catalyst for SI engine exhaust emission control," *IEEE Trans. Control Syst. Technol.*, vol. 8, no. 5, pp. 767–776, 2000.

[191] Y. Chen, V. Sima, W. Lin, J. Sterniak, and S. V. Bohac, "Lean HCCI/Rich SACI Gasoline Combustion Cycling and Three-Way Catalyst for Fuel Efficiency and NOx Reduction," *Jounal Eng. Gas Turbines Power*, vol. 137, no. 12, p. V001T04A005, Oct. 2015.

[192] H. Zhao, J. Li, T. Ma, and N. Ladommatos, "Performance and Analysis of a 4-Stroke Multi-Cylinder Gasoline Engine with CAI Combustion," in *SAE Technical Paper*, 2002, no. 2002-01–0420.

[193] H. Persson, R. Pfeiffer, A. Hultqvist, B. Johansson, and H. Ström, "Cylinder-to-Cylinder and Cycle-to-Cycle Variations at HCCI Operation With Trapped Residuals," in *SAE Technical Paper*, 2005, no. 2005-01–0130.

[194] N. Wermuth, H. Yun, and P. Najt, "Enhancing Light Load HCCI Combustion in a Direct Injection Gasoline Engine by Fuel Reforming During Recompression," *SAE Int. J. Engines*, vol. 2, no. 1, pp. 823–836, Apr. 2009.

[195] S. Klinkert, "An Experimental Investigation of the Maximum Load Limit of Boosted HCCI Combustion in a Gasoline Engine with Negative Valve Overlap," 2014.

[196] W. Lin, A. Arbor, and B. W. K. Twin-scroll, "Emissions Characterization During Transient Spark Assisted Compression Ignition (Saci) Engine Operation," in *ASME 2013 Internal Combustion Engine Division Fall Technical Conference*, 2013, pp. 1–9.

[197] S. Choi, M. Ki, K. Min, J. Kong, K. Chang, K. Kwon, and K. Shin, "An On-Line Model for Predicting Residual Gas Fraction by Measuring Intake / Exhaust and Cylinder Pressure in CAI Engine," in *SAE Technical Paper*, 2008, no. 2008-01–0540.

[198] M. Sellnau, J. Sinnamon, L. Oberdier, C. Dase, M. Viele, K. Quillen, J. Silvestri, and I. Papadimitriou, "Development of a practical tool for residual gas estimation in {IC} engines," in *SAE Technical Paper*, 2009, no. 2009-01–0695.

[199] G. Woschni, "A Universally Applicable Equation for the Instantaneous Heat Transfer Coefficient in the Internal Combustion Engine," in *SAE Technical Paper*, 1967, no. 670931.

[200] H. Persson, A. Hultqvist, B. Johansson, and A. Remón, "Investigation of the Early Flame Development in Spark Assisted HCCI Combustion Using High Speed Chemiluminescence Imaging," in *SAE Technical Paper*, 2007, no. 2007-01–0212.

[201] L. Tartakovsky, V. Baibikov, and M. Veinblat, "Comparative performance analysis of

SI engine Fed by ethanol and methanol reforming products," in *SAE Technical Paper*, 2013, no. 2013-01–2617.